Dynamic Synthesis/Design and Operation/Control Optimization Approach applied to a Solid Oxide Fuel Cell based Auxiliary Power Unit under Transient Conditions

Diego Fernando Rancruel

Dissertation submitted to the Faculty of the
Virginia Polytechnic Institute and State University
in partial fulfillment of the requirements for the degree of

DOCTOR OF PHILOSOPHY
in
Mechanical Engineering

Dr. Michael von Spakovsky, Chair
Dr. Walter O'Brien
Dr. Michael Ellis
Dr. Douglas Nelson
Dr. Sudip Mazumder
Dr. Donald Leo

Blacksburg, Virginia
February 11, 2005

Keywords: optimization, dynamics, control, decomposition, thermoeconomics, exergy, fuel cell, SOFC

Dynamic Synthesis/Design and Operation/Control Optimization Approach applied to a Solid Oxide Fuel Cell based Auxiliary Power Unit under Transient Conditions

by Diego Fernando Rancruel

Abstract

A typical approach to the synthesis/design optimization of energy systems is to only use steady state operation and high efficiency (or low total life cycle cost) at full load as the basis for the synthesis/design. Transient operation as reflected by changes in power demand, shut-down, and start-up are left as secondary tasks to be solved by system and control engineers once the synthesis/design is fixed. However, transient regimes may happen quite often and the system response to them is a critical factor in determining the system's feasibility. Therefore, it is important to consider the system dynamics in the creative process of developing the system.

A decomposition approach for dynamic optimization developed and applied to the synthesis/design and operation/control optimization of a solid oxide fuel cell (SOFC) based auxiliary power unit (APU) is the focus of this doctoral work. Called DILGO (Dynamic Iterative Local-Global Optimization), this approach allows for the decomposed optimization of the individual units (components, sub-systems or disciplines), while taking into account the intermediate products and feedbacks which couple all of the units which make up the overall system. The approach was developed to support and enhance current engineering synthesis/design practices by making possible dynamic modular concurrent system optimization. In addition, this approach produces improvements in the initial synthesis/design state at all stages of the process and allows any level of complexity in the unit's modeling.

DILGO uses dynamic shadow price rates as a basis for measuring the interaction level between units. The dynamic shadow price rate is a representation of the unit's cost

rate variation with respect to variations in the unit's coupling functions. The global convergence properties of DILGO are seen to be dependent on the mathematical behavior of the dynamic shadow price rate. The method converges to a "global" (system-level) optimum provided the dynamic shadow price rates are approximately constant or at least monotonic. This is likely to be the case in energy systems where the coupling functions, which represent intermediate products and feedbacks, tend to have a monotonic behavior with respect to the unit's local contribution to the system's overall objective function.

Finally, DILGO is a physical decomposition used to solve system-level as well as unit-level optimization problems. The total system considered here is decomposed into three sub-systems as follows: stack sub-system (SS), fuel processing sub-system (FPS), and the work and air recovery sub-system (WRAS). Mixed discrete, continuous, and dynamic operational decision variables are considered. Detailed thermodynamic, kinetic, geometric, physical, and cost models for the dynamic system are formulated and implemented. All of the sub-systems are modeled using advanced state-of-the-art tools. DILGO is then applied to the dynamic synthesis/design and operation/control optimization of the SOFC based APU using the total life cycle cost as objective function. The entire problem has a total of 120 independent variables, some of which are integer valued and dynamic variables. The solution to the problem requires only 6 DILGO iterations.

Acknowledgements

This work would not have been possible without the help of numerous people. Firstly, I would like to thank my advisor, Dr. Michael von Spakovsky, for providing me the opportunity to come to Virginia Tech and conduct this research. Dr. von Spakovsky's trust and faith in my capabilities were invaluable. Many thanks to Drs. Walter O'Brien, Michael Ellis, Doug Nelson, Sudip Mazumder, and Donald Leo for serving in my committee and for the valuable input they have given me over the course of this research.

This work was conducted under the sponsorship of the U.S. Department of Energy (DOE - Cooperative Agreement Number: DE-FC26-02NT41574)

The list of people in my family and friends who have helped me throughout the years is just too long to write in detail. I have been blessed with good people who have been with me in good and bad times. They should share the pride I feel because they are a big part of what I have been able to accomplish. I would like to thank as well my friends in Blacksburg, David, Vittorio, Pietro, Borja, Cristina, Nathan, and Todd. They have always been an important source of support.

This achievement would have been impossible to reach without the support, patience, company, and love of Elena. Thanks for being there for me.

This work is especially dedicated to my parents, Idalia and Carlos, thanks to whom I became the person I am. Through life they have given me support, freedom, example, and most importantly the love I need to reach my goals.

Diego Fernando Rancruel Arce

Table of Contents

List of Figures

List of Tables

Acronyms Index

AFR	Air to Fuel Ratio	MIMO	Multi-input/Multi-output
APU	Auxiliary Power Unit	NETL	National Energy Technology Laboratory
BOPS	Balance of Plant Sub-system	*ORS*	Optimum Response Surface
CFD	Computational Fluid Dynamics	PAFC	Phosphoric Acid Fuel Cell
DILGO	Dynamic Iterative Local-Global Optimization	PEMFC	Polymer Electrolyte Membrane Fuel Cell
DMFC	Direct Methanol Fuel Cell	*PES*	Power Electronics Sub-System
DMINLP	Dynamic Mixed Integer Non-linear Programming Problem	*SECA*	Solid State Energy Conversion Alliance
DOE	Department of Energy	SG	Steam Generator
EFA	Engineering Functional Analysis	SISO	Single-input/Single-output
FPS	Fuel Processing Sub-system	SMR	Steam-Methane Reformer Steam-to-Methane Ratio
FRR	Fuel Reformate Ratio	*SOFC*	Solid Oxide Fuel Cell
GRI	Gas Research Institute	*SS*	Stack Sub-system
ILGO	Iterative Local-Global Optimization	TFA	Thermoeconomic Functional Analysis
LGO	Local-Global Optimization	TI	Thermoeconomic Isolation
MCFC	Molten Carbonate Fuel Cell	*WRAS*	Work Recovery and Air Supply Sub-system

Chapter 1

Introduction

As the level of interaction between the various sub-systems of energy systems has increasingly become complex and performance a fundamental criteria for acquisition, the more important the need has become to carry out the synthesis/design[1] of the system in a completely integrated fashion in order that the demands imposed by all the sub-systems be accommodated in the best way possible. Unfortunately, when developing new systems or operating existing ones, the lack of comprehensive synthesis/design tools forces today's engineer to rely heavily on rules-of-thumb, individual experience, and a fairly non-integrated, non-interdisciplinary approach of basic calculations, i.e. simple *trade-off analysis.*

A typical approach to the synthesis/design optimization of energy systems is to only use steady state operation and high efficiency (or low total life cycle cost) at full load as the basis for the synthesis/design. Transient operation as reflected by changes in power demand, shut-down, and start-up are left as secondary tasks to be solved by system and control engineers once the synthesis/design is fixed. However, transient regimes may happen quite often and, thus, may be quite important in the creative process of developing the system. This is especially true for small power units used in transportation applications or for domestic energy supplies, where the load demand changes frequently and peaks in load of short duration are common. The duration of start-up is, of course, a major factor which must be considered since rapid system response is an important factor

[1] Note that *synthesis* refers to changes in system or component configuration while *design* here refers exclusively to, for example, the nominal (full load or design point) capacity, performance, and geometry of a given component or technology.

in determining the feasibility of, for example, solid oxide fuel cell (SOFC) based auxiliary power units (APUs). The need for more complex, efficient, and cost effective systems makes it imperative not only to analyze a greater number of possible configurations and technologies but also to synthesize/design systems in a way which optimizes these systems taking into account load and environmental variations over time and their effect on system performance and integrity.

Powerful software tools are accessible. However, these are designed for single point analysis or are not integrated with one another and do not consider all disciplines. In cases where optimization is considered, partially due to the fact that new and more potent computers have become available and optimization tools more popular, it is seen as a straightforward mathematical problem, which for large-scale, highly non-linear optimization problems can be very limiting to say the least. Even significant increases in computational power are not sufficient to offset the ever increasing complexity of energy systems and the ensuing synthesis/design problem. Therefore, the need for methods that permit effective solutions of large-scale optimization problems is still an area of research, which generates great interest.

In formulating the entire synthesis/design problem (i.e. identifying all the interacting sub-systems, choosing the possible configurations and decision variables, and defining the physical constraints), it may turn out that solving the entire problem as a single problem (as opposed to solving a set of multiple problems) is simply impractical. The reasons are multiple:

- The number of decision variables involved may simply be too large for an efficient solution. In fact, given the current state of mathematical optimization, a solution may not be obtainable at all in the most complex cases.
- A single group of engineers may not possess all the expertise required for dealing with the technologies, sub-systems, and components involved in the problem.
- The integration of different computer codes, which simulate different aspects of the system, may be difficult. Even in cases when code integration is possible, the overhead is simply too great to make the optimization viable.
- The synthesis/design of the different sub-systems may, in many cases, be done at different stages and times, crossing company lines, and even in different locations.

The overall problem being addressed is very complex and difficult to solve. In its entirety, it represents a dynamic mixed integer, non-linear programming (DMINLP) problem for which no general solution has been found. This is further complicated by the need to examine the largest number and most complete set of alternative syntheses and designs at each level of the problem in the shortest amount of time possible. Fundamental issues, which need to be examined, include the following:

1. the effects of decomposition on convergence to a global optimum[2] or a set of near-global optima for the system as a whole. As well as the effects on decomposition and the search for global optima that a mixed discrete, continuous, and dynamic decision variable space will have; this relates to the complete DMINLP.
2. the effects of material and geometric changes at the component or sub-component level on the thermodynamic, heat and mass transfer, kinetic and dynamic phenomena occurring within individual components or sub-components (e.g., heat exchangers, turbo-machinery, ram-air nozzles, zones within specific components, etc.);
3. the coupling between the physical phenomena at the component and sub-component levels and the thermodynamic, heat and mass transfer, kinetic and dynamic behavior found elsewhere in the system;
4. the coupling between the dynamics of the overall system and the dynamic or transient responses of individual sub-systems and components and the effects these have on component geometry and material selections as well as component and sub-system integration.
5. the relevance of using the 1st and 2nd Law of thermodynamics as a measure of the relative importance of the physical phenomena taking place in the system and as a guide to component and system level changes which alter these phenomena in ways consistent with the global optima sought for synthesis/design;

[2] It should be noted that reference to a "global optimum" here is not meant to be taken in a strictly mathematical sense, i.e. the concern here is not in proving that decomposition necessarily leads to a Kuhn-Tucker point, but instead that in using decomposition coupled to mathematical optimization that the synthesis/design of the system as a whole can be improved even for very complex, highly dynamic problems involving a large number of degrees of freedom. If this "global" or "system-level" optimum (improvement) happens to coincide with a Kuhn-Tucker point, that is all to the better. However, the impracticality of proving this for very large and complex problems of practical interest is simply a waste of time since we are concerned here with system-level (global) and component-level (local) improvements in synthesis/design and not mathematical proofs.

6. the limits on decomposition imposed by thermodynamic as well as cost-based considerations;

Fundamental issue 1 deals with the mathematical foundations of decomposition and the nature of the design spaces created by modeling and optimizing the system as well as its subsystems and components. Establishing and understanding the basis for decomposition and the characteristics of the design spaces involved is essential for being able to deal effectively with this highly complex problem of interrelated physical phenomena. A clearer understanding of these physical phenomena and their interrelationships is also essential.

The next four issues (2 to 4) deal with these, i.e. the fundamental aspects of how and why these occur at the component and sub-component levels as well as at the sub-system and system levels and how they are effected by other phenomena occurring locally, upstream / downstream, or in some place not directly linked to the phenomenon or phenomena in question. Obviously, the dynamic and off-design aspects of these phenomena are also of importance and need to be examined in order to deduce their impact on the overall problem. Studying these phenomena and their interrelationships could be enhanced by the use of CFD as well as experimental models (particularly as they relate to heat exchangers and their interactions within an overall system) coupled to the type of lumped-parameter models used at the sub-system and system levels for optimization.

The remaining three issues (5 to 6) are essential for establishing and understanding the fundamental basis for using the 1^{st} and 2^{nd} Laws of thermodynamics in modeling the physical phenomena present. The impact this has on approaches (e.g., trade-off analysis versus mathematical optimization) for effectively synthesizing and designing components/sub-components and sub-systems can and should be clearly delimited.

In conclusion, the research plan outlined here represents a unique opportunity to study the fundamental nature of the couplings which exist between the basic physical phenomena occurring within a given component / sub-component and those occurring elsewhere in the sub-system / sub-systems with which the component / sub-component interacts. Understanding the impact of these couplings is, in fact, as important as

understanding the individual phenomena, which occur locally. Thus, the work carried on over the last three years at Virginia Tech under the sponsorship of the U.S. Department of Energy (DOE) (Cooperative Agreement Number: DE-FC26-02NT41574) has aimed at addressing a number of these issues in the context of developing high fidelity, lumped parameters models for analysis and of SOFC based APU for transportation and distributed stationary applications.

1.1 System Synthesis/Design Process

Those involved in system synthesis/design can never quite agree as to just where exactly the process begins. The designer thinks it starts with a new system concept. The sub-system specialist thinks that nothing can begin until initial sub-system capabilities are estimated. The customer feels that the process starts with his/her requirements. They are all correct, since system synthesis/design is an integrated effort as shown in Figure 1.1. Requirements are set by customer needs, while concepts are developed to meet those needs. Synthesis/design points toward new concepts, technologies and requirements, which in turn can initiate a whole new system synthesis/design effort. The synthesis/design process can be broken into three major phases, as depicted in Figure 1.2.

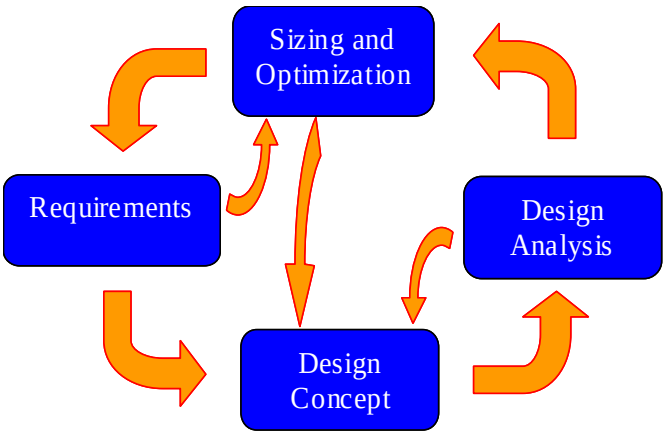

Figure 1.1: The synthesis/design wheel (Rancruel, 2002).

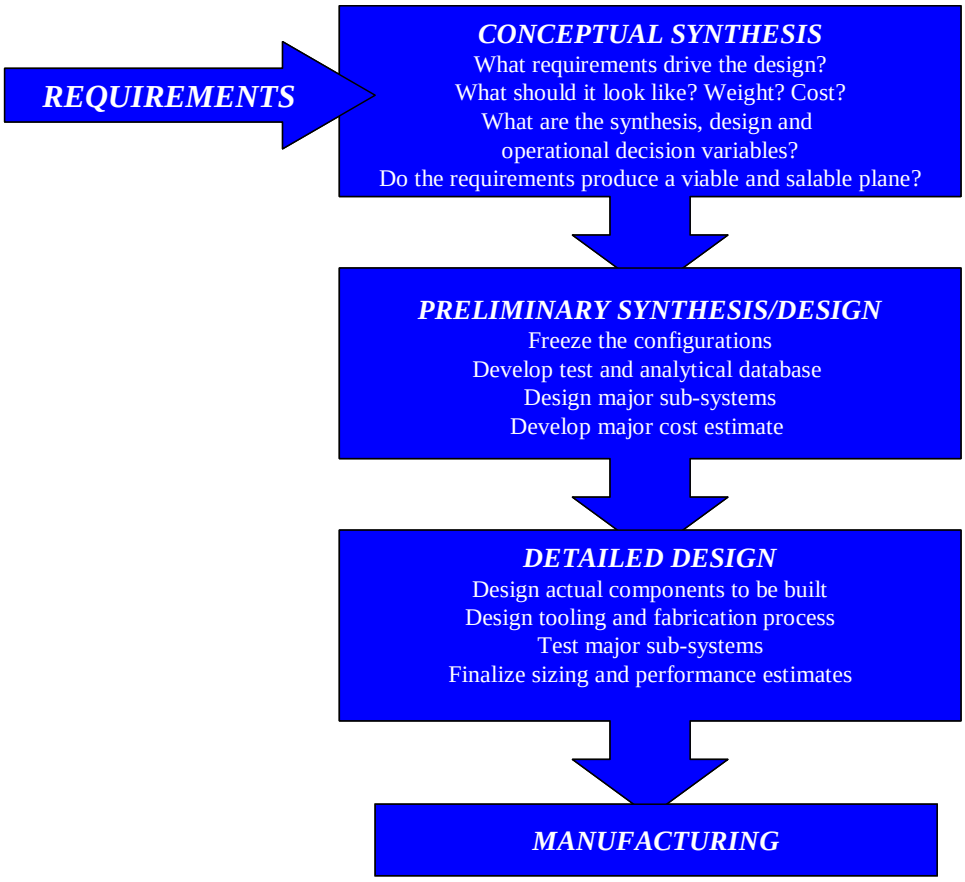

Figure 1.2 Three phases of system synthesis/design (Rancruel, 2002).

1.1.1 Conceptual System Synthesis Stage

It is in the conceptual system synthesis stage that many of the basic questions of configuration arrangement are answered. Conceptual synthesis is characterized by a large number of configuration alternatives and trade studies and a continuous, evolutionary change to the system concept under consideration. The first questions are asked and then explored, e.g., given a set of energy and performance needs:

- What types of sub-systems are available to meet these needs?
- Can any affordable system be built that meets the requirements?

If the answer to the latter is no, the customer may wish to review or relax the requirements. In the conceptual synthesis stage the requirements are used to guide and

evaluate the development of the overall system configuration. The level of detail in conceptual synthesis is not very deep. However, the constraints, limits and interactions among all the different components and sub-systems is so crucial that it requires years of expertise to be able to create good conceptual configurations at this point in the development process.

A key aspect of the conceptual synthesis stage is that it is a very fluid process. The configuration must be adaptable and is always changing both to incorporate new things learned during the process and to evaluate potential improvements. During the conceptual synthesis stage a number of alternative configurations are studied to determine which best meet the established requirements. The final result is a set of likely configurations or a super-configuration to evaluate in more detail during the preliminary system synthesis/design stage. As one goes through conceptual, preliminary, and detailed synthesis/design, the level of detail of the system, sub-systems, and components both in terms of modeling and analysis increases steadily.

1.1.2 Preliminary System Synthesis/Design Stage

The preliminary system synthesis/design can be said to begin when the major conceptual configurational changes are over. The big questions to be addressed are:

- What is the best system configuration (components and their inter-connections)?
- What are the best technical characteristics of each component (dimensions, material, capacity, performance, etc.)?
- What are the best flow rates, pressures, and temperatures of the various working fluids?
- What is the best operating point of the system at each instant of time?

During this stage, specialists in different areas synthesize/design and analyze their respective sub-systems or components. This stage as well as the previous are the ones on which this doctoral work is focused, offering a new approach for solving the integrated system synthesis/design optimization problem. The ultimate objective during the synthesis/design stage is to determine which single configuration and design is to be considered during the detailed system design stage.

1.1.3 Detailed System Design Stage

Assuming a favorable decision for entering full-scale development, the detailed system design stage seeks to define the actual pieces of equipment to be fabricated and assembled. This stage starts by identifying which phenomena must be modeled in greater detail; which analytical, numerical, and experimental high fidelity tools will be used; and what detailed costs are involved. This last and most expensive part of the system synthesis/design development process is characterized by a large number of designers, preparing detailed drawings or CAD/CAM files with actual fabrication geometries and dimensions. While, for instance, during an aircraft conceptual synthesis stage, the designers are concerned about such top-level issues as the number of engines required or the sweep of the wing, during the detailed system design stage, the designers concern themselves more with, for example, the exact radius of the corner of a pocket cutout on a flap track. Another important part of the detailed system design stage is what is called production design. Specialists determine how the system will be fabricated starting with the simplest sub-assemblies and building up to the final assembly process. Production designers often wish to modify the design for easy manufacture, modifications which can have a major impact on important figures of merit such as performance, weight, etc. At this point issues such as reliability/availability, material substitutions, and manufacturing and assembly criteria are addressed. Compromises are inevitable. However, the system must still meet the original requirements and constraints.

1.1.4 Synthesis/Design Stage: Tools

There are a number of tools and methodologies available to the engineer today. Of these, probably the most common and the least sophisticated is the system/component simulation package which aids the engineer in the synthesis and design process but forces the engineer, nonetheless, to rely heavily on rules-of-thumb and experience. Some exceptions to these tools are those based on pinch technology, exergy analysis, and expert systems[3]. A brief description of these is given in Chapter 2. There are, however,

[3] Note that all of the methodologies and tools described here are those which can in some way enhance an *integrated synthesis/design environment.* Such an environment facilitates *communication* between a set of synthesis / design tools as well as across platforms in order that the development process for new technologies be improved. However, as any such environment, its effectiveness depends very much on the tools of which it is comprised.

significant limitations as to what can be done with all of the above. Approaches for overcoming these limitations are mathematically based. They simultaneously model the physical and/or economic aspects of a system and its components. This permits the use, in a *single-level* approach, of optimization algorithms, whether deterministic (gradient-based) or heuristic (non-gradient based), which search the solution space of all possible solutions for the optimum synthesis, design, operation, and/or control of a system and its sub-systems and components. Furthermore, when such a single-level approach is unable to solve the synthesis/design optimization problem due to its complexity (both mathematical and cultural: see Muñoz and von Spakovsky, 2002), a *multi-level* approach using *decomposition* may be used to formulate the optimization problem in such a way as to permit the use of a gradient and or non-gradient based algorithm which can then successfully solve the problem. A discussion of these *optimization algorithms* and of *decomposition* is given in Chapter 2.

1.2. Operational and Dynamic Stage: Tools

Despite the progress made in recent year regarding the availability of reliable and affordable dynamic tools, the actual modelers fall short when it comes to robustness to support large, highly detailed systems and drastic changes in initial conditions. In the same manner, the simulation time increases exponentially as a function of the model detail and the magnitude of the disturbances impose on the model. There are, additionally, significant limitations of what can be done with these tools in order to apply dynamic optimization. Some commercial packages offer dynamic optimizers. However, again, they are not well-suit to handle highly complex systems for which each component's dynamic constant can present differences of several orders of magnitude difference. They also depend on the linearization, the normalization and the non-dimensionalization of the governing equations. Modern dynamic optimization algorithms such as optimal control theory or single and multiple shooting are limited, since they assume the system synthesis/design is already given. Additionally, their practical application depends on a relatively simple system dynamic model and on the assumption that the optimum control variable is a piecewise smooth function of time.

Currently control system design is limited to finding appropriate values of the controller parameters once the system synthesis and geometry has been determined, leaving no space for exploring the effects of the system dynamics on life cycle costs. Additionally, most times this approach yields changes in system configuration and geometry which separates the final system from the original synthesis/design, which in turn affects optimal performance. A brief description of the current dynamic tools will be presented in Chapter 3. In order to overcome the above mentioned difficulties a multi-level dynamic optimization technique must be developed and implemented in order to apply physical decomposition and at the same time take into account the control problem. This tool will be presented in Chapter 2 and 3 and is a major contribution of this doctoral work (see next section).

1.3 Thesis Objectives

Based on the discussion presented above, it is clear that there exists a need for a general methodology that will permit the integrated synthesis/design optimization of energy and non-energy systems at design and off-design while considering the system dynamic requirements and sub-system transient interactions. The required method should not only allow for the solution of the overall synthesis/design problem by dividing it into smaller sub-problems but facilitate as well the difficult task of sub-system integration. The general objective of this research is to develop the multi-disciplinary optimization concepts, tools, and application strategies that will allow the solution of the most general optimization problem for dynamic systems. These concepts, tools, and application strategies will be applied to the dynamic synthesis/design and operation/control optimization of a SOFC based APU for stationary application. The resulting optimization scheme is based on a decomposition approach called Dynamic Iterative Local Global optimization (DILGO) developed during this doctoral work. It is based on the decomposition optimization strategy for system synthesis/design called Iterative Local-Global Optimization (ILGO) (Muñoz, 2000; Muñoz and von Spakovsky, 200a,b, 2002). This multi-disciplinary decomposition optimization tool (DILGO) is specifically intended for solving the dynamic interaction of highly coupled systems. It also shows how the

dynamic optimization challenges mentioned above are met by satisfying the following requirements:

- It is able to evaluate the shadow (marginal) cost rates due changes is system-level variables (coupling functions) and the shadow (marginal) cost due to changes in the coupling functions integrated over time.
- is capable of using dissimilar modeling codes, possibly written on different platforms;
- supports multiple design points for dynamic systems in order to evaluate performance and cost through a complete load profile, and yet handle the complex dynamic simulations;
- effectively deals with dynamic operational decision variables and handles the coupling between these variables and the control system design.
- effectively deals with the synthesis problem (i.e. deals with the presence of integer and binary variables) so that advanced optimization algorithms to solve the complex mixed-integer problem (typically non-linear) are supported;
- is modular so that analyses and optimizations can be divided to the greatest extent possible into clearly separated tasks assigned to specialty organizations; therefore, permits geographically dispersed organizations to carry out optimization tasks aimed at optimizing the entire system;
- requires the minimum possible number of repetitions (i.e. re-optimizations);
- supports concurrent and parallel tasks;
- integrates as many parameters as possible within each sub-problem but not so many that it cannot be adequately defined and solved;
- is sufficiently general to handle systems in both stationary or transportation applications;
- guarantees, in the event of a premature stop in the process, a solution which is an improvement over the initial synthesis / design.

It is assumed in what follows that system modeling requires a high level of detail (and is, therefore, expensive to simulate and optimize) and involves large numbers of

independent, continuous, and discrete variables. In this doctoral work, the dynamic synthesis/design and operation/control problem is solved in an integral manner and is set up in a general way so that streams and couplings may be represented by energy (or exergy) or by any other relevant quantity, depending on which better facilitates the interface between the energy as well as any non-energy sub-systems present.

The specific goal of the work proposed for this doctoral research is the development of DILGO and the demonstration that the feasibility of using DILGO for the dynamic conceptual and preliminary synthesis/design and operational/control optimization of a SOFC based APU. It will, furthermore, be shown that DILGO can be used to generate optimum control strategies at the system level. Sub-systems for this SOFC include a fuel processing sub-system (FPS), an air and work recovery sub-system (WRAS), a fuel cell stack sub-system (SS), and a power electronics sub-system (PES). The latter does not participate in the optimization. This requires the development of a general, high fidelity, performance model for the system, which itself is based on high performance fuel cell technology. DILGO will be used for dynamically optimizing in an integrated fashion each of the sub-systems' syntheses/designs and operation/control, taking into account the optimal behavior of each sub-system for steady state at off-design as well as at its synthesis/design point and for transient behavior due to the dynamic loads present. Such a tool will enhance any integrated synthesis/design environment through a systematic and efficient selection of the best set of configurations (syntheses) and designs which comprise a system's synthesis/design space. The following is a list of the major specific objectives envisioned:

- Gain a fundamental understanding of how a high performance fuel cell system and its sub-systems operate at both steady state and transient state; and a general comprehension of the fundamental phenomena present in each part of the process.
- Create the physical, thermodynamic, and kinetic models for components and sub-systems and in turn describe their connectivities. Include models for off-design and dynamic behavior, which lead to the full modeling and optimization of the system over an entire load profile.

- Develop appropriate component geometry, fuel consumption, and cost functions, which relate cost to appropriate decision (synthesis/design and operation/control) variables.
- Develop and them apply a decomposition strategy, which permits both local/unit (i.e. component and sub-system) and global/system optimizations for both steady and transient states and provides for an on-going communication between these levels of optimization.
- Define the computational tools necessary for solving the set of mathematical optimization problems created.
- Use the models and computational tools for both optimizing the system locally (i.e. at the component and sub-system levels) and globally (i.e. at the system level).
- Document and analyze the results for the optimal synthesis/design of a high performance fuel cell system.

1.4 Original Contributions and Practical Impact

The originality of the proposed research is that it will provide the conceptual foundations for a completely general approach to the use of decomposition in large-scale dynamic optimization applied to the DMINLP problem. The case is made for dynamic behavior to be considered at the early stages of the synthesis/design process. This will have an immediate practical impact on the way energy systems in general and fuel cell systems in particular are synthesized/designed and dynamically operated/controlled in that it will

- advance the state-of-the-art beyond the isolated synthesis/design process and control system design approach, allowing for the dynamic operation to be part of the system life cycle.
- advance the state-of-the-art beyond simple trade-off analysis, bringing the power of real optimization to the complex dynamic synthesis/design and operation/control optimization problem for energy systems.

- allow for the decomposed optimization of sub-systems and components to facilitate the solution of the dynamic optimization problem, thus, simplifying the total system optimization without compromising the number of degrees of freedom possible.
- effectively deal with the complex problem of sub-system integration for dynamic segments.
- incorporate the highly dynamic nature of energy systems operation into the synthesis/design process through appropriate dynamic modeling and decomposition tools.
- establish the necessary and sufficient conditions for system-level dynamic synthesis/design and operation/control dynamic optimization.
- Develop comprehensive, high fidelity, fundamental dynamic models for all components of the balance of plant of a SOFC based APU, facilitating total system dynamic integration, analysis, and optimization. Complex non-linearities are modeled departing from the fundamental equations.
- Propose a novel system configuration that guaranties system dependability and makes feasible its application such that highly fluctuating load profiles are met.
- Generate control strategies in order to assure safe, efficient, and effective start-up and shut-down of the fuel cell system subject to drastic load cycling.
- Open a new field of research which considers the control system architecture a synthesis/design variable susceptible to being optimized at the very early stages of system development.

Chapter 2

State-of-the-Art of Energy Systems Synthesis/Design Analysis and Optimization

A current trend is to incorporate early on aspects of process control, energy utilization, and environmental impact into the synthesis/design process. This is because we are no longer simply interested in a narrowly defined optimal process. The process must be energy efficient, flexible, environmentally friendly, and easy to control. It has been shown that one way to accomplish this difficult task is to consider some aspects of the various sub-problems simultaneously and as early as possible. A number of algorithms involving general mathematical formulations and hybrid techniques have been proposed. The question of optimal solutions needs to be further analyzed as parametric objective functions are usually encountered. Thus, the optimal solution involves an optimal trade-off between the various terms (for example, between process design, energy utilization, control design, and environmental impact). In parallel with these integrated algorithms, integrated tools also need to be developed.

The synthesis/design of complex energy systems requires that sophisticated methodologies and tools be developed and applied. In fact, a number of these with varying degrees of sophistication have been the subject of research since the 1950s. Of these, probably the most common and the least sophisticated is the system/component simulation package which aids the engineer in the synthesis/design process but forces the engineer, nonetheless, to rely heavily on rules-of-thumb and experience. However, more structured tools exist. One can broadly classify the latter depending on the fundamental purpose for which they are used. Analysis methodologies and tools are typically used to gain a fundamental understanding of a process or system. The information is then used to

rationally define a set of possible configurations, designs, or modes of operation. Optimization methodologies and tools are used to determine a system's synthesis/design/operation so that a figure of merit is maximized or minimized. A description of the two types of methodologies/tools is given in the sections below. However, some fundamentals about system modeling and optimization are given first.

2.1 Energy System Synthesis/Design Modeling and Optimization Fundamentals

2.1.1 Modeling of an Energy System

The modeling of an engineering system typically begins with the selection of a number of degrees of freedom represented by parameters which can be varied at will within acceptable limits. These independent parameters or variables, hereby represented by a vector $\vec{z}$, are then used to create two systems of equations to represent the model of the system, i.e.

$$\vec{H} = \begin{Bmatrix} \vec{h}_1(\vec{x},\vec{y},\vec{z}) \\ \vec{h}_2(\vec{x},\vec{y},\vec{z}) \\ \vec{h}_3(\vec{x},\vec{y},\vec{z}) \\ \vdots \\ \vec{h}_n(\vec{x},\vec{y},\vec{z}) \end{Bmatrix} = \vec{0} \quad ; \text{and } \vec{G} = \begin{Bmatrix} \vec{g}_1(\vec{x},\vec{y},\vec{z}) \\ \vec{g}_2(\vec{x},\vec{y},\vec{z}) \\ \vec{g}_3(\vec{x},\vec{y},\vec{z}) \\ \vdots \\ \vec{g}_n(\vec{x},\vec{y},\vec{z}) \end{Bmatrix} \le \vec{0} \tag{2.1}$$

Where the vectors $\vec{x}$ and $\vec{y}$ at the modeling level represent fixed parameters which, as will be seen in the next section, are the set of independent synthesis/design and operational/control decision variables at the optimization level. The latter necessarily incorporates the modeling level as a sub-level. The vector of equality constraints $\vec{H}$ is composed of sub-vectors $\vec{h}_i$ each of which mathematically describes a phenomenon usually within the realm of a particular discipline. The elements of the sub-vectors $\vec{h}_i$ are known as the *state* equations. For energy systems, a number of different disciplines are represented by $\vec{H}$, the most common being the thermal sciences, materials, controls, and

economics[4]. The vector of inequality constraints $\vec{G}$ represents natural or artificial limitations imposed upon the system.

Any arbitrary vector $\vec{z}$ may not satisfy the constraints imposed by equations (2.1). In this case, equations (2.1) act as system *evaluators*. A feasible solution is one that has a vector of independent variables that satisfies equations (2.1). The process of finding a vector that leads to a feasible solution is typically iterative. The speed of this process is oftentimes slow because in practical systems the size of $\vec{x}$ is large and the systems of equations (2.1) are highly non-linear. A system evaluator coupled to the iterative scheme just described is called a system *analyzer*.

The representation of the relevant phenomena is accomplished by means of the software implementation of the mathematical models of the system. For obvious practical reasons, different "codes" are developed with each representing a particular aspect of the system. Thus, it is common to talk about thermodynamic, sizing, CFD, or costing codes, although exceptions exist. Examples of the latter are codes that are capable of blending in a single analysis fluid mechanics, heat transfer, and stress analysis. In addition, for reasons having to do with company organization, codes for different types of technologies, multi-disciplinary or not, are disaggregated. It is, therefore, common to have an engine code, a structures code, and so on.

2.1.2 Nonlinear Constrained Optimization

Once a model or a set of models of the engineering system has been developed, the option to optimize subject to a set of constraints exists. It is the model or set of models of the system described in the previous section that form the set of nonlinear constraints used in the formulation of the optimization problem. This problem is expressed in general terms by

Minimize $f(\vec{x}, \vec{y}, \vec{z})$ (2.2)

[4] In this work, the thermal sciences and economics are used directly. Controls are implicitly involved in the synthesis/design whenever there is a need for adjusting certain parameters over time. However, they can be explicitly involved during synthesis/design through the direct incorporation of controllers (e.g. PID controllers) into the overall model of the system as is done in this research work. Physical limitations on the components or materials used are incorporated into the model by constraints.

with respect to $\vec{x}$ and $\vec{y}$ (the independent decision variables) and subject to the following equality and inequality constraints:

$$\vec{H}(\vec{x},\vec{y},\vec{z}) = \vec{0} \tag{2.2.1}$$

$$\vec{G}(\vec{x},\vec{y},\vec{z}) \le \vec{0} \tag{2.2.3}$$

Note that an inequality constraint $g_j \le 0$ is active if $g_j = 0$ and inactive if not. By definition all equality constraints are active. Also note that the independent variables at the modeling level, i.e. the vector $\vec{y}$, are dependant variables at the optimization level. The first order necessary and sufficiency conditions for a point to be a local and a global minimum, respectively, are called the Karush-Kuhn-Tucker or Kuhn-Tucker conditions. The conditions are stated in the following theorem:

The Lagrange Multiplier Theorem

Let $\vec{x}^*$, $\vec{y}^*$, and $\vec{z}^*$ be a local minimizer for problem (2.2). Then there exist vectors $\vec{\lambda}^*$ and $\vec{\mu}^*$ such that

$$\vec{\mu}^* \ge \vec{0} \tag{2.3}$$

$$\nabla f\left(\vec{x}^*,\vec{y}^*,\vec{z}^*\right) + \vec{\lambda}^{*T}\nabla\vec{H}\left(\vec{x}^*,\vec{y}^*,\vec{z}^*\right) + \vec{\mu}^{*T}\nabla\vec{G}\left(\vec{x},\vec{y}^*,\vec{z}^*\right) = \vec{0} \tag{2.4}$$

$$\vec{\mu}^{*T}\vec{G}\left(\vec{x},\vec{y}^*,\vec{z}^*\right) = \vec{0} \tag{2.5}$$

One normally refers to $\vec{\lambda}^*$ and $\vec{\mu}^*$ as the Lagrange multiplier vectors of equality and inequality constraints. In the literature, $\vec{\mu}^*$ is sometimes called the Karush-Kuhn-Tucker multipliers.

In addition to these first order necessary conditions for a local minimum, first order sufficiency conditions, which guarantee that the local minimizer $\vec{x}^*$ and $\vec{y}^*$ is a global minimizer, also exist. These additional conditions place certain restrictions of convexity or concavity on the objective function $f(\vec{x},\vec{y},\vec{z})$ and the equality and inequality functions $\vec{H}(\vec{x},\vec{y},\vec{z})$ and $\vec{G}(\vec{x},\vec{y},\vec{z})$, respectively. For a detailed discussion of these conditions and others, the reader is referred to Floudas (1995). All of the conditions

briefly outlined above lay the foundations of optimality for the nonlinear optimization (programming) problem, problem (2.2). In practice, these conditions, especially those for sufficiency, are oftentimes difficult if not *impossible* to meet. Thus, an effective search of the space of all possible solutions is fraught with the uncertainties of knowing where the global optimum or a set of near-global optimums lie.

2.1.3 Basic Formulations for Energy System Analysis and Optimization[5]

Consider the energy system of Figure 2.1, which is composed of two units[6] or two disciplines. In the above figure, the $\vec{g}_i$ (i=1,2) are the vectors representing the limits or constraints imposed upon the units or disciplines; and the r_i's are the residuals in the state equations. The vectors $\vec{u}_{12}$ and $\vec{u}_{21}$ are the coupling functions. The two unit or discipline analyzers may be executed in parallel if values are set for the coupling functions, say $\vec{u}_{12}^{o}$ and $\vec{u}_{21}^{o}$.

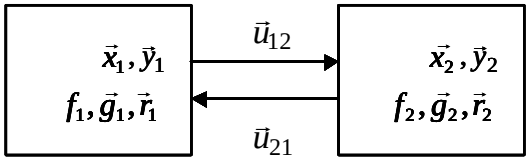

Figure 2.1. A simple energy system.

If one were now to optimize this system, it might be possible in some cases to define multiple objective functions which need be optimized simultaneously. The optimization is then carried out by assigning weights to each of them in order to obtain a unique objective. An area of mathematical optimization specializes in this type of multi-objective problems. In energy systems, one is oftentimes concerned with a single objective function (e.g., costs[7], thermodynamic efficiency, fuel consumption, specific

[5] In this section some of the terminology compiled by Balling and Sobieszczanski-Sobieski (1996) is used.
[6] A unit refers to either a component or a sub-system.
[7] For fuel cell systems, these costs include those traditionally associated with the manufacture and performance of each component as well as those associated with the impact of a component's size (volume) on system performance. Therefore, the goal of synthesis/design is not only one of minimizing the energy usage and capital costs of each sub-system/component but even more importantly, the indirect energy sub-system/component costs associated with the performance levels of the system itself.

fuel consumption, etc.). In this thesis work, the optimization problems are defined using a single objective function. The scalars f_1 and f_2 are the contributions of units or disciplines 1 and 2 to the overall objective function f. Other objectives (e.g., in the case of vehicle systems optimization, range, acceleration, etc.) are then cast as constraints. The optimization problem is, therefore, stated as minimizing $f = f_1 + f_2$.

A number of solution approaches to the above posed problem are possible depending on whether or not an analysis or a single- or multi-level optimization technique is applied. Before proceeding with a discussion of these, some additional observations are made.

2.1.4 Additional Comments

In mathematical optimization, the best system is the one that minimizes (or maximizes) an objective function. Let us assume that minimization of the total cost is the objective and that the optimization problem has a solution, i.e. a system has been determined that optimally satisfies the objective. Is this indeed the solution sought or must one also compare the performance of this system with the performance of other (non-optimal) systems based on other points of view, e.g., maintainability or environmental effects? There may be cases when such a comparison shows that the 'optimal' with respect to the cost of the system is not at all good when these other points of view are considered (attempts to translate other aspects into cost are made, but there may still be aspects that cannot be handled in this way). Multi-objective optimization is an attempt to correct such deficiencies. However, the solution then depends on subjective weighting factors or additional criteria. The point of all this is that the optimal solution may not be unique and is 'optimal' only in the strict mathematical sense. Thus, even if the synthesis/design procedure can be automated, expert human intervention is needed to evaluate the results and reach a final decision.

Another issue is the following. In the usual synthesis/design process of an energy system, the designer uses his knowledge and experience to select the type, configuration, and technical characteristics of a workable system (i.e. a system that is technically feasible and satisfies a given set of needs), which he then evaluates for its technical and

economic performance and for ways of improving it. If the system synthesis (type and configuration) is given, the decisions to be taken are of a rather quantitative nature. If, however, the synthesis is not given, in addition to quantitative decisions, there is need for many qualitative decisions, which may be non-deterministic. In such a case, innovation and creativity play a vital role. Given the multitude of energy system types and the variations in each type, one may question whether it is ever possible to replace the experienced designer's mental process with an algorithm consisting of a set of formulae and rules. On the other hand, in today's complex world, this same multitude of types and variations makes it rather impossible even for an experienced designer to evaluate all possible alternatives. Consequently, an automated procedure, if properly used, can be of invaluable help to the designer. Finally, the next section deals with the mathematical, algorithmic, and computational tools that are required to transform a set of synthesis/design requirements into a workable and eventually "best" or optimum energy system.

2.2 Energy System Synthesis/Design Analysis and Optimization Tools

2.2.1 Energy System Synthesis/Design Analysis Techniques

In Chapter 1, some well-known energy system analysis methodologies/tools were mentioned (e.g., pinch technology, exergy analysis, and expert systems). An explanation of each of these is given in the following sections.

2.2.1.1 Pinch Technology

The term "Pinch Technology" was introduced by Linnhoff and Vredeveld in 1982 to represent a new set of thermodynamically based methods that guarantee minimum energy levels in the design of heat exchanger networks. Over the last two decades, it has emerged as an unconventional development in process design and energy conservation. The term 'Pinch Analysis' is often used to represent the application of the tools and algorithms of Pinch Technology for studying industrial processes.

Pinch technology presents a simple methodology for systematically analyzing heat exchanger networks and the surrounding utility systems with the help of energy balances which provide the means for calculating the enthalpy changes (ΔH) in the streams passing through a heat exchanger. In addition, since energy in a heat interaction may only flow in the direction of hot to cold with out some type of work interaction, 'temperature crossovers' of the hot and cold stream profiles through the heat exchanger unit are prohibited. In practice, the hot stream can only be cooled to a temperature defined by the 'temperature approach' of the heat exchanger. The temperature approach is the minimum allowable temperature difference (ΔT_{min}) in the stream temperature profiles for the heat exchanger unit. The temperature level at which ΔT_{min} is observed in the process is referred to as "pinch point" or "pinch condition". The pinch defines the minimum driving force allowed in the heat exchanger unit.

A set of simple rules can be applied to guide the selection of a near optimum heat exchanger network. These rules simply stated are: do not transfer heat across the pinch, use a hot stream above the pinch and use a cold stream below the pinch. It has been claimed that pinch technology is a tool that can be used for process design (Linhoff, 1989), which indeed it can. However, based on the results of a challenge problem solved in the early 1990s (Linhoff and Alanis, 1991; Gaggioli et al., 1991), it would appear that exergy analysis as applied by an expert may be superior for that purpose, a fact which is not surprising since exergy analysis is based on both the 1st and 2nd Laws of thermodynamics and more complete as an overall analysis tool. An interesting (and spirited) comparison between pinch technology and exergy analysis is given by Sama (1995)

2.2.1.2 Exergy Analysis

Like pinch technology, exergy[8] analysis (e.g., Gaggioli et al., 1991) is a systematic but less structured way of analyzing alternative synthesis/design options for

[8] Exergy (some times refer as "availability" (Moran's book Availability Analysis) or "available energy" (Gyftopoulos and Beretta). The latter is in fact a broader and more general concept than that of "availability" or "exergy") is defined as the maximum theoretical useful work that could be obtained if a system were allowed to interact with a second idealized system called the *reference environment* (or "*dead state"*). Exergy is in fact a measure of the departure of the state of the system from that of the reference environment, i.e. it is the maximum potential for change or "departure from equilibrium" with the reference environment ("dead state").

energy systems and components. Though less structured than pinch technology or other 1st Law approaches, it does provide a more complete picture and a greater number of insights into the overall synthesis, design, and operational problem since it accounts both for the quantity and quality of all energy conversions present in a process. Furthermore, it is not primarily centered on heat exchange or mass exchange networks. It uses a set of common sense guidelines (e.g., Sama, 1995; Sama, Qian and Gaggioli, 1989) to detect and avoid or remove the so-called 2nd Law errors[9] in synthesis, design, and operation in order to guarantee a more cost-effective and/or better performing system. The objective of this type of analysis is the judicious expenditure of exergy[10] to reduce not just fuel costs but total costs. An incomplete list of "common sense guidelines", which would be used in an exergy analysis along with exergy balances of the system and each of its components and sub-systems, is the following:

- Do not use excessively large or excessively small thermodynamic driving forces in process operations.
- Minimize the mixing of streams with differences in temperature, pressure, or chemical composition.
- Do not discard energy at high temperatures to the ambient or to cooling water.
- Do not heat refrigerated streams with hot streams or with cooling water.
- When choosing streams for heat exchange, try to match streams where the final temperature of one is close to the initial temperature of the other.
- When exchanging heat between two streams, the exchange is more efficient if the flow heat capacities of the streams are similar. If there is a big difference between the two, consider splitting the stream with the larger heat capacity.
- Minimize the use of intermediate heat transfer fluids when exchanging heat between two streams.
- Heating (or refrigeration) is more valuable the further its temperature is from the ambient.

[9] It is somewhat misleading to simply call these 2nd Law errors since in fact, exergy and the concept of irreversibility and exergy destruction are based on both the 1st and 2nd Laws of thermodynamics (Gyftopolous and Beretta, 1991).
[10] The terms *exergy* combines the notions of the *quantity* of energy resulting from the 1st Law and the *quality* of energy resulting from the 2nd Law into a single entity which can be used to assess the real thermodynamic losses which occur within, to, and from a system.

- The economic optimum ΔT of a heat exchanger decreases as the temperature decreases and vice versa.
- Minimize the throttling of steam or other gases.
- The larger the mass flow, the larger the opportunity to save (or to waste) energy.
- Use simplified exergy (or availability or available energy) consumption calculations as a guide to process modifications.
- Some exergy inefficiencies cannot be avoided. Others can. Concentrate on those which can.

2.2.1.3 Expert Systems

Unlike the two systematic approaches just described, expert systems are not a type of analysis but a form of artificial intelligence (AI) which organizes and efficiently and quickly makes available the knowledge and experience of more than one person (Sciubba, 1998).

Expert Systems (ES) are based on *relational languages* that use the symbolism of formal propositional logic. They draw inferences from a number of *facts* stored in a particular database, properly called a *knowledge-base*. These facts can be synthesis/design data, synthesis/design rules, physical or logical constraints, etc. Each ES manipulates this knowledge in its own way, according to a logical procedure contained in its *inference engine*. AI and ES techniques are described and application examples presented in Frangopoulos, von Spakovsky, and Sciubba (2002).

Knowledge-based expert systems, or simply expert systems, use human knowledge to solve problems that normally would require human intelligence. These expert systems represent the expertise knowledge as data or rules within the computer. These rules and data can be called upon when needed to solve problems. Conventional computer programs perform tasks using conventional decision-making logic containing little knowledge other than the basic algorithm for solving that specific problem and the necessary boundary conditions. This program knowledge is often embedded as part of the programming code, so that as the knowledge changes, the program has to be changed and then rebuilt. Knowledge-based systems collect the small fragments of human know-how into a knowledge-base which is used to reason through a problem, using the knowledge

that is appropriate. A different problem, within the domain of the knowledge-base, can be solved using the same program without reprogramming. The ability of these systems to explain the reasoning process through back-traces and to handle levels of confidence and uncertainty provides an additional feature that conventional programming does not handle.

Most expert systems are developed via specialized software tools called shells. These shells come equipped with an inference mechanism (backward chaining, forward chaining, or both), and require knowledge to be entered according to a specified format. These shells qualify as languages, although certainly with a narrower range of application than most programming languages. For more detailed information on expert system shells, see the "Expert System Shells at Work" series by Schmuller (1991, 1992).

2.2.2 System Synthesis/Design Single-Level[11] Optimization Techniques

The single-level optimization techniques that can be employed to solve the problems posed above[12] depend on the type of optimization problem at hand. A general depiction of this problem for the synthesis/design optimization of energy systems is shown in Figure 2.2. Depending on its nature and level of complexity, such a problem can be classified in a number of ways (Rao, 1996), i.e.

- Classification Based on the Existence of Constraints: any optimization problem may be classified as constrained or unconstrained, depending on whether or not constraints exist in the problem.
- Classification Based on the Nature of the Decision (Independent) Variables: if the decision variables can be treated as parameters, the problem is classified as a static or parametric optimization problem. If, on the other hand, the decision variables are represented by functions, the problem is called a trajectory optimization problem.

[11] A "single-level" as opposed to "multi-level" technique refers to the fact that no *decomposition* is employed to break the optimization problem into a set of nearly equivalent smaller problems in order to facilitate the solution of the larger problem and overcome both the mathematical and cultural difficulties which exist with highly complex, highly dynamic problems (see *section 2.2.3*).

[12] This, of course, assumes that they are simple enough to be solved with a single-level approach which, in fact, they may not be (see Figure 2.2). If not, they could still be employed provided they were used in conjunction with a multi-level approach, i.e. with a *decomposition* technique (see *section 2.2.3*).

- Classification Based on the Nature of the Equations Involved: according to this classification, optimization problems can be linear, non-linear, geometric or quadratic programming problems. A problem is geometric if the objective function can be expressed as the sum of power terms (i.e. a polynomial). A quadratic problem is a non-linear programming problem with a quadratic objective function and linear constraints.
- Classification Based on the Permissible Values of the Independent Variables: depending on the values permitted for the decision variables, optimization problems can be classified as integer, real valued, or mixed integer programming problems.
- Classification Based on the Deterministic Nature of the Independent Variables: optimization problems can be classified as stochastic or deterministic programming problems.

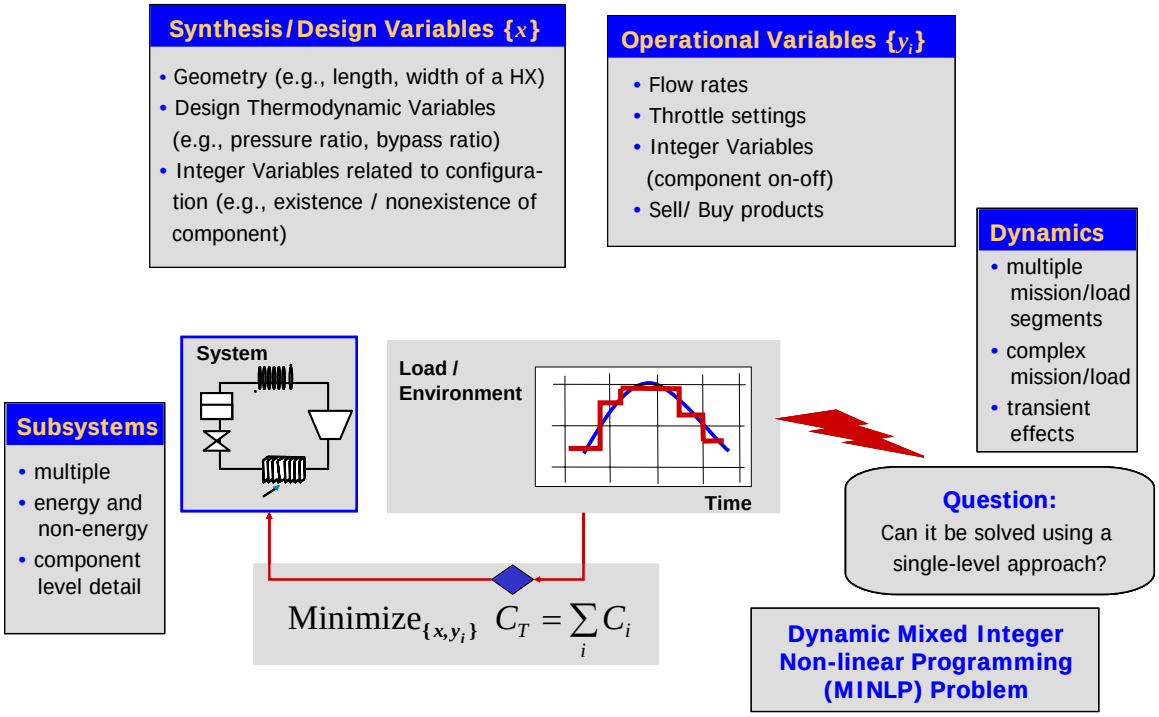

Figure 2.2. General depiction of the synthesis/design optimization problem for energy systems.

- Classification Based on the Separability of the Functions: optimization problems can be classified as separable or non-separable depending on whether the objective function or constraint functions can be written as the sum of n functions.

- Classification Based on the Number of Objective Functions: optimization problems can be classified as single and multi-objective programming problems.
- Classification Based on the Synthesis/Design Stage: Optimization problems can be addressed in different ways according to the synthesis/design stage. For early stages (Synthesis), the following approaches are primarily used. First, heuristics search, which are rules based on engineering experience and on physical concepts (e.g., exergy), are applied to generate feasible configurations, which are subsequently improved by applying a set of evolutionary rules in a systematic way (i.e., evolutionary search). These rules may come from special techniques, such as exergy analysis. Artificial Intelligence and Expert Systems have proven effective in generating appropriate configurations. Next, techniques are used to find optimum configurations, which attempt to reach pre-determined targets that have been identified by the application of physical rules. Principles from thermodynamics and other physical sciences are applied to obtain the targets for the optimal system configuration. These targets can correspond to upper or lower bounds on the best possible configuration and provide vital information for improvement of existing configurations. Attempts have been made to introduce economics at a second level, but the whole approach is mathematically non-rigorous and, consequently, the configuration obtained may be non-optimal. In addition, methods starting with a superstructure are also used (Olsommer, von Spakovsky, and Favrat (1999); Munoz and von Spakovsky (2000)). The final objective is to reduce this superstructure to the optimal configuration. A superstructure is considered with all the possible (or necessary) components and interconnections. An objective function is specified and the optimization problem is formulated. The solution of the optimization problem gives the optimal system configuration, which, inevitably, depends on (and is restricted by) the initial superstructure.

Many of the most difficult energy system synthesis/design optimization problems are single-objective, mixed integer, non-linear, deterministic optimization problems. The focus here is on techniques which can be used to solve these types of problems directly or indirectly in conjunction with some *decomposition* approaches (see *section 2.2.3* below).

These techniques will be broadly divided into two categories: gradient-based and non-gradient-based algorithms.

2.2.2.1 Gradient-Based Algorithms

The gradient-based algorithms of optimization are a class of search methods for real-valued functions. These methods use the gradient of a given function as well as function values. Although most energy system synthesis/design problems are constrained, it is useful to start with a general description of the methods for unconstrained problems. Thus, consider the unconstrained optimization problem

Minimize $f(\vec{x})$ (2.6)

w.r.t. $\vec{x}$

The resulting iterative algorithm is given by

$$\vec{x}^{k+1} = \vec{x}^{k} - \alpha^{k} \nabla f(\vec{x}^{k}) \tag{2.7}$$

where α is a sufficiently small step-size. The choice of the step-size α_k leads to a number of algorithms: the steepest descent method, Newton and quasi-Newton methods (e.g., the Fletcher and Powell and the BFGS methods), conjugate direction methods (e.g., the methods of Fletcher-Reeves, Polar-Ribiere, and Hestenes-Stiefel).

A number of gradient-based methods exist for solving non-linear programming problems such as the one given above. Optimization methods that handle the constraints explicitly are known as direct methods. Indirect methods attempt to find an optimum by solving a sequence of unconstrained problems. Examples of the latter are the Interior ands Exterior Penalty and the Augmented Lagrange Multiplier methods. Examples of direct methods are the Sequential Linear and Quadratic programming methods, the Method of Feasible Directions (MFD), the Generalized Reduced Gradient Method, and the Rosen Projection Method. Two of the most popular methods are briefly described below.

Method of Feasible Directions (MFD)

The iterative algorithm that results from this method begins by choosing a feasible starting point and moving to a better point according to the iterative formula

$$\vec{x}^{k+1} = \vec{x}^{k} + \alpha \cdot \vec{S}^{k} \tag{2.8}$$

where $\vec{x}^{k}$ is the starting point, $\vec{S}^{k}$ is the direction of movement, and α is the step length. The value of α is chosen so that $\vec{x}^{k+1}$ lies in the feasible region. The search direction $\vec{S}^{k}$ is found such that (1) a small move in that direction does not violate any constraint and (2) the value of the objective function decreases in that direction. A vector $\vec{S}$ is a usable feasible direction if (Chong and Zak, 1996)

$$\frac{d}{d\alpha} f(\vec{x}^{k} + \alpha \cdot \vec{S})\Big|_{\alpha=0} = \vec{S}^{T} \nabla f(\vec{x}^{k}) < 0 \tag{2.9}$$

$$\frac{d}{d\alpha} g_{j}(\vec{x}^{k} + \alpha \cdot \vec{S})\Big|_{\alpha=0} = \vec{S}^{T} \nabla g_{j}(\vec{x}^{k}) \leq 0 \tag{2.10}$$

In the Zoutendijk's implementation of the method, the usable feasible direction is taken as the negative of the gradient direction if the initial point of the iteration lies in the interior, i.e.

$$\vec{S}^{k} = \nabla f(\vec{x}^{k}) \tag{2.11}$$

Otherwise, equations (2.9) and (2.10) are used to find an adequate search direction.

Sequential Quadratic Programming (SQP)

The SQP method has a theoretical basis that is related to the solution of a set of nonlinear equations using Newton's method and the derivation of simultaneous nonlinear equations using the Kuhn-Tucker conditions, which form the Lagrangian of the constrained optimization problem. For a complete derivation of the method, see for example Rao (1996).

Algorithmically SQP is identical to equation (2.8) where the feasible search direction, $\vec{S}$, is found from solving the following quadratic problem, i.e. find the $\vec{S}$ which minimizes

$$Q(S) = \nabla f(x)^T S + \frac{1}{2} S^T [H] S \tag{2.12}$$

subject to

$$\beta_j g_j(\vec{x}) + \nabla g_j(\vec{x})^T \vec{S} \le 0 \tag{2.12.1}$$

$$\beta_j h_j(\vec{x}) + \nabla h_j(\vec{x})^T \vec{S} = 0 \tag{2.12.2}$$

where $[\vec{H}]$ is a positive definite matrix that is taken initially as the identity matrix and is updated in subsequent iterations so as to converge to the Hessian matrix of the Lagrangian of the original problem (2.6). The last two constraints are linearized by taking $\beta_j = 1$ if $g_j(\vec{x}) \le 0$ and $\beta_j = 0.9$ if $g_j(\vec{x}) > 0$. Problem (2.12) is then easily solved using a linear quadratic programming algorithm.

2.2.2.2 Non-gradient-Based Optimization Algorithms

Most practical energy system synthesis/design problems are characterized by mixed continuous and discrete variables and discontinuous and nonconvex synthesis/design surfaces. If standard nonlinear programming techniques such as the ones presented above are used exclusively for this type of problem, they may very likely be insufficient and in most cases find a relative optimum that is closest to the starting point (i.e. a local minimum or maximum). In addition to this, gradient-based methods cannot use discrete variables since gradients with respect to integer numbers are not defined.

A number of methods circumvent the above problems by means of specialized search schemes. These types of algorithms specialize in performing a complete search of the entire synthesis/design space and as a consequence are often referred to as global search algorithms[13]. Among these are rule-based expert systems (AI) and their more advanced implementations such as Tabu search and Hybrid expert systems. The latter are heuristic methods and have received considerable attention lately. However, the most popular and most developed methods for global search are Neural Networks, Simulated

[13] It should be noted that since such algorithms do not use Lagrange's method or some derivative thereof for finding a local or a global optimum, one cannot strictly speaking from a mathematical standpoint claim that one has found a Kuhn-Tucker point at the end of the search. On the other hand, this is not an issue here since the designer's primary concern is not in mathematical proofs but in improved syntheses/designs, and practice has shown that such methods can indeed find significant configurational, system, sub-system, and component improvements.

Annealing, connectivity matrix method, and Genetic Algorithms. Here a brief description of some of these methods is given.

Simulated Annealing (SA)

Simulated annealing (SA) is a very smart variant of the connectivity matrix method described next and, in spite of some limitations that are discussed below, is a very reliable process synthesizer. Though originally conceived as a multi-variable optimization tool, it was later adapted to function as a synthesis/design optimizer.

Simulated annealing was introduced by Metropolis et al. (1953) and is used to approximate the solution of very large combinatorial optimization problems (e.g., NP-hard problems). The technique originates from the theory of statistical mechanics and is based upon the analogy between the annealing of solids and solving optimization problems. Assuming that the objective is to find the configuration that minimizes a certain cost function E, the algorithm can then be formulated as follows. Starting off at an initial configuration, a sequence of iterations is generated. Each iteration consists of the random selection of a configuration from the neighborhood of the current configuration and the calculation of the corresponding change in a cost function ΔE. The neighborhood is defined by the choice of a generation mechanism, i.e. a ”prescription” to generate a transition from one configuration into another by a small perturbation. If the change in cost function is negative, the transition is unconditionally accepted; if the cost function increases, the transition is accepted with a probability based upon the Boltzmann distribution, namely,

$$P_{acc}(\Delta E) \approx \exp\left(-\frac{\Delta E}{kT}\right) \tag{2.13}$$

where k is a constant and the temperature T is a control parameter. This temperature is gradually lowered throughout the algorithm from a sufficiently high starting value (i.e. a temperature where almost every proposed transition, both positive and negative, is accepted) to a “freezing”' temperature, where no further changes occur. In practice, the temperature is decreased in stages, and at each stage the temperature is kept constant until thermal quasi-equilibrium is reached. All parameters which determine the temperature

decrease (the initial temperature, stop criterion, temperature decrease between successive stages, number of transitions for each temperature value) factor into what is called the cooling schedule.

Consequently the four key “ingredients” for the implementation of simulated annealing are: the definition of configurations, a generation mechanism, i.e. the definition of a neighborhood on the configuration space, the choice of a cost-function (i.e. objective function), and a cooling schedule.

The Connectivity Matrix Method

This method is a direct application of Graph Theory to process design. It consists of the following steps:

1. Create a logical process scheme, which entails the selection of the chemical/physical sub-processes that constitute the main process.
2. Construct the Connectivity Matrix (CM) for the logical process scheme. The rows of CM represent fluxes of matter or of energy, while the columns represent "operations" to be performed on these fluxes.
3. "Translate" each operation listed in CM into a series of physical transformations and devise one elementary sub-process scheme for each transformation.
4. Substitute into each transformation in every sub-process the component that performs it. Notice that at this point technical and operational constraints may come into play and limit or deny altogether the feasibility of a certain solution.
5. The resulting matrix is the Connectivity Matrix of the real process P. A proper quantitative simulation of P must now be performed to obtain the optimal set of operational parameters.

It is apparent that this method is a direct translation of the "mental scheme" a process engineer applies to a synthesis/design task, and it is entirely deterministic. Unfortunately, it is also clear that the method is strongly biased by the choices made in steps 1 and 3. Choosing a process scheme in fact sets a major structural constraint on the resulting process configuration, and this step is entirely left to the "experience" of the designer.

Genetic Algorithms (GAs)

Genetic Algorithms (GAs) are based on the principles of genetics and Darwin's theory of natural selection. The basic elements of natural genetics - crossover, mutation, and selection - are used in the genetic search procedure. Genetic algorithms were formally introduced in the United States in the 1970s by John Holland at the University of Michigan. The continuing price/performance improvement of computational systems has made them attractive for some types of optimization. In particular, genetic algorithms work very well on mixed (continuous and discrete), combinatorial problems. When properly conditioned, they are less susceptible to getting 'stuck' at local optima than gradient search methods. But they tend to be computationally expensive.

The algorithm is started with a set of solutions (represented by chromosomes) called a population. Solutions from one population are taken and used to form a new population. This is motivated by a hope that the new population will be better than the old one. Solutions which are selected to form new solutions (offspring) are selected according to their fitness - the more suitable they are the more chances they have of reproducing.

In Holland's original algorithm, GAs are characterized by bit string representations (chromosomes) of possible solutions to a given problem and by transformations used to vary those coded solutions. The algorithm is based on an elitist reproduction strategy where the individuals considered most fit are allowed to reproduce, thus, strengthening the chromosomal makeup of the new generation. Although many schemes to represent syntheses / designs as chromosome-like strings are possible (Hajela, 1999), the most popular is the use of binary quantities[14]. Thus, each synthesis/design variable is represented as strings of 0s and 1s, with the string length defining the desired precision. A number of such strings constitute a population of syntheses / designs. The recommended number of individuals in a population is in the range 2n to 4n where n is the number of independent variables (Rao, 1996)[15]. Each has a corresponding fitness

[14] Note, that depending on the application, other representations, e.g., floating point numbers, maybe more appropriate or useful than using a binary representation. An example of this is found in Olsommer, von Spakovsky, and Favrat (1999a).

[15] Note that this is not a hard and fast rule since in the work by Olsommer, von Spakovsky, and Favrat (1999a) and Muñoz and von Spakovsky (2001a,b), the authors have shown that even with a vary large number of degrees of freedom that the GA works best when the population is kept between 50 and 150 members.

value, F_v. The fitness value could be the objective function in a maximization problem (or its inverse in a minimization problem).

Once a chromosomal representation of the synthesis/design variables for a given population is available, the evolutionary mechanisms of selection, crossover and mutation are applied. One simplistic approach to selecting members of a population is to eliminate the individuals whose fitness value is below the average for the entire population. The selection proceeds by making copies of the fittest individuals so that the size of the new generation is equal to the original. The crossover process allows for an exchange of synthesis/design characteristics among members of a population. From the many ways in which crossover can be done (Goldberg, 1989), the most widely used approach is to randomly select two mating parents followed by a swap of binary numbers at a random position. Mutation safeguards[16] the search from a premature loss of information during reproduction and crossover. The fundamental idea is to choose a few members of the population using a probabilistic scheme and then switch a 0 to a 1 or vice-versa at a random place on the string. The GA then proceeds from generation to generation until no further improvements in the fitness function are achieved.

The three most important aspects of using genetic algorithms are: (1) definition of the objective function, (2) definition and implementation of the genetic representation, and (3) definition and implementation of the genetic operators. Once these three have been defined, the generic genetic algorithm should work fairly well. Beyond that many different variations to improve performance can be implemented, including niching (i.e. the ability to find multiple optima), improved selection and reproduction schemes, non-binary chromosomal representations, and parallelization of the algorithm.

Artificial Intelligence

In the preceding, it is tacitly assumed that *all* process synthesis/design calculations can be carried out by properly implemented automated routines. Process synthesis/design is a highly labor intensive and highly interdisciplinary task and is, therefore, by necessity performed by a team of specialists. As a consequence, it is also

[16] This is only true up to a point. Additional considerations such as the chromosomal representation as well as the methods of selection and crossover can have significant impacts on assuring that there is no significant loss of information too early in the search process (see Olsommer, von Spakovsky, and Favrat, 1999a).

very expensive in monetary terms; and there is a strong incentive to reduce this labor intensity (measured in man-hours). The only task that has as of yet not been fully automated is the *conceptual* one: the choice of the type and of the characteristics of the process itself. This automation can be implemented by a direct application of Artificial Intelligence (AI) techniques, whose specific task is to allow the codification of procedures that somehow mimic the thinking patterns of the human mind. Artificial Intelligence is defined as the part of computer science that investigates symbolic, non-algorithmic reasoning processes, and the representation of symbolic knowledge for use in machine inference (Sciubba, 19998). Currently, only a subset of these techniques, called Expert Systems (ES), has been successfully applied to system optimization. As discussed before, ESs can be used to reproduce the engineer's decisional path that proceeds from the synthesis/design data and constraints to possible process configurations.

Despite the fact that the mechanisms of brains are very different in detail from those of computers, they may, nonetheless, be doing similar sorts of things (storing, transforming, using information). This has led to the investigation of neural networks partly inspired by ideas about how the brain works. Some artificial neural networks have developed entirely as practical solutions to engineering problems without much concern for the accurate modeling of brain mechanisms. More recent work attempts to move towards more and more accurate models of real neurons, which are incredibly complex and varied.

Another recent development related to AI is the work on simulated evolution, which is based on biological theories of evolutionary processes. By modeling these on computers, it turns out that it is possible to evolve solutions to problems that we were previously unable to find. Genetic algorithms (GAs) are increasingly being used both as research tools and as a means of using computers to solve practical problems. Genetic Programming (GP) extends these ideas by using structures which are better suited to the problem than those used by GAs. For instance, a GP system may directly manipulate tree-like structures representing rules or computer programs. This work links up with studies in Artificial Life (Alife), which is concerned with simulated evolution of various kinds of artificial organisms, possibly competing or collaborating with one another.

Evolutionary techniques may use AI in the systems they evolve. Similarly AI systems may use evolutionary techniques to help with some of the harder problem solving tasks.

2.2.3 System Synthesis/Design Multi-Level Optimization Techniques

The use of the gradient and non-gradient based optimization techniques outlined above to solve the synthesis/design optimization problem in a single-level approach assumes that the problem is simple enough to be solved in this way. It may, in fact, not be. If not, these techniques can still be employed provided they are used in conjunction with a multi-level approach, i.e. with some *decomposition* technique(s) (e.g., Frangopoulos, von Spakovsky, and Sciubba, 2002). *Decomposition* is employed to break the optimization problem into a set of nearly equivalent smaller problems in order to facilitate the solution of the larger problem and overcome both the mathematical and cultural difficulties, which exist with highly complex, highly dynamic systems. Thus, *decomposition* can make an intractable, highly complex, highly dynamic problem with a large number of degrees of freedom tractable. *Decomposition* may also be warranted when certain software, hardware, company, and geographical boundaries (e.g., design teams located far from each other) do not permit solution of the original problem as a single-level problem.

Conceptually, decomposition can be viewed as an interface between a designer's models, simulators and/or analyzers and the optimization algorithms (i.e. gradient and non-gradient based) to which they would be coupled (see Figure 2.3). This defines a multi-level approach which contrasts with the traditional single-level approach in which the interface is absent. Four principal types of decomposition define such a multi-level approach: *disciplinary*, *conceptual*, *time*, and *physical*. The first of these, *disciplinary decomposition*, decouples, for example, a problem's thermodynamics and economics (e.g., the costs associated with the manufacture, weight, and volume of components) and optimizes each discipline independently (e.g., El-Sayed, 1989; Zimering, Burnes, Rowe, 1999). *Physical decomposition* decomposes the system across unit (component or sub-system) boundaries (e.g., Muñoz and von Spakovsky, 2001a,b, 2002; Georgopoulos, von Spakovsky, and Muñoz 2002; Rancruel and von Spakovsky, 2003; El-Sayed, 1989). For dynamic problems, it is also possible to divide the independent variables into

synthesis/design variables (those which remain constant over time) and control or *operational* variables (those that can be varied in time). This breakdown is called *conceptual decomposition* (Frangopoulos, 1990; Olsommer, von Spakovsky, Favrat, 1999; Muñoz and von Spakovsky, 2001a,b, 2002; Georgopoulos, von Spakovsky, and Muñoz 2002; Rancruel and von Spakovsky, 2003; El-Sayed, 1989). Finally, one additional form of decomposition, called *time decomposition* (e.g., Frangopoulos, 1990; Olsommer, von Spakovsky, Favrat, 1999; Muñoz and von Spakovsky, 2001a,b, 2002; Georgopoulos, von Spakovsky, and Muñoz 2002; Rancruel and von Spakovsky, 2003; El-Sayed, 1989), decomposes or transforms a dynamic problem into a quasi-stationary one consisting of a series of stationary time segments.

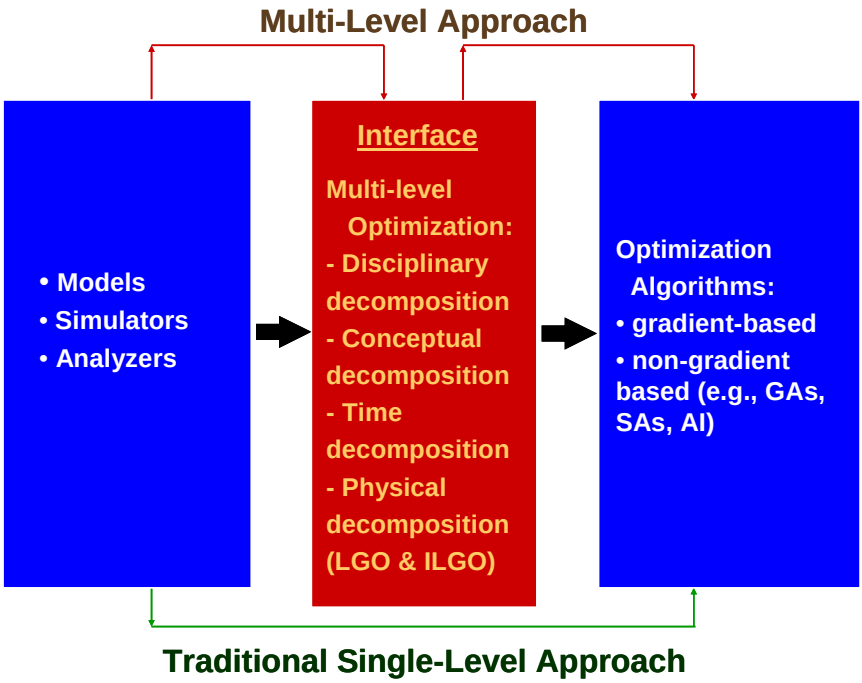

Figure 2.3. A conceptual view of decomposition.

In this work, only physical decomposition is used to solve the dynamic SOFC based APU system synthesis/design optimization problem. A brief description of each of the four types of decomposition is given in the following sections.

2.2.3.1 Disciplinary Decomposition

The decision variables in energy system synthesis/design may be broken down into purely thermo-physical and transport variables (discipline: thermodynamics) and others which are purely geometrical (discipline: economics). Examples of the former are component adiabatic efficiencies, pressures, temperatures, and flow rates. Examples of the latter are the physical dimensions of a heat exchanger, the number of blades in a turbine, the technology level of the component (including the choice of material), etc.

With the above considerations in mind, it is possible to define a two-level optimization problem. At the highest level the problem would be one of minimizing the amount of fuel required to perform a given task. Typically the thermo-physical and transport variables are chosen by the high-level optimizer. These values are set as boundary parameters for each of the units in the system. The material (cost or weight) used in each component is then minimized using the geometric parameters as the synthesis/design variables. The latter set of low-level problems uses geometry, technology, and material choices as decision variables. The low level problem is nested within the high-level problem.

2.2.3.2 Conceptual Decomposition

With conceptual decomposition the conceptual aspects of the optimization problem, i.e. synthesis, design, and operation, are broken into two or three levels of optimization: i) *synthesis*, implying the set of components appearing in a system and their interconnections; ii) *design*, implying the technical specifications of the components and the properties of substances flowing throughout the system at the nominal load; and iii) *operation*, implying the operating properties of components and substances under specified conditions. An iterative procedure is used to move back and forth between the three levels of optimizaton, terminating once the global optimum[17] for the objective

[17] See footnotes 2 and 13 above.

function has been found. This type of decomposition results in a set of nested optimization problems simpler than the original but much more computationally intensive (Olsommer, von Spakovsky, and Favrat, 1999a; Frangopoulos, 1990). To avoid this type of nesting, an approach used by Muñoz and von Spakovsky (2001a,b, 2002) completely separates the synthesis/design level(s) from the operational level, optimizing for the most stringent of the load/environmental conditions and a set of optimum and near-optimum feasible solutions determined for the given synthesis/design point. The overall computational burden is significantly reduced by the fact that only a limited number of feasible solutions need be optimally evaluated at off-design

2.2.3.3 Time Decomposition

The next type of decomposition is time decomposition, which decomposes the operational optimization problem into a series of quasi-stationary sub-problems each of which correspond to a given time interval. These can be optimized individually with respect to a set of unique operational/control variables and the results summed over all intervals. This form of decomposition complements the others.

2.2.3.4 Physical Decomposition

The final type of decomposition is physical decomposition, which looks at the system itself and breaks it down into a set of units (sub-systems, components, or sub-components), each of which forms a sub-problem within the context of the overall system optimization problem. The majority of these approaches within the literature can be classified as Local-Global Optimization (LGO). An exception is the approach developed by Muñoz and von Spakovsky (2001a,b; 2002). This approach called Iterative Local-Global Optimization (ILGO) is the only one in the literature, which due to its unique features, successfully leads, for highly complex, highly dynamic systems, to what in the thermoeconomic literature is called a close approach to "thermoeconomic isolation" (Frangopoulos and Evans, 1984; von Spakovsky and Evans, 1993). The latter is defined as the ability to optimize independently each unit of a system and yet still arrive at the

optimum for the system as a whole. The term "isolation" does not refer here to the individual optimization of a system component resulting from the optimization of the system as a whole. It is the opposite process of isolating components, optimizing their design, and then letting them interact in a system with the result that the system behaves optimally as well. A more complete discussion of "thermoeconomic isolation" is given in Chapter 3, Section 3.4.

In both LGO and ILGO, it is assumed that a number of disjoint sub-sets of the set of synthesis/design decision variables (one set for each unit[18]) can be established. Each set at the unit-level is used to optimize its respective sub-problem while the system-level set[19] in LGO is used to optimize the overall problem at the system-level. For LGO, this results in a nested set of optimizations of unit-level problems within an overall system-level problem. In ILGO, there is no nesting due to the fact that these system level decision variables are replaced by coupling functions and a set of shadow prices (see the discussions in Chapter 3) which are then used to incorporate system-level information directly at the unit level, eliminating in the process the necessity of having to optimize explicitly at the system level.

Finally, the technique of physical decomposition (ILGO in particular) has the advantage of breaking the overall optimization problem into a set of much smaller, unit sub-problems, which can simplify a highly complex, non-linear problem of synthesis/design optimization and allow one to take into account a larger number of decision variables (degrees of freedom) than would otherwise be possible. Physical decomposition makes it possible to simultaneously optimize not only at a system level, i.e. with respect to the system's performance and configuration, but also at a detailed component/sub-system level, i.e. with respect to the detailed geometry of the components themselves.

[18] Those decision variables which cannot be placed in a disjoint sub-set are by default system-level variables and must, thus, be considered at the system level.
[19] See footnote 14.

2.2.4 Control Systems Architecture and Design

2.2.4.1 Feedback Control

A control system is an interconnection of components forming a system configuration that will provide a desired response. The basis for analysis of a system is provided by linear systems theory, which assumes a cause-effect relationship for the components of a system. The input-output relationship represents the cause-effect of a process, which in turn represents the processing of the input signal to provide an output signal variable. All control systems consist of the same basic structure and the same basic components (Mutambara, 1999):

- Process: The dynamic system whose output is to be controlled. Usually, a mathematical model is required in order to understand and control the system.
- Actuator: A device used to physically influence the process.
- Controller: The algorithm that takes an input signal and generates the control signal required to drive the actuator.
- Sensor: A device that measures the actual system output and produces the measured output.
- Desired Output: The desired value of the output of the process being controlled.
- Actual Output: The actual state of the process that is to be controlled
- Comparator: Generates an error signal by comparing the actual output to the desired output.

Figures 2.4 and 2.5 show the two general control system categories. The open-loop control system utilizes the controller and actuator to obtain the desired response without using the measurement of the actual system response. Thus, the objective of an open-loop control system is to achieve the desired output by utilizing the actuating device to control the system directly without the use of feedback. In particular, open-loop control is sufficient when the system inputs and outputs are known with total certainty, and the mathematical model is perfect, and there are no external disturbances. Despite the obvious disadvantages of open-loop control, they are very convenient to use when obtaining the output measurement is either difficult or not economically feasible.

In order to address the apparent disadvantage of using an open-loop control system a closed-loop (feedback) control configuration can be applied. The closed-loop control utilizes a measure of the actual output to compare it with the desired output response (reference or command input). The measure of the output is called the feedback signal. The difference between the two quantities (the error signal) is then used to drive the output closer to the reference input through the controller and actuator. The elements of a general closed-loop control configuration are shown in Figure 2.5.

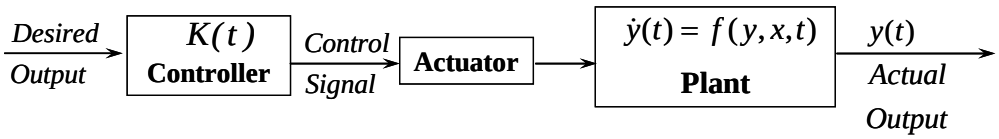

Figure 2.4. Elements of an open-loop control system.

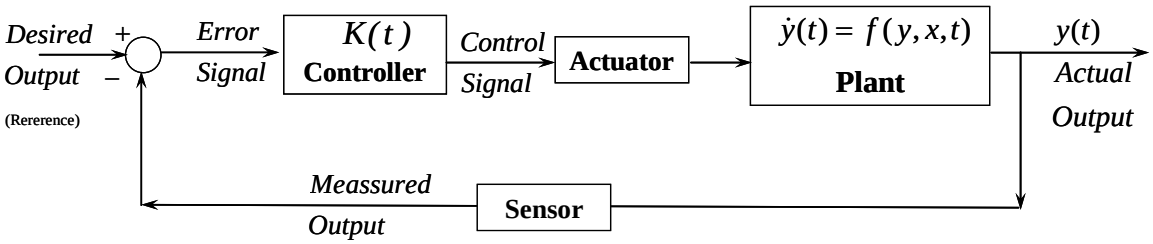

Figure 2.5. Elements of a closed-loop control system.

The introduction of feedback enables the engineer to control the desired output in order to improve accuracy. However, it requires that special attention to the issue of te stability of the response be taken (Mutambara, 1999). The feedback system is the basis of control system analysis and design. The following are the advantages of introducing feedback control:

- Faster response to an input signal
- Effective disturbance rejection
- Better tracking of reference signal
- Low sensitivity to system parameter error
- Low sensitivity to changes in calibration error
- More accurate control under disturbances and internal variations

- Effective and flexible control tuning by varying control gains
- Used to stabilize systems that are inherently unstable in the open-loop form

In the following sections a summary of modern feedback control techniques is presented

2.2.4.2 Proportional Integral Derivative (PID)Controller

In order to better explain the feedback control application the closed-loop control, the architecture shown in Figure 2.5 is simplify in Figure 2.6. The control problem is then defined as in Equation 2.14. This equation represents the dynamic governing equation for any given dynamic system. This equation is referred to in the literature as the system dynamics, the system realization, or the system state space (Bequette, 2003).

$$\dot{y}(t) = f\left(y, t, w\right) = Ay + Bw \tag{2.14}$$

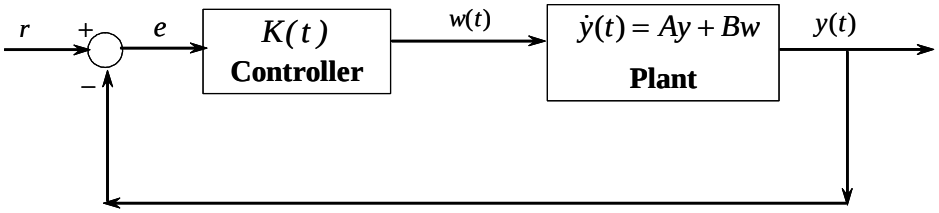

Figure 2.6. Closed-loop (Feedback) control system.

where A and B represent the system characteristics, t is time, y is the state variable, and w is the control variable.

From Figure 2.6 it follows that

$$e(t) = r - y(t) \tag{2.15}$$

$$w(t) = e(t)K(t) \tag{2.16}$$

$$\dot{y}(t) = Ay(t) + Be(t)K \tag{2.17}$$

The following is a brief description of the standard PID control algorithm used in most controllers. The first element of PID control to be developed is the proportional control. This means the controller output is the error times a constant.

$$w(t) = e(t)K_1 \tag{2.18}$$

Note that the action may be either direct or reverse. In a direct acting control loop, an increase in the process measurement causes an increase in the output to the final control element. Some control systems (such as Foxboro products) use proportional band rather than gain. The proportional band and the gain are related by

$$Gain = \frac{100\%}{\text{Proportional Band}} = \frac{\text{Output Change}}{\text{Input Change}} \tag{2.19}$$

where gain is the ratio of the change in the output to the change in the input, and proportional band is the amount the input would have to change in order to cause the output to move from 0 to 100% (or vice versa). With proportional only control, the controller will not bring the process measurement to the set-point without a manual reset. The proof of this results from combining equation 2.15 to 2.17 and considering that at steady state $\dot{y} = 0$. Then,

$$y = \frac{-BK_1}{A - BK_1} r \tag{2.20}$$

And as $t \to \infty, y \to r$ which implies $A = 0$. Obviously the *A* is not equal to zero since it is a vector or matrix of parameters depending on the system physics. As a result, there will always be an offset between the desired output and the measured output. In other words, if *K(t)* is a constant, as soon as the error approaches zero, the input signal becomes weak, thus, producing a reduction in the state variable, *y*, which in turn increases the steady state error. The offset occurs because the controller output (process input) and the process outputs come to equilibrium values before the error reaches zero.

Rather than to require that the operator "manually reset" the control loop whenever there is a load change, control functions are developed to "automatically reset" the controller. This "automatic reset" is also known simply as "integral" control. The equations for the proportional integral (PI) control and the control output are

$$K(t) = K_1 + \frac{K_2}{e(t)} \int_t e(t)dt \tag{2.21}$$

$$w(t) = e(t)K(t) = e(t)K_1 + K_2 \int_t e(t)dt \tag{2.22}$$

The proof of the PI controller ability to take the error to zero is a follows: at steady state $\dot{y}(t) = 0$ and from equation 2.17 and 2.22,

$$Ay - BK_1 y + BK_1 r + K_2 \int_t (r)dt - K_2 \int_t (y)dt = 0 \tag{2.23a}$$

Now, taking the derivative of equation 2.23a yields

$$A\dot{y} - BK_1 \dot{y} + 0 + K_2 r - K_2 y = 0 \tag{2.23b}$$

Which results in $r = y$ and of course, $e = 0$.

The next level of controller complexity is to add a term that accounts for the current rate of change of the error (error derivative). This allows the controller to "predict" what the direction of the error is and compensate for it. The time domain representation of a PID controller and the controller output are as follow:

$$K(t) = K_1 + \frac{K_2}{e(t)} \int_t e(t)dt + \frac{K_3}{e(t)} \frac{de(t)}{dt} \tag{2.24}$$

$$w(t) = e(t)K(t) = e(t)K_1 + K_2 \int_t e(t)dt + K_3 \frac{de(t)}{dt} \tag{2.25}$$

The derivative term in a PID controller speeds up the convergence at the beginning of the process when the error and its derivative are large and reduces its effects as the system approaches steady state. Additionally, it speeds up the system response to external disturbances, e.g., changes in the environment. A complete explanation of PID controller design, analysis, tuning, and optimization is given in Bequette (2003). Since PID control is the most widely used control approach because of its simplicity and adaptability to almost any type of system, the question arises whether the control can be approached in a different way? The answer to that question is not absolute. There may exist other general forms (architectures) for control systems (Bequette, 2003). However, the integral term should always remain for zero steady state error. Additionally, deep analysis of the newly proposed control forms yield that these are just variations of the

PID controller, which have been adjusted for specific applications. In general, the control design technique consists of how to compute and schedule the controller gains (K_1, K_2, K_3) for optimality and robustness. This is called tuning.

Proportional Integral Derivative (PID) control is what control process designers use for plant control because the process level of complexity is very high, the operational conditions fluctuate over wide ranges, and the external and internal disturbances are impossible to prevent or predict. The biggest disadvantage of PID control is that it is a single-input, single-output (SISO) architecture. This mean a controller can only control a state variable based on a single control variable. Obviously, the system at hand, the SOFC based APU with which this research deals, is not a SISO process because there is a high level of coupling among the various state variables. Fortunately, there are a number of techniques to decouple the process, e.g., relative gain array, RGA, (Bequette, 2003), and consider the control system as a sequence of SISO problems. These techniques have been applied to this research work successfully.

Finally, although there do exist modern control architectures other than SISO and decoupling that allow one to consider multi-input, multi-output systems, they present serious applicability problems when dealing with a system as complex as the SOFC based APU considered here. These difficulties will be clarified in the next sections.

2.2.4.3 Internal Model Control (IMC)

Internal model control (IMC) is a model based procedure, where a process model is “imbedded” in the controller. By explicitly using process knowledge and by virtue of the process model, improved performance can be obtained. Consider the IMC structure show in figure 2.7. The distinguishing characteristic of this structure is the process model which is run in parallel with the actual process sharing the same control variable input. The difference between the plant output and the model output is compared to the reference point in order to generate the controller input.

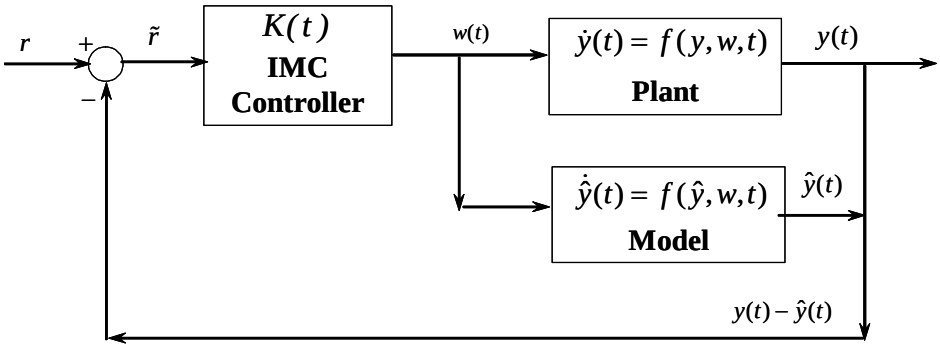

Figure 2.7. Internal model control structure.

The main advantage of IMC is that it provides a transparent framework for control system design and tuning as proposed by Bequette (2003). The IMC control can be formulated as a standard feedback control. For many processes, this procedure will result in a PID controller (some times cascaded with a filter). This is pleasing because the designer can use standard algorithms and equipment to implement an “advanced” control concept. The main disadvantage of IMC over standard feedback control is that it does not handle integrating or open-loop unstable systems (Bequette, 2003). Moreover, the practical implementation of IMC is based in the existence of “accurate” models capable of running in real time in order to predict the process behavior for a given input. However, due to increasing system complexity, external disturbances, internal parameter changes over time, and the wide range of operational conditions, these types of real-time models are very difficult to realize. A procedure based on IMC has been developed to form a standard feedback control system that can handle open-loop unstable systems (called IMC based PID). However, model complexity versus accuracy remains an important issue.

Finally, the applicability of IMC to fuel cells systems is constrained among other things by the fact that the natural gain of the stack experiences a change in sign as the current density increases (i.e. the power versus current density curve experiences a maximum). The exact point sign change is very difficult to predict with a model for a given operational condition due to material aging and other factors.

2.2.4.4 Multi-variable Control

PID controller can only handle SISO processes. However many industrial processes are multivariable, that is, they have multiple control variables (*w*) and multiple measurements (*y*). There are many approaches to the control of such systems, and the theoretical basis for the analysis and synthesis of these systems has been well developed (Balchen and Mumme, 1998). Figure 2.8 shows the general structure of a multivariable control. Notice that the feedback structure remains. However, the set of control variables, state variables, and reference points are not single values any longer. Instead, they become vectors. In fact, the controller is made up of a set of controllers, each one of which takes global information in order to regulate a particular control variable.

Theoretically, the multivariable control structure (Balchen and Mumme, 1998) is capable of controlling the system in a more effective manner that multiple SISO controllers. This due to the fact that it takes into account the tight coupling between state variables and how a single control variable can affect in a different manner several state variables. Furthermore, multivariable control in fact uses elements of IMC theory. Thus, the controller structure design is a function of the process transfer function (mathematical dynamic model).

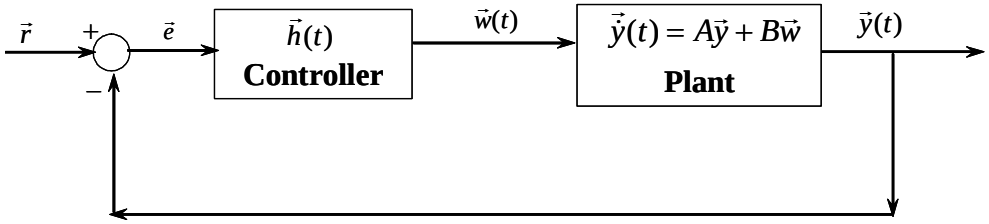

Figure 2.8. Multi-variable control structure.

Multivariable control techniques solve issues of complex specification and modeling errors elegantly but the complexity of the underlying mathematics is much higher than presented in traditional single-input, single-output control courses. The advantages of using multivariable control are evident, since it captures the system-level interactions and uses this information to better control the system at hand. Nonetheless, as is the case for all modern control techniques, its practical applicability is restricted due

to several reasons. First, the multivariable control concept needs the system model to be a set of linear differential equations with time invariant parameters. This is not the case when dealing with processes such as those found in fuel cell systems. A fuel cell system mathematical model includes a set of algebraic, non-linear partial, differential equations with time variant phenomena (e.g. chemical kinetics and equilibrium, electrochemical reactions, gas compression and expansion, heat transfer devices, etc.). Secondly, as for IMC, the controller quality depends on the model accuracy. Traditionally, linearization around a particular operational point and spatial discretization are used in order to apply multivariable control. However, this only aggravates the model accuracy issue. Consequently, multivariable control has so far been restricted to applications in relatively non-complex systems, for which the dynamics is well known and the level of coupling with other systems or components is restricted (e.g. robotic arms, tank level control, etc). Thus, at this point, their applicability to process control is a matter of research.

2.2.4.5 Model Predictive Control (MPC)

Model Predictive Control (MPC) refers to a class of algorithms that compute a sequence of manipulated variable adjustments in order to optimize the future behavior of a plant. Originally developed to meet the specialized control needs of power plants and petroleum refineries, MPC technology can now be found in a wide variety of application areas including chemicals, food processing, automotive, aerospace, metallurgy, and pulp and paper. Several authors have published excellent reviews of MPC theoretical issues, including Balchen and Mumme (1998).

The development of modern control concepts can be traced to the work of Kalman in the early 1960's, who sought to determine when a linear control system can be said to be optimal. Kalman studied a Linear Quadratic Regulator (LQR) designed to minimize a quadratic objective function. The process to be controlled can be described by a discrete-time, deterministic linear state-space model such as

$$\vec{y}_{k+1} = A\vec{y}_k + B\vec{w}_k \tag{2.26}$$

The vector $\vec{w}$ represents process inputs or manipulated variables; the vector y represents process states. The state vector is defined such that knowing its value at time k

and future inputs allows one to predict how the plant will evolve for all future times. Much of the power of Kalman's work relies on the fact that this general process model (equation 2.26) was used. The objective function (J to be minimized penalizes squared input and state deviations from the origin and includes separate state and input weight matrices Q and R to allow for tuning trade-off, i.e.

$$J = \sum_{j=1}^{\infty} \left(\left\| \vec{y}_{k+1} \right\|_Q^2 + \left\| \vec{w}_{k+1} \right\|_R^2 \right) \tag{2.27}$$

where the norm terms in the objective function are defined as follow:

$$\left\| \vec{y} \right\|_Q^2 = \vec{y}^T \vec{\vec{Q}} \vec{y} \tag{2.28a}$$

$$\left\| \vec{w} \right\|_R^2 = \vec{w}^T \vec{\vec{R}} \vec{w} \tag{2.28b}$$

Implicit in the representation is the assumption that all variables are written in terms of deviations from a desired steady-state. The solution to the LQR problem was shown to be a proportional controller, with a gain matrix K computed from the solution of a matrix Ricatti equation, namely,

$$w_k = -K y_k \tag{2.29}$$

The infinite prediction horizon of the LQR algorithm endowed the algorithm with powerful stabilizing properties. It was shown to be stabilizing for any reasonable linear plant (stabilizable and detectable) as long as the objective function weight matrices Q and R are positive definite. A dual theory was developed to estimate plant states from noisy input and output measurements, using what is now known as a *Kalman Filter*. The combined LQR controller and Kalman filter is called a Linear Quadratic Gaussian (LQG) controller. Constraints on the process inputs, states, and outputs were not considered in the development of LQG theory. Although LQG theory provides an elegant and powerful solution to the problem of controlling an unconstrained linear plant, it had little impact on

control technology development in the process industries. The most significant of the reasons cited for this failure include the existence of

- constraints
- process nonlinearities
- model uncertainties (robustness)
- unique performance criteria
- cultural reasons (people, education, etc.)

It is well known that the economic operating point of a typical process unit often lies at the intersection of constraints. A successful industrial controller must, therefore, maintain the system as close as possible to constraints without violating them. In addition, process units are typically complex, nonlinear, constrained, multivariable systems whose dynamic behavior changes with time due to such effects as changes in operating conditions and material aging. Process units are also quite individual so that the development of process models from fundamental physics and chemistry is difficult to justify economically. Indeed, the application areas where LQG theory has had a more immediate impact, such as in the aerospace industry, are characterized by physical systems for which it is technically and economically feasible to develop accurate fundamental models. Process units may also have unique performance criteria that are difficult to express in the LQG framework, requiring time-dependent output weights or additional logic to delineate different operating modes. However, the most significant reasons that LQG theory has failed to have a strong impact may be more related to the culture of the industrial process control community in which instrument technicians and control engineers either have had no exposure to LQG concepts or regard them as impractical.

This environment has led to the development *in industry* of a more flexible model based control methodology in which the dynamic optimization problem is solved on-line at each control execution. Process inputs are computed so as to optimize future plant behavior over a time interval known as the *prediction horizon*. In the general case, any desired objective function can be used. Plant dynamics are described by an explicit process *model* which can take, in principle, any required mathematical form. Process

input and output constraints are included directly in the problem formulation so that future constraint violations are anticipated and prevented. The first input of the optimal input sequence is injected into the plant and the problem is solved again at the next time interval using updated process measurements. In addition to developing more flexible control technology, new process identification technology was developed to allow quick estimation of empirical dynamic models from test data, substantially reducing the cost of model development. This new methodology for industrial process modeling and control is what is now referred to as Model Predictive Control (MPC) technology.

In modern process plants, the MPC controller is part of a multi-level hierarchy of control functions. At the top of the structure, a plant-wide optimizer determines optimal steady-state settings for each unit in the plant. These may be sent to local optimizers at each unit which run more frequently or consider a more detailed unit model than is possible at the plant-wide level. The unit optimizer computes an optimal economic steady-state and passes this to the dynamic constraint control system for implementation. The dynamic constraint control must move the plant from one constrained steady state to another while minimizing constraint violations along the way. In the conventional structure, this is accomplished by using a combination of PID algorithms, Lead-Lag (L/L) blocks, and High/Low select logic.

Nonlinear MPC

MPC, which uses nonlinear models, is likely to become more and more common as users demand higher performance and new software tools make nonlinear models more readily available. Developing adequate nonlinear, real-time, empirical models may, however, be very challenging. Also, there is no model form that is clearly suitable to represent general nonlinear processes. Froisy (1995) points out that second order Volterra models may bridge the gap between linear empirical models and nonlinear fundamental models in the near future. Nonetheless, nonlinear empirical models such as Volterra series or neural networks do not seem to extrapolate well.

An alternative approach would be to use first-principles models developed from well known mass, momentum, and energy conservation laws. However, the cost of developing a reasonably accurate first-principles model is likely to be prohibitive until

new software tools and validation procedures become available. Hybrid models that integrate steady state nonlinear first-principles models with dynamic empirical models (linear or nonlinear) may prove most promising for the near future. Gain-scheduling with linear dynamic models is an example of this approach. However, real-time execution remains an issue. Industrial MPC controllers rely solely on brute-force simulation to evaluate the effects of model mismatch. However, robust stability guarantees would significantly reduce the time required to tune and test industrial MPC algorithms. Furthermore, it is likely that the powerful theoretical results recently presented for MPC with a perfect model will be extended to include model mismatch in the near future. New robust stability guarantees will then be combined with uncertainty estimates from identification software to greatly simplify design and tuning of MPC controllers.

However, from a theoretical point of view, using a first principles nonlinear model changes the control problem from a convex quadratic programming (QP) problem to a non-convex non-linear program (NLP), the solution of which is much more difficult. There is no guarantee, for example, that the global optimum can be found. Bequette (2003) describes several approaches to solving the general nonlinear MPC problem in his review of nonlinear control for chemical processes. Although solving the nonlinear MPC problem at each time step is much more difficult, Rawlings et al. (2001) have shown that the nominal Lyapunov stability argument presented for linear models carries over to the general nonlinear case with minor modifications. The most important change is that a constraint must be included to zero the states at the end of the input horizon. They point out, however, that nonlinear MPC may require unexpected input adjustments. They present an interesting example in which a simple nonlinearity in the process model leads to a discontinuous feedback control law. This implies that tuning nonlinear MPC controllers may be very difficult, particularly for the case of model mismatch.

An important observation is that industrial MPC controllers almost always use empirical dynamic models identified from test data. The impact of identification theory on process modeling is perhaps comparable to the impact of optimal control theory on model predictive control. It is probably safe to say that MPC practice is one of the largest application areas of system identification. The current success of MPC technology may be due to carefully designed plant tests. Another observation is that process identification

and control design are clearly separated in current MPC technology. Efforts towards integrating identification and control design may bring significant benefits to industrial practice. For example, uncertainty estimates from process identification could be used more directly in robust control design. Ill-conditioned process structures could be reflected in the identified models and also used in control design.

Research needs as perceived by industry are mostly control engineering issues, not algorithm issues. Industrial practitioners do not perceive closed-loop stability, for example, to be a serious problem. Their problems are more like: Which variables should be used for control? When is a model good enough to stop the identification plant test? How do you determine the source of a problem when a controller is performing poorly? When can the added expense of an MPC controller be justified? How do you design a control system for an entire plant? How do you estimate the benefits of a control system? Answering these questions could provide control practitioners and theoreticians with plenty of work in the foreseeable future.

Finally, the future of MPC technology is bright. Next-generation MPC technology is likely to include multiple objective functions, an infinite prediction horizon, nonlinear process models, better use of model uncertainty estimates, and better handling of ill-conditioning. Because it is so difficult to express all of the relevant control objectives in a single objective function, next-generation MPC technology will probably utilize multiple objective functions. The infinite prediction horizon has beneficial theoretical properties and will probably become a standard feature. Output and input trajectory options will include set points, zones, trajectories and funnels. Input horizons will include options for multiple moves or parameterization using basis functions.

2.2.4.6 Adaptive Control

It is often desirable to adjust the parameters of a control system when the process operational point changes or there are internal disturbances (e.g., material aging). A system that does this automatically is known as an adaptive system. Because it is also sometimes necessary to automatically adjust the control parameters during start-up, even if the process parameters are relatively constant, a control system that does this is known

as a self-tuning controller. The similarities between these two control systems are so strong than they can be treated as one.

Many adaptive control structures have been developed. However, the practical developments in this area have been limited to adaptive controllers for single-input, single-output systems. The literature contains very few practical examples of adaptive, multivariable control based on parametric estimation in multivariable models. This is certainly due to the complexity of the problem. A complex solution requires considerable computer hardware and software capability, which increases the probability of failure someplace in the control system. The practical development of a complex system program requires much time and manpower.

There are many ways to realize an adaptive control system. The most important adaptive architectures presented in the literature are: gain schedule, model reference, self-tuning regulators, and stochastic. Figure 2.9 shows the most fundamental adaptive control structure. It is important to distinguish between the problems associated with the control algorithm and those connected directly with adaptive action itself. For example, it is possible to adapt a PID controller in order to achieve adaptive characteristics. There is general disagreement in the control community about what characteristics a control system must have in order to be called adaptive. The most common definition maintains that the adaptive system optimizes an objective function with respect to variations of the control parameters.

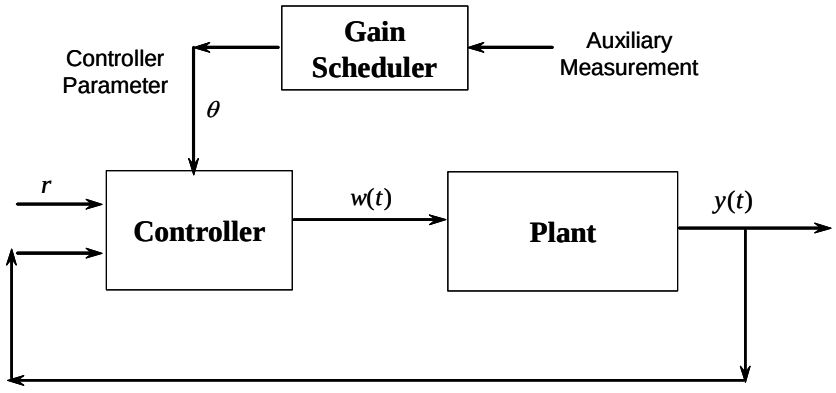

Figure 2.9. Gain schedule adaptive control architecture.

Finally, it is important to recognize that ordinary feedback control systems always have a potential stability problem. This characteristic may become even more significant

as control architectures such as adaptive control with parameter estimation are applied. Therefore, in practice the process to which the adaptive control is applied to should have very high reliability and be fundamentally stable. This, of course, is not always the case when dealing with highly dynamic systems. For a very comprehensive study on adaptive control, the reader is referred to Sastry and Bodson (1989).

2.2.5 Optimal Control (OPC)

Optimal control refers to systems designed to generate control variables that minimize (or maximize) a scalar objective function that includes the process states and control variables. This problem has been widely discussed in the control literature since 1962 when Pontryagin introduced the maximum principle. In fact, one of the best-known methods to solve the optimal control problem is "Pontryagin's maximum principle". A summary of the main points of this method follow.

A non-linear process (with no disturbances, for the moment) can be described by

$$\dot{y} = f(y, w, t) \tag{2.30}$$

The goal is to find $w(t) \in W$ which gives the maximum of the objective functional (optimal criterion) expressed as

$$J = S(y(t_2)) + \int_{t_1}^{t_2} L(y, w)dt \tag{2.31}$$

A scalar function (the Hamiltonian) is introduced such that

$$H(y, p, w) = L(y, w) + p^T f(y, w) \tag{2.32}$$

The optimal control is the *w(t)* that at any time maximizes *H* when *y(t)* and *p(t)* are given by the solution of the equations

$$\dot{y} = \frac{\partial H(\cdot)}{\partial p} \tag{2.33}$$

$$\dot{p} = -\frac{\partial H(\cdot)}{\partial y} \tag{2.34}$$

The boundary conditions for equations 2.33 and 2.34 depend on how $y(t_2)$ is specified. Usually the boundary conditions are given as:

$$y(t_1) = \text{given} \tag{2.35}$$

$$p(t_2) = -\left.\frac{\partial S(\cdot)}{\partial y}\right|_{t=t_2} \tag{2.36}$$

The solution of the optimization problem by this method requires the solution of a two-point boundary value problem. There are several ways of doing this which are reported in the literature. In all cases, this demands a real-time computation, which must be done rapidly by means of some iterative computational scheme. A condition for the successful application of the maximum principle is the availability of a good mathematical model of the system, and the objective functional equation must express accurately what has to be accomplished.

If the process in equation 2.30 also has a disturbance vector ($v(t)$), the problem is best solved by first developing a mathematical model of the generation of the disturbance as a response of a vector of uncorrelated "white noise sources" through a dynamic process. The state vector (y) for the process model is augmented by the disturbance state to form a super-process having the state vector (Y). This vector replaces the original vector (y) in the equations above and leads to an optimal solution for the disturbed process. The vector y and Y must be completely available in order to derive the optimal control. Therefore, it is often necessary to use a state estimator to compute those state variables that can not be directly measured.

The major disadvantage of the optimal control problem as stated above is that it yields the solution to an open-loop control problem. Thus, optimal control will yield an optimum trajectory of the control variables (w) as a function of time in order to achieve a predetermined goal, given a set of known initial conditions and disturbances. The solution would not include a control law adaptable to innumerable possible scenarios. One approach may be to implement an on-line, real-time OPC. However, the level of complexity related to a high-fidelity model of a non-linear dynamic process, as required by OPC, makes a practical application difficult. Furthermore, the OPC implementation depends on the availability of an accurate process model.

In order to develop an optimal control suitable to be implemented in a feedback control, the process described by equation 2.30 must be linear and time invariant and the objective functional must be a scalar quadratic function. The result is what is known as the linear quadratic problem, which can be solved using the Riccati equation (Balchen and Mumme, 1998). Again, the original optimization problem must be reduced in such a way that the result cannot be considered sufficiently accurate of system or process behavior.

There is extensive ongoing research on the application of the advance control techniques described above to introduce them into the complex dynamic systems in industrial process, including fuel cell applications (e.g., Golbert and Lewin, 2004; Varingola, Pukrushpan, and Stefanopoulon, 2003). Even though their applicability is restricted for practical issues, it is suggested as a subject of future research in dynamic optimization to investigate the possibility of applying ILGO/DILGO[20] when using controller architectures different from PIDs.

[20] DILGO stand for "dynamic iterative local-global optimization" and is the version of ILGO uniquely developed for the research work presented in this doctoral dissertation.

Chapter 3

Decomposition for the Large-Scale Optimization of Energy System Synthesis/Design

This chapter outlines three different decomposition strategies, i.e. *conceptual, time,* and *physical*, that address the need for large-scale, non-linear optimization. In the case of *physical decomposition*, two specific approaches are presented, namely, Local-Global Optimization (LGO) and Iterative Local-Global Optimization (ILGO). Dynamic Iterative Local-Global Optimization (DILGO) is a decomposition approach based on ILGO and a definition of shadow prices which is capable of handle highly dynamic systems optimization. DILGO is original to this research work.

For a deeper understanding of the concepts presented in this chapter, the reader is referred to the work by Muñoz and von Spakovsky (2000a,b,c,d; 2001a,b) and Rancruel and von Spakovsky (2003). The case is first made for the need of decomposition in the large-scale optimization of energy system synthesis/design. Indeed, the problem in its full complexity is defined as a dynamic, non-linear, mixed integer programming problem (DMINLP). These presentations set the theoretical foundation for the work given in Chapters 4, 5 and 6.

3.1 The Dynamic, Nonlinear Mixed Integer Programming Problem (DMINLP)

The synthesis/design optimization of an energy system in its most general form is a dynamic mixed integer non-linear programming problem with equality and inequality constraints. In general terms, this is expressed as

Minimize $f(\vec{x},\vec{y})$ (3.1)

w.r.t $\vec{x},\vec{y}$

subject to $\vec{H}(\vec{x},\vec{y}) = \vec{0}$ (3.2)

$\vec{G}(\vec{x},\vec{y}) \leq \vec{0}$ (3.3)

where $f(\vec{x},\vec{y})$ represents the figure of merit or objective of the optimization[21], the vector $\vec{x}$ the set of independent synthesis/design variables of the system, and $\vec{y}$ the set of operational/control variables[22]. The synthesis/design variables typically correspond to geometric parameters (physical dimensions of components), design flow rates, design pressure ratios, and in a wider sense some discrete (e.g., material or technology choice) or binary (e.g., existence or nonexistence of a unit or connection in the system configuration) parameters. Operational/control variables can be continuous variables (flow rates, valve settings) or binary variables (e.g., units on or off). The vector of equality constraints, $\vec{H}(\vec{x},\vec{y}) = \vec{0}$, represents the mass and energy balances (or other balances such as, for example, those for exergy, momentum, etc.) as well as the performance constraints that the energy system must obey. The vector of inequality constraints, $\vec{G}(\vec{x},\vec{y}) \leq \vec{0}$, represents physical or artificial limitations imposed upon the system.

The modeling of an energy system typically begins with the selection of a number of degrees of freedom represented by parameters which can be varied at will within acceptable limits. These independent parameters or variables are then used to create two systems of equations to represent the energy system, i.e. equations (3.2) and (3.3).

The DMINLP problem can be a highly complex problem which may not just be difficult to solve but may in fact be impossible to solve given the usual techniques of applied optimization. The complexity arises by virtue of the fact that a large number of degrees of freedom (both synthesis/design and operational variables) might be involved due to a desire to simultaneously optimize not only at a system level but at a detailed component/sub-system level. The complexity also arises because of detailed load profiles, of highly non-linear models, and of a mix of discrete and continuous variables. One option is to simplify the DMINLP problem greatly by, for example, reducing the

[21] In the field of thermoeconomics, this is the total cost of the system.

[22] Note that the modeling variable vector $\vec{z}$ is written apart of the functional description of the general optimization problem presented in Chapter 2 is dropped from the functional descriptions here since $\vec{z}$ represents the set of dependent variables for the optimization.

number of independent variables, considering only a single instant in time (i.e. only part of the load profile), assuming only steady state operation and/or perhaps even linearizing certain or all of the aspects of the problem. The drawback, of course, to any of these measures is a loss of information, which may in fact not be necessary if the problem can be decomposed into a set of smaller problems, the solution to which closely approximates the solution to the combined problem.

3.2 Conceptual Decomposition

Two different types of *conceptual* decomposition[23] were defined in *Chapter 2*: one which nests the operational-level optimizations within the synthesis/design level(s) of optimization and one which does not. The latter avoids this sort of nesting by completely separating the synthesis/design level(s) from the operational level. This type of decomposition reduces the computational burden seen with the nested conceptual decomposition approach by assuming that only a limited number of feasible solutions need be optimally evaluated at off-design.

Most if not all energy systems must meet a set of loads (e.g., electricity, heat, cooling, thrust, etc.) under a varying set of environmental conditions (e.g., ambient temperature and pressure). Thus, the synthesis/design optimization of the system must be done in such a way that the system is able to meet the most, for example, stringent load(s) and set of conditions as well as all other loads and conditions in the most efficient or cost effective manner. However, considering all load points simultaneously, especially for a very detailed load profile over a long period of time, further complicates an already complex problem. The non-nested conceptual decomposition surmounts this particular difficulty by decomposing the time variant features of synthesis/design into the synthesis/design at the most stringent load point, segment δ, followed by that at all other load points and conditions – i.e. a set, including the optimum and a number of near optimum syntheses/designs at the most stringent load point, are evaluated at all other load points in order to determine the optimal synthesis/design at all points[24]. The most

[23] As will be seen in Chapter 5, with the application of DILGO, neither conceptual nor time decomposition are used with the application presented in this research work. Thus, only physical decomposition is employed.

[24] Obviously, conceptual decomposition makes the assumption that the global optimum found in this way approximates what would be found without conceptual decomposition. This is an assumption made on physical not mathematical

stringent time segment (i.e. load point and set of environmental conditions) depends on the purpose of the system. In particular, for a fuel cell system the most stringent time segment is defined by the load profile. The synthesis/design of the system is initially optimized with respect to this particular point that mathematically and on a thermoeconomic (thermodynamic and economic) basis is expressed in the following terms:

$$\text{Minimize} \quad C_\delta = \left[\left(\sum_{r=1}^{R} c_r \dot{R}_r + \sum_{i=1}^{M} C_i^{operational} \right) \cdot \tau \right]_\delta + \sum_{i=1}^{M} C_i \tag{3.4}$$

$$\text{w.r.t.} \quad \tilde{x}_\delta = \{\vec{x}_1, \vec{x}_2, \cdots, \vec{x}_m\}_\delta \qquad \tilde{y}_\delta = \{\vec{y}_1, \vec{y}_2, \cdots, \vec{y}_m\}_\delta \tag{3.4.1}$$

Subject to

$$\begin{aligned} \left[\vec{H}\right]_\delta &= \vec{0} \\ \left[\vec{G}\right]_\delta &\le \vec{0} \end{aligned} \tag{3.4.2}$$

where C_δ is the total cost of the energy system, C_i the capital cost of the i^{th} unit (sub-system or component), M the number of units, τ the length of time considered for time segment i, $\dot{R}_r$ the rate of consumption of the r^{th} resource, and c_r its unit cost. Finally, $C_i^{operational}$ represent other related operational costs of the i^{th} unit such as maintenance. As is pointed out in Rancruel, von Spakovsky, and Muñoz (2001), the objective function, equation (3.4), deals with one time segment and can also be expressed in purely physical terms such as weight or fuel.

The result obtained from solving equation (3.4) for a single synthesis / design is a set of feasible solutions (one optimal with respect to equation (3.4) and the others near-optimal) that satisfies the constraints given by equations (3.4.2). These solutions have a corresponding set of vectors $\tilde{x}_\delta$ and $\tilde{y}_\delta$ which are the set of synthesis/design and operational/control decision variables, respectively. The most promising of these feasible solutions are then used to minimize the total cost over the entire load/environmental profile for each of these feasible solutions. In order to obtain the synthesis/design that minimizes the total cost (or weight or fuel or other objective function) of the energy

basis, a discussion of which is beyond the scope of this dissertation work. However, even if in certain cases this assumption is not true, the likelihood of a good solution is high (Muñoz and von Spakovsky, 2001a,b).

system over the entire load/environmental profile, the following off-design optimization problem needs to be defined and solved for each time segment t where $t \neq \delta$

$$\text{Minimize} \quad C_T^{operational} = \sum_{t=1}^{T-1}\left(\sum_{r=1}^{R} c_{rt}\dot{R}_r\right)\cdot\tau_t + \sum_{t=1}^{T-1}\left(\sum_{i=1}^{M} C_{it}^{operational}\right)_t \tag{3.5}$$

$$\text{w.r.t.} \quad \vec{y}_t = \left\{y_{1_t}, y_{2_t}, \ldots, y_{n_t}\right\} \tag{3.5.1}$$

$$\text{subject to} \quad \left[\vec{H}\right]_{off-design} = \vec{0} \quad , \quad \left[\vec{G}\right]_{off-design} \leq \vec{0} \tag{3.5.2}$$

$$\vec{x} - \vec{x}^{\,pf} = \vec{0} \tag{3.5.3}$$

where $C_T^{operational}$ is the total operational cost of the system, $C_{it}^{operational}$ and c_{rt} represent other operational costs such as maintenance and resources unit cost, respectively, for the i^{th} unit, which take into account the time value of money, and $\vec{y}_t$ the set of system operational/control variables associated with the particular off-design time segment t of the load/environmental profile. Initially, the off-design optimization problem has to be solved for the T-1 off-design time segments with values of the synthesis/design independent (decision) variable vector $\vec{x}$ equal to $\vec{x}^{best}$, where $\vec{x}^{best}$ is the vector of the independent synthesis/design variables corresponding to the best (from the standpoint of the system-level objective) solution obtained by solving Problem (3.4). The solution to Problem (3.4) is actually a family of feasible solutions[25] that satisfy the constraints given by equations (3.4.1) and (3.4.2). However, the best solution, i.e. $\left(\vec{x}^{best}, \vec{y}_\delta^{best}, C_\delta^{best}\right)$, is not necessarily the best when the various off-design conditions are taken into account. The vector $\vec{x}^{pf}$, appearing in equation (3.5.3), indicates that the T-1 off-design optimization problems have to be solved for each one of the promising feasible solutions obtained from Problem (3.4), i.e. $\left(\vec{x}^{pf}, \vec{y}_\delta^{pf}, C_\delta^{pf}\right)$. The first term in equation (3.5) is used to evaluate each of the off-design time segments of the

[25] This family consists of the global minimum solution C_δ^{best} with corresponding decision variable vectors $\vec{x}^{best}$ and $\vec{y}_\delta^{best}$, plus a set of near global minimum solutions C_δ^{pf} with corresponding vectors $\vec{x}^{pf}$ and $\vec{y}_\delta^{pf}$. All of these solutions are constrained in the set of promising feasible solutions represented by $\left(\vec{x}^{pf}, \vec{y}_\delta^{pf}, C_\delta^{pf}\right)$

load/environmental profile, while the second term in equation (3.5) accounts for the maintenance costs which vary from one time segment to the next. The solution to Problem (3.5) effectively results in a set of optimal steady state operational variable values $\vec{Y}_t$ for each time segment and an optimal total cost C_T for each promising solution from which the final synthesis/design for the system is chosen, i.e.

$$C_T^* = C_\delta^* + C_T^{operational^*} \tag{3.6}$$

where, $$C_\delta{}^* = \left[\left(\sum_{r=1}^{R} c_r \dot{R}_r{}^* + \sum_{i=1}^{M} C_i^{operational*} \right) \cdot \tau \right]_\delta + \sum_{i=1}^{M} C_i^* \tag{3.6.1}$$

and equation (3.6) is valid for each promising solution.

As mentioned earlier, conceptual decomposition transforms the overall time-dependent problem of synthesis/design into two separate but linked problems (Problems (3.4) and (3.5)). In particular, it decomposes a problem with *d*+*ot* variables (*d* synthesis/design variables, *o* operational variables, and *t* time segments) into two smaller problems of *d*+o and *o(t-1)* variables, respectively. However, as a trade-off for reducing the number of variables which must be handled by any one problem, the expense of possibly having to carry out the optimization represented by Problem (3.5) for several possible promising solutions, i.e. those chosen in the synthesis/design optimization (Problem (3.4)), arises. In addition, even with conceptual decomposition, further decomposition for a very complex problem of synthesis/design optimization may be needed. When this is the case, both time and physical decomposition can be used.

3.3 Time Decomposition

Time decomposition transforms the operational optimization problem into a quasi-stationary problem consisting of a series of stationary sub-problems each of which correspond to a given time interval. Transient (unsteady) behavior within a given time interval is handled by breaking the interval into a series of smaller time segments and then numerically or analytically integrating over all the segments in order to capture the unsteady behavior of a component or sub-system. Each time interval is optimized individually with respect to a set of unique operational/control variables and the results

summed over all intervals. This form of decomposition complements conceptual as well as physical decomposition. The form in which equation (3.5) above is written already assumes that time decomposition has been applied, if this were not the case, equation (3.5) would have been written with integrals and not summations.

3.4 Physical Decomposition

Most energy systems can be decomposed into a set of units (sub-systems and/or components), each of which must have a clearly defined set of feedback or coupling functions with the other units of the system. Such a physical decomposition reduces the overall system optimization problem of synthesis/design into a number of unit optimization sub-problems. Two main approaches to physical (unit) decomposition are presented in the following sections. The first is a Local-Global Optimization (LGO) approach characteristic of all other such approaches in the literature and the second is an original development by Muñoz and von Spakovsky (2000a,b,c,d; 2001a,b) called the Iterative Local-Global Optimization (ILGO) approach. A third approach, an original contribution of this doctoral work is Dynamic Iterative Local-Global Optimization (DILGO). A discussion of this approach appears in section 3.5.2.

Unit (physical) decomposition, as opposed to time decomposition, tries to isolate the influence that each of the units that form a system has in terms of the overall (system-level) objective function. The unit's impact may be multi-disciplinary as shown below. To illustrate the fundamental differences between the leading decomposition methods (LGO and ILGO) for energy system synthesis/design, the simple two-unit system of Figure 3.1 will be considered where $\vec{z}_1$ and $\vec{z}_2$ are the decision variable sets, each unit is subject to a set of constraints which describe the physical processes present, and u_{12} and u_{21} are functions (in the general case, vectors of functions) that couple the two units. The typical objective function, *C*, is written as the sum of the contributions of each of the units, i.e. $C_1 + C_2$. In turn, the contribution of each unit is composed of two terms as, for example, indicated below for unit 1, namely,

$$C_1 = k_1 R_1 + C_{capital1} \tag{3.7}$$

In equation (3.7), R_1 is some external resource used by unit 1 (typically fuel) and $C_{capital_1}$ is a function related to the size of the unit (weight/volume or cost) while k_1 is a conversion factor. In a thermoeconomic problem, $C_{capital_1}$ is the capital cost. In a thermodynamic problem $C_{capital_1}$ is either ignored, as may be the case for a stationary system, or translated into physical terms such as weight, as would be the case for a transportation system.

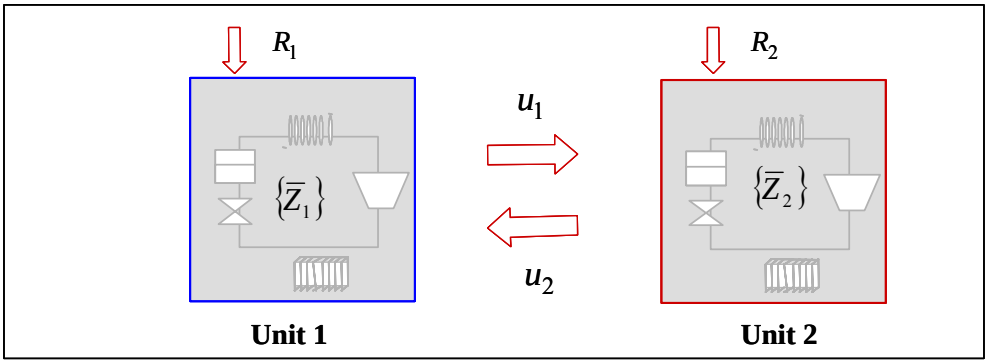

Figure 3.1 Physical decomposition of a 2-unit system.

Before proceeding with a comparison of LGO and ILGO as applied to the system of Figure 3.1, a few words are in order about the origins of the various methods for physical decomposition of energy systems[26] which come from the field of thermoeconomics. The first to devise a scheme for physical decomposition where Evans and El-Sayed (1970), which has come to be known as the Evans–El-Sayed Formalism. Without a doubt, this is the single most influential work in thermoeconomics, which also applies decomposition. Many of the leading cost assignment and optimization methods such as Engineering Functional Analysis - EFA (von Spakovsky and Evans, 1993; Evans and von Spakovsky, 1993), Thermoeconomic Functional Analysis - TFA (Frangopoulos, 1994), Exergy Structural Theory (Valero et al., 1994) and others (e.g., Tsatsaronis and Pisa, 1994) are to a certain extent variations of the original Evans–El-Sayed method. This method was based on the Lagrange multiplier theorem of optimization and made possible, under certain very specific conditions, the decomposition of a system into units

[26] Physical decomposition has also been used extensively for years on aerospace applications. For a brief overview the reader is referred to Munoz and von Spakovsky (2003).

(for a brief discussion of the essential features of the original Evans–El-Sayed method, the reader is referred to Muñoz and von Spakovsky, 2002).

Based on the thermoeconomic approaches developed by Evans, Frangopoulos, and von Spakovsky (i.e. TFA and EFA), the concept of "thermoeconomic isolation (TI)" was introduced (Evans et al., 1980; Frangopoulos, 1983; Frangopoulos and Evans, 1984; von Spakovsky and Evans, 1984). As mentioned in the previous chapter, TI is defined as the ability to optimize independently each unit of a system and yet still arrive at the optimum for the system as a whole. TI is, in fact, a stronger condition than mere *decomposition*. In the latter, the complete set of decision variables for the system and its components can only partially be distributed to the units into which the system is decomposed, i.e. although each unit has its own local set of decision variables independent of those of the other units, there is still a subset of decision variables at the system level which cannot be uniquely assigned to any given unit. Thus, not all of the decision variable sets can be said to be disjoint, i.e. assignable to one and only one unit. TI, on the other hand, assumes that under certain conditions complete disjointness is possible so that simply optimizing at the unit level is sufficient for ensuring a system level optimum. The conditions required for TI in these earlier methods (e.g., von Spakovsky and Evans, 1991) included an adequate functional breakdown of the system (i.e. a breakdown into units as described by the functional diagram of EFA or TFA), system and component cost functions and constraints based on exergy and negentropy, and system and component cost functions linearized with respect to each corresponding function's (unit's) product.[27]

However, the practicality of linearazing in very complex systems as well as the negative associated with a possible loss of information makes the use of EFA and TFA in particular and the Evans / El-Sayed formalism in general questionable for achieving TI. In addition, TI has only been successfully achieved or closely approached using this formalism for very simple systems. Furthermore, none of these methods was developed

[27] Note that in ILGO which is described later, these conditions are completely eliminated and TI is closely approached by embedding system-level information (i.e. that due to the decision variables which are not disjoint and, thus, exist at the system-level) explicitly at the unit level through the use of coupling functions and their associated shadow prices (see the discussions on LGO and ILGO below). Achieving or closely approaching TI in effect requires that the system-level optimum response surface (again, see the discussions below on LGO and ILGO) is either a hyperplane or a convex hypersurface.

for units coupled to non-energy systems as is the case in aircraft; and, thus, the conditions for closely approaching TI were never studied for those cases. Finally, the Evans / El-Sayed formalism indirectly assumes that a single group of analysts has access to and the expertise to work with all of the disciplines and the different technologies (units) that compose the system. This may, in fact, not be the case and more often than not is.

To overcome the difficulties mentioned above and eliminate the conditions required by these earlier methods for achieving or closely approaching TI, ILGO was developed. In order to compare the characteristics of LGO[28] with ILGO, a description of the LGO approach is given next.

3.4.1 The Local-Global Optimization (LGO) Approach

In the LGO approach, two levels of optimization instead of one are used. At the local or unit level, an optimization for each unit and each set of values of the coupling functions between units is carried out. These optimum results are then used at a global or system level at which the system synthesis/design is optimized[29] with respect to the coupling function values. In order to get a better understanding of the LGO approach, let us consider the following optimization problem applied to a system decomposed into two units as shown in Figure 3.1.

Minimize

$$C = k_1 R_1\left(\vec{z}_1, u_{12}(\vec{z}_1,\vec{z}_2), u_{21}(\vec{z}_1,\vec{z}_2)\right) + k_2 R_2\left(\vec{z}_2, u_{12}(\vec{z}_1,\vec{z}_2), u_{21}(\vec{z}_1,\vec{z}_2)\right) \tag{3.8}$$

w.r.t. $\vec{z}_1, \vec{z}_2$

subject to the primary constraints

$$\vec{H} = \begin{bmatrix} \vec{h}_1 \\ \vec{h}_2 \end{bmatrix} = \vec{0} \tag{3.8.1}$$

[28] By definition, LGO is unable to achieve TI unless by happenstance all decision variables can be distributed into disjoint sets, each of which can be assigned to one and only one unit.

[29] Again, as in a previous footnote it must be emphasized that "optimized" need not be taken here in a strictly mathematical sense of guaranteeing that a Kuhn-Tucker point at the system-level is found. What is guaranteed and what is of importance here is that with such decomposition approaches an "improved" synthesis/design is guarantee unless the initial point already is global optimum.

$$\vec{G} = \begin{bmatrix} \vec{g}_1 \\ \vec{g}_2 \end{bmatrix} \leq \vec{0} \tag{3.8.2}$$

and to the additional (secondary) constraints

$$u_{12}(\vec{z}_1, \vec{z}_2) - \xi = 0 \tag{3.8.3}$$

$$u_{21}(\vec{z}_1, \vec{z}_2) - \psi = 0 \tag{3.8.4}$$

where R_1 and R_2 are the resources used by units 1 and 2, respectively, k_1 and k_2 their respective unit costs, and $\vec{z}_1$ and $\vec{z}_2$ the set of independent variables for each unit used in the optimization of the system. Constraints (3.8.3) and (3.8.4) require that the coupling functions take on values of ξ and ψ such that

$$u_{12\,max} \leq \xi \leq u_{12\,min} \tag{3.8.5}$$

$$u_{21\,max} \leq \psi \leq u_{21\,min} \tag{3.8.6}$$

The cost of operating each unit is clearly identified in Problem (3.8). The contribution of each unit to the overall objective C is a function of the variables of each unit and the values ξ and ψ of the coupling functions. Therefore, for a given set of values ξ and ψ of the coupling functions, Problem (3.8) can easily be decomposed into two sub-problems, one for each of the units, i.e.

Sub-problem 1:

Minimize $\quad C_1 = k_1 R_1 \left(\vec{z}_1, \xi, \psi\right)$ (3.9)

w.r.t. $\vec{z}_1$

subject to $\quad \vec{h}_1 = \vec{0}$ (3.9.1)

$\vec{g}_1 \leq \vec{0}$ (3.9.2)

Sub-problem 2:

Minimize $\quad C_2 = k_2 R_2 \left(\vec{z}_2, \xi, \psi\right)$ (3.10)

w.r.t. $\vec{z}_2$

subject to $\vec{h}_2 = \vec{0}$ (3.10.1)

$\vec{g}_2 \leq \vec{0}$ (3.10.2)

where for purposes of simplification it has been assumed that the capital costs are zero. Thus, Problem (3.8) is effectively reduced to two smaller problems (Problems (3.9) and (3.10)) by physical decomposition. Problems (3.9) and (3.10) have to be solved several times for different values of ξ and ψ of the coupling functions u_{12} and u_{21}. The values selected for the coupling functions must be included within the limits given by expression (3.8.5) and (3.8.6). It is assumed in using LGO that it is possible to find different sets of values for the independent variable vectors $\vec{z}_1$ and $\vec{z}_2$ which correspond to particular values ξ and ψ of u_{12} and u_{21}.

The results for sub-problems 1 and 2 are a set of optimum values for each objective as a function of the coupling functions such that

$$C_1^* = \min\left(k_1 R_1\left(\vec{z}_1, \xi, \psi\right)\right) \tag{3.11}$$

$$C_2^* = \min\left(k_2 R_2\left(\vec{z}_2, \xi, \psi\right)\right) \tag{3.12}$$

Equations (3.11) and (3.12) imply that there exists a set of unit optimum independent variable vectors $\vec{z}_1^*$ and $\vec{z}_2^*$ that satisfy

$$C_1^* = k_1 R_1\left(\vec{z}_1^*, \xi, \psi\right) \tag{3.13}$$

and $$C_2^* = k_2 R_2\left(\vec{z}_2^*, \xi, \psi\right) \tag{3.14}$$

for each set of values ξ and ψ of the coupling functions u_{12} and u_{21}. Graphically this is shown in Figure 3.2 where each local or unit-level optimum of the local objectives C_1 and C_2 are plotted as a function of the coupling functions u_{12} and u_{21}. A vector of optimum values for the system-level objective function results from combinations of the sum of the optimum solutions found by solving the local sub-problems, Problems (3.9) and (3.10), i.e. $C^* = C_1^* + C_2^*$.

In fact, every point of C^*_1 and C^*_2 versus u_{12} and u_{21} represents a local or unit-level optimum. When these two surfaces called unit-level Optimum Response Surfaces (ORSs) are combined, they form what is called the system-level ORS[30] for the system as a whole (see Figure 3.2). The system-level ORS defines the global or system-level problem given by

$$\text{Minimize } C^* = k_1 R_1(\xi,\psi) + k_2 R_2(\xi,\psi) \tag{3.15}$$

w.r.t. ξ, ψ

subject to

$$\vec{G} = \begin{bmatrix} \xi - u_{12\,\max} \\ -\xi + u_{12\min} \\ \psi - u_{21\,\max} \\ -\psi + u_{21\min} \end{bmatrix} \le \vec{0} \tag{3.15.1}$$

This system-level optimization problem consists of finding the optimum values of the coupling functions, ξ^* and ψ^*, that minimize the global or system-level objective. At the system-level, the independent variable vectors $\vec{z}_1$ and $\vec{z}_2$ of each unit do not appear. This is because of the assumption made earlier that there are a unique set of local or unit-level optimum values $\vec{z}_1^*$ and $\vec{z}_2^*$ for every combination of ξ and ψ.

The LGO technique has the advantage of breaking a large problem into smaller sub-problems that can be solved simultaneously. The drawback is the computational burden that this approach has for large, complex systems since each sub-problem must be solved independently many times in order to generate the system-level ORS. This is further compounded by the need for heuristic algorithms to deal with a mix of real and integer variables in the optimization and by the use of computationally expensive (unit) analyzers. To circumvent these drawbacks, Muñoz and von Spakovsky (2000a,b,c,d; 2001a,b) developed the Iterative Local-Global Optimization (ILGO) approach.

[30] For a system with more than two coupling functions, the ORS is in fact a hyper-surface.

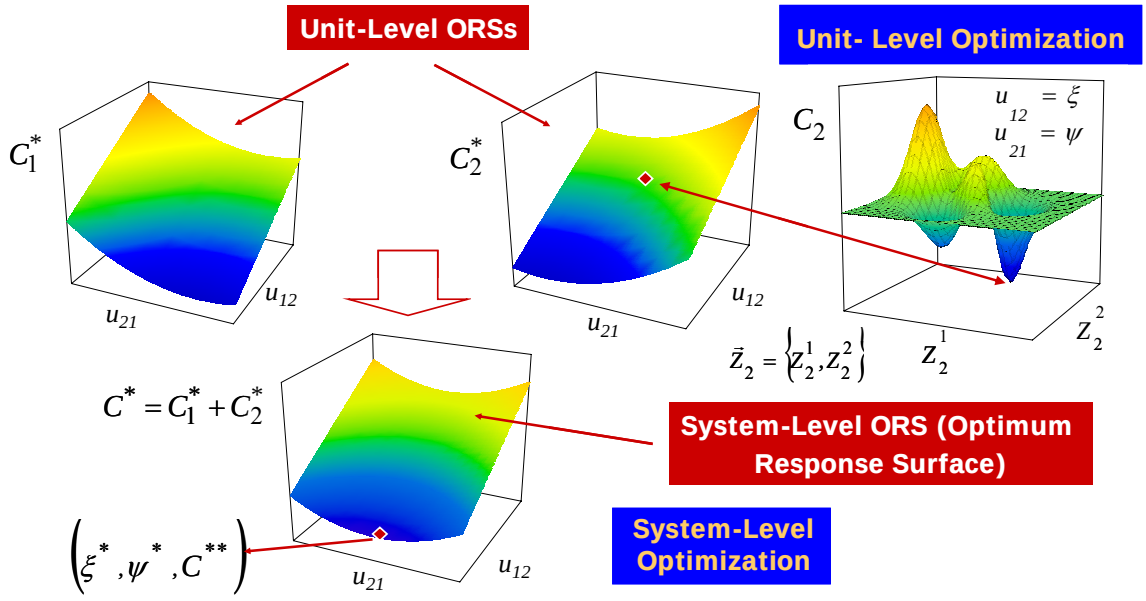

Figure 3.2. Local (unit-level) and global (system-level) optimizations.

There are two complementary versions of this approach: ILGO-A and ILGO-B. Both are presented in the following sections. However, before proceeding, the algorithm for LGO is summarized as follows[31]:

- Identify the independent variable vectors ($\vec{z}_1$ and $\vec{z}_2$) and the coupling functions (u_{12} and u_{21}).
- Define and solve the unit-level optimization problems (Problems (3.9) and (3.10)) for different values of ξ and ψ of the coupling functions u_{12} and u_{21} and find a set of local or unit optimum values $\vec{z}_1^*$ and $\vec{z}_2^*$ for every combination of ξ and ψ.
- Define and solve the system-level optimization problem (Problem (3.15)).

[31] Note that LGO always results in a explicit or implicit nesting of unit-level optimizations (problems (3.9) and (3.10)) within an overall system-level optimization (problem (3.15)).

3.4.2 Advantage of ILGO over standard LGO Approach.

In addition to not having the drawbacks outlined in the previous section for LGO, the ILGO decomposition strategy is an advance over LGO in that it

- eliminates the nested optimizations (whether implicit or explicit) required in standard local-global decomposition approaches;
- uses an intelligent search based on shadow prices to effectively search the system-level ORS(s) without having to actually generate the ORS(s);
- assures consistency between all local objectives and the system-level objective;
- introduces no constraint inconsistencies from one sub-problem to another;
- is conducive to the parallelization of the various sub-problem optimizations.

In addition, ILGO makes possible the decentralized, integrated synthesis/design optimization of systems by allowing multiple platforms and software tools as well as geographically dispersed and discipline diverse teams of engineers to effectively interact both at the unit (local) and the system (global) levels. In the following sections, two versions of the ILGO approach (ILGO-A and ILGO-B) are presented. Even though the presentation is only given for a two unit system (as was done with the LGO approach), both approaches are completely general and applicable to any multiple unit system. In addition, they are applicable whether or not a system is hierarchical[32] or non-hierarchical.

3.4.3 The Iterative Local-Global Optimization (ILGO) Approach

The Iterative Local-Global Optimization (ILGO) approach eliminates the need for implicitly or explicitly (Muñoz and von Spakovsky, 2000a,b,c,d; 2001a,b) creating the ORSs by using a first order Taylor series expansion to approximate the local behavior of the system-level ORS. A formal presentation of this method is given below. Consider a modified version of Problems (3.9) and (3.10) where the two sub-problems are now solved for particular values ξ_o and ψ_o of the coupling functions u_{12} and u_{21}, i.e.

[32] In a hierarchical system, all the components flow from a principal component.

Sub-problem 1:

Minimize $C_1 = k_1 R_1\left(\vec{z}_1, \xi_o, \psi_o\right)$ (3.16)

w.r.t. $\vec{z}_1$

subject to $\vec{h}_1 = \vec{0}$ (3.16.1)

$\vec{g}_1 \le \vec{0}$ (3.16.2)

Sub-problem 2:

Minimize $C_2 = k_2 R_2\left(\vec{z}_2, \xi_o, \psi_o\right)$ (3.17)

w.r.t. $\vec{z}_2$

subject to $\vec{h}_2 = \vec{0}$ (3.17.1)

$\vec{g}_2 \le \vec{0}$ (3.17.2)

The resulting values for the optimum solutions are $(C_1^*)_o$ and $(C_2^*)_o$ with corresponding independent variable vectors $(\vec{z}_1^*)_o$ and $(\vec{z}_2^*)_o$. The subscript o that accompanies the optimum solutions serves as a reminder that they are calculated at the initial or reference point. At this point, a Taylor series expansion of the unit-level objective functions is performed about the ORS reference point and the linear terms are taken so that

$$C_1^* = \left(C_1^*\right)_o + \left(\frac{\partial C_1^*}{\partial u_{12}}\right)_o \Delta u_{12} + \left(\frac{\partial C_1^*}{\partial u_{21}}\right)_o \Delta u_{21} \tag{3.18}$$

$$C_2^* = \left(C_2^*\right)_o + \left(\frac{\partial C_2^*}{\partial u_{12}}\right)_o \Delta u_{12} + \left(\frac{\partial C_2^*}{\partial u_{21}}\right)_o \Delta u_{21} \tag{3.19}$$

The partial derivatives in equation (3.18), which are in fact "shadow prices[33]" (von Spakovsky and Evans, 1993), are evaluated at the optimum value C_1^* of the objective for sub-problem 1 based on the choice of ξ_o and ψ_o for u_{12} and u_{21}, respectively. In fact geometrically, these partial derivatives or shadow prices are the slopes of the unit-level ORS at each local (unit-level) optimum point in the u_{12} and u_{21} directions. The shadow prices indicate the relative importance of the coupling functions in terms of the overall system-level objective. Similarly, for sub-problem 2, a set of shadow prices, i.e. slopes, of the surface for unit 2 at ξ_o and ψ_o can be found. Using a more compact notation, equations (3.18) and (3.19) can be written as follows:

$$C_1^* = \left(C_1^*\right)_o + \lambda_{12}^1 \Delta u_{12} + \lambda_{21}^1 \Delta u_{21} \tag{3.20}$$

$$C_2^* = \left(C_2^*\right)_o + \lambda_{12}^2 \Delta u_{12} + \lambda_{21}^2 \Delta u_{21} \tag{3.21}$$

Depending on the sign and absolute value of the partial derivatives or shadow prices for units 1 and 2, an improved restricted optimum value of the system-level objective given by

$$C^* = \left(C_1^*\right)_o + \left(C_2^*\right)_o + \left(\lambda_{12}^1 + \lambda_{12}^2\right)_o \Delta u_{12} + \left(\lambda_{21}^1 + \lambda_{21}^2\right)_o \Delta u_{21} \tag{3.22}$$

can be obtained by changing the values of the coupling functions in the directions and with the magnitudes indicated by the shadow prices. Equation (3.22) is obviously a construction of the restricted optimum local objectives, equations (3.18) and (3.19), and furthermore represents the restricted system-level optimum point which appears on the ORS for the system-level optimization given in Figure 3.3.

The feasibility of solving the optimization problem as stated in equations (3.16) and (3.17) is based on the existence of a set of vectors $\vec{z}_1^*$ and $\vec{z}_2^*$ for each set of values ξ and ψ that minimizes each unit objective function and satisfies the unit constraints. However, this assumption, that every combination of ξ and ψ leads to a feasible solution, may not be warranted for some systems. In fact, it is possible to find

[33] A "shadow price" is a type of "marginal cost" since it represents the marginal cost associated with marginal changes in a unit-level or local objective's optimum value with respect to marginal changes in the value of an associated coupling function.

simultaneous increases in u_{12} and u_{21}, which due to the characteristics of the units are not physically possible. For these reasons, it is necessary to reformulate the unit-level optimization problems as follow.

Sub-problem 1[34]:

$$\text{Minimize } C_1^{'} = C_1 + \left(C_2^*\right)_o + \left(\lambda_{12}^2\right)_o \Delta u_{12}{}^{(1)} + \left(\lambda_{21}^2\right)_o \Delta u_{21}{}^{(1)} \tag{3.23}$$

w.r.t. $\vec{z}_1$ and subject to the same constraints as in Problem (3.16)

Sub-problem 2:

$$\text{Minimize } C_2^{'} = C_2 + \left(C_1^*\right)_o + \left(\lambda_{12}^1\right)_o \Delta u_{12}{}^{(2)} + \left(\lambda_{21}^1\right)_o \Delta u_{21}{}^{(2)} \tag{3.24}$$

w.r.t. $\vec{z}_2$ and subject to the same constraints as in Problem (3.17).

The above sub-problems have the advantage that only values of the independent variables close to $\left(\vec{z}_1^*\right)_o$ and $\left(\vec{z}_2^*\right)_o$, which lead to feasible solutions, are allowed to participate in the optimization in its search for the global optimum.[35] The expressions for the objective functions $C_1^{'}$ and $C_2^{'}$, i.e. equations (3.23) and (3.24), take into account the fact that variations in the independent (decision) variables of the unit being optimized have an impact on the local (unit-level) objective function of both units. For example, variations in the decision variables of unit 1, namely, $\vec{z}_1$, cause changes $\Delta u_{12}{}^{(1)}$ and $\Delta u_{21}{}^{(1)}$ in the coupling functions u_{12} and u_{21}, respectively, according to the following relationships:

$$\Delta u_{12}^{(1)} = \frac{\partial u_{12}}{\partial \vec{Z}_1} \Delta \vec{z}_1 \tag{3.25}$$

and $$\Delta u_{21}^{(1)} = \frac{\partial u_{21}}{\partial \vec{Z}_1} \Delta \vec{z}_1 \tag{3.26}$$

[34] Note that this problem is the minimization of cost in unit 1 plus the projected change in cost in the rest of the system (in this case, unit 2) as a consequence of the variation of the local independent variables.
[35] Again, the term "global optimum" is used in a "engineering" sense and not a strictly "mathematical one.

where the superscript (1) indicates that the changes in the coupling functions are due to a variation in $\vec{z}_1$ only[36]. These changes translate into a variation in the optimum value of the local objective function of unit 1 *and* unit 2. The impact on the local objective function of unit 2 (when solving Problem (3.23)) is taken into consideration through the shadow prices (the λ's), i.e.

$$\lambda_{12}^2 \equiv \left(\frac{\partial C_2^*}{\partial u_{12}} \right)_o \tag{3.27}$$

and $$\lambda_{21}^2 \equiv \left(\frac{\partial C_2^*}{\partial u_{21}} \right)_o \tag{3.28}$$

Therefore, Problems (3.23) and (3.24) are not strictly speaking local or unit-level sub-problems. In the work of Muñoz and von Spakovsky (2000a,b,c,d; 2001a,b) such problems are called *unit-based, system-level optimization problems* since in effect system-level information has now been embedded directly into each local or unit-level objective. It is this embedding that leads to the more general nature of ILGO over LGO and to the very desirable ILGO feature of eliminating the nested optimizations from which LGO suffers.

Thus, an iterative procedure called ILGO is established where by starting with random values of the coupling functions, new values (ξ and ψ) for these functions are selected based on the slopes. ILGO, therefore, moves intelligently using the shadow prices towards the global (system-level) optimum[37] without having to actually create the ORS in Figure 3.4 or any of the local surfaces shown in Figure 3.3. This and the fact that no nested optimizations of local (unit-level) within global (system-level) are required prove to be major advantages.

The algorithm for the ILGO approach as given in Muñoz and von Spakovsky (2000a,b,c,d; 2001a,b) is as follows:

1- Obtain an initial point of the optimum response surface with u_{12} and u_{21} equal to ξ_o and ψ_o by solving the optimization sub-problems.

[36] In the same fashion, superscript (2) indicates that the changes in the coupling functions are due to a variation in $\vec{z}_2$ only.
[37] Again this is meant in an engineering sense.

2- Calculate the partial derivatives (shadow prices) of the restricted optimum values of the local objective functions C_1^* and C_2^* with respect to ξ and ψ

3- Estimate the maximum allowable values of Δu_{12} and Δu_{21} [38]. If no information is available, assume that the partial derivatives are constant over most of the optimum response surface.

4- The unit-based system-level optimization Problems (3.23) and (3.24) are defined and solved subject to the additional constraint that the values of the increment have to be constrained by a maximum (see Georgopoulos, 2002).

5- Finally, the solutions from the previous step are used to update $\left(\bar{z}_1^*\right)_o$, $\left(\bar{z}_2^*\right)_o$ and ξ_o and ψ_o. Repeat the procedure until no improvement is achieved or until the coupling functions have reached the minimum allowable values.

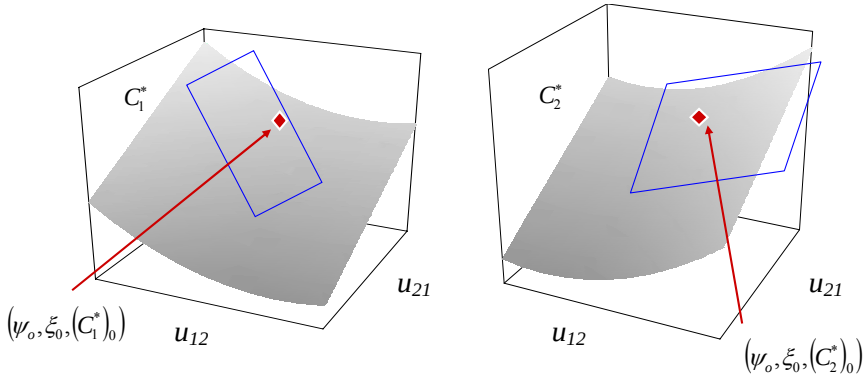

Figure 3.3: Initial restricted unit or local optimum points.

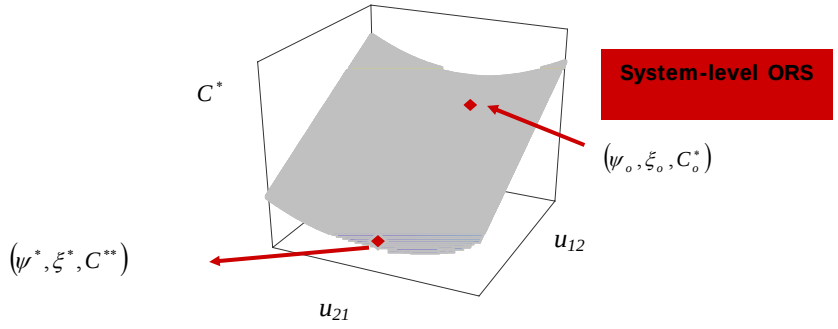

Figure 3.4. The restricted system-level optimum point on the system-level ORS

[38] Note that the values of the coupling function could be limited by physical constraints within the system.

3.5 Dynamic Optimization

3.5.1 Conceptual and Time Decomposition Applied to Dynamic Optimization Problems

The conceptual decomposition approach presented in section 3.2 is well suited for handling energy systems whose operational life is fundamentally steady state. In other words, it makes two fundamental assumptions. The first is that transient effects have little or no effect on operational costs and performance. Secondly, and more importantly, it assumes that the resulting synthesis/design optimum is adequate for handling transients, especially start-up, shut-down, and abrupt load changes. From an engineering point of view, the first assumption may be acceptable for large scale power systems such as power plants with capacities on the order of megawatts. Due to market, economic and engineering reasons, these sort of systems are intended to operate at load levels close to the design point and transients are avoided as much as possible. It they happen, they are intentionally scheduled to be slow. However, not even for these type of systems is the second assumption reasonably sustainable. Start-up and shut-down are inevitable, in fact they are critical from an economic and system integrity point of view. Therefore, these type of events should at least be considered at the earliest stages of synthesis/design and, of course, during the optimization process.

For small power generation systems (e.g., solid oxide fuel cell based auxiliary power units), abrupt load changes all over the system capacity range are common. These, changes are very sudden and can happen on the order of tens to hundreds of times a day. In the same way these system can go through start-up-shut-down cycles many times a day, Therefore, it is not possible to employ the two assumptions on which the traditional conceptual decomposition approach is based. To address this challenge of transient, traditional conceptual decomposition is formulated in a different manner. Thus, the synthesis/design optimization is defined as

$$\text{Minimize} \quad C_\delta = \left[\int_{t=0}^{\tau} \sum_{r=1}^{R} c_r \dot{R}_r(t) dt + \int_{t=0}^{\tau} \sum_{i=1}^{M} C_i^{operational}(t) dt \right]_\delta + \sum_{i=1}^{M} C_i \tag{3.29}$$

w.r.t. $\tilde{x}_\delta = \{\vec{x}_1, \vec{x}_2, \cdots, \vec{x}_m\}_\delta \quad \tilde{y}_\delta = \{\vec{y}_1, \vec{y}_2, \cdots, \vec{y}_m\}_\delta \quad \tilde{K}_\delta = \{\vec{K}_1, \vec{K}_2, \cdots, \vec{K}_m\}_\delta$ (3.29.1)

subject to

$$\begin{aligned} \left[\vec{H}\right]_\delta &= \vec{0} \\ \left[\vec{G}\right]_\delta &\le \vec{0} \end{aligned} \tag{3.29.2}$$

where the integral terms are added to account for the fact that the synthesis/design point may very well be a transient event. Again, the result obtained from solving equation (3.29) for a single synthesis/design is a set of feasible solutions (one optimal with respect to equation (3.29) and the others near-optimal) that satisfies the constraints given by equations (3.29.2). These solutions have a corresponding set of vectors $\tilde{x}_\delta$ and $\vec{y}_\delta$. Additionally, the system is optimized in terms of the set of vectors $\tilde{K}_\delta$, representing the control system gains[39]. The most promising of these feasible solutions are then used to minimize the total cost over the entire load/environmental profile for each of these feasible solutions. In order to obtain the synthesis/design that minimizes the total cost (or weight or fuel or …) of the energy system over the entire load/environmental profile, the following off-design optimization problem need to be defined and solved for each time segment t where $t \neq \delta$

$$\text{Minimize} \quad C_T^{operational} = \sum_{t=1}^{T-1} \int_0^t \sum_{r=1}^{R} c_{rt} \dot{R}_r(t) dt + \sum_{t=1}^{T-1} \int_0^t \sum_{i=1}^{M} C_{it}^{operational}(t) dt \tag{3.30}$$

$$\text{w.r.t. } \vec{y}_t = \{y_{1_t}, y_{2_t}, \ldots, y_{n_t}\} \quad \vec{K}_t = \{K_{1_t}, K_{2_t}, \cdots, K_{n_t}\} \tag{3.30.1}$$

$$\text{subject to} \quad \left[\vec{H}\right]_{off-design} = \vec{0} \quad , \quad \left[\vec{G}\right]_{off-design} \le \vec{0} \tag{3.30.2}$$

$$\vec{x} - \vec{x}^{\,pf} = \vec{0} \tag{3.30.3}$$

[39] Of course, this assumes that one or more control sub-systems are included in the system configuration and, thus, in the overall system synthesis/design optimization process. Furthermore, the $\tilde{K}_\delta$ has been pulled out of the synthesis/design variable vector $\tilde{x}_\delta$ to emphasize the actual presence of one or more control system configuration. In a similar vain, the $\vec{K}_t$ vector in problem (3.30) has been pulled out of the operational/control variable vector $\vec{y}_t$ for the case when an optimal gain schedule is developed for the operational segments. The vector $\vec{y}_t$, thus, becomes simple a vector of operational state variables.

where, $C_T^{operational}$ is the total operational cost of the system, $C_{it}^{operational}$ and c_{rt} represent other operational costs such as maintenance and resource unit cost, respectively, for the i^{th} unit, which take into account the time value of money, $\vec{y}_t$ the set of system operational/control variables associated with the particular off-design time segment t of the load/environmental profile, and $\vec{K}_t$ the set of system control gain variables. As for the traditional conceptual decomposition approach, the off-design optimization problem has to be solved for the T-1 off-design time segments. The vector $\vec{x}^{pf}$, appearing in equation (3.30.3), indicates that the T-1 off-design optimization problems have to be solved for each one of the promising feasible solutions obtained from Problem (3.29), i.e. $\left(\vec{x}^{pf}, \vec{y}_\delta^{pf}, c_\delta^{pf}\right)$. The first term in equation (3.30) is used to evaluate each of the off-design time segments of the load/environmental profile, while the second term in equation (3.30) accounts for the maintenance costs which vary from one time segment to the next. The solution to Problem (3.30) effectively results in a set of optimal dynamic state operational/control variable values $\vec{y}_t$ and $\vec{K}_t$ for each time segment and, as before, an optimal total cost C_T for each promising solution from which the final synthesis/design for the system is chosen, i.e.

$$C_T^* = C_\delta^* + C_T^{operational^*} \tag{3.31}$$

Positing the optimization problem in the manner just outlined allows one to consider each control sub-system as a separate discipline or unit in the optimization process to which conceptual and physical decomposition along with the dynamic shadow prices defined in the next section can be applied. Furthermore, the assumption of quasi-stationary states when applying time decomposition is no longer required. This is fundamental for the optimization of highly dynamic systems, for which quasi-stationary states do not apply or the required number of dynamic segment subdivisions would be too many to be practical. It is also important to point out that time decomposition, even when the number of subdivisions is enough to closely simulate the optimal operational variable path, is not suited for any control sub-systems which may be present in the system configuration.

3.5.2 Physical Decomposition Applied to Dynamic Optimization Problems: Dynamic Iterative Local-Global Optimization (DILGO)

3.5.2.1 Treatment of Control Sub-system Optimization

Two approaches are proposed for optimizing a dynamic system with one or more control sub-systems present. In the first approach each unit is optimized using DILGO[40] along with optimal control theory, i.e. the latter results directly in an optimum trajectory of the dynamic/control variables, $\vec{w}$, without consideration for feedback control system effects. Once $\vec{w}^*$ is known, a second optimization problem is posed, namely,

$$\text{Minimize } f = (\vec{w}^* - \vec{w}_c)^2 \tag{3.32}$$

$$\text{w.r.t. } \vec{K}_c$$

where $\vec{w}_c$ is the controller output and $\vec{K}_c$ is the controller gain set. The objective is to find the optimum controller gain set which yields the closest dynamic/controller output trajectory $\vec{w}_c$ to the optimum control variable trajectory $\vec{w}^*$ found in the previous step. Figure 3.5 depicts the physical decomposition required for this first approach in which units 1 and 2 are optimized first followed by units 3 and 4 (the controller) in a second optimization problem (problem (3.32)).

In the second approach, the controllers are incorporated into the corresponding sub-system models (see Figure 3.6) and optimization problems, defining the dynamic/control variables as a function of the system operational state variables, the reference point, and the controller gains. In this case the controller gains are set as additional synthesis/design decision variables (see Problem (3.29)). In fact, if advanced controllers are being used, the controller gains can be handled as dynamic/control variables (i.e. scheduled gain, predictive control, etc.).

[40] DILGO is the dynamic version of ILGO applied to the dynamic optimization of system using physical decomposition.

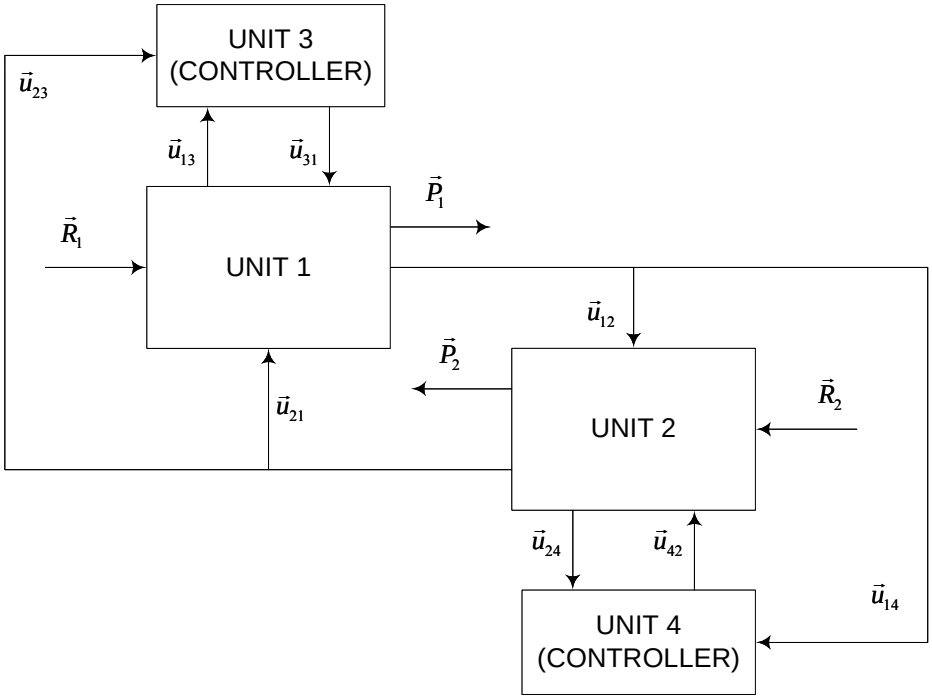

Figure 3.5. Schematic of the physical decomposition required when using the first approach to optimize the controller sub-system(s) as a separate unit(s).

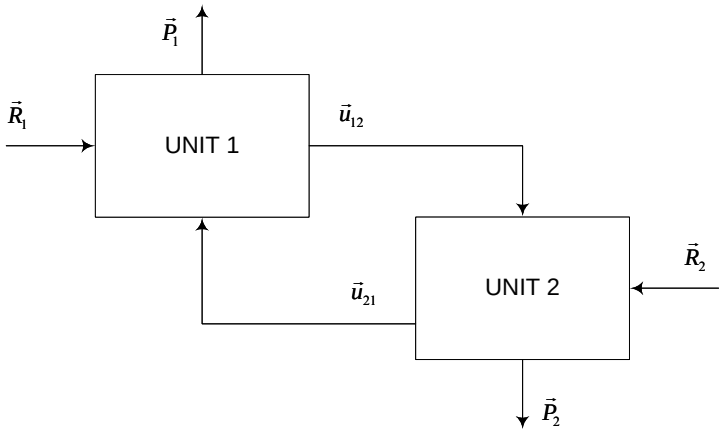

Figure 3.6. Schematic of the physical decomposition required when using the second approach to optimize the controller sub-system(s) integrated to the system[41].

A comparison between the two approaches yields the following comments:

- Both approaches consider the controller design effect on system performance.
- Both approaches can incorporate the controller costs into the objective function.

[41] Each unit includes the respective controllers

- The first approach shows the designer directly and more quickly the optimum dynamic/control variable trajectory $\vec{w}^*$.
- The first approach shows the difference between the optimum dynamic control variable trajectory $\vec{w}^*$ and the dynamic controller output trajectory generated by the controller. This shows how close the resulting system is to the global optimum. In addition, if the controller is far from the optimum performance, new controller architectures can be added into the optimization problem in the form of synthesis/design decision variables.
- The first approach is computationally (time) more expensive since the number of optimization problems is duplicated.
- The second approach simplifies the designer's work. However, the resulting optimum may not be the global optimum if the controller architecture can not simulate the optimum trajectory.
- The second approach is more practical, since for most systems the best practical controller architecture has already been defined experimentally. Thus, the controller problem is reduced to finding optimum values for the controller gains. In addition, the gains are considered design variables (i.e. not time dependant) for each transient; and with the resulting information, a controller gain schedule can be generated.

In this doctoral work the first approach was used for the dynamic synthesis/design and operational/control optimization of a SOFC system. The application of the second approach is suggested as future work.

3.5.2.2 System-Level Unit-Based Optimization Problem Definition for DILGO

Figure 3.7 shows the physical decomposition of a dynamic system made up of two sub-systems applying ILGO. The feedback controllers generate a set of controlled inputs $\vec{w}$ to each unit, which are intended to regulate the set of inputs $\vec{R}$ in order to produce the set of outputs $\vec{P}$ according to pre-defined outputs reference values $\vec{S}$. As

before the streams connecting the two units (i.e. coupling functions) are represented by $\vec{u}$.

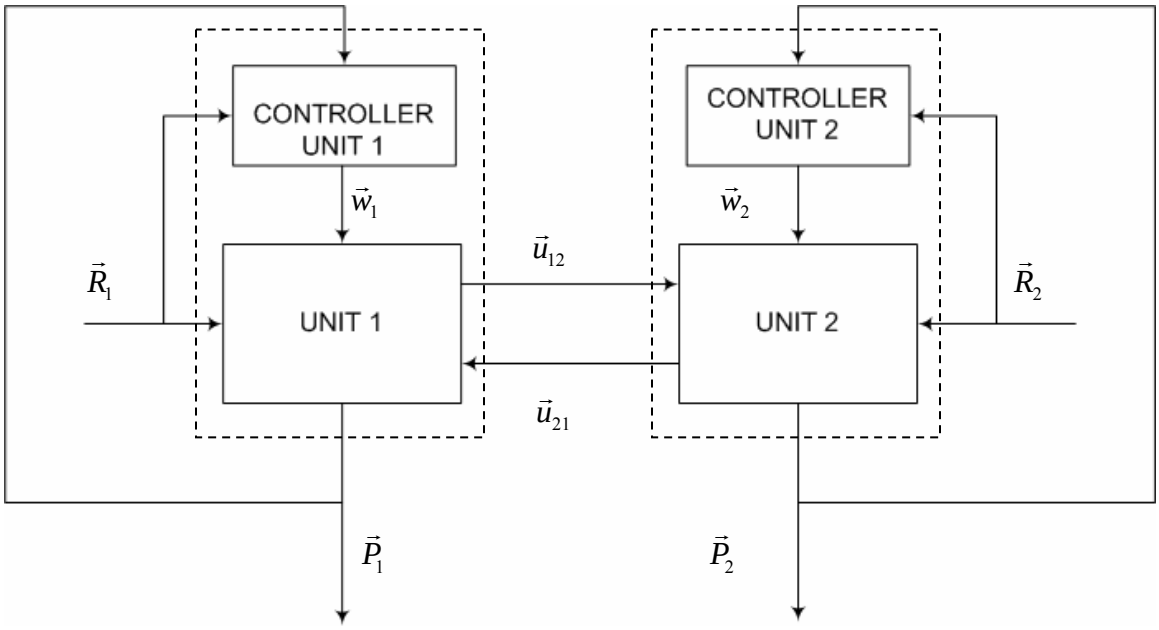

Figure 3.7. Physical Decomposition and Control system Consideration

Applying physical decomposition (i.e. ILGO) to this two unit system, the following are system-level, unit-based optimization problems for each unit are defined:

Sub-problem 1:

$$\text{Minimize } C_1' = C_1 + \left(C_2^*\right)_o + \left(\frac{\partial C_2^*}{\partial u_{12}}\right)_o \Delta u_{12}{}^{(1)} + \left(\frac{\partial C_2^*}{\partial u_{21}}\right)_o \Delta u_{21}{}^{(1)} \tag{3.33}$$

w.r.t. $\vec{x}_1, \vec{y}_1, \vec{K}_1$ and subject to a known set of constraints

Sub-problem 2:

$$\text{Minimize } C_2' = C_2 + \left(C_1^*\right)_o + \left(\frac{\partial C_1^*}{\partial u_{12}}\right)_o \Delta u_{12}{}^{(2)} + \left(\frac{\partial C_1^*}{\partial u_{21}}\right)_o \Delta u_{21}{}^{(2)} \tag{3.34}$$

w.r.t. $\vec{x}_2, \vec{y}_2, \vec{K}_2$ and subject to a known set of constraints

Unfortunately, the optimization sub-problems defined in this way are not well suited for handling a dynamic process. For instance, the coupling functions $\vec{u}_{ij}$ are changing with time and, therefore the term Δu_{ij} can not be defined as the difference of steady state values or the difference of steady state values at the end of a transient. For the same reason the shadow price $\left(\frac{\partial C_1^*}{\partial u_{12}}\right)$ cannot be defined as is, because its value changes as well with the transient. Thus, in order to adequately use the concepts behind the ILGO approach, two techniques are proposed.

In order to understand the level of complexity of the problem at hand let us first define the unit-level optimization problems as follow:

Unit 1:

$$\text{Minimize} \quad \begin{aligned} C_1 &= \lim_{\delta\tau\to 0}\left(\sum_{t=1}^{T}\dot{C}_1\left(\vec{x}_1,\vec{y}_{1t},\dot{\vec{y}}_{1t},\vec{u}_{12t},\vec{u}_{21t},\vec{w}_1,\vec{K}_1\right)\Delta\tau_t\right) \\ &= \sum_{t=1}^{T}\int_0^t \dot{C}_1\left(\vec{x}_1,\vec{y}_{1t},\dot{\vec{y}}_{1t},\vec{u}_{12t},\vec{u}_{21t},\vec{w}_1,\vec{K}_1\right)dt \end{aligned} \tag{3.35}$$

w.r.t. $\vec{x}_1,\vec{y}_{1t},\vec{K}_1$ and subject to a known set of constraints

where $\dot{\vec{y}}_{1t}$ is the vector of unit 1 time rate of change of the operational state variables, and $\vec{w}_1$ and $\vec{u}_{12t}$ are defined as

$$\vec{w}_1 = f\left(\vec{x}_1,\vec{y}_{1t},\dot{\vec{y}}_{1t},\vec{u}_{12t},\vec{u}_{21t},\vec{S}_1,\vec{P}_1,\vec{K}_1\right) \tag{3.35a}$$

$$\vec{u}_{12t} = f\left(\vec{x}_1,\vec{y}_{1t},\dot{\vec{y}}_{1t},\vec{u}_{21t},\vec{w}_1\right) \tag{3.35b}$$

Unit 2:

$$\text{Minimize} \quad \begin{aligned} C_2 &= \lim_{\delta\tau\to 0}\left(\sum_{t=1}^{T}\dot{C}_2\left(\vec{x}_2,\vec{y}_{2t},\dot{\vec{y}}_{2t},\vec{u}_{21t},\vec{u}_{12t},\vec{w}_2,\vec{K}_2\right)\Delta\tau_t\right) \\ &= \sum_{t=1}^{T}\int_0^t \dot{C}_2\left(\vec{x}_2,\vec{y}_{2t},\dot{\vec{y}}_{2t},\vec{u}_{21t},\vec{u}_{12t},\vec{w}_2,\vec{K}_2\right)dt \end{aligned} \tag{3.36a}$$

w.r.t. $\vec{x}_2,\vec{y}_{2t},\vec{K}_2$ and subject to a known set of constraints

where $\vec{\dot{y}}_{2t}$ is the vector of unit 1 time rate of change of the operational state variables, and $\vec{w}_2$ and $\vec{u}_{21t}$ are defined as

$$\vec{w}_2 = f\left(\vec{x}_2, \vec{y}_{2t}, \vec{\dot{y}}_{2t}, \vec{u}_{21t}, \vec{u}_{12t}, \vec{S}_2, \vec{P}_2, \vec{K}_2\right) \tag{3.36b}$$

$$\vec{u}_{21t} = f\left(\vec{x}_2, \vec{y}_{2t}, \vec{\dot{y}}_{2t}, \vec{u}_{12t}, \vec{w}_2\right) \tag{3.36c}$$

These definitions of the optimization sub-problems show a highly coupled dynamic system where transient response not only depends on the systems synthesis/design but also on the controller design, the coupling functions, the actual values of the dynamic operational state variables (initial conditions) and the product and reference values. Additional complexity appears due to the fact that the boundary between coupling functions, unit products, reference values, and control variables is not always clear, i.e. the coupling functions and control variables can be defined as unit products or unit resources.

Combining the system-level, unit-based optimization problem definition presented in equations (3.35a) and (3.36a) and the concept of the cost rate $\dot{C}$ introduced in equations (3.35a) and (3.36a) the system-level, unit-based objective functions can be expressed as

Unit 1:

Minimize

$$C_1' = \sum_{t=1}^{\tau}\left((\dot{C}_1)_t + (\dot{C}_2^*)_t + \left(\frac{\partial \dot{C}_2^*}{\partial u_{12}}\right)_t \Delta u_{12t} + \left(\frac{\partial \dot{C}_2^*}{\partial u_{21}}\right)_t \Delta u_{21t}\right)\Delta\tau_t \tag{3.37}$$

w.r.t. $\vec{x}_1, \vec{y}_{1t}, \vec{K}_1$ and subject to a known set of constraints

Unit 2:

Minimize

$$C_2' = \sum_{t=1}^{\tau}\left((\dot{C}_2)_t + (\dot{C}_1^*)_t + \left(\frac{\partial \dot{C}_1^*}{\partial u_{21}}\right)_t \Delta u_{21t} + \left(\frac{\partial \dot{C}_1^*}{\partial u_{12}}\right)_t \Delta u_{12t}\right)\Delta\tau_t \tag{3.38}$$

w.r.t. $\vec{x}_2, \vec{y}_{2t}, \vec{K}_2$ and subject to a known set of constraints

The partial derivatives above are by definition the shadow prices or marginal costs of the coupling functions except that now they are defined in terms of the unit cost rates. These, however, in turn are changing with time and, therefore, a definition of dynamic shadow prices is necessary. Equations (3.37) and (3.38) assume a set of discrete steady state load segments. Since, this is in fact not the case for dynamic systems; the system-level unit-based optimization problems quasi-stationary given above must be integrated over time yielding the time dependent forms of the system-level, unit-based optimization problems, i.e.

Unit 1:

Minimize

$$\begin{aligned} C_1' &= \sum_{t=1}^{\tau}\left(\int_0^t \dot{C}_1(t)dt + \int_0^t \dot{C}_2^*(t)dt + \int_0^t \left(\frac{\partial \dot{C}_2^*(t)}{\partial u_{12}(t)} \right) \Delta u_{12}(t)dt + \int_0^t \left(\frac{\partial \dot{C}_2^*(t)}{\partial u_{21}(t)} \right) \Delta u_{21}(t)dt \right) \\ &= \sum_{t=1}^{\tau}\left(C_1 + C_2^* + \int_0^t \left(\frac{\partial \dot{C}_2^*(t)}{\partial u_{12}(t)} \right) \Delta u_{12}(t)dt + \int_0^t \left(\frac{\partial \dot{C}_2^*(t)}{\partial u_{21}(t)} \right) \Delta u_{21}(t)dt \right) \end{aligned} \tag{3.39}$$

w.r.t. $\vec{x}_1, \vec{y}_{1t}, \vec{K}_1$ and subject to a known set of constraints

Unit 2:

Minimize

$$\begin{aligned} C_2' &= \sum_{t=1}^{\tau}\left(\int_0^t \dot{C}_2(t)dt + \int_0^t \dot{C}_1^*(t)dt + \int_0^t \left(\frac{\partial \dot{C}_1^*(t)}{\partial u_{21}(t)} \right) \Delta u_{21}(t)dt + \int_0^t \left(\frac{\partial \dot{C}_1^*(t)}{\partial u_{12}(t)} \right) \Delta u_{12}(t)dt \right) \\ &= \sum_{t=1}^{\tau}\left(C_2 + C_1^* + \int_0^t \left(\frac{\partial \dot{C}_1^*(t)}{\partial u_{21}(t)} \right) \Delta u_{21}(t)dt + \int_0^t \left(\frac{\partial \dot{C}_1^*(t)}{\partial u_{12}(t)} \right) \Delta u_{12}(t)dt \right) \end{aligned} \tag{3.40}$$

w.r.t. $\vec{x}_2, \vec{y}_{2t}, \vec{K}_2$ and subject to a known set of constraints

where the dynamic shadow price rate based on the dynamic restricted local (unit-based) optimum cost rate and coupling function is defined as

$$\dot{\lambda}_{ij}^i = \dot{\lambda}_{ij}^i(u_{ij}, t) \equiv \left(\frac{\partial \dot{C}_i^*(t)}{\partial u_{ij}(t)} \right) \tag{3.41}$$

With this in mind, problems (3.39) and (3.40) simplify to

Unit 1:

$$C_1^{'} = \sum_{t=1}^{\tau}\left(C_1 + C_2^{*} + \int_0^t \dot{\lambda}_{12}^2(u_{12},t)\Delta u_{12}(t)dt + \int_0^t \dot{\lambda}_{21}^2(u_{21},t)\Delta u_{21}(t)dt \right) \tag{3.42}$$

w.r.t. $\vec{x}_1, \vec{y}_{1t}, \vec{K}_1$

subject to

$$\vec{h}_{1t} = \vec{0} \tag{3.42.2}$$

$$\vec{g}_{1t} \le \vec{0} \tag{3.42.3}$$

Unit 2:

$$C_2^{'} = \sum_{t=1}^{\tau}\left(C_2 + C_1^{*} + \int_0^t \dot{\lambda}_{21}^1(u_{21},t)\Delta u_{21}(t)dt + \int_0^t \dot{\lambda}_{12}^1(u_{12},t)\Delta u_{12}(t)dt \right) \tag{3.43}$$

w.r.t. $\vec{x}_2, \vec{y}_{2t}, \vec{K}_2$

subject to

$$\vec{h}_{2t} = \vec{0} \tag{3.43.2}$$

$$\vec{g}_{2t} \le \vec{0} \tag{3.43.3}$$

where, for example, for the two unit system of problem (3.42) and (3.43)

$$\Delta u_{12t} = \nabla_{x_1}\left(u_{12t}\right)^T \Delta\vec{x}_1 + \nabla_{y_{1t}}\left(u_{12t}\right)^T \Delta\vec{y}_{1t} + \nabla_{K_1}\left(u_{12t}\right)^T \Delta\vec{K}_1 \tag{3.44}$$

In general the effect of the decision variables on the coupling functions is given by

$$\Delta u_{ijt} = \nabla_{x_i}\left(u_{ijt}\right)^T \Delta\vec{x}_i + \nabla_{y_{it}}\left(u_{ijt}\right)^T \Delta\vec{y}_{it} + \nabla_{K_i}\left(u_{ijt}\right)^T \Delta\vec{K}_i \tag{3.45}$$

In addition, the additional set of constraints

$$\Delta u_{ij\,t} - \varepsilon\ \Delta u_{ij\,t\max} \le 0 \tag{3.46}$$

are imposed. In this expression, $\Delta u_{ijt\max}$ are the maximum allowable values for the coupling functions and the factor ε is added to ensure that the linear Taylor series expansions are a good local representation of the optimum response surface.

The definition of dynamic shadow price rate (equation (3.41)) and its utilization in the dynamic system-level, unit-based optimization Problems (3.42) and (3.43) is well suited for handling the optimization of highly dynamic systems for which no quasi-stationary state assumption can be made. However, the computation of the actual value of the dynamic shadow price rates may become rather time consuming if the system at hand has a very fast dynamic behavior or the transient segments make up most of the load profile. If this is the case it may be useful to define a shadow price not in terms of a dynamic shadow price rate but instead in term of a shadow price based on the integral of coupling function change over time. To do this one defines the total coupling function over time U_{ij} as

$$U_{ij} = \int_0^t u_{ij}(t)dt \tag{3.47}$$

so that the total coupling function change over time based on the optimal coupling function value at the end of a operational segment is written as

$$\Delta U_{ij} = U_{ij}^* - U_{ij} = \int_0^t \left(u_{ij}^*(t) - u_{ij}(t)\right)dt \tag{3.48}$$

with this definition a shadow price based on the change of the total optimal cost over time with respect to the total coupling function over time, U_{ij} is given by

$$\Lambda_{ij}^{i} \equiv \frac{\partial C_i}{\partial U_{ij}} \tag{3.49}$$

The integral system-level, unit-based objective optimization problems corresponding to these new definition can be expressed as

Unit 1:

Minimize

$$C_1^{'} = \sum_{t=1}^{\tau}\left((C_1)_t + (C_2^*)_t + \left(\frac{\partial C_2^*}{\partial U_{12}}\right)_t \Delta U_{12t} + \left(\frac{\partial C_2^*}{\partial U_{21}}\right)_t \Delta U_{21t}\right)\Delta\tau_t \tag{3. 50}$$

w.r.t. $\vec{x}_1, \vec{y}_{1t}, \vec{K}_1$

subject to

$$\vec{h}_{1t} = \vec{0} \tag{3. 50.2}$$

$$\vec{g}_{1t} \le \vec{0} \tag{3. 50.3}$$

Unit 2:

Minimize

$$C_2^{'} = \sum_{t=1}^{\tau} \left((C_2)_t + (C_1^*)_t + \left(\frac{\partial C_1^*}{\partial U_{21}} \right)_t \Delta U_{21t} + \left(\frac{\partial C_1^*}{\partial U_{12}} \right)_t \Delta U_{12t} \right) \Delta \tau_t \tag{3. 51}$$

w.r.t. $\vec{x}_2, \vec{y}_{2t}, \vec{K}_2$

subject to

$$\vec{h}_{2t} = \vec{0} \tag{3. 51.2}$$

$$\vec{g}_{2t} \le \vec{0} \tag{3. 51.3}$$

where in general the effect of the decision variables on the total coupling functions over time is given by

$$\Delta U_{ijt} = \nabla_{x_i} \left(U_{ijt} \right)^T \Delta \vec{x}_i + \nabla_{y_{it}} \left(U_{ijt} \right)^T \Delta \vec{y}_{it} + \nabla_{K_i} \left(U_{ijt} \right)^T \Delta \vec{K}_i \tag{3. 52}$$

In addition to the above constraints, the additional constraints

$$\Delta U_{ij_t} - \varepsilon \, \Delta U_{ij_{t\max}} \le 0 \tag{3.52}$$

are imposed upon the problem. In expression (3.53), the $\Delta U_{ij_{t\max}}$ are the maximum allowable values for the total coupling functions changes over time and the factor ε is added to ensure that the linear Taylor series expansions are a good local representation of the integral optimum response surface. It is readily seen that one of the advantages of ILGO and DLGO is that the $\vec{x}_1$ and $\vec{y}_{1t}$ may be chosen so that the internal constraints (both the models system of equations and the desired unit's products or tasks) are met.

Finally, this latter formulation, Problem (3.50) and (3.51), is recommended when conceptual decomposition is used because a unit's cost for each operational segment is a value which falls directly out of the solution of the optimization problem. The main

disadvantage of this particular formulation is the fact that the duration time may not be a fixed parameter for some segments.

3.6 Some Final Comments and Discussion

3.6.1 Model Complexity, Reliability, and Development

It is necessary to remain open-minded in relation to the level of complexity of dynamic models. A very detailed dynamic model necessarily requires longer execution time, and, the time required to build the model is longer. In addition, the more detailed the model is, the more difficult it is for the simulation to converge for all possible scenarios.

Simplified, reduced order, dynamic models, on the other hand, do not capture real system behavior through the whole range of operational variables, initial conditions, and disturbances. Therefore, from an engineering point of view, the trade-offs between less or more detail should be closely looked at before model development begins. Furthermore, the computational tools used to solve the dynamic model should be carefully selected according to the problem at hand. A dynamic model tool is required (e.g., Simulink, gProms, ect.) and should be chosen according to the model size, type of dynamic equations (e.g., exponential terms in PDE systems are not easy to solve), optimization approach to be followed, and the available optimization software.

3.6.2 Choice of Coupling function Quantities

Coupling functions can be expressed in terms of thermodynamic or flow quantities or even non-energy based quantities. The choice of quantities depends on how the total objective behaves with respect to the system's coupling functions (i.e. the optimum response surface) when represented in terms of any of the candidate quantities (e.g., energy, exergy, thrust, negentropy, mass flow, etc.). Based on the work by Muñoz and von Spakovsky (1999; 2000a,b,c) and by Rancruel and von Spakovsky (2002), the following comments are made:

- When dealing with dynamic systems optimization, an additional variable must be considered when constructing the ORS. Both the system total cost and the coupling functions are time dependent. However, it is not possible to show the systems total objective function evolution as a function of time for more than one coupling function. In order to show this behavior, a new definition of the ORS is introduced by defining the total objective function in terms of the integral over time of the coupling functions (i.e. $C_T = f(\vec{U}_{ij})$).

- If the ORS is smoothly convex (or concave) the ILGO or DILGO approach necessarily leads to the "global" optimum;

- Linear or almost linear behavior of the ORS increases the convergence speed of the algorithm. Of course, if this is not the case, linearization or piecewise linearization are possible. A technique which has been used by a number of researchers (e.g., Frangopoulos, 1984, von Spakovsky, 1986). However, linearization comes with an inherent loss of information.

Chapter 4

Total System Description and Synthesis/Design Problem Definition

4.1 Fuel Cell Systems

The fuel cell is an electrochemical device, which converts the chemical energy of a fuel and an oxidant into electric power. Its benefits are that the electric power is generated at high energy efficiency and with very low environmental emissions. For the last thirty years, federal and private industrial support to develop fuel cell technologies has been considerable. The use of fuel cell systems has been strongly promoted in the United States and in Japan for medium scale cogeneration plants. Nowadays, this interest has been extended to a smaller scale, namely, that at the residential level. At the same time, increased interest has arisen for the application of fuel cell systems to automotive propulsion and auxiliary power unit applications, although there is not yet a clear choice on the direct use of hydrogen stored on-board or the installation of a hydrogen generating plant on-board (Azevedo et al., 2000). The present research work is focused on the use of this newly emerging technology for auxiliary power unit applications for both stationary (residential) and transport (trucks) applications.

4.1.1 Historical Development of Fuel Cell Technology

In 1839, William Robert Grove, a British jurist and amateur physicist, first discovered the principle of the fuel cell. Grove utilized four large cells, each containing hydrogen and oxygen, to produce electric power which was then used to split the water in the smaller upper cell into hydrogen and oxygen. However, it was Ludwig Mond and Charles Langer who first used the term "fuel cell" in 1889, when they tried to build a

power generating device using air and industrial coal gas. It was not until 1932 that Francis Bacon developed the first successful fuel cell. It would take another 27 years to apply their invention to a practical application, a 5 kWe system capable of powering a welding machine. More recently, NASA used fuel cells during the 1960's to power on-board electronics for the Gemini and Apollo spacecraft. In fact, NASA still uses fuel cells to provide electricity and water for its space shuttle missions.

Today, fuel cells are on a trajectory to break through economic and technical barriers in a multitude of applications ranging from portable devices to homes and vehicles. For energy providers, fuel cells offer a safe, efficient, and reliable power solution that addresses critical issues such as deregulation, rising energy costs, increasing load factors, severe power outages, and increasing power consumption. For vehicle manufacturers, fuel cells represent the single greatest technology advancement in the last 100 years to replace the internal combustion engine and address growing environmental concerns over issues such as global warming and air pollution.

4.1.2 Fuel Cells for Stationary and Transport Applications

In the recent years, more awareness has been given to clean energy concepts. Fuel cells, with their dramatically reduced emissions, few moving parts, and high electric energy conversion efficiency at full and especially at partial load, seem to be ideally suited for a variety of stationary applications in urban centers and metropolitan areas. The stationary applications that are of greatest interest today concern small- and medium-scale plants for combined heat and power generation, especially in situations where reliability of supply is important (i.e. hospitals, hotels, etc).

The four major fuel cell technologies for stationary power generation are the following:

- Phosphoric Acid Fuel Cell (PAFC) systems.
- Molten Carbonate Fuel Cell (MCFC) systems.
- Solid Oxide Fuel Cell (SOFC) systems.
- Polymer Electrolyte Membrane Fuel Cell (PEMFC) systems.

At present, the most developed or mature of them is the PAFC system, which has reached the stage of commercial use for stationary applications. For example,

International Fuel Cells, with its subsidiary ONSI, began manufacturing 200 kW_e PAFC stationary cogeneration systems in 1992 (Kordesch and Simader, 1996).

The MCFC system represents a potentially less expensive solution, with costs that can be one third or one fourth of those for the PAFC (Escombe, 1995). The main problem presently being investigated is the durability of the electrodes and of the cells, which is still about 8000 hours against a target of at least 20,000 hours. Investigations on alternative cathode materials and on doping of the electrolyte are being carried out (Lane et al., 1995).

SOFC systems have some strategic interest especially because their operation at high temperature (1000°C) allows the use of a wide variety of fuels (Escombe, 1995). In the U.S., they have followed essentially three paths. The tubular design of Siemens Westinghouse with 1 to 2 m long tubes, external fuel gas feed (anode), an internal cathode, and yttrium-stabilized zirconium forming the solid electrolyte structure. A monolithic design (a corrugated sequence of electrodes and electrolyte) is used by Allied Signal Corporation (now General Electric). Other companies are developing a thin planar disk arrangement.

PEMFC technology has had a very rapid development in the last several years. It has been successfully implemented for aerospace applications (Kordesch and Simader, 1996) and is seen now as potentially interesting for stationary power generation applications. While large utility applications are envisioned as belonging to the MCFC and SOFC, there are many applications such as utility peak power generation and dispersed distributed power generation for which the PEMFC will probably compete directly with the PAFC. In the long term and in light of recent advancements, the life-cycle cost of the PEMFC system could be more favorable (Wilson et al., 1996). Ballard Power Systems Inc. has developed PEMFC demonstration units of 30 kW_e (hydrogen fueled) and 10 kW_e (natural gas fueled). The 10 kW_e PEMFC unit with compact natural gas reformer was the first integrated PEMFC unit to be operated with natural gas (Wurster, 1997). Until recently, large-scale production of PEMFCs was inhibited by the large amounts of high cost materials required. However, due to design and integration improvements, overall PEMFC system costs have as of today been substantially reduced, making commercialization feasible.

The electric efficiencies of these four different types of fuel cell technologies can be considerably higher than those achievable with gas motors or gas turbines, an aspect especially important for power production with the lowest emissions of pollutants and noise. The following table (Table 4.1) provides an overview of the fields of application foreseen for the four types of fuel cells as well as a comparison of the electric, thermal, and total system efficiencies that can be achieved.

Table 4.1. Comparison of fuel cell technologies for stationary applications (Wurster, 1997).

Criterion	PAFC	PEMFC	MCFC	SOFC
Utilizable Type of Energy	- Electricity - Heat	- Electricity - Heat	- Electricity - Heat - Steam	- Electricity - Heat - Steam
Electrical Efficiency	40% – 45%	≤ 50%	50% – 55%	50% – 60%
Thermal Efficiency	45%	≤ 40%	> 40%	> 40%
Utilization Ratio	85% – 90%	80% – 90%	> 90%	> 90%
Electric to Thermal Energy Ratio	≈ 1	≈ 1.2	≈ 1.4	≈ 1.5
Application	Commercial Cogeneration	Domestic and Commercial Cogeneration	Commercial and Industrial Cogeneration Power Plants	Domestic, Commercial and Industrial Cogeneration Power Plants

Commercial and industrial facilities will probably take the lead in implementing fuel cell systems. According to the Gas Research Institute (GRI), approximately 18,000 MW_e of the power market in the U.S. should be economical for fuel cell cogeneration systems, provided the installed cost is $1000/kW. The industrial sector is similar to the commercial sector in size and required fuel cell characteristics. Approximately 10% of this potential market is for small (less than 1 MW_e) cogeneration systems. Since waste heat is at a premium in these applications, fuel cells may need to operate as a cogeneration system in order to be competitive (Cleghorn et al., 1996).

Since the late 1980s, there has been a strong push to develop fuel cells for use in light-duty and heavy-duty vehicle propulsion. A major drive for this development is the need for clean, efficient cars, trucks, and buses that can operate on conventional fuels (gasoline, diesel), as well as renewable and alternative fuels (hydrogen, methanol, ethanol, natural gas, and other hydrocarbons).

With hydrogen as the on-board fuel, such vehicles would be zero emission vehicles. With on-board fuels other than hydrogen, the fuel cell systems would use an appropriate fuel processor to convert the fuel to hydrogen, yielding vehicle power trains with very low acid gas emissions and high efficiencies. Further, such vehicles offer the advantages of electric drive and low maintenance because of the few critical moving parts. This development is being sponsored by various governments in North America, Europe, and Japan, as well as by major automobile manufacturers worldwide. Several fuel cell-powered cars, vans, and buses have operated on hydrogen and methanol.

In the early 1970s, K. Kordesch modified a 1961 Austin A-40 two-door, four-passenger sedan to an air-hydrogen fuel cell/battery hybrid car. This vehicle used a 6-kW alkaline fuel cell in conjunction with lead acid batteries and operated on hydrogen carried in compressed gas cylinders mounted on the roof. The car was operated on public roads for three years and about 21,000 km. In 1994 and 1995, H-Power (Belleville, New Jersey) headed a team that built three PAFC/battery hybrid transit buses. These 9 meter (30 foot), 25 seat (with space for two wheel chairs) buses used a 50 kW fuel cell and a 100 kW, 180 amp-hour nickel cadmium battery.

The major activity in transportation fuel cell development has focused on the polymer electrolyte fuel cell (PEFC). In 1993, Ballard Power Systems (Burnaby, British Columbia, Canada) demonstrated a 10 m (32 foot) light-duty transit bus with a 120 kW fuel cell system, followed by a 200 kW, 12 meter (40 foot) heavy-duty transit bus in 1995. These buses use no traction batteries. They operate on compressed hydrogen as the on-board fuel. In 1997, Ballard provided 205 kW (275 HP) PEFC units for a small fleet of hydrogen-fueled, full-size transit buses for demonstrations in Chicago, Illinois, and Vancouver, British Columbia. Working in collaboration with Ballard, Daimler-Benz built a series of PEFC-powered vehicles, ranging from passenger cars to buses. The first such vehicles were hydrogen-fueled. A methanol-fueled PEFC Aclass car unveiled by

Daimler-Benz in 1997 has a 640 km (400 mile) range. Plans are to offer a commercial vehicle by 2004. A hydrogen-fueled (metal hydride for hydrogen storage), fuel cell/battery hybrid passenger car was built by Toyota in 1996, followed in 1997 by a methanol-fueled car built on the same (RAV4) platform.

In February 2002, UTC Fuel Cells and Nissan signed an agreement to develop fuel cells and fuel cell components for vehicles. Renault, Nissan's alliance partner, is also participating in the development projects. UTC Fuel Cells will provide proprietary ambient-pressure proton exchange membrane fuel cell technology. Ballard's fuel cell engine powered DaimlerChrysler's NECAR 5 fuel cell vehicle in a 13-day, 3,000-mile endurance test across the United States. The drive provided Ballard and DaimlerChrysler with testing experience in a variety of conditions. Toyota Motor Corp. and Honda Motor Co. have announced they will advance their initial vehicle introduction plans for fuel cell vehicles to late in 2002 from 2003. Honda achieved a significant milestone for its product launch by receiving both CARB and EPA certification of its zero emission FCX-V4 automobile. This is the first vehicle to receive such certification. Ballard's fuel cell powered this Honda vehicle.

Other major automobile manufacturers, including General Motors, Volkswagen, Volvo, Chrysler, Nissan, and Ford, have also announced plans to build prototype polymer electrolyte fuel cell vehicles operating on hydrogen, methanol, or gasoline. IFC and Plug Power in the U.S., and Ballard Power Systems of Canada are involved in separate programs to build 50 to 100 kW fuel cell systems for vehicle motive power. Other fuel cell manufacturers are involved in similar vehicle programs. Some are developing fuel cell-powered utility vehicles, golf carts, etc.

The application of fuel cells in the space program (1 kW PEFC in the Gemini program and 1.5 kWe AFC in the Apollo program) was demonstrated in the 1960s. More recently, three 12 kWe AFC units have been used for at least 87 missions with 65,000 hours flight time in the Space Shuttle Orbiter. In these space applications, the fuel cells use pure reactant gases. IFC has produced a H2/O2 30 kWe unit for the Navy's Lockheed Deep Quest vehicle. It operates at depths of 1500 meters (5000 feet). Ballard Power Systems has produced an 80 kWe PEFC unit for submarine use (methanol fueled) and for portable power systems.

4.1.3 Fuel Cell Auxiliary Power Systems

In addition to high-profile fuel cell applications such as automotive propulsion and distributed power generation, the use of fuel cells as auxiliary power units (APUs) for vehicles and residencies has received considerable attention (Fuel Cell Handbook, 2204). APU applications may be an attractive market because it offers a true mass-market opportunity that does not require the challenging performance and low cost required for propulsion systems for vehicles. In this section, a discussion of the technical performance requirements for such fuel cell APUs, as well as the current status of the technology and the implications for fuel cell system configuration and cost is given. Even though the term APU is generally use for mobile applications in this doctoral work the DOE terminology is applied, i.e. the term is used equally for both mobile and stationary applications. Auxiliary power units are devices that can provide all or part of the non-propulsion power for vehicles or all the power required by a residence. Such units are already in widespread use in a range of vehicle types and for a variety of applications, in which they provide a number of potential benefits (see Figure 4,1). Although each of these applications could provide attractive future markets for fuel cells, this research work will focus on applications to on-road vehicles (specifically trucks) and single residence applications.

Vehicles Types	Loads Serviced	Potential Benefits
• Heavy-duty & utility trucks • Airplanes • Trains • Yachts & Ships • Recreational vehicles • Automobiles & light trucks (not commercial yet)	• Space conditioning • Refrigeration • Lighting and other cabin amenities • Communication and information equipment • Entertainment (TV, radio)	• Can operate when main engine unavailable • Reduce emissions and noise while parked • Extend life of main engine • Improve power generation efficiency when parked

Figure 4.1. Overview of APU for transportation applications (Fuel Cell Handbook, DOE/NETL 2002).

In 1997, the Office of Naval Research initiated an advanced development program to demonstrate a ship service fuel cell power generation module. The ship

service generator supplies the electrical power requirements of the ship. This program will provide the basis for a new fuel cell-based design that will be an attractive option for the future Navy surface ships. This program will provide the Navy with a ship service that is more efficient and incorporates a distributive power system that will remain operating even if the engine is destroyed.

Fuel cells can serve as a generator, battery charger, battery replacements and heat supply. They can adapt to most environments, even locations in Arctic and Antarctic regions. One effort, being run in collaboration with the Army Research Office, has demonstrated a prototype fuel cell designed to replace in many applications a popular military standard battery.

The target application is the Army's BA-5590 primary (i.e., use-once-and-dispose) lithium battery. The Army purchases approximately 350,000 of these batteries every year at a cost of approximately $100 per battery, including almost $30 per battery for disposal. Fuel cells, on the other hand, are not thrown away after each use but can be reused hundreds of times. Mission weight savings of factors of 10 or more are projected. The prototype fuel cell, which has the same size and delivers the same power as a battery, has been tested in all orientations and under simulated adverse weather conditions, and was enthusiastically received by Army senior management.

General Electric has developed a 5-kW prototype of a SOFC power system for stationary application (Minh, 2004). The system consists of all the required components for a self-contained unit, including SOFC stack, fuel processing sub-system, fuel and oxidant delivery sub-system, thermal management sub-system, and control sub-system. The concept is in a testing stage.

System Performance Requirements

A key reason for interest in fuel cell APU applications is that there may be a good fit between APU requirements and fuel cell system characteristics. Fuel cells can be efficient and quiet, and APUs do have the load following requirements and physical size and weight constraints associated with propulsion applications. However, in order to understand the system requirements for fuel cell APUs, it is critical to understand the required functionality (refer to Figure 4.2) as well as competing technologies. To provide

the functionality of interest and to be competitive with internal combustion engine (ICE) driven APUs, fuel cell APUs must meet various requirements; an overview is provided in Figure 4.2.

Key Parameter	Typical Requirements	Expected fuel cell performance
Power output	12 – 42 V DC is acceptable for most applications, 110 / 220 V AC may be desirable for powering power tools etc.	DC power output simplifies the power conditioning and control for fuel cells
System Capacity	1 – 5 kW for light duty vehicles and truck cabins up to 15 kW for truck refrigeration	Fits expected range for PEFCs and probably also advanced SOFCs
System Efficiency	More than 15-25% based on LHV	Efficiency target should be achievable, even in smallest capacity range
Operating life and reliability	Greater than about 5,000 hours stack life, with regular service intervals less than once every 1,000 hours	Insufficient data available to assess whether this is a challenge or not

Figure 4.2. Overview of typical system requirements (Fuel Cell Handbook, 2002).

Fuel cell APUs for transportation will likely have to operate on gasoline and for trucks preferably on diesel fuel in order to match the infrastructure available and preferably be able to share on-board storage tanks with the main engine. For residential applications the fuel of choice would be natural gas. The small amount of fuel involved in fueling APUs would likely not justify the establishment of a specialized infrastructure (e.g., a hydrogen infrastructure) for APUs alone. Similarly, fuel cell APUs should be water self-sufficient, as the need to carry water for the APU would be a major inconvenience to the operator and would require additional space and associated equipment. In addition to the requirement for stationary operation mentioned in Figure 4.2, fuel cell APUs must be able to provide power rapidly after start-up and must be able to effectively follow loads. While the use of batteries to accomplish this is almost a given, a system start-up time of about ten minutes or less will likely be required to arrive at a reasonable overall package. Finally, fuel cell APUs are clean. These attributes may well be the key competitive advantage that fuel cell APUs have over conventional APUs, and hence their performance must more than match that of internal combustion engines APUs.

Technology Status

Active technology development efforts in both PEFC and planar SOFC technology, driven primarily by the interest in distributed generation and automotive propulsion markets, have achieved significant progress in the development of these technologies. For distributed power applications, refined and even early commercial prototypes are being constructed. However, in the case of planar SOFC a distinction must be made between different types of SOFC technologies. Neither the tubular nor the electrolyte supported SOFC technology is suitable for APU applications due to their very high operating temperature, large size, and weight. Only the electrode supported planar SOFC technology may be applicable to APU applications. Since it has only been developed over the past nine years, as opposed to several decades for the PEFC and other SOFC technologies, it has not developed as far, although it appears to be catching up quickly (see Figure 4.3). Most importantly, SOFC offer the advantage over PEFC that the fuel processing sub-system is much simpler, requiring less components and demanding less space.

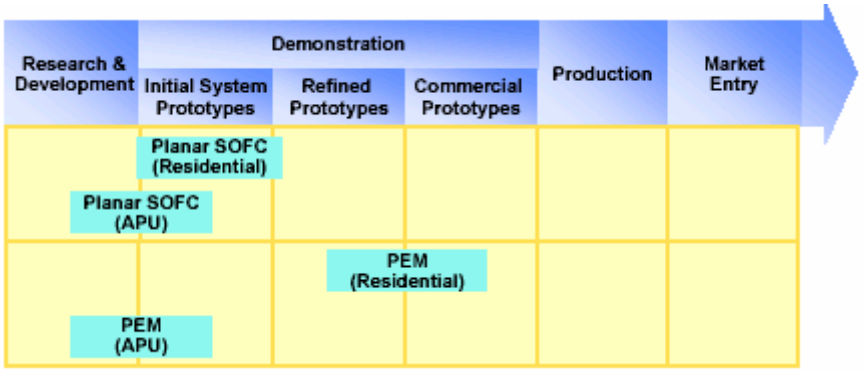

Figure 4.3. Stage of development for fuel cells for APU applications (Fuel Cell Handbook, 2002).

Fuel cell APU applications could benefit significantly from the development of stationary generation systems, especially from residential scale systems, because of the similarity in scale and duty cycle. In fact, stationary generation systems are designed mostly for operation on natural gas and do not face as stringent weight and volume requirements as APU transportation applications. As a result, fuel cell APUs are in the early initial system prototype stage.

Several developers, including Nuvera, Honeywell, and Plug Power are active in the development for residential PEFC power systems. Most of the PEFC system technology can be adapted for APU applications, except that a fuel processor capable of handling transportation fuels is required. However, most of the players in the residential PEFC field are also engaged in the development of PEFC systems for automotive propulsion applications, which are targeting the ability to utilize transportation fuels for PEFC systems.

Relatively few developers of SOFC technology have paid attention to non-stationary markets. All are focused on small- to medium-sized distributed generation and on-site generation markets. Only Global Thermoelectric (Calgary, Canada) has been active in the application of its technology to APUs. A recent study conducted a detailed conceptual design and cost estimate of a 5-kWnet SOFC-based truck APU and concluded that, provided improvement in several technology areas continued, planar SOFCs could ultimately become a realistic option for this mass-market application.

System Configuration and Technology Issues

Based on the system requirements discussed above, fuel cell APUs will consist of a fuel processor, a stack system, and the balance of plant. Figure 4.4 lists the components required in SOFC and PEFC based systems. The components needed in a PEFC system for APU applications are similar to that needed in distributed power. The main issue for components for PEFC-based systems is the minimization or elimination of the use of external supplied water. For both PEFC and SOFC systems, start-up batteries (either existing or dedicated units) will be needed since external electric power is not available. Detailed cost and design studies for both PEFC and SOFC systems at sizes ranging from 5 kW to 1 MW were made that point to the fundamental differences between PEFC and SOFC technology that impact the system design and by implication the cost structure. These differences will be discussed in the following paragraphs.

The main components in a SOFC APU are the fuel cell stack, the fuel processor, and the thermal management system. In addition, there are several balance of plant components, which are listed in Figure 4.4. The relatively simple reformer design is possible because the SOFC stack operates at high temperatures (around 800°C) and is

capable of utilizing both carbon monoxide and certain hydrocarbons as fuel. Since both the anode and cathode exhaust at temperatures of 600-850°C, high temperature recuperators are required to maintain system efficiency. These recuperators are made of expensive materials (due to a high temperature reducing and oxidizing atmosphere), making it an expensive component in the system. However, if hydrocarbons are converted inside the stack, this leads to a less exothermic overall reaction so that the stack cooling requirements are reduced. However, internal reforming produces undesired thermal gradients in the stack, which are aggravated during transient operation. Current materials have constraints on the temperature gradients they can support. Therefore, in this doctoral work, the internal reformer is eliminated in order to favor the dynamic response.

Further system simplification would occur if a sulfur-free fuel were used or if the fuel cell were sulfur tolerant. In that case, the fuel can be provided directly from the reformer to the fuel cell. In order to minimize system volume (and minimize the associated system weight and start-up time), integration of the system components is a key design issue.

Figure 4.5 shows a simplified layout for an SOFC-based APU. The air for reformer operation and cathode requirements is compressed in a single compressor and then split between the unit operations. Unreacted anode tail gas is recuperated in a tail gas burner. Additional energy is available in a SOFC system from energy recovery from tail gas effluent streams that are typically 400-600°C. Current thinking is that reformers for transportation fuel based SOFC APUs will be of the exothermic type (i.e. partial oxidation or autothermal reforming), as no viable steam reformers are available for such fuels.

The power requirements for auxiliary power applications require smaller fuel cell stack duties. The heat losses for a SOFC stack operating at a smaller power duty are a larger proportion of the gross rating than in a stationary power application. Insulation, required for specified system skin temperature requirements, could conceivably result in a large proportion of the total system volume. Integration of the high temperature components is important in order to reduce the system volume and insulation

requirements. SOFC APU systems will require inexpensive high performance insulation materials to decrease both system volume and cost.

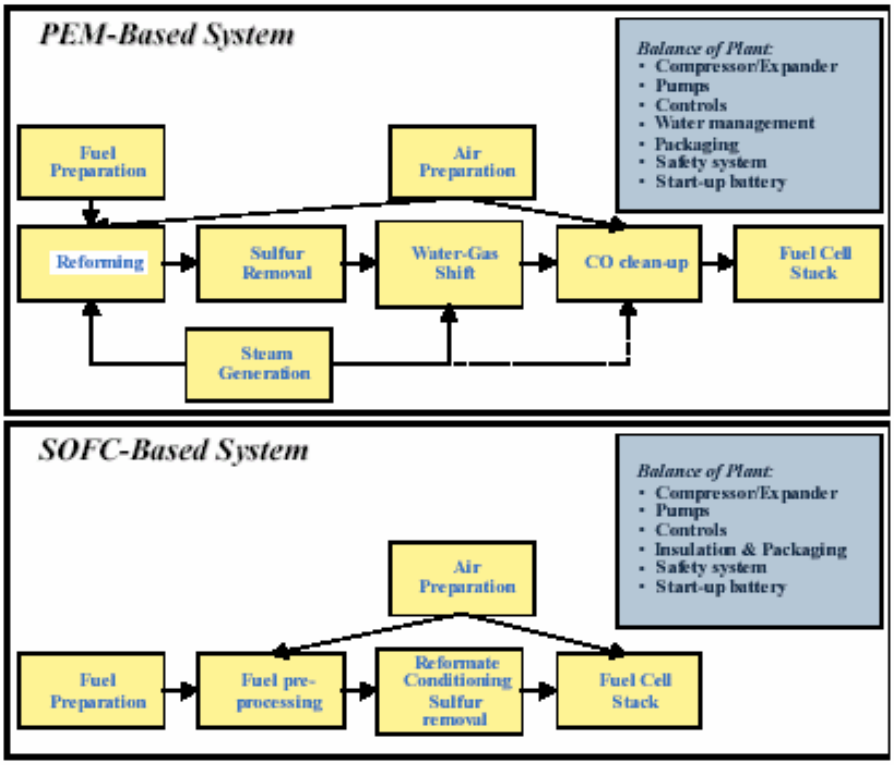

Figure 4.4. Overview of subsystems and components for SOFC and PEFC systems (Fuel Cell Handbook 2002).

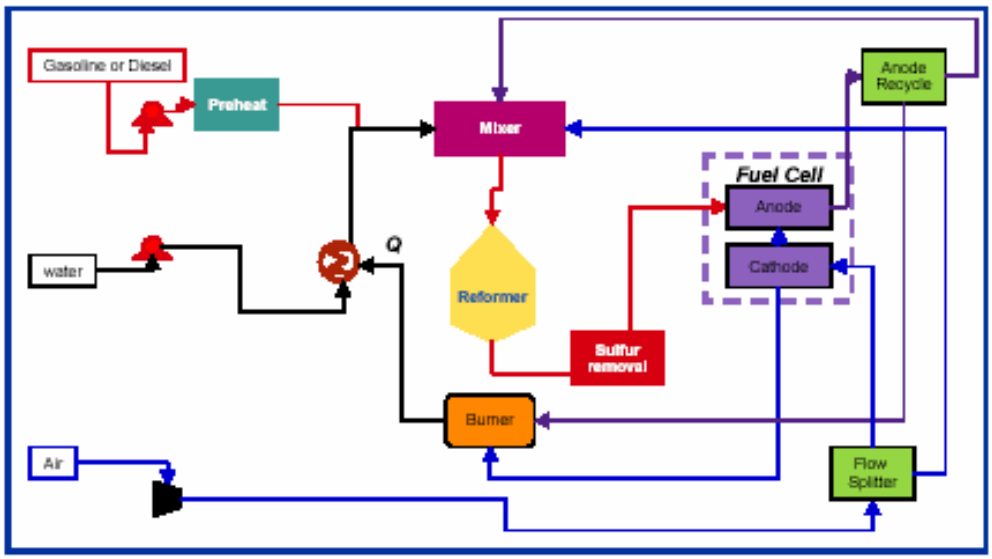

Figure 4.5. Simplified System process flow diagram of pre-reformer/SOFC system (Fuel Cell Handbook 2002).

As to the operating requirements of PEFC stack technology, shift reactors and a carbon monoxide removal step are required to produce reformate of sufficient quality. Similarly, the stack operating temperature and its humidity requirements require a water management system as well as radiators for heat rejection. Some developers are developing pressurized systems to benefit from higher reactant partial pressures on both anode and cathode. Fuel processing for PEFC APU systems is identical to that needed in distributed power or propulsion applications. The additional issue for the PEFC is the minimization of the steam needed for the fuel processor system. Since an APU is a mobile and/or remote (independent) unit, the need for external sources of water should be minimized. In addition, the reformate stream is further diluted by additional steam if that water is not removed prior to the fuel cell stack.

Another design integration issue in PEFC systems is water management for hydrating the electrolyte and providing the necessary steam for reforming and water-gas shift operations. Additional steam may be required for the CO clean-up device. Some reformate-based PEFC systems are run under pressure to increase the partial pressure of reactants for the PEFC anode and cathode, increasing efficiency. Pressure operation also aids in heat integration for the internal generation of steam at pressures greater than atmospheric (i.e. steam generated at temperatures greater than 100°C). PEFC system integration involves the integration of a reformer (either exothermic or endothermic overall, ~850-1000°C), shift reactors (exothermic, 150-500°C), CO-cleanup (primarily exothermic, 50-200°C), and the fuel cell stack (exothermic, 80°C). Each reaction zone operates at a significantly different temperature, thus, providing a challenge for system integration and heat rejection. To alleviate some of these drawbacks, and further reduce the cost of the PEFC systems, developers are now investigating the possibility of using higher temperature membranes (e.g. operating slightly above 100°C). This would increase the carbon monoxide tolerance, potentially simplifying the fuel processor design as well as simplifying the heat rejection.

System Cost Considerations

As for any new class of product, total cost of ownership and operation of fuel cells will be a critical factor in their commercialization, along with the offered

functionality and performance. This total cost typically has several components for power systems such as fuel cells. These components include fuel cost, other operating costs such as maintenance cost, and the first cost of the equipment. This first cost has a significant impact on fuel cells' competitiveness. The main component of a fuel cell's first cost is the manufacturing cost, which is strongly related to the physical configuration and embodiment of the system, as well as to the manufacturing methods used. System configuration and design in turn are directly related to the desired system functionality and performance, while the manufacturing methods used are strongly linked to the anticipated production volume.

The main difference in SOFC stack cost structure as compared to PEFC cost relates to the simpler system configuration of the SOFC-based system. This is mainly due to the fact that SOFC stacks do not contain the type of high-cost precious metals that PEFCs contain. This is off-set in part by the relatively complex manufacturing process required for the manufacture of the SOFC electrode-electrolyte plates and by the somewhat lower power density in SOFC systems. Low temperature operation (enabled with electrode supported planar configurations) enables the use of low cost metallic interconnects which can be manufactured with conventional metal forming operations.

The balance of plant contains all the direct stack support systems, reformer, compressors, pumps, and the recuperating heat exchangers. Its cost is low by comparison to the PEFC because of the simplicity of the reformer. However, the cost of the recuperating heat exchangers partially offsets that. To provide some perspective on the viability of SOFCs in APU applications from a cost perspective, NETL sponsored an estimate of the cost structure of small-scale (5 kW), simple cycle SOFC, anode-supported system operated on gasoline. The estimated manufacturing cost for such systems (see Figure 4.6) could well be close to that estimated for comparable PEFC systems, while providing somewhat higher system efficiency. While the stack, insulation and stack balance in this simple-cycle system is a key component, the balance of plant is also an important factor. The stack cost again mainly depends on the achievable power density. Small systems like these will likely not be operated under high pressure. While this simplifies the design and reduces cost for compressors and expanders (which are not readily available at low cost for this size range in any case) it might also negatively affect

the power density achievable. Furthermore, one of the key challenges with small-scale SOFC systems is to overcome heat losses. The higher the heat losses are, the higher the cost since more recuperation is required to maintain the fuel cell within an acceptable operating temperature range and hence to ensure good performance.

Finally, the large fraction of cost related to balance of plant issues is mainly due to the very small scale of these types of systems, which results in a significant reverse economy of scale. While design work is still ongoing, it is anticipated that the cost structure of this system will change rapidly to reduce the cost of the balance of plant further, and further improve the competitiveness of these systems.

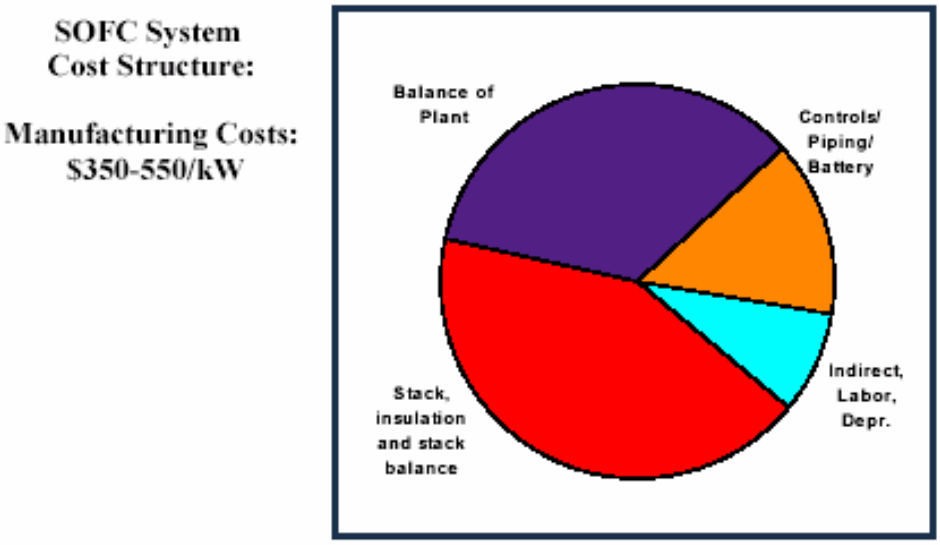

Figure 4.6. Projected cost structure of a 5kWnet APU SOFC system with gasoline fueled POX reformer, fuel cell operating at 300mW/cm^2, 0.7 V, 90 % fuel utilization, and 500,000 units per year production volume (Fuel Cell Handbook, 2002).

Outlook and Conclusions

In conclusion, both PEFCs and SOFCs have the potential to meet the allowable cost targets, provided successful demonstrations prove the technology. It is critical, however, that for the current technologies to be commercially successful, especially in small-capacity markets, high production volumes be reached. APU applications might provide such markets. It is similarly critical that the technologies be demonstrated to perform and achieve the projected performance targets and demonstrate long life. These are the challenges ahead for the fuel cell industry in the APU market segment.

Derivative Applications

Because of the modular nature of fuel cells, they are attractive for use in small portable units, ranging in size from 5 We or smaller to 100 We power levels. Examples of uses include the Ballard fuel cell, demonstrating 20 hours of operation of a portable power unit, and an IFC military backpack. There has also been technology transfer from fuel cell system components. The best example is a joint IFC and Praxair, Inc. venture to develop a unit that converts natural gas to 99.999% pure hydrogen based on using fuel cell reformer technology and a pressure swing adsorption process.

4.2 Balance of Plant Description

4.2.1 Hydrogen Production by Steam Reforming of Natural Gas

Many hydrocarbons and alcohols can be considered as candidate fuels for stationary applications of fuel cells. The fuel considered in this research work is natural gas, which is a naturally occurring gas mixture, consisting mainly of methane. Table 4.2 outlines the typical components of natural gas in the Union Gas system and the typical ranges for these values allowing for the different sources. Based on this table, the assumption of natural gas consisting of 100% methane was made. Due to its low electrochemical reactivity, methane, as indeed any other hydrocarbon, is not used directly in fuel cells, an exception, of course, being the use of methanol in Direct Methanol Fuel Cells (DMFCs). A process such as steam reforming[42] is required to convert this fuel to a hydrogen-rich gas appropriate for the operation of the fuel cell.

A simplified flow diagram of the most general steam-methane production process is shown in Figure 4.7. In order to protect the catalysts used in the reactors, the methane must be desulfurized before being fed to the steam-methane reformer. One or more shift reactors are added to maximize hydrogen production, and a CO purifier is required for low temperature fuel cells in order to minimize the damage on the fuel cell stack catalyst. Due to the high operational temperatures of SOFC technology no CO purifier and shift

[42] Steam reforming involves catalytic conversion of the hydrocarbon and steam to hydrogen and carbon oxides. The process works only with light hydrocarbons that can be vaporized completely without carbon formation (Kordesch and Simader, 1996).

reactors are required. Additionally, if the feed fuel is methane or natural gas desulphurization stage is not required provided no oderants (which are sulfur based) are contained in the gas. All these considerations reduce the fuel processing to the steam-methane reactor and a heat recovery device, which in fact most times is integrated into the SMR.

Table 4.2: Chemical composition of natural gas (Union Gas, 2001).

Component	Typical Analysis (mole %)	Typical Range (mole %)
Methane	94.69	88.3 – 96
Ethane	2.58	2.20 – 4.32
Propane	0.20	0.16 – 0.98
iso-Butane	0.03	0.01 – 0.12
normal-Butane	0.03	0.01 – 0.18
iso-Pentane	0.01	trace – 0.06
normal-Pentane	0.01	trace – 0.03
Hexanes plus	0.01	trace – 0.03
Nitrogen	1.60	1.38 – 5.50
Carbon dioxide	0.81	0.50 – 0.92
Oxygen	0.02	0.01 – 0.05
Hydrogen	trace	trace – 0.02

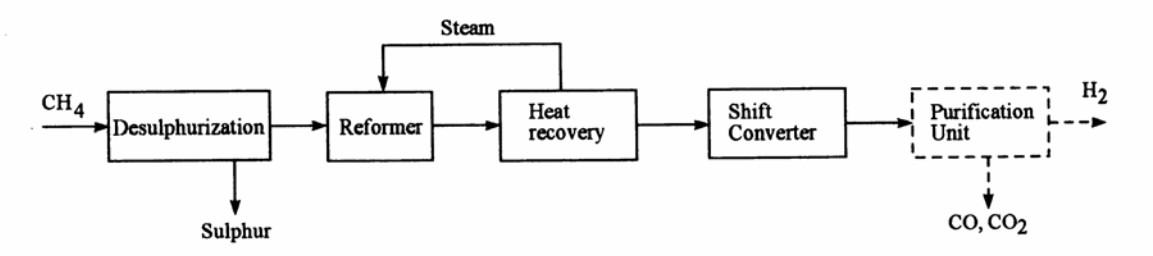

Figure. 4.7. Flow diagram of hydrogen production by catalytic steam reforming.

A schematic diagram of a steam-methane reformer (SMR) reactor, similar to that developed by United Technologies Corporation for fuel cell applications, is shown in Figure 4.8. The SMR consists of a pressure shell, a catalyst basket, and a combustion chamber with a burner. The pressure shell is equipped with a flanged cover to facilitate the installation of the catalyst basket. The catalyst consists of two catalyst beds in series and a number of annuli for the process mixture flow. The SMR reactor uses a combination of co-current and counter-current heat exchange between the process gas

and the flue gas in order to maximize thermal efficiency and to optimize usage of construction materials. In particular, the process feed is passed downwards through the first catalyst bed receiving heat from the partly cooled combustion gas and the product gas, both in counter-current flow with the process feed. The process gas is then transferred from the first catalyst bed to the top of the second catalyst bed through a number of tubes or a channel where it flows down through that bed, receiving heat from the hot combustion gas in co-current flow with the process gas. The product gas from the second catalyst is finally passed through an annular space supplying part of its heat back to the process gas flowing in the first catalyst bed in counter-current flow.

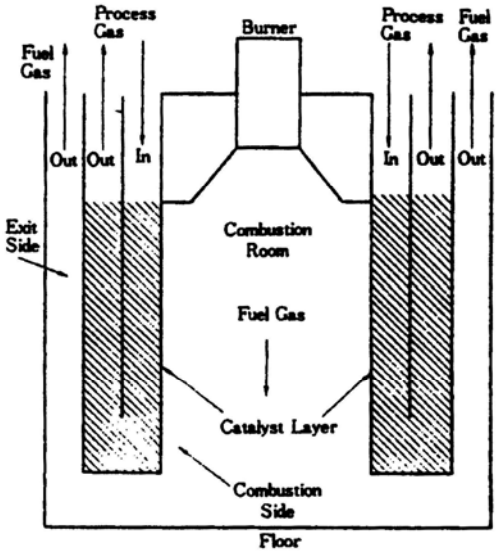

Figure. 4.8. Schematic diagram of a steam methane reformer reactor.

The configuration just described is the industry most used. However, it is volume demanding. Therefore, for SOFC based APU applications, a compact SMR configuration is proposed. The reactor looks like a single-pass shell and tube heat exchanger. The catalyst is placed in the tube side. The reactor works as a counter-flow heat exchanger in order to facilitate the endothermic reaction. The combustion takes place at the burner in a separate chamber in order to facilitate the hot gas flow into the reformer. Figure 4.9 shows the typical shapes of the catalyst particle. The catalyst has a 4-hole cylindrical shape and normally contain nickel oxide dispersed on a calcium aluminate ceramic support promoted with alkali.

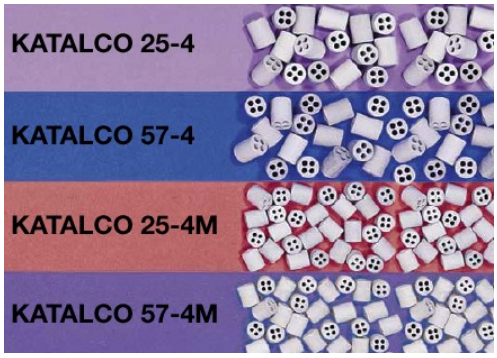

Figure 4.9. Shape of the catalyst particles inside the tubes of the steam methane reformer reactor (Synetix Product Brochure, 2001).

There are up to eleven possible reactions that can take place between the constituents of the process of the reformate gas[43] inside the reformer tubes (Xu and Froment, 1989). However, due to the presence of the catalysts, three out of the eleven are favored and, therefore, chosen to describe the steam reforming of methane. They are as follow:

- Demethanation reaction (endothermic):

$$CH_4 + H_2O \leftrightarrow CO + 3H_2 \qquad (\Delta H_{298} = 206 \text{ kJ/mol}) \tag{4.1}$$

- Water-gas shift (WGS) reaction (exothermic):

$$CO + H_2O \leftrightarrow CO_2 + H_2 \qquad (\Delta H_{298} = -40.6 \text{ kJ/mol}) \tag{4.2}$$

- Overall demethanation reaction (endothermic):

$$CH_4 + 2H_2O \leftrightarrow CO_2 + 4H_2 \qquad (\Delta H_{298} = 165 \text{ kJ/mol}) \tag{4.3}$$

All of the above reactions are reversible at reforming temperatures. Also note, that at higher temperatures, less methane and more carbon monoxide (CO) is present in the reformate gas and that methane content increases with pressure and decreases with increasing steam to carbon ratio (He, 1997).

4.2.2 Fuel Processing Sub-system (FPS) Configuration

Figure 4.10 shows the proposed solid oxide fuel cell based auxiliary power unit super-configuration. This super-configuration was developed taking into account all the

[43] From this point forward it will be referred to as reformate gas or simply reformate.

equipment and recovery loops necessary to maximize total system efficiency. Departing from it and using parametric studies and dynamic optimization tools, the optimum system synthesis/design and optimum dynamic operational/control are found as part of this doctoral work in order to minimize total life cycle cost. Thus, the final optimal configuration will be some sub-set of this super-configuration. What follows is a general description of the fuel processing and work recovery- air supply sub-systems, which together compose the balance of plant sub-system. More component details will be given as the system model is develop later in this chapter.

The main objective of the fuel processing sub-system (FPS) is to convert the natural gas (methane), obtained from a natural gas tank, to the hydrogen-rich reformate gas that will provide the hydrogen fuel required for the operation of the SOFC stack. The FPS configuration (see Figure 4.10) initially developed for the processing of this hydrocarbon feedstock is described below. The necessary amount of fuel feed, consisting primarily of methane as shown in Table 4.2, is taken from a pressurized source (tank or district grid); and then a part of it is supplied to the reforming line while the remaining fuel is intended for combustion. The methane flowing down the reforming line is mixed with a fraction of the products of the anode during regular operation. Tthese products are water rich and are a high temperature. At start-up the steam is produced in a steam generator and mixed with the methane before entering the SMR reactor. The anode products recirculation is a very good example of the thermal and kinetic integration applied to the FPS configuration. Additionally, a large amount of thermal energy contained in the combustion gases exiting the SMR reactor is used to preheat the air stream and is also used in the expander and steam generator during start-up. At this point, a synthesis or configurational variation can be proposed. The methane and steam could be mixed before the mixture is preheated and sent to the reformer or not. Which configuration is finally implemented should be the result of an optimization process of synthesis/design and operation. For the moment the two streams are preheated independently.

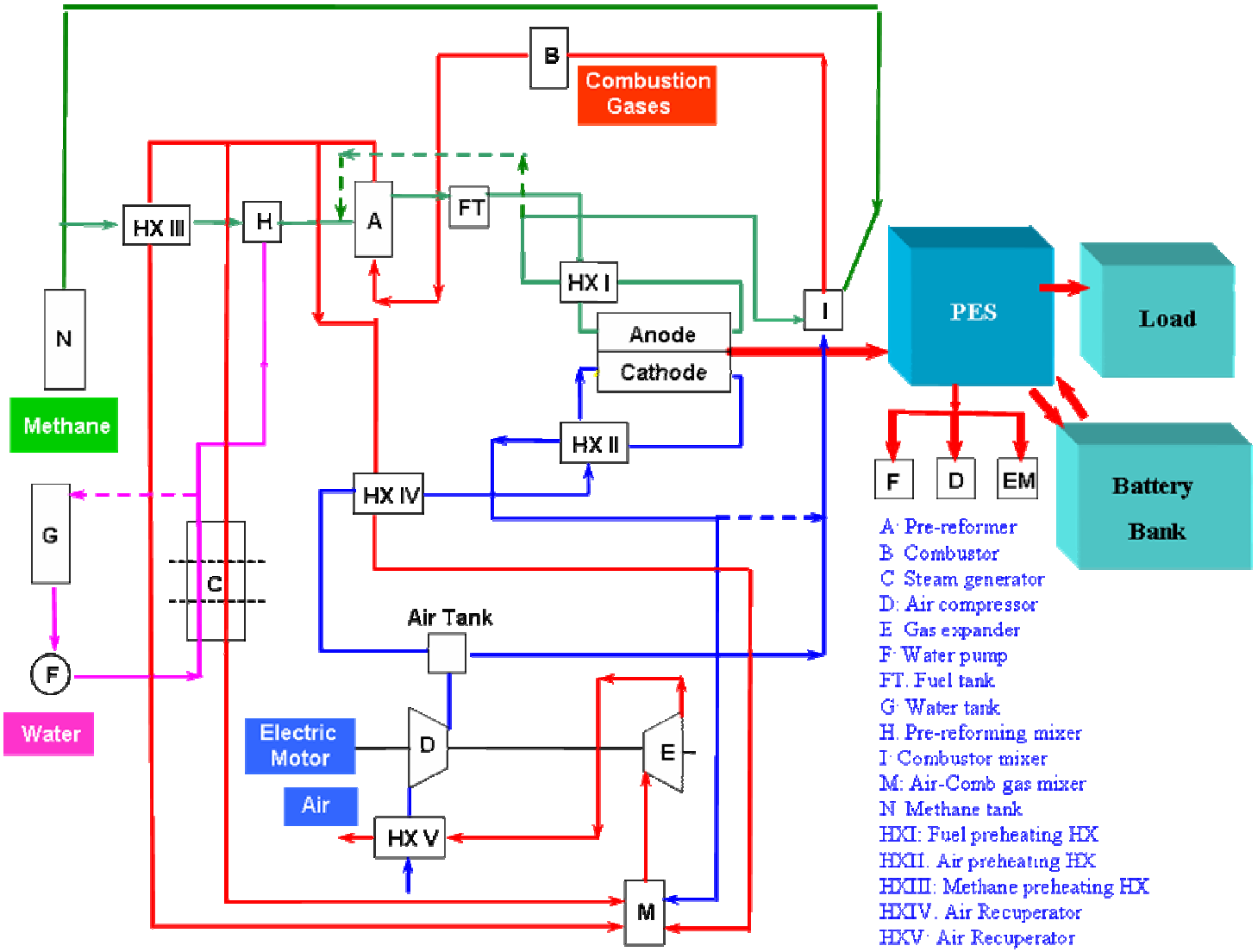

Figure 4.10. Super-configuration of the proposed SOFC based power system established prior to the parametric study and optimization process.

The reforming of the above mentioned mixture into hydrogen and carbon monoxide is carried out inside the SMR reactor. The heat needed to drive the endothermic reforming reaction is provided by the combustion gases leaving the burner. The details concerning the geometry of the steam-methane reactor as well as the chemical reactions taking place inside it and the appropriate catalysts used were given earlier. The reformate gases coming out of the steam reformer are stored in a tank designed specifically for the transient and not steady state operation of the SOFC based APU. This tank, thus, acts as an energy buffer between the balance of plant sub-system (BOPS) and the stack sub-system (SS). This allows almost immediate supply of fuel to the stack at operational points (perturbations due to load changes) where the stack demand rate is larger than the reformer production rate. Before being delivered to the fuel cell stack, the hydrogen-rich reformate gas is brought to the desired anode inlet conditions by use of a heat exchanger.

The combustion mixture supplied to the burner consists of air taken from the air tank and the output of the cathode, the fraction left after recirculation of the hydrogen-depleted anode exhaust gas, and the compressed methane that bypasses the reforming line. Burning the residual hydrogen in the stack tail gas translates to decreased consumption of additional methane in the burner and, therefore, to increased efficiency of the configuration. Furthermore, using air bleed from the stack introduces additional increments in efficiency by eliminating the compression stage. However, air coming from the stack is rich in nitrogen, the amount depending on stack requirements. Therefore, using it depends on whether or not its heat capacity is enough to meet the thermal management needs. After providing the required thermal energy for the endothermic reforming reaction, the combustion gases are split into three streams, the first preheats the methane and the second is passed through the steam generator where it supplies the necessary heat for producing the steam consumed in the reforming process. The third is used to preheat the air going into the stack. Finally, prior to being expanded and exhausted to the atmosphere, the combustion gas streams are mixed together.

4.2.3 Work Recovery and Air Supply Sub-System (WRAS) Description

In the BOPS and SS, the temperatures of a number of critical components (particularly the SOFC stack and the pre-reformer of the FPS) have to be carefully controlled, and the flow and utilization of heat from several sources within the configuration have to be managed effectively in order to achieve high overall efficiency. Therefore, the thermal management plays a significant role in the operation of the SOFC power system. Its major functions include maintaining the stack operating temperature in the appropriate range, bringing the hydrogen-rich reformate gas and compressed air to the desired anode inlet conditions before exiting the FPS and the work recovery and air supply sub-system (WRAS), respectively, and controlling the steam reformer operational conditions and the generation of the steam required for the FPS. A number of high performance heat exchangers are used within the configuration in order to meet these objectives. Furthermore, since the SOFC operates at a high temperature, this high-grade waste heat is of importance for preconditioning the streams coming into the stack. Thermal energy available from the conditioning of the reformate gas, the steam, the compressed air, and the methane are used in the WRAS.

In the WRAS, the combustion gases coming from the steam generator, the compressed air heat exchanger, and the methane heat exchanger are mixed together with the air coming from the stack. Thus, the mixed gases are expanded through an expander for purposes of energy recovery, i.e. to offset some of the parasitic power requirements. The work generated by the gas mixture is used to drive the air compressor, which in turn compresses the air to be stored in the air tank and then used in the stack and the combustor. For some operating conditions, the work produced by the expander does not match the work required by the compressor. This additional work is supplied by an electrical motor which takes power from the SS/PES (power electronics sub-system)

4.3 Modeling of the Fuel Processing Sub-system (FPS)

4.3.1 FPS Thermodynamic, Kinetic, and Geometric Models

The mathematical model of the FPS consists of a set of equations that describe the mass and associated energy flows in each of the lines of the sub-system, based on the chemical reactions inside each reactor and on the laws of conservation of mass and energy for each component in the sub-system. In the case where the sub-system is in a transient state, the conservation of molar mass and energy for each component can be written as follows:

$$\sum_{in} \dot{n}_{mix} - \sum_{out} \dot{n}_{mix} = \frac{dn_{cv}}{dt} \tag{4.4}$$

$$\sum_{q} \dot{Q}_q - \dot{W} + \sum_{in} \dot{n}_{mix} h_{mix} - \sum_{out} \dot{n}_{mix} h_{mix} = \frac{dE_{cv}}{dt} \tag{4.5}$$

where the indices in and out refer to the inlet and outlet flow streams, respectively, and q to the number of heat interactions $\dot{Q}_q$ of the component with other components or sub-systems. Moreover, $\dot{W}$ represents the work done by the component, $\dot{n}_{mix}$ the inlet or outlet mixture molar flow rate, and h_{mix} the corresponding specific enthalpy. The terms n_{cv} and E_{cv} refer to the control volume moles and energy.

The mixture's molar flow rate, $\dot{n}_{mix}$, is defined as the sum of the molar flow rates of its constituents, while the corresponding specific enthalpy, h_{mix}, is given by the following relation

$$h_{mix}(T, \mathbf{y}) = \sum_{p=1}^{7} y_p h_p(T) \tag{4.6}$$

which is valid for a Gibbs-Dalton (ideal gas) mixture. In the above equation, y_p represents the mole fraction of the pth constituent and h_p its corresponding partial enthalpy. Since there are chemical reaction mechanisms that are active within the system, the constituent's partial enthalpy is expressed as

$$h_p(T) = \left(\Delta h_f^o\right)_p + h_p^{'}(T) - h_p^{'}(T_o) \tag{4.7}$$

where $\left(\Delta h_f^o\right)_p$ is the enthalpy of formation of constituent p at standard temperature T_o and pressure P_o. The value of the enthalpy $h_p^{'}$ of the p[th] constituent is determined by the approximate expression

$$h_p^{'}(T) = a_p T + \frac{4}{5} b_p T^{5/4} + \frac{2}{3} c_p T^{3/2} + \frac{4}{7} d_p T^{7/4} \tag{4.8}$$

which is based on a regression of data from the JANAF Thermochemical Tables (1971). The values of the coefficients a_p, b_p, c_p, and d_p in the above equation are tabulated in Gyftopoulos and Beretta (1991). The range of application for this correlation is for temperatures ranging from 300 ^{o}K to 4000 ^{o}K

Chemical equilibrium calculations are necessary in the modeling of the FPS reactor in order to determine the composition of their inlet and outlet streams. The equilibrium constant of the reaction, $K(T)$, is defined as

$$K(T) = \exp\left[-\frac{\Delta g^o(T)}{RT}\right] \tag{4.9}$$

where $\Delta g^o(T)$ is the Gibbs free energy of reaction at temperature T given by

$$\Delta g^o(T) = \Delta h^o(T) - T\Delta s^o(T) \tag{4.10}$$

Here $\Delta h^o(T)$ is the enthalpy of reaction at temperature T and pressure P_o, and $\Delta s^o(T)$ to the entropy of reaction at the same conditions. The values of these functions can be determined by using the following two relations:

$$\Delta h^o(T) = \Delta h^o + \sum_{p=1}^{7} \nu_p \left[h_p^{'}(T, P_o) - h_p^{'}(T_o, P_o)\right] \tag{4.11}$$

$$\Delta s^o(T) = \Delta s^o + \sum_{p=1}^{7} \nu_p \left[s_p(T, P_o) - s_p(T_o, P_o)\right] \tag{4.12}$$

where

$$s_p(T,P) = a_p \ln T + 4b_p T^{1/4} + 2c_p T^{1/2} + \frac{4}{3} d_p T^{3/4} - R \ln P \tag{4.13}$$

and ν_p is the stoichiometric coefficient of the p[th] constituent in the reaction. The term Δh^o, appearing in equation (4.11), is called the enthalpy of reaction at standard conditions, i.e. $T_o = 25$ °C and $P_o = 1$ atm, and is expressed as

$$\Delta h^o = \sum_{p=1}^{7} \nu_p \left(\Delta h_f^o\right)_p \tag{4.14}$$

The term Δs^o, appearing in equation (4.12), is called the entropy of reaction at standard conditions and is given by

$$\Delta s^o = \sum_{p=1}^{7} \nu_p \left(\Delta s_f^o\right)_p \tag{4.15}$$

where $\left(\Delta s_f^o\right)_p$ is the entropy of formation of constituent *p* at standard temperature T_o and pressure P_o. Finally, one more variable appearing in the chemical equilibrium calculations is the degree of reaction, ξ, which is defined as

$$\xi = \frac{\epsilon}{\dot{n}_{mix,i}} \tag{4.16}$$

where ϵ is the reaction coordinate and $\dot{n}_{mix,i}$ is the molar flow rate of the mixture entering the reactor.

In addition to the thermophysical property correlations given above, the necessary heat transfer calculations of the FPS component models require additional thermophysical property correlations as well as those for transport properties. These are included in the simulation code as fitted correlations of data obtained directly from the Engineering Equation Solver (EES) software (1995). In particular, the EES software contains subroutines for calculating the thermophysical and transport properties of various substances assuming either ideal or real gas behavior. Therefore, appropriate correlations (Bird, steward, and lighfoot, 1960) for the thermal conductivity k, and dynamic viscosity μ of the seven different mixture constituents (i.e. CH_4, H_2O, CO, CO_2, H_2, O_2, and N_2) are extracted from the software based on the temperature and

pressure ranges of interest. The thermophysical and transport properties of the ideal gas mixture are determined using standard mixing rules such that:

$$Z_{mix}(T,y) = \sum_{p=1}^{7} \frac{y_p Z_p}{\sum_{j=1}^{7} y_j \Phi_{pj}} \tag{4.17a}$$

Whre Φ_{pj} is given by

$$\Phi_{pj} = \frac{1}{\sqrt{8}} \left(1 + \frac{\mu_p}{M_j}\right)^{-1/2} \left[1 + \left(\frac{\mu_p}{\mu_j}\right)^{1/2} \left(\frac{M_p}{M_j}\right)^{1/4}\right]^2 \tag{4.17b}$$

All thermophysical and transport properties are evaluated at the arithmetic mean of the inlet and outlet mixture temperatures unless otherwise specified.

As to the thermal analysis of the heat exchangers included in the FPS configuration, two different methods are applied, namely, the log mean temperature difference (LMTD) method and the number of transfer units (NTU) method based on the concept of a heat exchanger effectiveness. The effectiveness, ε, of a heat exchanger is the ratio of the actual heat transfer rate to the thermodynamically limited maximum possible heat transfer rate if an infinite heat transfer surface area were available in a counter-flow heat exchanger. The actual heat transfer is obtained either by the energy given off by the hot fluid or the energy received by the cold fluid. Therefore,

$$\varepsilon = \frac{\dot{Q}_{actual}}{\dot{Q}_{max}} = \frac{\dot{n}^h_{mix}\left[h^h_{mix}\left(T_{h,i}\right) - h^h_{mix}\left(T_{h,o}\right)\right]}{\dot{Q}_{max}} = \frac{\dot{n}^c_{mix}\left[h^c_{mix}\left(T_{c,o}\right) - h^c_{mix}\left(T_{c,i}\right)\right]}{\dot{Q}_{max}} \tag{4.18}$$

The fluid that undergoes the maximum temperature difference is the fluid having the minimum heat capacity. Thus, in this work, the maximum possible heat transfer is expressed as

$$\dot{Q}_{max} = \dot{n}^h_{mix}\left[h^h_{mix}\left(T_{h,i}\right) - h^h_{mix}\left(T_{c,i}\right)\right] \quad \text{if} \quad \left(\dot{n}C_p\right)^h_{mix} < \left(\dot{n}C_p\right)^c_{mix} \tag{4.19}$$

or

$$\dot{Q}_{max} = \dot{n}^c_{mix}\left[h^c_{mix}\left(T_{h,i}\right) - h^c_{mix}\left(T_{c,i}\right)\right] \quad \text{if} \quad \left(\dot{n}C_p\right)^c_{mix} < \left(\dot{n}C_p\right)^h_{mix} \tag{4.20}$$

What follows is a description of the models developed for the compact heat exchangers, the steam generator, and the reactor included in the FPS configuration.

4.3.2 Modeling of the Compact Heat Exchanger (HE)

The heat exchangers used in the FPS in particular and the BOPS in general are all plate-fin type, compact heat exchangers with a single-pass, cross-flow arrangement. Their modeling details are presented in Table 4.3. The heat transfer and pressure drop models used are based on the work of Shah (1981) and Kays and London (1998). A dynamic energy balance and empirical correlations for the heat transfer coefficients are applied in order to relate the geometric models of the heat exchangers to the thermodynamic ones. The NTU method was used to validate the dynamic model results at steady state. The expression for the heat exchanger effectiveness is obtained from Incropera and DeWitt (1990) and is valid for single-pass, cross-flow arrangements with both fluids unmixed. It should be made clear that the equations appearing in Table 4.3 are valid for both the hot and the cold stream sides. Therefore, they should be taken into account twice in order for the heat exchanger model to be complete. Exempt are the equations that refer to the height and number of plates of the heat exchanger, the volumes of the hot and cold sides, as well as the overall heat transfer coefficient and the heat exchanger effectiveness.

The following assumptions are made in the thermal analysis of each section of the heat exchanger:

- Fluid flow on each side is one-dimensional.
- Longitudinal conduction in the fluid or wall is negligible.
- The effective conductance (hA) is known for each fluid as a function of Reynolds number.
- Conduction resistances through the wall are negligible.
- The heat exchanger is adiabatic overall.
- Since the fluid is a gas, its thermal capacitance is assumed to be small compared to the wall.

Table 4.3. Geometric and heat transfer models of a plate-fin heat exchanger.

Variable Description		Model Equation
L_h	Hot-side length	Assigned value
L_c	Cold-side length	Assigned value
H	Height	$H = b_h + 2a + n_{plates}\left(b_h + b_c + 2a\right)$
n_{plates}	Number of plates	
l_f	Fin length	$l_f = \frac{b}{2} - t_f$
V_p^h	Hot-side volume	$V_p^h = L_c L_h b_h \left(n_{plates} + 1\right)$
V_p^c	Cold-side volume	$V_p^c = L_c L_h b_c n_{plates}$
A	Heat transfer area	$A = \beta V_p,\ A_o = \frac{D_h A}{4L}$
A_o	Minimum free flow area	
Variable Description		**Model Equation**
A_f	Finned area	$A_{fr} = LH,\ m = \sqrt{\frac{2h}{k_f t_f}}$
A_{fr}	Frontal area	
η_f	Fin efficiency	$\eta_f = \frac{\tanh\left(ml_f\right)}{ml_f},\ \eta_o = 1 - \left(1 - \eta_f\right)\frac{A_f}{A}$
η_o	Outside overall surface efficiency	
$\dot{n}$	Mixture molar flow rate	$G = \frac{\dot{n}}{A_o}$
j	Colburn factor	$Pr = \frac{\mu C_p}{k}$
G	Maximum mass velocity	$h = jGC_p Pr^{-2/3}$
Pr	Prandtl number	
h	Heat transfer coefficient	
U	Overall heat transfer coefficient	$UA = \frac{1}{\frac{1}{\left(\eta_o Ah\right)_h} + \frac{1}{\left(\eta_o Ah\right)_c}}$

The following three partial differential equations show the dynamic energy balance performed on the cold and hot fluids and on the heat exchanger walls for the cross-flow section shown in Figure 4.11.

Hot side

$$\left(Mc_p\right)_h \frac{\partial T_h}{\partial t} = \left(\dot{m}c_p\right)_h L_x \frac{\partial T_h}{\partial x} + \left(hA\right)_h \left(T_h - T_w\right) \tag{4.21}$$

Cold side

$$\left(Mc_p\right)_c \frac{\partial T_c}{\partial t} + \left(\dot{m}c_p\right)_c L_y \frac{\partial T_c}{\partial y} + \left(hA\right)_c \left(T_c - T_w\right) \tag{4.22}$$

Wall

$$\left(Mc_p\right)_w \frac{\partial T_w}{\partial t} = \left(hA\right)_c \left(\overline{T}_c - T_w\right) + \left(hA\right)_h \left(\overline{T}_h - T_w\right) \tag{4.23}$$

where M is the mass in the control volume, the subscript h indicates the hot side, the subscript c indicates the cold side, the subscript w indicates the wall, and x and y are the longitudinal and transverse directions, respectively. A refers to the heat transfer area while h is the heat transfer coefficient.

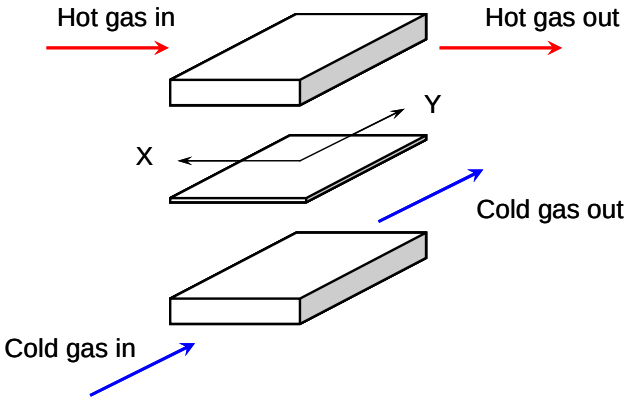

Figure 4.11. Compact heat exchanger section.

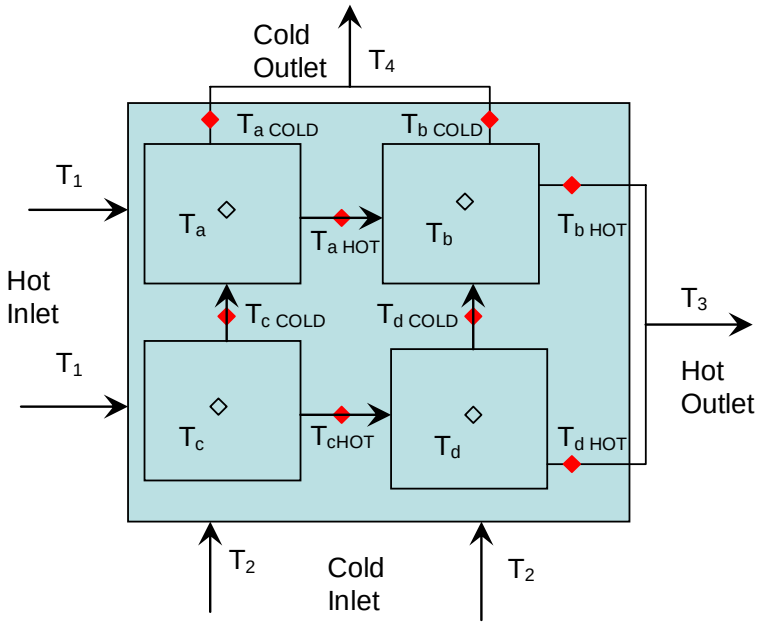

Figure 4.12. Compact heat exchanger spatial discretization.

In this research, a numerical approach was applied to solve the transient thermal response of the compact heat exchangers. This is due to the fact that the partial differential equations describing the wall and fluid temperature responses are complex and non-linear, and there are no general solutions. In order to guarantee adequate accuracy, spatial discretization as depicted in Figure 4.12 was applied to the heat exchanger. Figure 4.12 shows a top-view of a compact heat exchanger with four discrete segments in order to illustrate the numerical approach. Proper validation of the models shows that accurate results are reach with sixteen discrete segments or more. The result of applying spatial decomposition is a set of 3xn differential equation, where n is the number of discrete segments. This set of equations is easier to solve than the original PDF system.

4.3.3 Modeling of the Steam Generator (SG)

The steam generator (SG) considered in this research consists of an economizer, an evaporator, and a superheater. These three integrated component parts have been modeled as a cross-flow, shell-and-tube heat exchanger with a single-pass shell and one tube pass. Since the same type of shell-and-tube heat exchanger is taken into account to describe the economizer, evaporator, and superheater geometries, the geometric models developed are identical. The necessary equations are obtained from Kakaç and Liu (1998) and are the appropriate ones for this particular shell-and-tube configuration. The geometric model of the steam generator is presented in Table 4.4.

The economizer, evaporator, and superheater dynamic models are formulated similarly. In general, the steam generator is discretized spatially in n sections. For each section (index i), a dynamic energy balance for the pipe is formulated as follows:

$$\frac{1}{n}\left(mc_p\right)_w \frac{\partial T_{wi}}{\partial t} = \dot{Q}_{gas-steel\,i} - \dot{Q}_{steel-steam\,i} \tag{4.24}$$

where the heat flows are calculate by

$$\dot{Q}_{gas-steel\,i} = \frac{1}{n} U_{gas_i} A\left(T_{gas_i} - T_{steel\,i}\right) \tag{4.25}$$

$$\dot{Q}_{steel-steam\,i} = \frac{1}{n} U_{steam\,i} A \left(T_{steel\,i} - T_{steam\,i} \right) \tag{4.26}$$

The temperatures of the gas and steam for each section of the counter flow heat exchanger are calculated implicitly as follow:

$$\dot{Q}_{gas-steel\,i} = \left(\dot{m} c_p \right)_{gas} \left(T_{gas\,i-1} - T_{gas\,i} \right) \tag{4.27}$$

$$\dot{Q}_{steel-steam\,i} = \left(\dot{m} c_p \right)_{steam} \left(T_{steam\,i} - T_{steam\,i+1} \right) \tag{4.28}$$

For the evaporator the last equation is replaced by

$$\dot{Q}_{steel-steam\,i} = \left(\dot{m} \right)_{steam} \left(h_{steam\,i} - h_{steam\,i+1} \right) \tag{4.29}$$

Table 4.4. Geometric model of the steam generator (Kakaç and Liu, 1998).

Fixed Parameter Description		Value	Fixed Parameter Description		Value
t_w	Tube wall thickness (mm)	1.5	CTP	Tube count calculation constant	0.93
n_{passes}^{SG}	Number of passes	1	CL	Tube layout constant	1
Variable Description			**Model Equation**		
d_i^{SG}	Tube inner diameter		Assigned value		
n_{tubes}^{SG}	Number of tubes		Assigned value		
L_{SG}	Length		Assigned value		
d_o^{SG}	Tube outer diameter		$d_o^{SG} = d_i^{SG} + 2t_w$		
P_T^{SG}	Pitch		$P_T^{SG} = 1.25 d_o^{SG}$		
D_s^{SG}	Shell diameter		$D_s^{SG} = 0.637 \sqrt{\frac{CL}{CTP}} \sqrt{\pi n_{tubes}^{SG} \left(P_T^{SG} \right)^2}$		
B	Baffle spacing		$B = 0.6 D_s^{SG}$		

As far as the heat transfer analysis of the steam generator is concerned, three different heat transfer models are developed and presented in the following pages due to the fact that different convection heat transfer coefficients as well as methods are considered in the design/analysis of its three parts.

Two different expressions for the tube-side heat transfer coefficient are given depending on whether the water flow inside the tubes is fully developed laminar or turbulent. The correlation used for the shell-side heat transfer coefficient is the one suggested by Kern (1950). The details of the economizer's heat transfer model are given in Table 4.5.

For saturated convective boiling prior to dry-out, relations to predict the heat transfer coefficient have typically been formulated to impose a gradual suppression of nucleate boiling and a gradual increase in liquid film evaporation heat transfer as the quality increases. A number of correlations based on this approach have been developed. The one recently developed by Kandlikar (1989), which has been fit to a broad spectrum of data for both horizontal and vertical tubes, is used to calculate the tube-side heat transfer coefficient for the evaporator.

Table 4.5: Heat transfer model of the economizer (Kakaç and Liu, 1998).

Variable Description		Model Equation
Re_{eco}	Tube-side Reynolds number	$Re_{eco} = \left(\frac{4\dot{n}_{H_2O}}{\pi d_i \mu_{H_2O} n_{tubes}} \right)_{eco}$, $Pr_{eco} = \left(\frac{\mu_{H_2O} C_{p_{H_2O}}}{k_{H_2O}} \right)_{eco}$
Pr_{eco}	Tube-side Prandtl number	
$h_{H_2O}^{eco}$	Tube-side heat transfer coefficient	If $Re_{eco} \le 2300$ $\quad h_{H_2O}^{eco} = 4.36 \left(\frac{k_{H_2O}}{d_i} \right)_{eco}$ otherwise $h_{H_2O}^{eco} = 0.023 \left(\frac{k_{H_2O}}{d_i} \right)_{eco} \left(Re_{eco} \right)^{0.8} \left(Pr_{eco} \right)^{0.4}$
D_{eq}^{eco}	Shell-side equivalent diameter	$D_{eq}^{eco} = \frac{4\left(P_T^{eco} \right)^2 - \pi \left(d_o^{eco} \right)^2}{\pi d_o^{eco}}$
A_s^{eco}	Bundle cross-flow area	$A_s^{eco} = \frac{D_s^{eco} \left(P_T^{eco} - d_o^{eco} \right) B_{eco}}{P_T^{eco}}$, $G_s^{eco} = \frac{\dot{n}_{gas}}{A_s^{eco}}$
G_s^{eco}	Shell-side mass velocity	
h_{gas}^{eco}	Shell-side heat transfer coefficient	$h_{gas}^{eco} = 0.36 \left(\frac{k_{gas}}{D_{eq}} \right)_{eco} \left(\frac{D_{eq} G_s}{\mu_{gas}} \right)_{eco}^{0.55} \left(\frac{C_{p_{gas}} \mu_{gas}}{k_{gas}} \right)_{eco}^{1/3} \left(\frac{\mu_{gas}}{\mu_{wall}} \right)_{eco}^{0.14}$
U_{eco}	Overall heat transfer coefficient	$U_{eco} = \frac{1}{\frac{1}{h_{H_2O}^{eco}} + \frac{1}{h_{gas}^{eco}}}$, $A_{eco} = \left(\pi d_o L n_{tubes} n_{passes} \right)_{eco}$
A_{eco}	Heat transfer area	
ΔT_{lm}^{eco}	Log mean temperature difference	$\Delta T_{lm}^{eco} = \frac{\left(T_{gas,i} - T_{H_2O,o} \right)_{eco} - \left(T_{gas,o} - T_{H_2O,i} \right)_{eco}}{\ln \left[\frac{\left(T_{gas,i} - T_{H_2O,o} \right)_{eco}}{\left(T_{gas,o} - T_{H_2O,i} \right)_{eco}} \right]}$
$\dot{Q}_{eco}$	Heat transfer rate	$\dot{Q}_{eco} = \dot{n}_{gas} C_{p_{gas}}^{eco} \left(T_{gas,i}^{eco} - T_{gas,o}^{eco} \right) = U_{eco} A_{eco} \Delta T_{lm}^{eco}$

Table 4.6: Heat transfer model of the evaporator Kandlikar (1989).

Variable Description		Model Equation
A_{cr}^{evap}	Cross-sectional area	$A_{cr}^{evap} = \frac{\pi\left(d_i^{evap}\right)^2}{4}$, $G_{tube}^{evap} = \frac{\dot{n}_{H_2O}}{n_{tubes}^{evap} A_{cr}^{evap}}$
G_{tube}^{evap}	Tube-side mass velocity	
Co	Convection number	$Co = \left(\frac{1-\chi}{\chi}\right)^{0.8}\left(\frac{\rho_{H_2O}^{vap}}{\rho_{H_2O}^{liq}}\right)^{0.5}$
Fr_{le}	Froude number	$Fr_{le} = \frac{\left(G_{tube}^{evap}\right)^2}{\left(\rho_{H_2O}^{liq}\right)^2 g d_i^{evap}}$
Bo	Boiling number	$Bo = \frac{q''_{evap}}{G_{tube}^{evap} h_{fg}}$
h_{liq}	Heat transfer coefficient for the liquid phase	$h_{liq} = 0.023\frac{k_{H_2O}^{liq}}{d_i^{evap}}\left(\frac{G_{tube}^{evap}(1-\chi)d_i^{evap}}{\mu_{H_2O}^{liq}}\right)^{0.8}\left(\frac{\mu_{H_2O} C_{p_{H_2O}}}{k_{H_2O}}\right)_{liq}^{0.4}$
$h_{H_2O}^{evap}$	Tube-side heat transfer coefficient	$h_{H_2O}^{evap} = h_{liq}\left[C_1 Co^{C_2}\left(25 Fr_{le}\right)^{C_5} + C_3 Bo^{C_4}\right]$
D_{eq}^{evap}	Shell-side equivalent diameter	$D_{eq}^{evap} = \frac{4\left(P_T^{evap}\right)^2 - \pi\left(d_o^{evap}\right)^2}{\pi d_o^{evap}}$
A_s^{evap}	Bundle cross-flow area	$A_s^{evap} = \frac{D_s^{evap}\left(P_T^{evap} - d_o^{evap}\right)B_{evap}}{P_T^{evap}}$, $G_s^{evap} = \frac{\dot{n}_{gas}}{A_s^{evap}}$
G_s^{evap}	Shell-side mass velocity	
h_{gas}^{evap}	Shell-side heat transfer coefficient	$h_{gas}^{evap} = 0.36\left(\frac{k_{gas}}{D_{eq}}\right)_{evap}\left(\frac{D_{eq}G_s}{\mu_{gas}}\right)_{evap}^{0.55}\left(\frac{C_{p_{gas}}\mu_{gas}}{k_{gas}}\right)_{evap}^{1/3}\left(\frac{\mu_{gas}}{\mu_{wall}}\right)_{evap}^{0.14}$
U_{evap}	Overall heat transfer coefficient	$U_{evap} = \frac{1}{\frac{1}{h_{H_2O}^{evap}} + \frac{1}{h_{gas}^{evap}}}$
A_{evap}	Heat transfer area	$A_{evap} = \left(\pi d_o L n_{tubes} n_{passes}\right)_{evap}$
ΔT_{lm}^{evap}	Log mean temperature difference	$\Delta T_{lm}^{evap} = \frac{\left(T_{gas,i} - T_{gas,o}\right)_{evap}}{\ln\left[\frac{\left(T_{gas,i} - T_{H_2O}\right)_{evap}}{\left(T_{gas,o} - T_{H_2O}\right)_{evap}}\right]}$
q''_{evap}	Surface heat flux (single tube)	$q''_{evap} = \frac{\dot{n}_{gas} C_{p_{gas}}^{evap}\left(T_{gas,i}^{evap} - T_{gas,o}^{evap}\right)}{n_{tubes}^{evap} A_{evap}} = \frac{U_{evap}\Delta T_{lm}^{evap}}{n_{tubes}^{evap}}$

Table 4.7: Heat transfer model of the superheater (Kakaç and Liu, 1998).

Variable Description		Model Equation
Re_{super}	Tube-side Reynolds number	$Re_{super} = \left(\frac{4\dot{n}_{H_2O}}{\pi d_i \mu_{H_2O} n_{tubes}} \right)_{super}$, $Pr_{super} = \left(\frac{\mu_{H_2O} C_{p_{H_2O}}}{k_{H_2O}} \right)_{super}$
Pr_{super}	Tube-side Prandtl number	
$h_{H_2O}^{super}$	Tube-side heat transfer coefficient	$h_{H_2O}^{super} = 0.023 \left(\frac{k_{H_2O}}{d_i} \right)_{super} \left(Re_{super} \right)^{0.8} \left(Pr_{super} \right)^{0.4}$
D_{eq}^{super}	Shell-side equivalent diameter	$D_{eq}^{super} = \frac{4\left(P_T^{super} \right)^2 - \pi \left(d_o^{super} \right)^2}{\pi d_o^{super}}$
A_s^{super}	Bundle cross-flow area	$A_s^{super} = \frac{D_s^{super} \left(P_T^{super} - d_o^{super} \right) B_{super}}{P_T^{super}}$, $G_s^{super} = \frac{\dot{n}_{gas}}{A_s^{super}}$
G_s^{super}	Shell-side mass velocity	
h_{gas}^{super}	Shell-side heat transfer coefficient	$h_{gas}^{super} = 0.36 \left(\frac{k_{gas}}{D_{eq}} \right)_{super} \left(\frac{D_{eq} G_s}{\mu_{gas}} \right)_{super}^{0.55} \left(\frac{C_{p_{gas}} \mu_{gas}}{k_{gas}} \right)_{super}^{1/3} \left(\frac{\mu_{gas}}{\mu_{wall}} \right)_{super}^{0.14}$
U_{super}	Overall heat transfer coefficient	$U_{super} = \frac{1}{\frac{1}{h_{H_2O}^{super}} + \frac{1}{h_{gas}^{super}}}$, $A_{super} = \left(\pi d_o L n_{tubes} n_{passes} \right)_{super}$
A_{super}	Heat transfer area	

The equations of the evaporator's heat transfer model are presented in detail in Table 4.6. As to the heat transfer model of the superheater, this is presented in Table 4.7. The correlations used to calculate the tube-side and shell-side heat transfer coefficients are the same as those appearing in the model for the economizer. It is important to notice that the state of the water along the pipes is tracked by considering its pressure and temperature. This allows one to know the phase change location in order to use the proper heat transfer coefficient in the energy equation.

4.3.4 Modeling of the Steam-Methane Reformer

A number of simplifying assumptions are introduced to facilitate the modeling of the SMR reactor described in the previous sections. These are outlined below:

- A single reactor tube is analyzed. Thus, all the tubes in the reactor behave independently of one another.
- Reforming and combustion gases behave ideally in all sections of the reactor.
- The gas flow pattern through the channels is assumed to be plug flow.

- All reactions are considered to be the kinetically controlled. The rate expressions consider equilibrium.
- A uniform temperature exists throughout each catalyst particle.
- No carbon deposition is allowed in the SMR reactor.
- Axial dispersion and radial gradients are negligible.
- The outside shell wall is adiabatic.

The three reactions chosen to describe the steam reforming of methane are the ones presented in the previous section, i.e. the endothermic demethanation reactions and the exothermic water-gas shift reaction. The third reaction results from combining these two partial chemical reaction mechanisms. What follows is a derivation of the kinetic laws that allow one to predict the chemical composition of the reactants along the SMR.

Reaction 1	$CH_4 + H_20 \Leftrightarrow CO + 3H_2$
Reaction 2	$CO + H_20 \Leftrightarrow CO_2 + H_2$
Reaction 3	$CH_4 + 2H_20 \Leftrightarrow CO_2 + 4H_2$

Chemical Kinetics Theory

Given the stoichiometric reaction mechanism: $aA + bB \leftrightarrow rR + sS$, where a, b, r, and s are the stoichiometric coefficients and A, B, R, and S the chemical symbols for the reactants and products, the most general expression for the forward and backward reactions, respectively, takes the following form:

$$\vec{r} = \vec{k}[A]^{\alpha}[B]^{\beta}[R]^{\varsigma}[S]^{\sigma} \tag{4.30.a}$$

$$\bar{r} = \bar{k}[A]^{\alpha'}[B]^{\beta'}[R]^{\varsigma'}[S]^{\sigma'} \tag{4.30.b}$$

where $\vec{k}$ and $\bar{k}$ are the forward and backward reaction constants. Also, A, B, R, and S in these equations represent either reactants or products concentrations, mole fractions, or partial pressures (see Giftopoulos and Beretta, 1991). Now, the net rate of reaction is then given by combining the previous equations such that

$$r = \vec{r} - \bar{r} = \vec{k}[A]^{\alpha}[B]^{\beta}[R]^{\varsigma}[S]^{\sigma} - \bar{k}[A]^{\alpha'}[B]^{\beta'}[R]^{\varsigma'}[S]^{\sigma'} \tag{4.31}$$

At stable chemical equilibrium, the forward and backward reaction rates must be equal. Therefore, r is zero and

$$\frac{\vec{k}}{\overleftarrow{k}} = [A]^{\alpha'-\alpha}[B]^{\beta'-\beta}[R]^{\varsigma'-\varsigma}[S]^{\sigma'-\sigma} \tag{4.32}$$

where, $\vec{k}$ and $\overleftarrow{k}$ are expressed by the Arrhenius equation: $A_1 \exp\left(\frac{-EA}{RT}\right)$, A_1 is the Arrhenius coefficient, EA the Arrhenius activation energy, and R the gas constant. Since A_1, EA, and R are constants, $\vec{k}$ and $\overleftarrow{k}$ depend only on the temperature T. Using chemical equilibrium theory (Giftopoulos and Beretta, 1991), one can express the equilibrium constant $K_e(T)$ as a function of temperature (see section 4.3.1). Thus, one can express the ration of the reaction rate constants as a function of K_e, i.e.

$$\frac{\vec{k}}{\overleftarrow{k}} = f(K_e) \tag{4.33}$$

Moreover, from the stable chemical equilibrium condition,

$$K_e = \frac{[R_e]^r[S_e]^s}{[A_e]^a[B_e]^b} \tag{4.34}$$

where the quantities in brackets are concentration, mole fractions, or partial pressures. Combining equation (4.32) and (4.34) results in

$$[A]^{\alpha'-\alpha}[B]^{\beta'-\beta}[R]^{\varsigma'-\varsigma}[S]^{\sigma'-\sigma} = f\left([R_e]^r[S_e]^s[A_e]^{-a}[B_e]^{-b}\right) \tag{4.35}$$

This constraint must be satisfied for all stable chemical equilibrium concentrations. Therefore, the function f must be a power function such that:

$$[A]^{\alpha'-\alpha}[B]^{\beta'-\beta}[R]^{\varsigma'-\varsigma}[S]^{\sigma'-\sigma} = \left([R_e]^r[S_e]^s[A_e]^{-a}[B_e]^{-b}\right)^n \tag{4.36}$$

This equality is satisfied if and only if

$$\frac{\alpha'-\alpha}{-a} = \frac{\beta'-\beta}{-b} = \frac{\varsigma'-\varsigma}{r} = \frac{\sigma'-\sigma}{s} = n \tag{4.37}$$

Therefore,

$$\frac{\vec{k}}{\overleftarrow{k}} = K_e{}^n \tag{4.38}$$

This result implies that

- If experimental data are available, the order of the forward and backward reaction $\alpha', \alpha, \beta', \varsigma', \varsigma, \sigma', \sigma$ can be determined; and, therefore, n is known.
- If the order of the one reaction is known from experimental data, and *n* is known form experimental data close to stable chemical equilibrium, the order of the other reactions can be determined.

Now, from equation (4.37):

$$\alpha' = \alpha - an, \beta' = \beta - bn, \varsigma' = \varsigma + rn, \sigma' = \sigma + sn\,. \tag{4.39}$$

Thus, using those equalities and equation (4.38), equation (4.31) can be rewritten such that

$$r = \vec{r} - \overleftarrow{r} = \vec{k}[A]^{\alpha}[B]^{\beta}[R]^{\varsigma}[S]^{\sigma} - \overleftarrow{k}[A]^{\alpha-an}[B]^{\beta-bn}[R]^{\varsigma+rn}[S]^{\sigma+sn} \tag{4.40}$$

$$r = \vec{k}\left([A]^{\alpha}[B]^{\beta}[R]^{\varsigma}[S]^{\sigma} - \frac{[A]^{\alpha-an}[B]^{\beta-bn}[R]^{\varsigma+rn}[S]^{\sigma+sn}}{\frac{\vec{k}}{\overleftarrow{k}}}\right) \tag{4.41}$$

$$r = \vec{k}\left([A]^{\alpha}[B]^{\beta}[R]^{\varsigma}[S]^{\sigma} - \frac{[R]^{\varsigma+rn}[S]^{\sigma+sn}}{[A]^{an-\alpha}[B]^{bn-\beta}K_e{}^n}\right) \tag{4.42}$$

where A_1, EA, α, β, ζ, σ, and *n* are constants, which are determined experimentally. Thus, the general form of the kinetic reaction rate used in this doctoral work in which both the forward and backward reactions and equilibrium are considered is given by

$$r = A_1 \exp\left(\frac{-EA}{RT}\right)\left([A]^{\alpha}[B]^{\beta}[R]^{\varsigma}[S]^{\sigma} - \frac{[R]^{\varsigma+rn}[S]^{\sigma+sn}}{[A]^{an-\alpha}[B]^{bn-\beta}K_e{}^n}\right) \tag{4.43}$$

Chemical Kinetics Application and Reactor Design

The geometric and kinetic models presented in Tables 4.8 to 4.11 are used in order to complete the SMR modeling. Among the different rate equations found in the literature for the three chemical reactions in the SMR reactor, the one developed by Xu and Froment (1989) was selected to represent the reaction rate in the kinetic modeling of the

SMR reactor. The values of the frequency factor K_0 and the activation energy EA, appearing in the reaction rate expression, were determined experimentally by Xu and Froment (1989). The methane partial pressure is written in terms of the total pressure, the steam-to-methane ratio, and the actual (kinetic) methane conversion. Finally, achieving equilibrium at the exit of the SMR reactor is desired since it translates in maximum conversion of the methane to hydrogen.

Table 4.8. Geometric model of the SMR reactor.

Variable Description		Model Equation
n_{tubes}^{SMR}	Number of tubes	Assigned value
d_i^{SMR}	Tube inner diameter	Assigned value
A_{cr}^{SMR}	Cross-sectional area (single tube)	$A_{cr}^{SMR} = \frac{\pi \left(d_i^{SMR} \right)^2}{4}$
t_w	Tube wall thickness	$d_o^{SMR} = d_i^{SMR} + 2t_w$
d_o^{SMR}	Tube outer diameter	
P_T^{SMR}	Pitch	$P_T^{SMR} = 1.2 d_o^{SMR}$
D_s^{SMR}	Shell diameter	$D_s^{SMR} = 0.661 \sqrt{\pi n_{tubes}^{SMR} \left(P_T^{SMR} \right)^2}$

Table 4.9. Kinetic model of the SMR reactor.

Variable Description		Model Equation
ζ_{H_2O/CH_4}	Steam-to-methane ratio	Assigned value
$\dot{n}_{CH_4,i}$	Inlet methane molar flow rate	$X_{CH_4} = \frac{\dot{n}_{CH_4,i} - \dot{n}_{CH_4,o}}{\dot{n}_{CH_4,i}}$
$\dot{n}_{CH_4,o}$	Outlet methane molar flow rate	
X_{CH_4}	Actual (kinetic) methane conversion	
P_{CH_4}	Methane partial pressure	$P_{CH_4} = y_{CH_4} P_{SMR} = \frac{1 - X_{CH_4}}{1 + 2X_{CH_4} + \zeta_{H_2O/CH_4}} P_{SMR}$
P_{SMR}	Reformate gas mixture pressure	
T_{avg}^{SMR}	Average reformate gas temperature	$-R_a = r_1 + r_2 + r_3$
R_a	Demethanation reaction rate	
L_{SMR}	SMR reactor length for the design point	$L_{SMR} = \frac{\dot{n}_{CH_4,i}}{\left(n_{tubes} A_{cr} \rho_B \right)_{SMR}} \int_0^{X_{CH_4,eq}} \frac{dX_{CH_4}}{\left(-r_{CH_4} \right)}$

Variable Description		Model Equation
r_1	1st reaction rate	$r_1 = \dfrac{\dfrac{k_1}{P_{H2}^{2.5}}\left[P_{CH4}P_{H2O} - \dfrac{P_{H2}^3 P_{CO}}{K_{eq_1}}\right]}{DEN^2}$
r_2	2nd reaction rate	$r_2 = \dfrac{\dfrac{k_2}{P_{H2}}\left[P_{CO}P_{H2O} - \dfrac{P_{H2}P_{CO2}}{K_{eq_2}}\right]}{DEN^2}$
r_3	3rd reaction rate	$r_3 = \dfrac{\dfrac{k_3}{P_{H2}^{3.5}}\left[P_{CH4}P_{H2O}^2 - \dfrac{P_{H2}^4 P_{CO2}}{K_{eq_3}}\right]}{DEN^2}$
r_K	jth reaction rate	$r_{CH4} = -r_1 - r_3$ $r_{H2O} = -r_1 - r_2 - 2r_3$ $r_{CO} = r_1 - r_2$ $r_{CO2} = r_2 + r_3$ $r_{H2} = 3r_1 + r_2 + 4r_3$
k_i	ith kinetic parameter	$k_i = A_i \exp\left(\dfrac{-E_i}{RT}\right)$
K_j	jth adsorption parameter	$K_j = B_j \exp\left(\dfrac{-\Delta H_j}{RT}\right)$
$DEN = 1 + K_{CO}P_{CO} + K_{H2}P_{H2} + K_{CH4} + P_{CH4} + K_{H2O}\dfrac{P_{H2O}}{P_{H2}}$		

Table 4.10: Kinetic parameters.

Reaction No.	$A_i \quad \left[mol \cdot MPa^{0.5} \cdot (g_{cat})^{-1} \cdot h^{-1}\right]$	$E_i \quad \left[kJ \cdot mol^{-1}\right]$
1	$1.336 \cdot 10^{12}$	240.1
2	$1.955 \cdot 10^{4}$	67.13
3	$3.226 \cdot 10^{11}$	243.9

Table 4.11. Adsorption constants.

Species	$B_j \quad \left[MPa^{-1}\right]$	$\Delta H_j \quad \left[kJ \cdot mol^{-1}\right]$
CO	$8.23 \cdot 10^{-4}$	-70.65
H2	$6.12 \cdot 10^{-8}$	-82.90
H2O	$1.77 \cdot 10^{5}$	88.69
CH4	$6.65 \cdot 10^{-3}$	-38.28

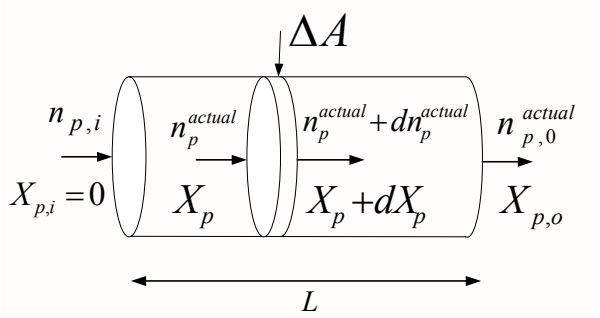

Fig. 4.13. Steam reformer differential discretization.

Mass balance

Once the kinetic expressions have been defined and the corresponding flow rates of the mixture's constituents have been determined, the corresponding mass balance can be applied. Figure 4.13 shows the reformer differential control volume over which the mass and energy balances are applied. For plug flow conditions, dispersion is assumed to be negligible. Thus, the material balance that includes transport, reaction, and accumulation of the reforming gas, can be written as

$$\frac{\partial(-UC)}{\partial x} - R_a \rho_C = \frac{\partial C}{\partial t} \tag{4.44}$$

where C is the methane molar concentration (g-mole/m3), U is the superficial velocity (m/hr), R_a is the methane reaction rate per unit mass of catalyst, ρ_C is the catalyst bed density (kg catalyst / m^3 reactor), x is the axial direction (m), t is time (hr). Let Y be the mole fraction of methane and ρ the molar density of bulk gas. Then, $C = \rho Y$ and the concentration balance is replaced by

$$\frac{\partial \dot{n} Y}{\partial x} - R_a \rho_C \frac{\pi d^2}{4} = \frac{\pi d^2}{4}\left(\rho \frac{\partial Y}{\partial t} + Y \frac{\partial \rho}{\partial t}\right) \tag{4.45}$$

where $\dot{n}$ is the molar flow rate inside the reactor (g-mole/hr) and *d* is the inside diameter (m). Now the mass flow, density, methane mole fraction, and methane conversion along the reactor are given respectively by

$$\dot{n} = \dot{n}_0 + 2X_1\dot{n}_1 \tag{4.46}$$

$$\rho = \frac{P}{RT}\left(\frac{\dot{n}}{\dot{n}_0}\right); \quad Y = \frac{\dot{n}_1(1-X_1)}{\dot{n}_0 + 2X_1\dot{n}_1}; \quad X_1 = \frac{\dot{n}_1 - \dot{n}_0 Y}{\dot{n}_1 + 2Y\dot{n}_1} \tag{4.47}$$

where X_1 is the methane conversion, $\dot{n}_0$ is the initial total molar flow onside the reactor, and $\dot{n}_1$ is the initial methane flow rate. Rewriting the time derivative of ρ yields

$$\frac{\partial\rho}{\partial t} = \frac{\partial\rho}{\partial X_1}\frac{\partial X_1}{\partial Y}\frac{\partial Y}{\partial t} \tag{4.48}$$

A most general expression for the mass balance for species *i* is given by equation (4.49), where the reaction rates r_K comes from Table 4.9, and the transient terms with respect to the walls and the chemical reaction are negligible compared to the heat transfer dynamics.

$$\frac{\partial\dot{n}_i}{\partial x} = -r_i\rho_C\pi A_T \tag{4.49}$$

Pressure Drop

The pressure drop along the catalyst bed (along the tube) is given by (Scott, 1999)

$$\frac{\partial P_i}{\partial x} = \frac{-G_x}{\rho_x g_c D_p}\frac{1-\phi}{\phi}\left[\frac{150(1-\phi)\mu}{D_p + 1.75G_x}\right] \tag{4.50}$$

where $G_x = \rho_x Vel$ (4.51)

and ρ is the gas density, D_p is the particle equivalent average diameter, g_c is the gravity constant, μ is the gas viscosity, and ϕ is the void factor.

Energy balances

Energy balances for the tube-side of the reformer, for the tube-wall, for the combustion gases (shell–side), and for the catalyst are given next.

Reformer gas side energy balance:

The reformer gas energy balance includes the gas sensible enthalpy change, reaction enthalpies, heat transfer from the hotter tube-wall, heat transfer from the catalyst particles, and the accumulation or storage term. The energy equation is as follows:

$$-\frac{\partial\left(\dot{n}c_pT\right)}{\partial x}=h_iA_i\left(T_w-T\right)+h_cA_cA_i\left(T_c-T\right)-A_ic_p\frac{\partial\left(\rho T\right)}{\partial t}-\frac{\partial\left(\dot{n}h_{mix}\right)}{\partial x} \tag{4.52}$$

where c_p is the heat capacity of the tube-side flow (J/g-mole-K), A_c is the external surface area of particles per volume of catalyst bed (m^3/m^2), T_c is the catalyst temperature (K), h_i is the inside heat transfer coefficient (J/hr-m-K), h_c is the catalyst-fluid heat transfer coefficient (j/hr-m-K), ΔH_1 the demethanation reaction enthalpy (J/g-mole CH_4), ΔH_2 the water-gas shift reaction enthalpy (J/g-mole CO). The reaction enthalpies are evaluated at the reactor average temperature. Negative values indicate an exothermic reaction. The heat transfer coefficients (h) are a function of the characteristics of the fluid and the geometry of the reactor.

Shell side energy balance:

The energy balance equation for the shell-side gas includes sensible enthalpy change, heat transfer with the tube wall, and accumulation of internal energy. It can be written as

$$\rho_0A_0c_{p0}\frac{\partial T_0}{\partial t}=-\rho_0V_0A_0c_{p0}\frac{\partial T_0}{\partial x}-h_0A_0\left(T_0-T_w\right) \tag{4.53}$$

where A_0 is the heat transfer area, ρ_0 is the gas density, T_0 is the gas temperature, T_w is the tube wall temperature, h_0 is the heat transfer coefficient.

Tube wall energy balance:

The energy balance for the tube wall includes convective heat transfer with the reformate gas and shell-side gas (combustion gases) and accumulation of internal energy. This balance is written as

$$\rho_w\left(d_0^2 - d_i^2\right)c_{p_w}\frac{\partial T_w}{\partial t} = 4h_0 d_0\left(T_0 - T_w\right) - 4h_i d_i\left(T_w - T_i\right) \tag{4.54}$$

where d_0 and d_i are the external and internal diameter, respectively, ρ_w is the metal density, T_0 is the reformate gas temperature, T_w is the tube wall temperature, T_i is the combustion gases temperature, h_0 is the reformate gas-side heat transfer coefficient, h_i is the combustions gas side heat transfer coefficient, and c_{p_w} is the wall specific heat.

Catalyst energy balance:

The energy balance equation for the catalyst is

$$c_{p_C}\rho_C\frac{\partial T_C}{\partial t} = h_C A_C\left(T - T_C\right) \tag{4.55}$$

where ρ_C is the catalyst density, T is the reformate gas temperature, A_C is the external surface area of particles per volume of catalyst bed (m^3/m^2), T_C is the catalyst temperature (K), h_C is the catalyst-fluid heat transfer coefficient(J/hr-m-K), and c_{p_C} is the catalyst specific heat.

4.3.5 Modeling of the Hydrogen and Air Tanks

Thermodynamic models are developed by applying dynamic mass and energy balances to the fuel and air tanks in order to determine the required inlet and exit mass flows. Creation of robust and detailed thermodynamic models of these components is complemented by geometric models, which are widely applicable and can be used to simulate the buffering requirements at both full and part loads. The final dimensions of the tanks are found by simulating the biggest possible disturbance under the most demanding condition, taking into account the power demand profile and final operating conditions, and by finally computing the fuel demand during the transient.

The mass flow output of the tanks is determined by the stack hydrogen and air requirements, which in turn are defined by the load conditions and load controller. The tank's output is regulated according to the demand using servo valves, which are operated by an electric signal. The mass flow input is determined by the reference pressure in the

tanks. The reference pressure is a parameter required by the control system and is a product of the system optimization. For the hydrogen tanks the inlet mass flow comes from the steam methane reformer, which in turn is feed by a high pressure methane tank. The methane output from this high pressure tank is regulated again by a servo valve and depends, as mentioned above on the hydrogen tank pressure. For the air tank, the inlet mass flow comes from the screw air compressor, whose mass flow output is determined by regulating the compressor speed. The required compressor work input is supply by the expander and the electrical motor. The dynamic energy and mass balance presented next are general and are applied to all three tanks.

$$\frac{dn_i}{dt} = n_{in} y_{i_{in}} - n_{out} y_{i_{out}} \tag{4.56}$$

$$n_T = \sum_{i=1}^{7} n_i \tag{4.57}$$

$$y_{i_{out}} = \frac{n_i}{n_T} \tag{4.58}$$

$$n_T c_{p_T} \dot{T} + \dot{n}_T c_{p_T} T = n_{in} c_{p_{in}} (T_{in} - T_{amb}) - n_{out} Cp_T (T - T_{amb}) - hA(T - T_{amb}) \tag{4.59}$$

where n is the moles of species i in the tank, n_T is the total moles in the tank n_{in} and n_{out} are the molar flow coming in and out of the tank, respectively, y_i is the molar fraction of species i, T is temperature in the tank, c_p is the stream specific heat, h is the tank's heat transfer coefficient, and A is the tank's heat transfer area. In equation 4.59, the sub-script *in* denotes the inlet stream, the sub- script *out* denotes the outlet stream, and the sub-script T denotes the tank.

4.3.6 Modeling of the mass flow control servo-valves

From fluid dynamics, the friction loss through a pipe obstruction is related to the flow rate by a resistant coefficient or a loss coefficient. Thus, the pressure drop through a valve is given by

$$\frac{\Delta P}{\rho} = K\frac{v^2}{2} \tag{4.60}$$

where ΔP is the in static pressure due to friction, ρ is the fluid density, K is the loss coefficient, and ν is the cross-section average velocity at the entrance or exit. The valve capacity $\dot{m}_{full}$ (mass flow rate when fully open) is designated by the flow coefficient C_v as follow. C_v is the manufacturer specification and a characteristic of a fully open valve such that

$$\dot{m}_{full} = C_v\sqrt{\frac{\Delta P}{\rho/\rho_{ref}}} \tag{4.61}$$

Here the reference density is that of water at 60 ^{o}F. From the two previous equations, the loss coefficient K can be expressed in terms of C_v as follow.

$$K = \frac{2}{\rho_{ref}}\left(\frac{A}{C_v}\right)^2 \tag{4.62}$$

As a valve closes, it admits less flow for a given pressure drop. Thus, flow is a function of pressure drop and γ, the fractional opening of the valve ($0 < \gamma < 1$). On which the inherent characteristic function Φ(γ) of the valve depends. Φ(γ) decreases monotonically from 1, for a fully open valve, to zero for a closed valve. The mass flow rate, $\dot{m}$, through the valve in terms of this function is defines as:

$$\dot{m} = C_v\Phi(\gamma)\sqrt{\frac{\Delta P}{\rho/\rho_{ref}}} \tag{4.63}$$

Manufacturers determine Φ(γ) experimentally, measuring pressure drop and flow at various valve openings. Ideally, the pressure drop would be kept constant, as if the valve were installed between two tanks at constant pressure. However, equation (4.63) can be used with any pair of flow and pressure drop measurements. In this doctoral work, a linear inherent characteristic function has been implemented and made a property of the valve such that

$$\Phi(\gamma) = \left(\frac{\dot{m}}{\dot{m}_{full}}\right) = \gamma \tag{4.64}$$

To make use of the valve, it is installed in a pipe, so that in this case the dependence of the flow on the valve opening is defined differently. The installed characteristics are, thus,

$$\frac{\dot{m}}{\dot{m}_{full}} = \Phi(\gamma)\sqrt{\frac{\Delta P\big|_{\gamma}}{\Delta P\big|_{\gamma=1}}} \tag{4.65}$$

In general, installed characteristics differ from inherent characteristics. This does not represent some alteration in the valve (Φ(γ) has not change). Rather this behavior is the result of the pressure drop across the valve varying as the valve is opened. The installed characteristics become even more important while designing the control system, because the dependence of $\dot{n}$ on γ should not show sensitive regions that would make control difficult. The control input to the valve is converted by a transducer into an electrical signal V that varies between 24 and 4 volts. The valve transfer function (a function in Laplace space) relates the voltage in the control actuator to the flow that passes through valve. For linear installed characteristics, the following expression shows the gain at steady state:

$$\dot{m} = \dot{m}_{full}\gamma = \dot{m}_{full}\frac{V-4}{24-4} \tag{4.66}$$

In terms of the deviation V-4, a change of variables results in

$$\dot{m}' = \frac{\dot{m}_{full}}{20}V' \tag{4.67}$$

Transforming this steady state equation into an unsteady state equation using Laplace transform such that the valve transfer function can be written in terms of function *f(s)* in the Laplace domain as follow:

$$G_v(s) = \frac{\dot{m}'(s)}{V'(s)} = \frac{\dot{m}_{full}}{20}f(s) \tag{4.68}$$

where $\dot{m}'(s)$ now represents the dynamic characteristic of the valve. Thus, the gain, i.e. the impact the controller can have on manipulating the flow, increases with $\dot{m}_{full}$ as supplied by a large valve. The transfer function for a valve with linear characteristics is defined by

$$G_v(s) = K_v\left(\frac{1}{\tau s + 1}\right) = \frac{\dot{m}'(s)}{V'(s)} = \frac{\dot{m}_{full}}{20} f(s) \tag{4.69}$$

where *f(s)* equals $1/(\tau s + 1)$, s is the coordinate in the Laplace domain, τ is the valve time constant and K_v is the valve gain. Now, converting the transfer function into the time domain yields the following expression

$$\frac{d\dot{m}}{dt} = \frac{K_v}{\tau} V - \frac{K_v}{\tau} 4 - \frac{\dot{m}}{\tau} \tag{4.70}$$

4.4. Modeling of the Work Recovery and Air-Supply Sub-system (WRAS)

4.4.1 Description of the WRAS

The WRAS is a small but important part of the whole fuel cell system. Figure 4.14 shows a compressor (C) which provides the fuel cell with air. The compressor is driven by an expander (E), which is fed with hot gases from the FPS and air from the stack cathode. An electric motor is used to supply additional power to the compressor in case the power extracted from the expander is not enough to run the compressor. In order to model the WRAS of a fuel cell, it is necessary to model the individual parts, namely, the compressor, the expander, and the motor, followed by a coupling of all elements to an operating sub-system.

It has become very evident through research that the performance and overall efficiency of a fuel cell system is very dependent on the air management sub-system. Unfortunately, no off-the-shelf compressor/expander/motor technologies are available that simultaneously meet the entire unique air supply requirements of fuel cell systems (efficiency, performance, cost, pressure-flow, size and weight). Due to this, a great deal of information from various literature sources and internet homepages were evaluated in order to produce the model of the sub-system described here. To begin with, compressor, expander, and motor performance maps that describe component behavior as a function

of inlet and outlet pressures, mass flow rate, rotor speed, and inlet temperature were developed based on Larminie and Dicks (2003). The compressor map for a general screw compressor (see Figure 4.17) is also the basis for the expander map.

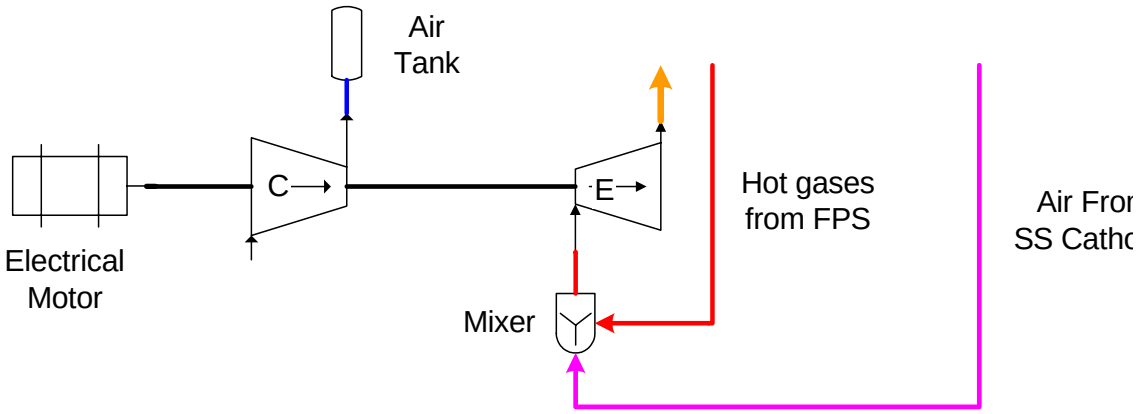

Figure 4.14. WRAS configuration

Kovacevic (2003) was used in the design of the screw compressor in order to determine its dimensions from which moment of inertia and speed could be determined. The governing equation for the compressor and expander were deduced from Bianchi, Peretto, and Spina (1998) as well as from the technical report of The Boeing Company (1977). Equations for modeling the motor were taken from Palm (1986). While motor specifications were taken from the homepage of Minarik Drives & Control (2004). After studying the available literature, it was decided to use a DC motor for running compressor.

4.4.2 Turbomachinery Model Development

In this section the fundamental equations and assumptions used to derive the turbomachonery models are described. Before modeling the entire three coupled components sub-system – compressor, expander, motor – each component is first. The turbomachinery models (i.e. compressor and expander) were developed departing from dynamic mass balance, momentum balance, energy balance as given by equations (4.71), (4.72), and (4.73) respectively and applied to the control volume given in Figure 4.15.

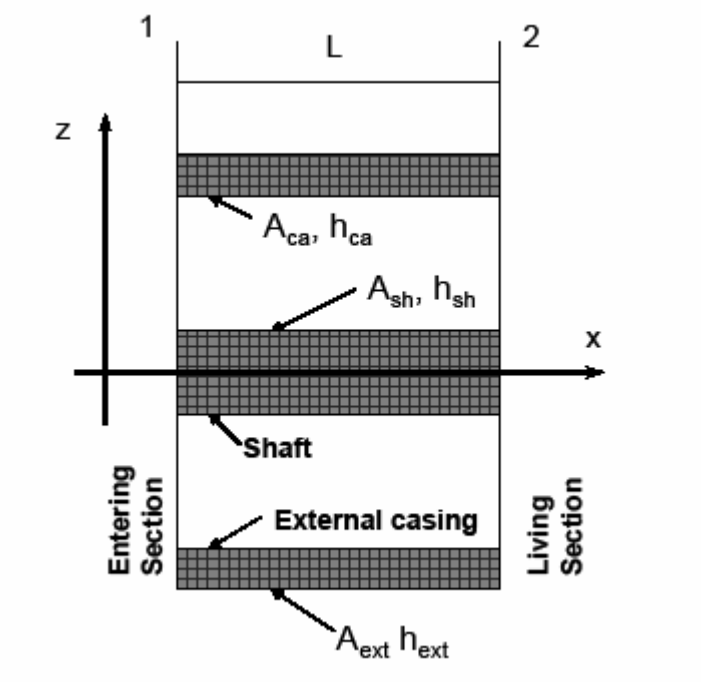

Figure 4.15: Cylindrical portion of turbomachine components.

Mass balance equation:

$$\frac{\partial(\rho v)}{\partial x}+\frac{\partial \rho}{\partial t}=0 \tag{4.71}$$

Momentum balance equation:

$$\frac{\partial\left(p+\rho v^2\right)}{\partial x}+\frac{\partial(\rho v)}{\partial t}=\frac{\partial p}{\partial x}+2\rho v\frac{\partial v}{\partial x}+\rho\frac{\partial v}{\partial t}=-f_a-f_p \tag{4.72}$$

where

$$f_a=\frac{\lambda}{D_h}\rho\frac{v^2}{2} \quad \text{and} \quad f_p=\rho g\frac{dz}{dx} \tag{4.73}$$

Energy balance equation:

$$\begin{aligned}&\frac{\partial}{\partial x}\left[\rho v\left(\frac{p}{\rho}+u+\frac{v^2}{2}+gz\right)\right]+\frac{\partial}{\partial t}\left[\rho\left(u+\frac{v^2}{2}+gz\right)\right]\\&\qquad=\frac{\partial}{\partial x}\left[\rho v\left(h+\frac{v^2}{2}+gz\right)\right]+\frac{\partial}{\partial t}\left[\rho\left(u+\frac{v^2}{2}+gz\right)\right]=q-w\end{aligned} \tag{4.74}$$

where λ is the friction coefficient, g is the acceleration of gravity, ρ is the gas density, p is the pressure, x is the horizontal direction of the flow along the shaft, z is vertical direction, h is the enthalpy, u is the internal energy, and v is the velocity.

The following assumptions are made in the thermal analysis of turbomachinery (i.e. compressor and expander)

- Fluid flow is one-dimensional.
- Since the fluid is a gas, its thermal capacitance is assumed to be small compared to the wall.
- perfect gas $\left(\frac{p}{\rho} = RT \, , c_p = c_p(T) \right)$
- constant gas property in each x section
- $dp = kRTd\rho$ (isentropic transformation)
- negligible elevation variations (dz=0)
- Kinetic energy change between inlet and outlet gas flow negligible
- The heat transfer is calculated assuming single thermal mode representing the casing, impeller and duct wall temperature.

Based on the previous assumptions equation (4.71) to (4.73) are simplified. The resulting equations for the compressor and expander are presented in Tables 4.12 and 4.13 respectively along with the heat transfer model for each the components. Notice that the heat transfer equations apply in the same manner to both compressor and expander. $T_{\infty sh}$ and $T_{\infty ca}$ are assumed to be equal to the ambient temperature. The time component of the energy balance has been neglected since the gas thermal capacitance is assumed to be small compared to the wall.

Although screw compressors are expensive to manufacture, they have important advantages that lead to the choice of that type of compressor. For one, hand screw compressors provide the oil-free output required by the fuel cell system and provide an extended range of pressure ratios. In addition, they operate at a high efficiency over a wide range of flow rates.

Table 4.12. Compressor dynamic governing equation.

Variable Description		Model Equation
Heat transfer between gas and shaft		
U_r	Overall heat transfer coefficient between the shaft and lub system	$C_{sh}\frac{\partial T_{sh}}{\partial t}+U_r\left(T_{sh}-T_{\infty sh}\right)=h_{sh}A_{sh}\left(T-T_{sh}\right),$ $C_{sh}=\rho c_{sh}V$
$T_{\infty sh}$	Cooling temperature of the shaft	
T_{sh}	Shaft Temperature	
C_{sh}	Shaft thermal capacity	
c_{sh}	Specific heat	
h_{sh}	Shaft heat transfer coefficient	
T	Gas mean temperature	
A_{sh}	Shaft heat transfer area	
Heat transfer between gas and external case		
$T_{\infty ca}$	temperature of the ambient	$A_{ca}h_{ca}\left(T-T_{ca}\right)=A_{ext}h_{ext}\left(T_{ca}-T_{\infty ca}\right)+C_{ca}\frac{\partial T_{ca}}{\partial t}$, $C_{ca}=\rho c_{ca}V$
C_{ca}	casing thermal capacity	
c_{ca}	Specific heat	
h_{ca}	casing heat transfer coefficient	
A_{ca}	casing heat transfer area	
h_{ext}	casing external heat transfer coefficient	
A_{ext}	casing external heat transfer area	
T_{ca}	casing Temperature	
Mass balance		
p	Compressor mean pressure	$\frac{\partial p}{\partial t}=\frac{kRT_2}{V_c}\left(m_1-m_2\right)$ $p=\frac{p_1+p_2}{2}$ $T=\frac{T_1+T_2}{2}$ $k=\frac{c_p}{c_v}$
p_1	Compressor inlet pressure	
p_2	Compressor exit pressure	
m_1	Compressor inlet mass flow	
m_2	Compressor exit mass flow	
T	Compressor mean temperature	
T_1	Compressor inlet temperature	
T_2	Compressor exit temperature	
V_c	Compressor volume	

Momentum balance		
A_c	Compressor transversal area	$\frac{\partial m_2}{\partial t} = \frac{A_c}{L_c}\left[(p_1 - p_2) - \Delta p_s\right],$
L_c	Compressor length	
Δp_s	Pressure ratio at steady state	$\Delta p_s = (p_{1s} - p_{2s}),$
p_{1s}	Inlet pressure at steady state	$\frac{A_c}{L_c}(p_{1s} - p_{2s}) = \frac{\lambda}{2D_h}\frac{R}{A_c}\frac{m^2 T}{p}$
p_{2s}	Exit pressure at steady state	$+\frac{R}{A_c L_c}\left(m_2^2\frac{T_2}{p_2} - m_1^2\frac{T_1}{p_1}\right)$
λ	Friction Coefficient	
D_h	Hydraulic diameter	
Energy balance		
h_1	Inlet gas enthalpy	$m_2 h_2 - m_1 h_1 = Q - P,$
h_2	Exit gas enthalpy	
Q_s	heat exchanged in steady state	$Q = Q_s + Q_d,\ \ Q_s = W_c = \Delta T_s \dot{m} Cp$
ΔT_s	Temperature difference at steady state	
T_{2s}	Exit temperature at steady state	$Q_d = \left[C_{sh}\frac{\partial T_{sh}}{\partial t} + C_{ca}\frac{\partial T_{ca}}{\partial t}\right]$
		$\Delta T_s = T_1 - T_{2s} = \frac{T_1}{\eta_c}\left(\left(\frac{P_2}{P_1}\right)^{\frac{\gamma-1}{\gamma}} - 1\right)$
		$T_2 = \frac{1}{\dot{m}c_p}\left\{\left[C_{sh}\frac{\partial T_{sh}}{\partial t} + C_{ca}\frac{\partial T_{ca}}{\partial t}\right] - Q_s\right\} + T_1$
W_c	compressor work	$W_c = c_p\frac{T_1}{\eta_c}\left(\left(\frac{P_2}{P_1}\right)^{\frac{k-1}{k}} - 1\right)m$

Heat transfer from the fluid in a compressor to the impeller and casing is a complex phenomenon, particularly during start-up transients. Heat flows go from the fluid to the casing and then to the ambient; and from the fluid to the impeller and then to the casing and to the ambient through the bearings, seals, and shaft. A more direct approach to model these phenomena is to assume the thermal capacitance of the casing, impeller and inlet duct to be approximated by a single thermal.

Compressor Off-Design Characteristics

The compressor map used in the model is based on Larmine and Dicks (2003). Figure 4.16 below shows the typical performance map for a screw compressor based on four dimension less groups, namely, the pressure ratio, the mass flow factor equal to $\dot{m}\sqrt{T_1}/P_1$, the rotor speed factor equal to $N/\sqrt{T_1}$, and the compressor efficiency. In the model used in this doctoral work pressure ratio and speed are used to obtain the mass flow factor and the efficiency from the map. Since it was not possible to find such a map in the literature for the applications at hand the compressor map with modifications was used for the expander model. These modifications entailed the change of slope of the rotational speed factor lines from negative for the compressor to positive for the expander. Additionally, the mass flow factor axis was properly scaled.

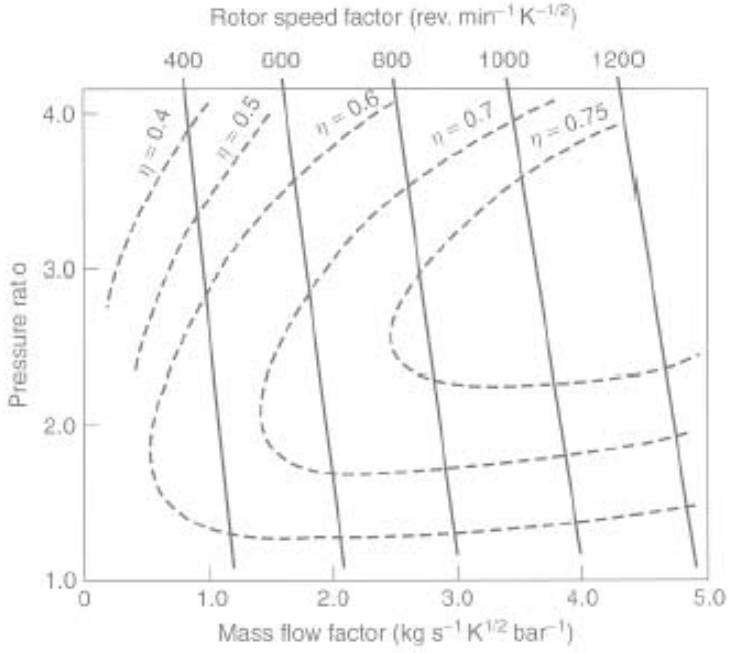

Figure 4.16. Compressor Performance map.

Table 4.13. Expander dynamic governing equation.

Variable Description		Model Equation
Mass balance		
p	Expander mean pressure	$\frac{\partial p}{\partial t} = \frac{kRT_2}{V_E}(m_1 - m_2)$ $p = \frac{p_1 + p_2}{2}$ $T = \frac{T_1 + T_2}{2}$ $k = \frac{c_p}{c_v}$
p_1	Expander inlet pressure	
p_2	Expander exit pressure	
m_1	Expander inlet mass flow	
m_2	Expander exit mass flow	
T	Expander mean temperature	
T_1	Expander inlet temperature	
T_2	Compressor exit temperature	
V_E	Compressor volume	
Momentum balance		
A_E	Expander transversal area	$\frac{\partial m_2}{\partial t} = \frac{A_E}{L_E}[(p_1 - p_2) - \Delta p_s]$, $\Delta p_s = (p_{1s} - p_{2s})$, $\frac{A_E}{L_E}(p_{1s} - p_{2s}) = \frac{\lambda}{2D_h}\frac{R}{A_E}\frac{m^2 T}{p} + \frac{R}{A_E L_E}\left(m_2^2 \frac{T_2}{p_2} - m_1^2 \frac{T_1}{p_1}\right)$
L_E	Expander length	
Δp_s	Pressure ratio at steady state	
p_{1s}	Inlet pressure at steady state	
p_{2s}	Exit pressure at steady state	
λ	Friction Coefficient	
D_h	Hydraulic diameter	
Energy balance		
h_1	Inlet gas enthalpy	$m_2 h_2 - m_1 h_1 = Q - P$, $Q = Q_s + Q_d$, $Q_s = W_E = \Delta T_s \dot{m} c_p$ $Q_d = \left[C_{sh}\frac{\partial T_{sh}}{\partial t} + C_{ca}\frac{\partial T_{ca}}{\partial t}\right]$ $\Delta T_s = T_1 - T_{2s} = \eta_E T_1\left(1 - \left(\frac{P_2}{P_1}\right)^{\frac{\gamma-1}{\gamma}}\right)$ $T_2 = \frac{1}{\dot{m}c_p}\left\{\left[C_{sh}\frac{\partial T_{sh}}{\partial t} + C_{ca}\frac{\partial T_{ca}}{\partial t}\right] - Q_s\right\} + T_1$
h_2	Exit gas enthalpy	
Q_s	heat exchanged in steady state	
ΔT_s	Temperature difference at steady state	
T_{2s}	Exit temperature at steady state	
W_E		$W_E = \eta_E c_p T_1\left(1 - \left(\frac{P_2}{P_1}\right)^{\frac{\gamma-1}{\gamma}}\right)\dot{m}_2$

4.4.3 Electric Motor Model Development

The WRAS requires a motor to back up the power of the expander to run the compressor. It also has the function to balance changes in power requirements. The literature survey (e.g., Minarik Drives & Control, 2004) shows that it is common to use brushless DC motors to run compressors. The motor specifications are presented in Figure 4.17 and the selected specifications of the motor are highlighted. The dynamic equations used for the transient motor model are form by performing an electric power balance in the equivalent electric circuit and a torque balance on the shaft. The resulting equations are presented in Table 4.14.

BOSS BRUSHLESS DC MOTORS SPECIFICATIONS

Minarik Drive	Minarik P/N 530-0X-XXX(N)	Max EMF or Terminal Voltage (V)	Rated Voltage w/Minarik Brushless Drive (V)	No Load Max Speed at Rated Voltage (RPM)	Resistance (ohms)	Inductance (mH)	Torque Constant (Kt = in-lb/A)	Voltage Constant (KeVolts/KRPM)	Motor Peak Torque (in-lb)	Motor Cont. Stall Torque (in-lb)	Motor Max Peak Current (Amps)	Motor Cont. Stall Current (A)	Drive-Motor System Cont. Torque (in-lb)	Drive/Motor System Peak Torque (in-lb)	Weight (lbs)
LVBL02	530-04-210	64	24	2500	3.9	3.2	0.7	8	6.3	1.6	10.4	2.4	1.4	2.1	2.9
LVBL06	530-04-210	64	24	2500	3.9	3.2	0.7	8	6.3	1.6	10.4	2.4	1.4	3.5	2.9
MMBOSS05	530-04-210	64	24	2500	3.9	3.2	0.7	8	6.3	1.6	10.4	2.4	1.4	3.5	2.9
LVBL06	530-04-230	88	24	1800	2.5	2.5	0.9	11	12.7	3.1	15	3.3	2.7	7.4	3.3
MMBOSS05	530-04-230	88	24	1800	2.5	2.5	0.9	11	12.7	3.1	15	3.3	2.7	7.4	3.3
LVBL06	530-04-212	64	24	2500	0.57	0.96	0.7	8	22	4.9	35	7.2	3.5	6.3	4.9
BOSS04 (115 or 230 VAC)	530-08-310	530	260	2500	73	210	7.4	88	26	6	4.3	0.81	5.2	26	4.4
	530-08-270	380	130/260	2000/3000	30	38	5.4	64	26	6	5.3	1.11	6.0/5.3	22.7	7.7
	530-08-312	380	130/260	2000/3000	37	114	5.4	64	22	7	5.9	1.11	7.0/5.2	18.4	7.7
	530-08-272	350	130	2500	14	18	3.7	44	26	6	7.6	1.6	5.3	26	4.4
	530-08-314	350	130/260	2000/3000	18	54	3.7	44	22	7	11.9	2.2	5.3	22	4.4
	530-08-330	530	260	2500	18	82	7.4	88	53	13.3	8.8	1.8	11.1	53	9.5
	530-08-274	260	130	3000	9.3	28	2.7	32	26	6	10.4	2.2	5.3	21.6	4.4
	530-08-316	260	130	3000	9.3	28	2.7	32	22	7	11.9	2.2	5.2	21.6	7.7
	530-08-332	380	130/260	2000/3000	10.4	43	5.4	64	53	13.3	12.2	2.4	13.3/11.1	43.2	9.5
	530-08-350	530	260	2500	10.2	57	7.4	88	76	19	12.7	2.6	17.7	59.2	11.5
	530-08-352	380	130/260	2000/3000	5.4	30	5.4	64	76	19	18	3.6	19/17.7	43.2	11.5
	530-08-370	530	260	2500	6.1	36	7.4	88	104	27	18	3.6	21.3	59.2	12.8
	530-08-334	260	130/260	2500/4000	4.6	20	3.7	44	53	13.3	18	4.8	11.1/11.1	29.6	9.5
	530-08-336	190	130	3000	2.6	10.8	2.7	32	53	13.3	24	4.8	10.8	21.6	11.5
	530-08-372	380	130/260	2000/4000	3.4	19	5.4	64	104	27	24	4.9	21.6/21.3	43.2	11.5
BOSS08 (115 or 230 VAC)	530-08-354	260	130	2500	2.8	14	3.7	44	26	19	25	5.2	17.7	26	11.5
	530-08-410	380	130	2000	2.7	15	5.4	64	94	33	20	6.1	28.4	86.4	15
	530-08-374	260	130	2500	1.5	8.9	3.7	44	104	27	35	7.1	21.3	59.2	12.8
	530-08-356	190	130	3600	1.34	7.5	2.7	32	76	19	35	7.2	17.7	43.2	11.5
	530-08-430	530	260	2500	1.7	12.6	7.4	88	180	60	29	8.1	46.1	118.4	20
	530-08-420	380	130/260	2000/2500	1.5	9.4	5.4	64	139	46	30	8.5	43.2/37.2	86.4	17
	530-08-426	530	260	2500	2.9	18	7.4	88	139	46	22	6.2	37.2	118.4	17
	530-08-412	260	130	2500	1.29	6.9	3.7	44	94	33	30	8.8	28.4	59.2	15
BOSS15 (115VAC)	530-08-412	260	130	2500	1.29	6.9	3.7	44	94	33	30	8.8	28.4	94	15
	530-08-376	190	130	3000	0.86	4.7	2.7	32	104	27	48	9.8	21.3	81	12.8
	530-08-432	380	130	2000	0.9	6.7	5.4	64	180	60	41	11.1	60	162	20
	530-08-416	190	130	2500	0.67	3.6	2.7	32	94	33	41	12.1	28.4	81	15
	[illegible]	[illegible]	[illegible]	[illegible]	[illegible]	[illegible]	[illegible]	[illegible]	[illegible]	[illegible]	[illegible]	[illegible]	[illegible]	[illegible]	[illegible]
	530-08-424	190	130	2500	0.35	2.3	2.7	32	139	46	61	17	37.2	81	17

Figure 4.17. Electrical motor specifications. Minarik Drives & Control (2004).

Table 4.14. Electrical motor dynamic governing equation.

Variable Description		Model Equation
Electric balance		
V_t	Motor voltage	$V_t = RI_a + L\frac{dI_a}{dt} + K\omega$ $W_M = I_a * V_t$
R	Motor electric resistance	
I_a	Motor current	
L	Motor inductance	
K	Manufacturer constant	
ω	Shaft angular velocity	
W_M	Motor work	
Torque balance		
J	Total moment of inertia	$J\frac{d\omega}{dt} = T_M - T_L$ $T_M = \eta\frac{W_M}{\omega}$ $T_L = \frac{W_L}{\omega}$ $W_L = W_c - W_E$ $W_L = \eta W_M$
T_M	Motor torque	
T_L	Required load torque	
W_L	Required load power	
η	Motor efficiency	

Note from table 4.14 that a change in the required power will result in an instantaneous change in the required torque which results in the dynamic variation of the angular velocity. Additionally, a variation in the angular velocity causes a variation in the current. The change in current results in the variation of efficiency obtained from the map. This dynamic variation takes place until the power required is equal to the output power produced by the motor and steady state is reached.

Motor Off-Design Characteristics

The performance map for the motor to determine the motor's off-design behavior was developed using data derived from Minarik Drives & Control (2004). The motor map provides the motor's efficiency versus voltage and current. Maps for two voltages 12 and 24 volts are shown in Figures 4.18 and 4.19, respectively. The efficiency of the motor depending on the current for a 12 Volt and a 24 Volt motor are shown. Linear

interpolation between several voltage versus efficiency maps was used to determine the motor performance.

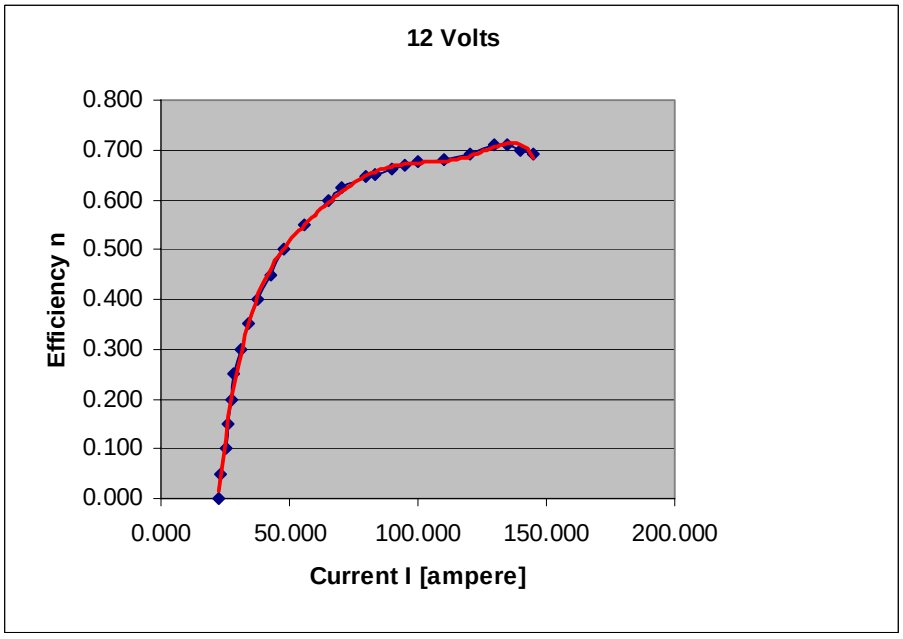

Figure 4.18. Performance motor map (12 volt). Minarik Drives & Control (2004).

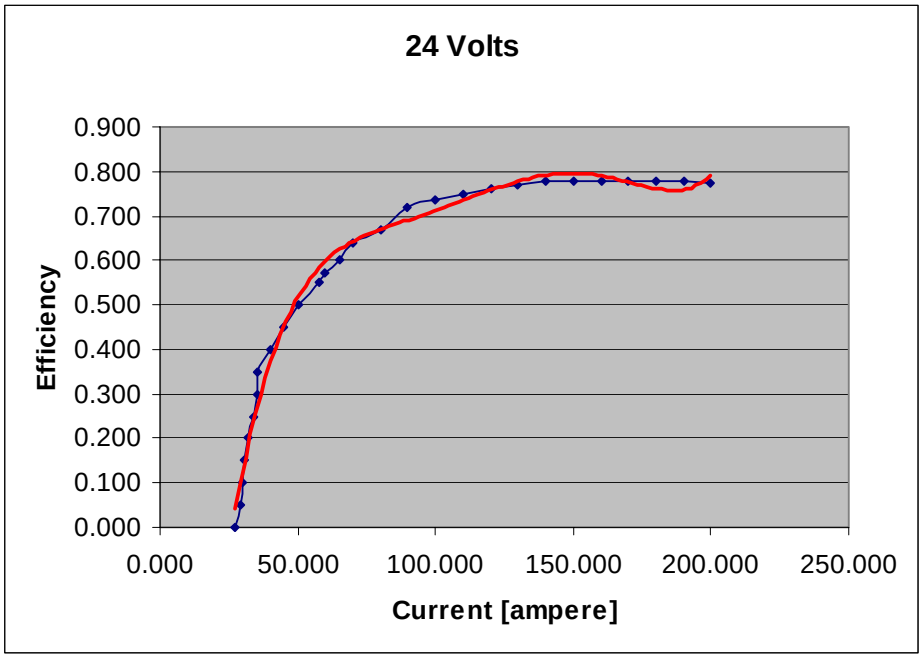

Figure 4.19. Performance motor map (24 volt). Minarik Drives & Control (2004).

Coupling of the Compressor Expander and Motor

The required load on the motor is given by:

$$W_L = W_{comp} - W_{Turb} \tag{4.75}$$

Furthermore, since the compressor, expander, and motor are coupled to each other through the same shaft the rotational speed of all the three components must be the same due to the rigidity of the shaft. Thus, the rotational speed N acts as a coupling constraint variable on the coupled unit such that.

$$N_M = N_{Comp} = N_{Turb} \tag{4.76}$$

The implication of this constraint is that under transient conditions, for example, when the inlet mass flow rate requirement is increased for the compressor, the rotational speed and the power requirement must be varied and correspondingly the rotational speeds of motor and expander are changed. This is done by the control system which adjusts the voltage of the motor instantaneously resulting in the desired conditions. All the state variables of the three components vary according to the dynamic relations and constraint relations described above until the required conditions are satisfied and the system reaches steady state.

As an illustration of the behavior of the complete compressor-expander-motor unit, the dynamic behavior of the rotational speed N for a step change in motor inlet voltage is shown in Figure 4.20. After a step change in sped of about 70 rpm the unit again reaches steady state conditions after about 40 sec. Similarly, the dynamic behavior of the current can be seen in Figure 4.21. The dynamic behavior of the compressor mass flow rate is shown in figures 4.22. The purpose of the motor in this model is to provide the extra power required by the compressor which has not been provided by the expander. The transient behavior of the compressor power, expander power, and the motor power is described in figure 4.23.

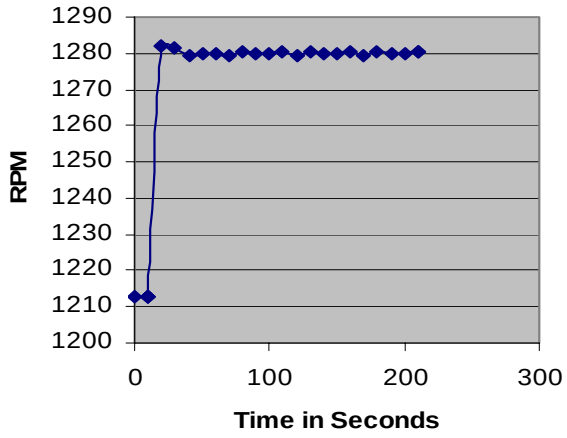

Figure 4.20. Transient behavior of the coupled model's rotational speed.

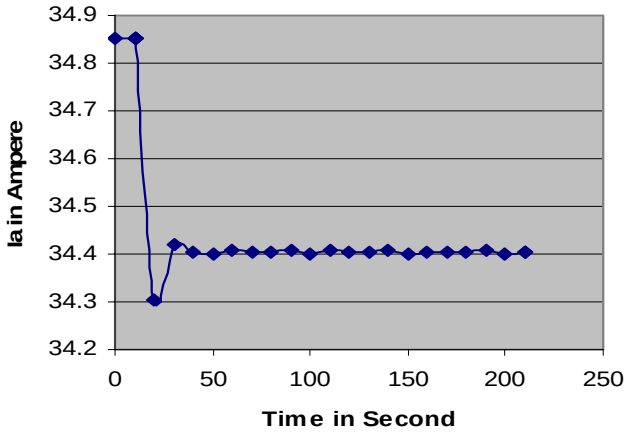

Figure 4.21. Transient behavior of the coupled model's motor current.

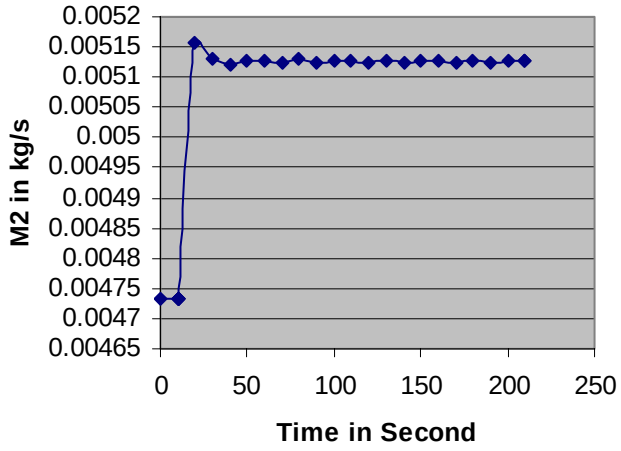

Figure 4.22. Transient behavior of the coupled model's compressor outlet mass flow rate.

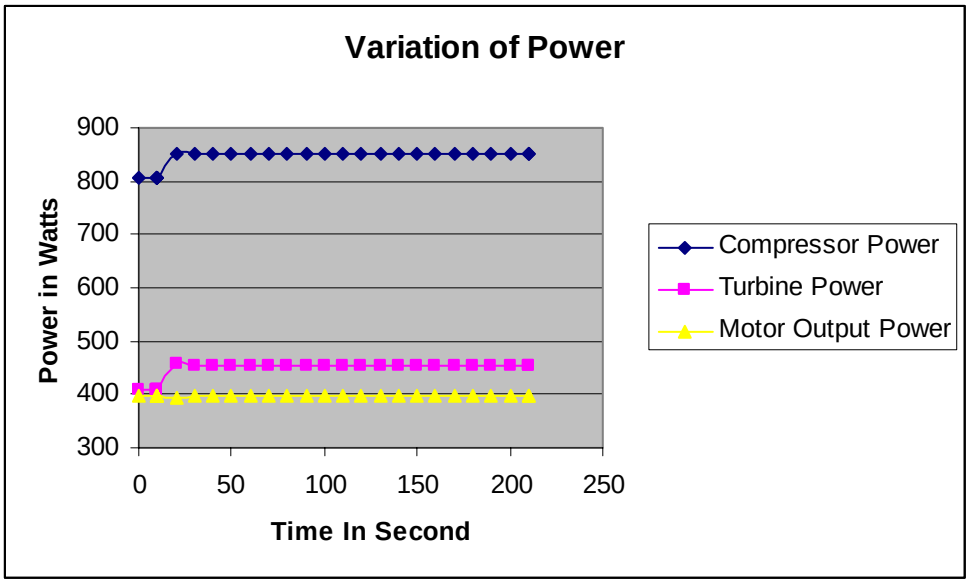

Figure 4.23. Transient behavior of coupled model's power in various components.

4.5 Cost Models of the FPS and WRAS

The FPS capital cost model is based on the development of appropriate cost functions for its components that relate cost to appropriate geometric variables (e.g., volume, heat transfer area, mass). The expressions for the cost functions comprising the FPS purchase cost model are given in Table 4.15. The main sources of component purchase cost information used to obtain the desirable FPS cost correlations are summarized below. The cost functions of the FPS reactors and their catalyst beds are derived from data found in James et al. (1997), Peters and Timmerhaus (1980), and Sinott (1994). James et al. (1997) provide unit prices of the most commonly used catalysts as well as detailed material and manufacturing costs for the multiple reactor parts. Sinott (1994) and Peters and Timmerhaus (1980) suggest the form that a reactor's cost correlation should have, i.e. a power function of its volume, and give the appropriate values of the exponent for different reactor types.

The purchase cost model of the steam generator is obtained by applying regression analysis to data found in Sinott (1994) while the purchase cost information on compact heat exchangers is obtained from correlations developed in the early 1970's by Dieckmann et al. (1972). Finally, the purchase cost of the methane compressor is based

on data found in James et al. (1997). A markup factor of 1.54 (James et al., 1997) that accounts for overhead is applied to all the cost models mentioned above. Moreover, these cost equations have been updated to reflect 2001 U.S. dollars by using the Chemical Engineering Plant Cost Index (2003). The turbo-machinery purchase cost is based on data found in James et al. (1997).

Table 4.15. The FPS purchase cost model.

Variable Description		Model Equation
FPS Cost Model		
V_{SMR}	SMR reactor volume	$C_{bare\ reactors} = 3240\left(V_{SMR}\right)^{0.4}$
$C_{bare\ reactors}$	Bare reactors purchase cost	
$C_{catalyst}$	Catalyst beds purchase cost	$C_{catalyst} = 21,280.5V_{SMR}$
$C_{reactors}$	Reactors purchase cost	$C_{reactor} = 1.54\left(C_{bare\ reactor} + C_{catalyst}\right)$
A_{SG}	Steam generator heat transfer area	$C_{SG} = 1486.8A_{SG}^{0.7}$
C_{SG}	Steam generator purchase cost	
n_{HX}	Number of compact heat exchangers	$C_{HX} = 111.6n_{HX}m_{HX}$
m_{HX}	Compact heat exchanger mass	
C_{HX}	Compact heat exchangers purchase cost	
WRAS Cost Model		
$\dot{W}_{MC}$	Methane compressor duty	$C_{MC} = 162 + 5.746\dot{W}_{MC}$
C_{MC}	Methane compressor purchase cost	
$\dot{W}_{AirC}^{Design}$	Air compressor duty at design	$C_{Comp\_Mot} = \left(1052.058 + 2.74113\dot{W}_{AirC}^{Design}\right)1.5$
C_{Com_Mot}	Screw compressor, electrical motor cost	
$\dot{W}_{Exp}^{Design}$	Recover work at design	$C_{Exp} = 1052.058 + 2.74113\dot{W}_{Exp}^{Design}$
C_{Exp}	Expander cost	
$C_{FPS}^{purchase}$	FPS purchase cost	$C_{FPS}^{purchase} = C_{reactor} + C_{SG} + C_{HX} + C_{MC} + C_{Exp\_Mot} + C_{Exp}$

Table 4.16. Economic assumptions included in the cost models.

Parameter Description		Value	Parameter Description		Value
n_{units}	Number of units manufactured	200000	f_{maint}	Maintenance factor	0.1
t_{oper}	Operating hours per year	8000	i	Capitalization ratio (per year)	10%
n_{years}	Number of years	10	T	FCS lifetime (years)	10

The economic assumptions made in the evaluation of the FPS annualized capital cost are presented in Table 4.16. The capitalization ratio includes return on investment, federal, state, and local income taxes as well as depreciation and property insurance. Since the component purchase cost information is based on a production volume of 500,000 units per year, the effect of a change in the production volume on the unit cost is taken into account by applying an appropriate scale factor to the FPS annualized capital cost (see Table 4.17). This scale factor is derived using information available on the Directed Technologies website (2001). The estimate for the FPS capital cost includes the FPS amortized purchase cost together with its amortization costs as well as a maintenance cost. The FPS maintenance cost is assumed to be constant and equal to 10% of the FPS purchase cost.

The FPS operating cost is associated with the consumption of natural gas throughout the lifetime of the fuel cell system. The unit cost of natural gas over a twelve-month period is given in Table 4.18 and is based on available data from the Energy Information Administration website (2004). The method used to express the capital and operating costs is the method of annualized costs.

Table 4.17. The FPS annualized capital cost estimation model.

Variable Description		Model Equation
C_{FPS}^{maint}	FPS maintenance cost	$C_{FPS}^{maint} = f_{maint} C_{FPS}^{purchase}$
$\dot{C}_{FPS}^{amort}$	FPS annual amortization cost	$\dot{C}_{FPS}^{amort} = i C_{FPS}^{purchase}$
C_{FPS}	FPS capital cost	$C_{FPS} = \left(C_{FPS}^{purchase} + C_{FPS}^{maint} + \dot{C}_{FPS}^{amort} \mathrm{T} \right) \left(\frac{n_{units}}{500,000} \right)^{-0.362}$

Table 4.18. Natural gas unit prices per month (Energy Information Administration, 2000).

Month	Natural gas price ($/kft^3)	Month	Natural gas price ($/kft^3)
January	6.72	July	9.07
February	6.62	August	9.07
March	6.85	September	8.72
April	7.40	October	8.14
May	8.10	November	7.52
June	8.72	December	7.02

4.6 Stack Sub-system (SS) Thermodynamic, Geometric, and Cost Models

4.6.1 Modeling of the SOFC Stack

Since the focus of this doctoral work is the transient behavior of the BOPS and not the SS, a rather straightforward steady state SOFC stack model based on experimental data was developed. This consists mainly of the set of equations presented in Table 4.19. The expression for the polarization curves used to characterize cell performance is based on the Fuel Cell Handbook (2004). It is assumed that the fuel cell stack has a pressure drop of 10% of the inlet air's absolute pressure at full load and falls linearly as the air molar flow rate is reduced. The additional assumptions made in modeling the SOFC stack are shown in Table 4.20.

The required inlet flow rate of the cathode stream as well as the flow rate of the water produced from the reaction in the stack can be determined from the molar flow rate of the hydrogen consumed and stoichiometric calculations. The average oxygen partial pressure for the fuel cell stack air is found from the cathode inlet and outlet conditions along with psychometric calculations. No internal reforming was considered since it introduces temperature gradients that affect the stack life span. Other than the hydrogen reaction no other chemical reaction on the anode side was considered. Finally, the rate of

the heat rejected to the fuel cell coolant, $\dot{Q}_{rej}$, is calculated by performing an energy balance on the fuel cell stack.

Table 4.19. The SOFC steady state stack model.

Variable Description		Model Equation
n_{cells}	Number of cells	Assigned value
A_{act}	Cell active area	Assigned value
T_i^{FC}	Inlet stack temperature	Assigned value
T_o^{FC}	Outlet stack temperature	Assigned value
P_i^{FC}	Inlet stack pressure	Assigned value
T_{avg}^{FC}	Average stack temperature	$T_{avg}^{FC} = \frac{T_i^{FC} + T_o^{FC}}{2}$
$\dot{n}_{H_2}^{'}$	Hydrogen molar flow rate (consumed)	$\dot{n}_{H_2}^{'} = n_{cells}\frac{JA_{act}}{2F}$
P_{avg}^{FC}	Average stack pressure	Polarization curve equations regression $V_{cell}^{actual} = f(J, A_{act}, P_{avg}^{FC}, T_{avg}^{FC})$
J	Current density	
V_{cell}^{actual}	Actual cell voltage	
$\dot{E}_{stack}^{gross}$	Stack gross power produced	$\dot{E}_{stack}^{gross} = n_{cells}V_{cell}^{actual}JA_{act}$

Table 4.20. SOFC stack model assumptions.

Parameter Description		Value
η_F	Faradaic efficiency	100%
$\phi_i^{cathode}$	Relative humidity of atmospheric air	75%
$\zeta_{stoich}^{cathode}$	Cathode stoichiometric ratio	2.2
f_{H_2}	Hydrogen utilization factor	0.85

4.6.2 Cost Models of the SS

The SS purchase cost is broken down into the fuel cell stack purchase cost and the SS auxiliary equipment (i.e. sensors and control valves) purchase cost. The fuel cell stack

cost structure is presented in Table 4.21. As with the FPS capital cost model, the objective is to come up with cost functions that relate the above mentioned stack costs to appropriate geometric variables, i.e. cell active area and the total number of cells. The detailed fuel cell stack purchase cost model presented in Table 4.21 is derived from analyzing the cost information found in Oei et al. (1997) and in Arthur D. Little (2000). The SS auxiliary equipment purchase cost is assumed to be equal to 10% of that for the fuel cell stack. Since the above information is based on a production volume of 500,000 units per year, the same scale factor as the one appearing in the FPS cost model is applied to the SS capital cost to account for the SS unit cost variation due to a change in production volume.

Table 4.21. Cost models of the stack sub-system.

Variable Description		Model Equation	
C_{stack}	Fuel cell stack purchase cost	C_{ass}	Stack purchase cost
		$C_{ass} = (0.02687 A_{act} + .88) n_{cell}$	
		$C_{extra\ material}$	Endplates, collectors, insulators, and tie bolts
		$C_{extra\ material} = 248.96$	
		$C_{assembly}$	Stack assembly cost
		$C_{assembly} = 30.8 + 0.3465 n_{cells}$	
C_{aux}	Auxiliary equipment purchase cost	$C_{aux} = 0.1 C_{stack}$	
$C_{SS}^{purchase}$	SS purchase cost	$C_{SS}^{purchase} = C_{stack} + C_{aux}$	
C_{SS}^{maint}	SS maintenance cost	$C_{SS}^{maint} = f_{maint} C_{SS}^{purchase}$	
$\dot{C}_{SS}^{amort}$	SS annual amortization cost	$\dot{C}_{SS}^{amort} = i C_{SS}^{purchase}$	
C_{SS}	SS capital cost	$C_{SS} = \left(C_{SS}^{purchase} + C_{SS}^{maint} + \dot{C}_{SS}^{amort} \mathrm{T} \right) \left(\frac{n_{units}}{500,000} \right)^{-0.362}$	

The SS capital cost estimate is based on the same economic assumptions as those made in the calculation of the FPS capital cost and includes the SS purchase cost as well as amortization and maintenance costs (both given as a percentage of the purchase cost).

There are no SS operating costs since the only resource consumed in the SS is the hydrogen-rich reformate gas produced by the FPS.

4.7 Fuel Cell System Control Challenges, Control Problem Definition, and Synthesis/Design and Operational Issues

In recent years, rapid and significant advances in fuel cell stack technology, together with advances in power electronics and control systems, has enabled the development of high performance fuel cell systems for stationary and mobile applications. Apart from the obvious advantage of low emissions, the overall fuel cell system static and dynamic performance and power and energy efficiency are critically dependant on the intelligent design of the control system and control strategies. These include the control of fuel cell system's heat and steam management, fuel (hydrogen) and air supply and distribution, main and auxiliary power management, and system integration. For the case of using an onboard or in-place fuel processor as the hydrogen supply sub-system, the control challenges become even more extensive and difficult, requiring innovative management of slower heat transfer and chemical reactions effects for start-up, turn-down, and abrupt changes in load, as well as the control of the mass flow, pressure, and temperature of the fuel and air. This section describes the variety of control challenges being encountered and the strategies being used for the successful development of affordable SOFC based auxiliary power units.

4.7.1 WRAS Control Issues

Unlike a naturally aspirated internal combustion engine, a fuel cell stack requires a forced air supply at system pressure. It is important that the flow through each cell should be evenly distributed, especially when diluted reactant gas such as air used, in order to avoid trapping the partially depleted reactant gas in a relatively restricted flow area. Additionally, when changes in load occur, it is extremely important to keep the appropriate air/hydrogen ratio in the cell in order to avoid cell degradation, high parasitic loads, or starvation induced loads. To assure the flow through each cell at an optimum operating pressure, the air supply system requires coordinated pressure and flow control

systems. An air compressor with speed control features can be used to supply different amounts of air for a wide range of power demands in order to reduce parasitic power losses. Also, to recover energy from the gases exiting the FPS, an expander can be integrated with the compressor. Additionally, an electrical motor is needed in order to account for additional power demand by the compressor and for start-up. These three components operated on a single shaft.

Thus, the process of controlling the WRAS is complicated and should be integrated with that of the stack control sub-system. It is not possible to control both pressure and flow using a one variable flow control input with fixed downstream restrictions unless the exact amount of flow consumption is known. This would lead to an open-loop speed or flow control with inner feedback control loop which may, however, result in pressure variations due to parameter variations and disturbances. To achieve more precise and robust simultaneous control of both flow and pressure, an additional solenoid flow control valve is needed at the downstream end with both pressure and flow feedback measurements.

One of the most important performance criteria for both stationary and mobile fuel cell system is the transient response to power demands. The fuel cell itself has a very fast dynamic response. However, the response times of the FPS and WRAS sub-systems are dependent on system synthesis/design and will affect overall system transient performance. A speed controlled air compressor with long lines may produce significant first order transport delays in system response. Additionally, the fuel cell system fast transient response may cause degradation (e.g., due to sudden fuel depletion on the fuel cell stack) if in the event of load changes proper fuel and air supply is not provided rapidly enough and is not properly coordinated. To overcome the inevitable delays in the WRAS response, an accumulator type pressure tank with a solenoid control valve can be added near the fuel cell stack input port. This approach has additional benefits from a noise control stand point and may be used for fast start-up of the fuel cell at the cost of packaging space. Another simplistic approach is to provide excess air flow at a cost to system efficiency. A more cost effective approach is to use a predictive control method, which can be implemented in the form of adaptive gain control or feedforward control using look-up tables or fuzzy logics on top of the regular feedback control loop. It is

worth looking into research on predictive control. However, there is a big obstacle that makes its practical application not very effective yet. This barrier is the change in the stack's natural gain through the entire operational range, i.e. the power versus current density curve has a change in slope as the current density increases. At which power and current density point this change happens is difficult to predict as operational conditions change. For this reason, current control systems are PID based.

4.7.2 FPS Control Issues

For direct hydrogen fuel cell systems, liquid or compress gas hydrogen is stored in a tank. The control task in the hydrogen supply system is to keep the fuel cell flooded with hydrogen and circulated at the same pressure as the air supply pressure, independently of the hydrogen consumed and in proportion to the electrical current draw. It may also be important to minimize the pressure difference between the fuel-supplied anode and the air-supplied cathode. The same control issues apply to the of onboard or in-place fuel processors. However, in this case additional control issues arise. The control problem encountered in the fuel processor is very complicated. Like any other chemical process it is multi-input/multi-output (MIMO) control system; and to achieve highly efficient chemical conversion, it is important to have precise pressures, temperatures, and mass flow rates of the various reactants at different locations. Furthermore, on overall sub-system controllability analysis is critical in designing proper control algorithms. For instance, controlling the fuel flow to meet the fuel cell power demand and at the same time meet the energy demand at the reformer using exhaust gases may result in an uncontrollable situation. Therefore, accurate control of the reactant ratios at the reactor and at various operational conditions is critical in achieving good overall system performance, fuel economy, and emissions, quite a challenging control task.

Other that packaging issues, one of the most significant drawbacks of onboard or in-place fuel processing is the system time constant which can be considered dependent on the synthesis/design. Slow dynamic response is mainly due to the slow heat transfer, mass transfer, and mixture delays. There are several control difficulties imposed by these slow dynamics at various points of transient operation, such as cold start-up, turn-down, and shut-off as well as overall system instabilities for normal transient operation. The

optimum SOFC based APU's start-up strategy is presented in Chapter 6 with dynamic analysis focusing on the heat transfer effects. To compensate for such slow dynamics pressurized air and hydrogen tanks for energy buffering under transient conditions can be incorporated along with a battery bank. This of course, implies additional cost, weight, and packaging space but is an effective solution to dealing with transitions between high and low loads and, increase the feasibility of such systems for high performance, highly dynamic applications.

Three dynamic state variables must be controlled at the steam-methane reformer (SMR). These are the methane conversion, the reformate output temperature, and the steam-to-methane ratio. In order to perform this task, three control variables are defined, namely, the hot gas inlet temperature and mass flow and the recirculation factor. The latter is explained below. In order to pair the control variables and the state variables in the correct manner, a sensitivity matrix analysis was performed. The results are shown in next section. The SMR requires a methane mixture rich in steam. The steam can be produced using a steam generator. However, using this component requires extra energy to evaporate the water and to run the water pump. To avoid this burden a fraction of the water-rich cathode products are recirculated back to the inlet of the SMR. Due to transport delays, the steam to methane ratio changes during transient operation if the recirculation fraction is kept constant. In order to guarantee proper steam-to-methane ratio, a three-way control valve should be implemented at the cathode exit.

The cathode inlet pressure control can be designed using a pressure control valve with a reference pressure port directly connected to air the manifold. To have more flexibility in controlling the system pressure, the reformate tank pressure is controlled using a feedback controller to regulate the methane tank exit mass flow and pressure, which in turn uses the air tank pressure as the reference point. When designing the flow circuit, it is important to avoid choked flow to prevent fuel starvation at high power operation.

The output temperature in the burner is controlled by regulating the methane flow rate into the burner mixer. This requires an additional control valve at the methane tank exit. The hot gas mass flow is controlled by regulating the amount of air into the burner mixer. This requires a three-way valve at the cathode output.

4.7.3 Fuel Cell System Heat Management Issues

Most of the losses in the fuel cell electrochemical reaction process are converted into a thermal release of energy, resulting in a significant amount of stack heating, a substantial amount of which must be removed from the fuel cell stack. To recover this energy for use inside the fuel cell system is impractical for operational, packaging, and cost considerations. For example, the stack operational temperature is 1000 ^{o}K, which is lower than the required steam-methane reformer hot gas inlet temperature. Furthermore, transferring energy to the air stream requires additional heat exchangers which increase the system's capital cost and increases its packaging space. For these reasons, the stack excess thermal energy is removed using a fan which passes air across the stack. The air mass flow is determined by the stack reference temperature. The fan power is considered as a parasitic load. However, the output air is at a high temperature and can be used for heating a house in the case of stationary applications or a cabin in the case of transportation applications. The stack thermal management is more of a system synthesis/design issue than a feedback control. Once the system is synthesized/designed a simple temperature feedback control is sufficient to meet the control needs.

In order to reduce the temperature gradients across the fuel cell stack, the inlet stream temperatures are set equal to the stack output temperatures with a variation of five degrees (i.e. 1000 ^{o}K ± 5 ^{o}K). In order to achieve this temperature range, a compact heat exchanger network is implemented. The fundamental idea is to transfer energy from the stack output streams to the input streams. The precise configuration is shown in Chapter 6. Note that the heat exchanger required geometry is a product of the dynamic optimization problem as are the configuration and controller.

4.7.4 Power Electronics Sub-system Considerations

SOFC based power electronics sub-systems (PES) are used to provide direct or alternating current (ac or dc) to satisfy application specific power needs. Typically, they include multiple, interconnected power converters (typically a dc-dc converter followed by a dc-ac converter for stationary applications and a dc-dc converter for mobile

applications). The switching scheme in such power converters can be based on pulse-width modulation (PWM), resonant, quasi-resonant, soft-switched, or line-commutated. Furthermore, the topological structures of these converters can be vastly different from each other. As such, the mathematical models of the PES may include discontinuous differential equations, discrete differential equations, functional differential equations, digital automata, impulsive differential equations, non-smooth differential equations, ordinary and even partial differential equations. In addition, these models require system-level constraints.

Due to the lack of a PES model which can be coupled to the models in this doctoral work, it is assumed that the battery bank is part of the PES and is able to provide immediate power to the system or application. Therefore, the PES is not a part here of the optimization process. Currently, a research team from the University of Illinois, Chicago, and Virginia Tech led by Dr, Michael von Spakovsky and Dr. Sudip Mazumder are working to generate the software platform in order to perform a system-level dynamic optimization which includes PES and SS dynamic models as well as the FPS and WRAS dynamic models developed, optimized, and presented here.

4.7.5 Overall Control System and Control Law Strategies

Figure 4.24 shows the proposed control scheme for the FPS and WRAS integrated with the PES and SS. A multi-level control approach is used in order to help improve the time response of the BOPS. The first level is determined by the air and fuel tank pressures. An objective of the FPS and WRS is to keep the tank pressure at predefined values. Disturbances in tank pressures appear as the fuel and air stack requirements change. Control strategies should guarantee that the fuel in the tank is never depleted and should ensure that no shut-down process is complete before proper levels of fuel and air in the pressurized tanks are reached.

Two additional control actions are implemented for the SMR with the objective of regulating the reformate gases exit composition and temperature. As mentioned above, at the SMR, the reformate gases temperature and composition are controlled using the hot gases inlet temperature and mass flow, respectively, as control variables. The pairing of the state and control variables was determined using the relative gain array matrix

technique (i.e. a common technique of control theory). Table 22 shows the control and state variables pairing used in order to implement the proposed control strategy.

The second level of control is defined by the hydrogen and air stack requirements. As the load changes, the amount of hydrogen (reformate) out of the tank is changed by regulating the flow valve. The air tank valve is regulated to maintain the proper stoichiometric ratio in the stack.

The third level of control is defined by the rate change in load demand and battery bank charge level. For sudden changes in load, the difference between the produced and required power is supplied by the battery bank. The power required to keep the charge level is considered a parasitic power. Finally, for small increments in power demand, the system is able to assure direct stack response until proper hydrogen (reformate) mass flow is reached. This is done by increasing the fuel utilization up to safe levels. Reductions in power demand are easier to control, since these can be met by reducing fuel utilization, reducing hydrogen mass flow, and by switching the battery bank to charge mode.

Table 4.22. Control and state variables pairing[44]

Component	Control Variable	State Variable
Steam-methane reformer	Hot gases inlet temperature	Reformate gas exit temperature
	Anode recirculation fraction	Steam to methane ratio
Reformate tank	Methane mass flow	Tank Pressure
Air Tank	Electric Motor volts	Tank Pressure
Fuel Cell Anode	Valve volts	Reformate mass flow
Fuel Cell Cathode	Valve volts	Air mass flow

[44] The controller gains are treated as design decision variables in the optimization problem.

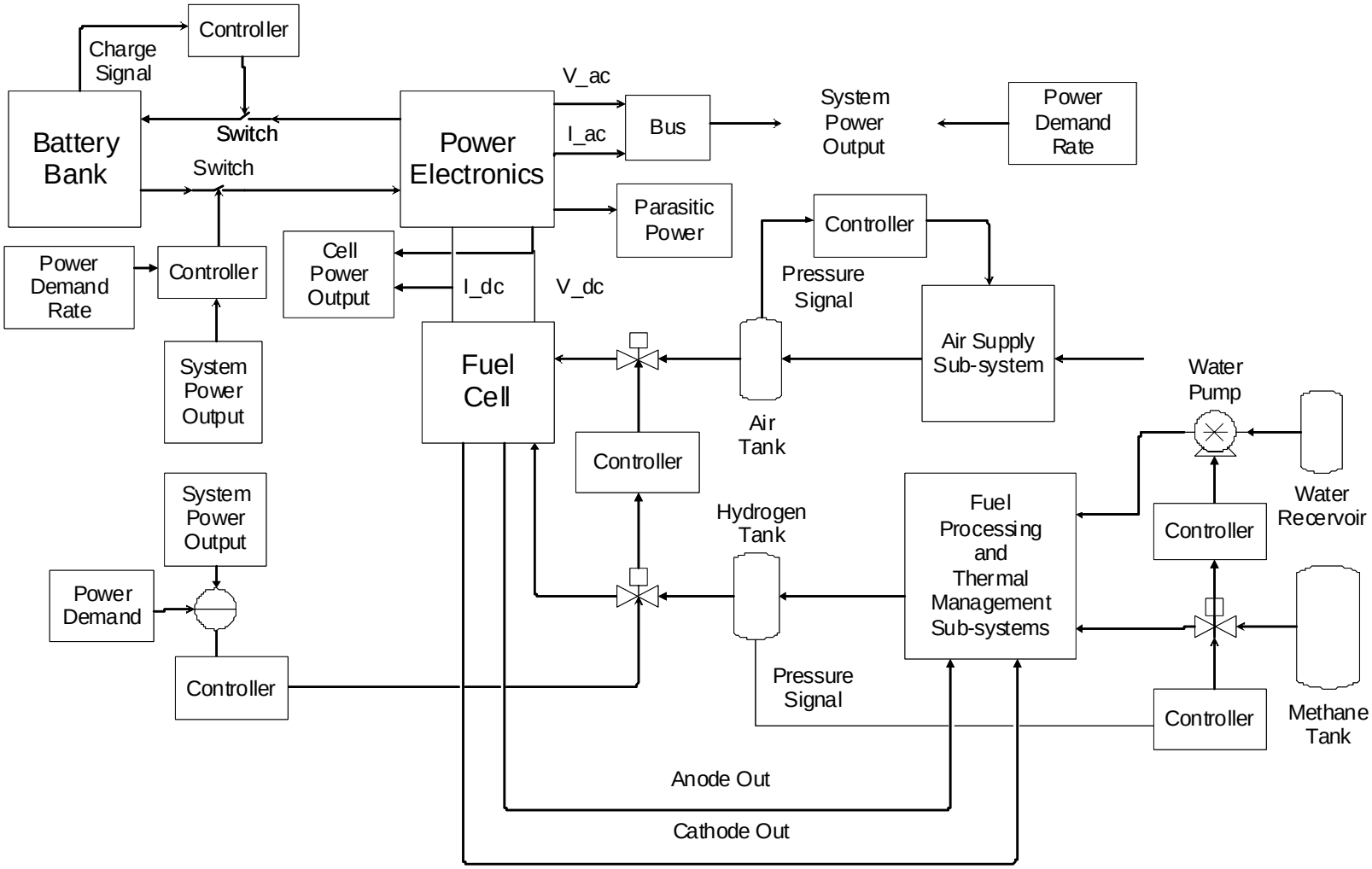

Figure 4.24. Multi-level control system configuration.

4.7.6 Control Parameter and Control Variable Set Definitions

A set of system-level operational/control parameters have been defined, whose purpose is to keep the component level dependent variables within acceptable ranges, which in turn can be initially defined as component control limits (e.g., design limitations such as maximum stack inlet temperature) or as the output of a trade-off or optimization process (e.g., steam reformer optimum operational temperature). The system-level control parameters for the BOPS are the steam-to-methane ratio (SMR), the fuel utilization (FU), the air to fuel ratio (AFR), and the fuel reformate ratio (FRR). The steam-to-methane ratio allows control of the chemical reaction inside the steam reformer and the reactants inlet temperature. FU directly controls the heat and work recovery and is important for characterizing the reaction in the stack. However, since the primary focus here is on the BOPS, it has been set constant. AFR directly controls the parasitic power requirements and the heat load in the reformer, which is directly tied to the methane conversion at the SMR. Finally, FRR allows control of the inlet temperatures to the stack and the outlet temperatures of the SMR by determining the hot gases temperature at the burner exit. In addition, during start-up the stream of combustion gases leaving the SMR is divided into two streams which go to the air pre-heating heat exchangers and the steam generator. The proportions into which this stream is divided can be used as a control parameter.

These system-level operational/control parameters, in the early stages of the synthesis/design process, are considered as synthesis/design choices, which are a valid subject for system optimization. The optimization process then determines an optimal system synthesis and a set of optimal component designs consistent with an optimal choice of values for these system level operational/control parameters both at design and off-design. Thus, transient phenomena (e.g., change in power demand, start-up, etc.) are taken into account in the optimal synthesis/design process by, for example, minimizing the time response or fuel consumption as a function of these parameters at off-design so that the optimal control of a system's operation affects (compromises) what would otherwise simply be a single-point synthesis-design.

4.7.7 Fuel (Reformate), Air, and Electrical Energy Buffering Considerations

SOFC stacks respond quickly to changes in load while the BOPS responds in times several orders of magnitude higher. This dichotomy diminishes the reliability and performance of SOFC electrodes with increasing load as do current and voltage ripples which result from particular PES topologies and operation. These ripples, load changes, and the difference in transient response between the electrical-electrochemical components for the PES and SS and those for the chemical-thermal-mechanical components of the BOPS must be approached in a way which makes operation of the entire system not only feasible but ensures that efficiency and power density, fuel utilization, fuel conversion, and system response is optimal at all load conditions. The undesirable effects of these orders of magnitude differences in transients can be approached by introducing fuel, (reformate), air, and electrical energy buffering into the system layout. Fuel (reformate) and air buffering have been shown to be a practical and efficient way of reducing the time delay due to the FPS. In the same way electrical energy buffering compensates the PES imbalance due to load perturbations, especially during start-up.

As can be seen in Figure 4.10 and in Chapter 6 for the optimal configuration, such buffering has been added to the system configuration. Typically, buffering is only used in stationary systems because of the additional weight and volume, which is an operational penalty for transportation systems. However, in this research, the air and fuel tanks considered are very small and light (initial tank designs have yielded 1 liter volumes), since the tanks are used to minimize transient effects, to increase response capabilities, and to minimize sub-system interaction effects during transients. They are not intended for long-term storage. With this in mind, it is reasonable to explore a trade-off between the advantages and disadvantages of using buffering devices.

The control strategy developed for the BOPS ensures that the fuel (reformate) and the air in the tanks are never depleted. In addition, during load transients, the load on the SOFC, which is not a stiff voltage source and is, thus, connected to the load through the PES, is met by the batteries until the BOPS is able to supply fuel (reformate) at the

required rates. However, because the batteries (depending on their size) discharge at relatively rapid rates, their duration of operation is relatively small and must, therefore, be combined with a pressurized fuel (reformate) tank which can rapidly supply fuel to the stack. In addition, for transportation applications, the intention is to use the actual battery set of the vehicle instead of a separate battery bank. For stationary applications, batteries could be replaced by the electrical grid.

4.7.8 Advantages of Using Fuel (Reformate), Air, and Electrical Energy Buffering

As already mentioned above, a significant increase in the load demand can cause anode degradation (i.e., oxidation) due to "fuel starvation" along the electrode. Fuel (reformate) buffering minimizes this effect by supplying, almost immediately; the required (reformate) fuel to the stack for any given load. Control strategies should be developed to guarantee that the fuel (reformate) in the tank is never depleted. Furthermore, since the fuel (reformate) and air tanks are pressurized, their contents can be immediately used for start-up. This improves the time response by minimizing the effects of the time delay due to the FPS.

As to electric energy buffering, because the SOFC is not a stiff voltage source, it is connected to a PES, which serves as an interface between the SOFC and the application load. The behaviors of the PES (for example, the magnitude and frequency of the current and voltage ripples) and that of the time-varying load have a direct impact on stack performance and the durability (lifetime) of the fuel cell. If the peak-current levels from these loads are high, it can lead to a low-reactant condition within the SOFC. Similarly, variations in the output voltage (of the SOFC) can directly affect the operation of the integrated PES and the application load. Thus, having a supply of electrical energy during operation at peak-current levels lessens undesirable effects on the SOFC stack.

4.7.9 Energy Buffering Devices for Load-Transient Mitigation

Results of a simple analysis of the impacts of battery[45] and pressurized hydrogen tank[46] on mitigating the degrading effects of load transients are shown below. Figure 4.25 shows a typical tubular solid oxide fuel cell (TSOFC) system, supplying stationary power to an electric grid. To mitigate the effects of load transients, a battery is connected between the DC-DC and DC-AC stages, while a pressurized hydrogen tank supplies the instantaneous requirements of hydrogen to the SOFC. During steady-state operation, the TSOFC provides power to meet the load demands as well as recharge the battery. For durable TSOFC systems, the energy-storage devices must be large enough to mitigate the effects of load transients. Figure 4.26 shows the variation of the response time[47] of the TSOFC system with the size of the battery and the hydrogen molar-flow rates of the pressurized hydrogen tank. From this figure one can observe that the smallest response time can be achieved using largest size battery and high hydrogen molar-flow rates. However, this comes at the cost of low-power-density and high cost. For the purpose of this study, we assume that response times in the range of 0.2 s to-0.35 s are acceptable for reliable TSOFC system operation.

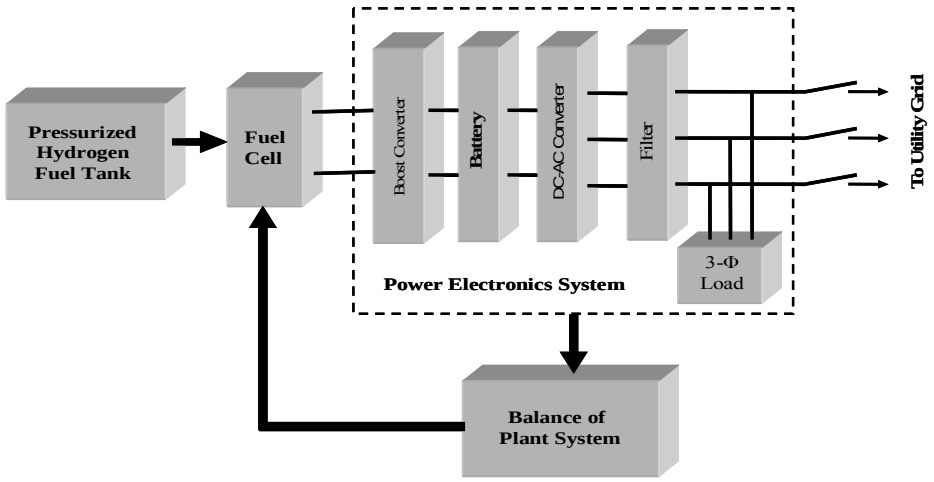

Figure 4.25. TSOFC system topology containing pressurized hydrogen fuel tank and battery for load-transient mitigation (Mazumder et. al., 2004).

[45] High-energy-density batteries are used to supply the instantaneous energy requirements during load transients. However, because the batteries (depending on their size), discharge at rapid rates, their operating life is very small.

[46] Fuel buffering using a pressurized hydrogen tank mitigates the effects of load transients by supplying, almost immediately, fuel at the required rates to the stack for any load condition. Suitable control strategies guarantee that the fuel in the tank is never depleted. Furthermore, since the fuel- and air-supply tanks are pressurized, their contents can also be used during start-up.

[47] A TSOFC system response times are a measure of its reliability. TSOFCS reliability increases with a decrease in the response times.

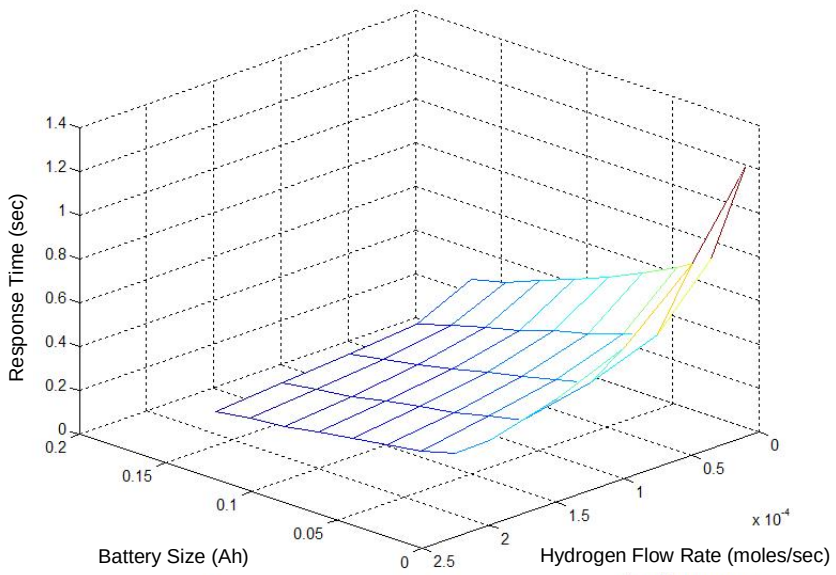

Figure 4.26. Variation of TSOFC response time with battery size and hydrogen flow rate (Mazumder et. al., 2004).

4.8. Computational Tools and Validation Efforts

In order to perform the simulation of the detailed dynamic models presented in this chapter gPROMS ® form Process Systems Enterprise's was used. gPROMS® is a powerful general-purpose process modeling and optimization environment used to enhance design and operation of continuous and batch processes. It allows one to build high-accuracy models of process and energy conversion systems.

gPROMS® stands for general Process Modeling System. It is an advanced general purpose process modeling, simulation and optimization software. gPROMS® is actually a family of products for process modeling which can be integrated to basic programming, CDF, and control tools among others, including other dynamic simulators. gPROMS® models can be used for steady-state and dynamic simulation, estimation and optimization within the gPROMS® user interface, or embedded in and external solution engine. Additionally, gPROMS® provides numerous facilities for design of control systems and their implementation.

At its core gPROMS® is an equation-based system, meaning that processes are described by their underlying physical and chemical relationships and the operational

task sequences superimposed on them. gPROMS® analyses the relationships governing the process and then performs your solution of choice - dynamic or steady-state simulation, optimization or parameter estimation. This enables designers to quantify process design and operation.

Te models developed in this research were validated using published data from different authors. Bianchi, Peretto, and Spina (1998) report experimental data of a compressor-turbine assembly, which along with data from Minarik Drives & Control (2004) were used to validate the WRAS model performance. Data from Kays and London (1998) where used to compare against the compact heat exchanger models. The work by Bausa and Tsatsaronis (1998) was referred in order to implements the steam methane generator. Alkasab and Lu (1991) show experimental data performance for steam reformer steady and dynamic operation.

Chapter 5

Optimization Strategy and Coupling Function Definitions for the SOFC based APU

This chapter presents in detail the procedure followed for the dynamic synthesis/design and operation/control optimization of the proposed fuel cell system (FCS). *Physical decomposition* is used for this purpose. *Time and conceptual* decomposition are avoided by using the dynamic models and applying DILGO using the dynamic shadow prices. In the case of physical decomposition, three different sub-systems, namely the FPS, SS, and WRAS are taken into account and their coupling functions described. The decomposed optimization problems for the three units considered are defined and the DILGO approach presented in the previous chapter is applied.

5.1 System-Level Dynamic Optimization Problem Definition

The interdependence between the three units (sub-system) being synthesized/designed (the SS, FPS, and WRAS) is quite tight. Although there are other units, namely, the battery bank and power electronics sub-systems (BBS and PES), they are not synthesized/designed, i.e. they do not have decision variables which are optimized. Thus, for example, the FPS's optimal synthesis/design is affected by the optimal synthesis/design decisions made in the SS and WRAS as well as by the load requirements dictated for the BBS and PES. The result is that the fuel cell system at hand constitutes the typical case of a system in which "everything influences everything else".

Thus, determining the optimal synthesis/design and dynamic operation of the fuel cell system requires that the optimal synthesis/design and dynamic operation of each of

the auxiliary power unit sub-systems be carried out in an integrated fashion. Individually optimizing each sub-system without consideration for their integration as a system does not lead to the optimum for the system as a whole. The decomposition approach (LGO and ILGO) described in *Chapter 3* are two means by which each sub-system can be individually optimized consistent with their integration into the overall system. However, they are not suited to handle the system dynamics. This is particularly important when optimizing a system operating under transient conditions for a big fraction of its life cycle. Additionally, these systems can be subject to sudden load changes of considerable magnitude.

For the reasons stated above[48] the DILGO approach is applied to the synthesis/design optimization problem at hand. How DILGO is applied is discussed in this chapter. However, the next section begins with a description of the overall dynamic system synthesis/design and operation/control optimization problem and is followed in the remaining sections of *Chapter 5* with a description of each of the sub-system optimization problems. What follows is the overall system problem definition in terms of total life cycle cost as the objective function.

5.1.1 System-Level Dynamic Synthesis/Design Optimization Problem Definition

Future fuel cell systems present a unique set of requirements not previously addressed. For example, fuel cell based auxiliary power units must be substantially more affordable than comparable systems (battery packs and generators) both in terms of acquisition and operational costs. Future fuel cell systems will likely be high efficiency, high performance systems. To permit an integrated approach to their and other dynamic systems' optimal synthesis/design and operation/control , it will be necessary to combine into a single comprehensive model thermodynamic, kinetic, geometry, and control as well as cost functions so that a large number of independent variables related to how different technologies optimally accommodate limited payload spaces can be investigated (Brown, 1999). Thus the system-level optimization problem would be that of minimizing

[48] An additional reason is the complexity and nonlinearity of the optimization problem as well as the large number and mix (discrete and continuous) decision variables.

the total cost of the system through its life cycle. It is formulated as follows in terms of the capital cost of each sub-system and the total operation/control cost:

Minimize

$$C_{\mathrm{T}} = C_{SS} + C_{FPS} + C_{WRAS} + C_{PES} + C_{BBS} + \int_{t=0}^{T} \dot{C}_{fuel}\, dt \tag{5.1}$$

w.r.t.

$$\left\{\vec{x}_{SS}, \vec{y}_{SS}, \vec{K}_{SS}\right\} \quad , \quad \left\{\vec{x}_{FLS}, \vec{y}_{FLS}, \vec{K}_{FLS}\right\} \quad , \quad \left\{\vec{x}_{WRAS}, \vec{y}_{WRAS}, \vec{K}_{WRAS}\right\}$$

subject to

$$\vec{H}_{SS} = \vec{0}, \quad \vec{G}_{SS} \le \vec{0} \tag{5.1.2}$$

$$\vec{H}_{FPS} = \vec{0}, \quad \vec{G}_{FPS} \le \vec{0} \tag{5.1.3}$$

and $$\vec{H}_{WRAS} = \vec{0}, \quad \vec{G}_{WRAS} \le \vec{0} \tag{5.1.4}$$

Note that C_{BB}, and C_{PES} are fixed costs and are, thus, not minimized along with the rest of the objective, which consists of the total cost of each sub-system and its associated fuel cost penalties. C_{SS}, C_{FPS}, and C_{WRAS} represent the capital, amortization, and maintenance costs. $\dot{C}_{fuel}$ is the fuel cost rate which is integrated along the total life cycle (from time zero to time T). For this research work it is important to note that the optimization problem is being solve not only in terms of the synthesis/design and operational decision variables, $\vec{x}$ and $\vec{y}$, but also in terms of a set of PID controller gains, $\vec{K}$, which are intended to optimize the system with respect to not only total cost but also the time response. Here, the system's time response to the changes in load is set as a constraint.

5.2 System-Level Operational/Control Optimization Problem Definition

The solution to the synthesis/design optimization problem for highly dynamic systems, operating over a wide range of conditions (the fuel cell system will be required

to go from 20% to 100% load and back in a matter of seconds) cannot be determined by only taking into consideration the most demanding load/environmental condition, the so-called synthesis/design point. Doing so will overlook the effects on system configuration and component synthesis/design of the operational (dynamic) variables during transient events. Moreover, this wrongly assumes that the control system design can overcome deficiencies which become part of the system during the synthesis/design stage. Even if it is the case that the control system can regulate the dynamic variables to appropriate values, the system for sure will not have an optimum synthesis/design. For instance, the synthesis/design of the fuel cell system that gives the lowest capital cost while meeting all constraints at maximum load may very well not be efficient at low loads and incapable of keep all operational constraints during transients. Additionally, if conceptual decomposition with no nesting were applied, the "best" and a set of promising feasible solutions found at the synthesis/design point when optimized at the operational/control level could not be guarantee an effective search of the solution space for dynamic operational segments. Therefore, in this doctoral work, in order to reach a more reliable solution of the dynamic fuel cell system optimization, the synthesis/design and dynamic operational optimization problem is solved all at once. Again, this was made possible using a high-fidelity, robust dynamic model and the definition of dynamic shadow prices.

Thus, the system-level dynamic operational/control optimization problem is defined as

Minimize

$$C_{oper} = C_{fuel} = \lim_{\Delta t \to 0} \left(\sum_{i=0}^{n} \dot{c}_{fuel} \dot{n}_{fuel} \Delta t \right) = \int_{t=0}^{T} \dot{c}_{fuel} \dot{n}_{fuel} dt = \int_{t=0}^{T} \dot{C}_{fuel} dt \tag{5.2}$$

w.r.t. $\vec{y}_{oper}, \vec{K}_{control}$

subject to

$$\vec{h}_{oper} = \vec{0} \tag{5.2.1}$$

$$\vec{g}_{oper} \leq \vec{0} \tag{5.2.2}$$

$$\vec{x} - \vec{x}^{pf} = \vec{0} \tag{5.2.3}$$

where C_{oper} is the operating cost of the fuel cell system (FPS, WRAS, and SS) and $\vec{y}_{oper}$ its set of operational variables associated with the operational time segments of the load/environmental profile, and $\vec{K}_{control}$ is the set of PID system control gains. $\dot{c}_{fuel}$ is the cost rate of fuel (e.g., methane) per kmol of fuel, $\dot{n}_{fuel}$ is the mole flow rate of fuel, and n is the number of operational segments. The only contribution to the objective function of the operational optimization problem is the cost of the fuel consumed during the time period Δt of each operational segment. Maintenance cost are not included he because they have been assumed to know as a percentage of the capital cost. Constraint (5.2.3) indicates that Problem (5.3) must be solved with values of the synthesis/design variable vector $\vec{x}$ equal to $\vec{x}^{pf}$, where $\vec{x}^{pf}$ is the vector of the design variable values corresponding to one particular configuration and set of component designs.

5.3 Residential Load Requirements

In order to synthesize/design the proposed fuel cell system (FCS), the energy requirements for a representative residential building[49] must be established. The types of residential loads considered are the following:

- Electrical load.
- Space heating load.
- Space cooling load.

The electrical load, in particular, includes the electricity needed to power the lights and appliances of the residence as well as the fans of the HVAC equipment. The profiles of these three different loads depend greatly on the geographical location of the residence and the corresponding weather conditions. The residential energy demands as well as the environmental conditions given in Figures 5.1 and 5.2 are representative of Atlanta, Georgia, and are based on an analysis of detailed load profile data obtained from Gunes and Ellis (2001).

[49] Based on the work by Gunes and Ellis (2001), a representative residential building is a 195 m^2 typical single-family residence for the United States. Residential energy surveys indicate that a typical family includes four members, i.e. two adults and two children.

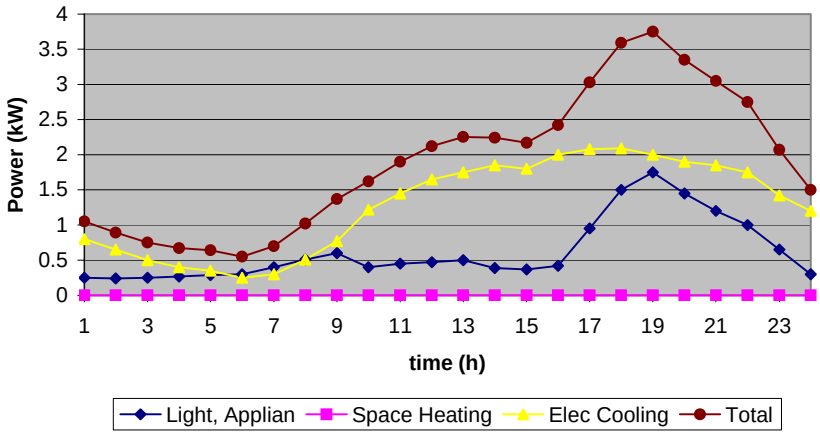

Figure 5.1. Electrical energy use for peak cooling day in Atlanta, Georgia on 07/11 (Gunes and Ellis, 2001).

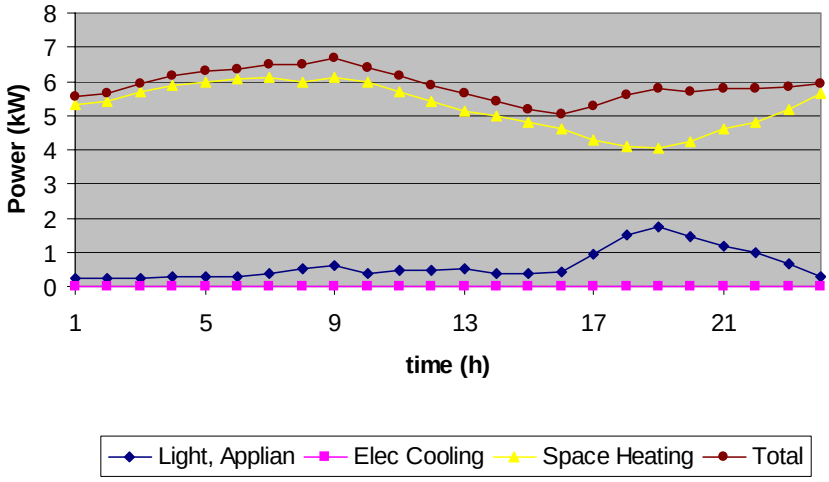

Figure 5.2. Electrical energy use for peak heating day in Atlanta, Georgia on 01/12 (Gunes and Ellis, 2001)

Now, for purposes of this doctoral work, the entire load/environmental profile has been simplified into a two-day load profile, i.e. typical summer day plus typical winter day. This two-day profile seen in Figures 5.3 and 5.4 is a simplification of the original profiles of Figures 5.1 and 5.2 in that only major load transitions are taken into account. It is believed that this sufficiently models the load changes for the synthesis/design process. However, to ensure conditions which properly challenge the control systems, two abrupt large changes in load have been introduced at time 1 and 24 hours. The resulting total load profile shown in Figures 5.3 and 5.4 is multiply by 180 days in order to account for a whole year.

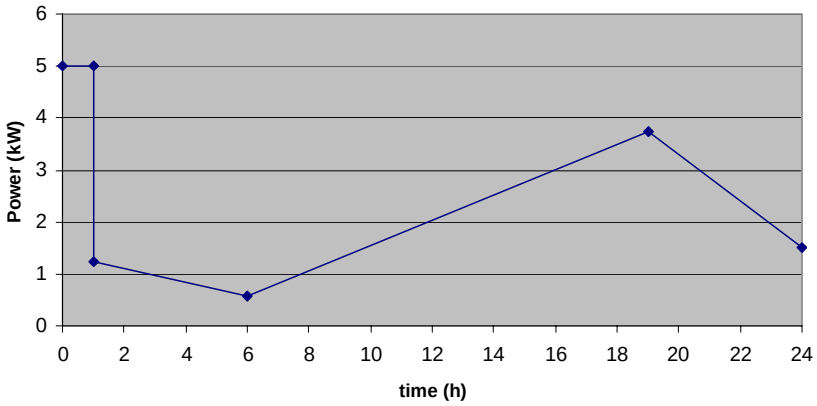

Figure 5.3. Approximated electric load profile of a peak cooling day in Atlanta, Georgia on 07/11 (Gunes and Ellis, 2001)

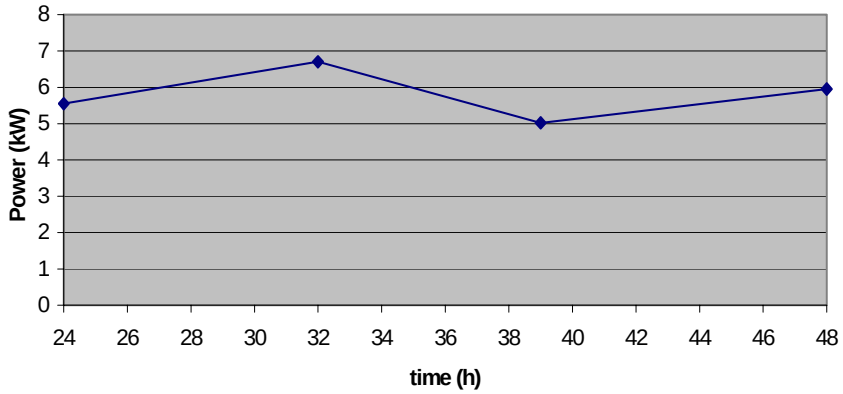

Figure 5.4. Approximated electrical load profile of a peak heating day in Atlanta, Georgia on 01/12 (Gunes and Ellis, 2001)

5.4 Decomposition and Coupling Function Definitions: Applying DILGO to the Dynamic SOFC based APU Synthesis/Design and Operational/Control Optimization Problem

In order to solve the system-level optimization problems (i.e. equations (5.1) to (5.1.4)) one could try using the local-global optimization (LGO) decomposition technique presented in Muñoz and von Spakovsky (2000b) and discussed in Chapter 3. In order to do this, the design of each sub-system would need to be carried out for multiple values of the coupling functions. This would mean that a number of unit-level optimization runs with respect to each unit's synthesis/design and operational decision variables would

have to be solved for innumerable combinations of values of the constraints related to the coupling functions space. The results would then be used to generate the optimum response surface (ORS) for the system, which in this case would be in the C_{FCS} versus the coupling functions. The latter problem involves finding the combination of the coupling functions that minimize the system-level objective function. From a practical standpoint, one of the principal difficulties associated with the implementation of the LGO technique in its general form for this case is the computational burden which it entails to generate enough points to build up the optimum response surfaces. However, the most important difficulty is that LGO is not conceptually suitable to handle dynamic optimization problems, except perhaps in quasi-stationary term which, of course, does not capture the real transients in the profile. Obviously, this is unsuitable for the FCS optimization problem consider here.

Thus, another decomposition approach is needed which significantly lessens the prohibitive computational burden and can handle the interaction effects among units during transients, i.e. DILGO, as discussed in *Chapter 3*[50]. DILGO departs from the same physical decomposition concept defined for ILGO. However, it uses a new definition of dynamic shadow prices.

One of the major objectives of this doctoral work is to demonstrate the usefulness of applying the DILGO method to the optimization problem described above. In order to do this, the FCS is broken down into the sub-systems mentioned earlier, i.e. the SS, FPS, and WRAS. This simplified breakdown of the FCS, as well as its interactions with the environment and the material and energy streams connecting its three sub-systems, are shown in Figure 4.10 and simplify in Figure 5.5. Therefore, the physical decomposition of the proposed FCS configuration into three units leads to the decomposition of the system-level synthesis/design optimization problem (Problem (5.1)) into three optimization sub-problems, one for the SS, one for the FPS, and one for the WRAS.

[50] Note that there are a number of other advantages that DILGO brings to the table (see Chapter 3) including the elimination of nested optimizations. The ability to be used across geographically dispersed teams of synthesis/design specialists is also possible with DILGO and is possible with LGO provided the off-line version of LGO is used, i.e., the unit-level ORS are generated prior to running the system-level optimization.

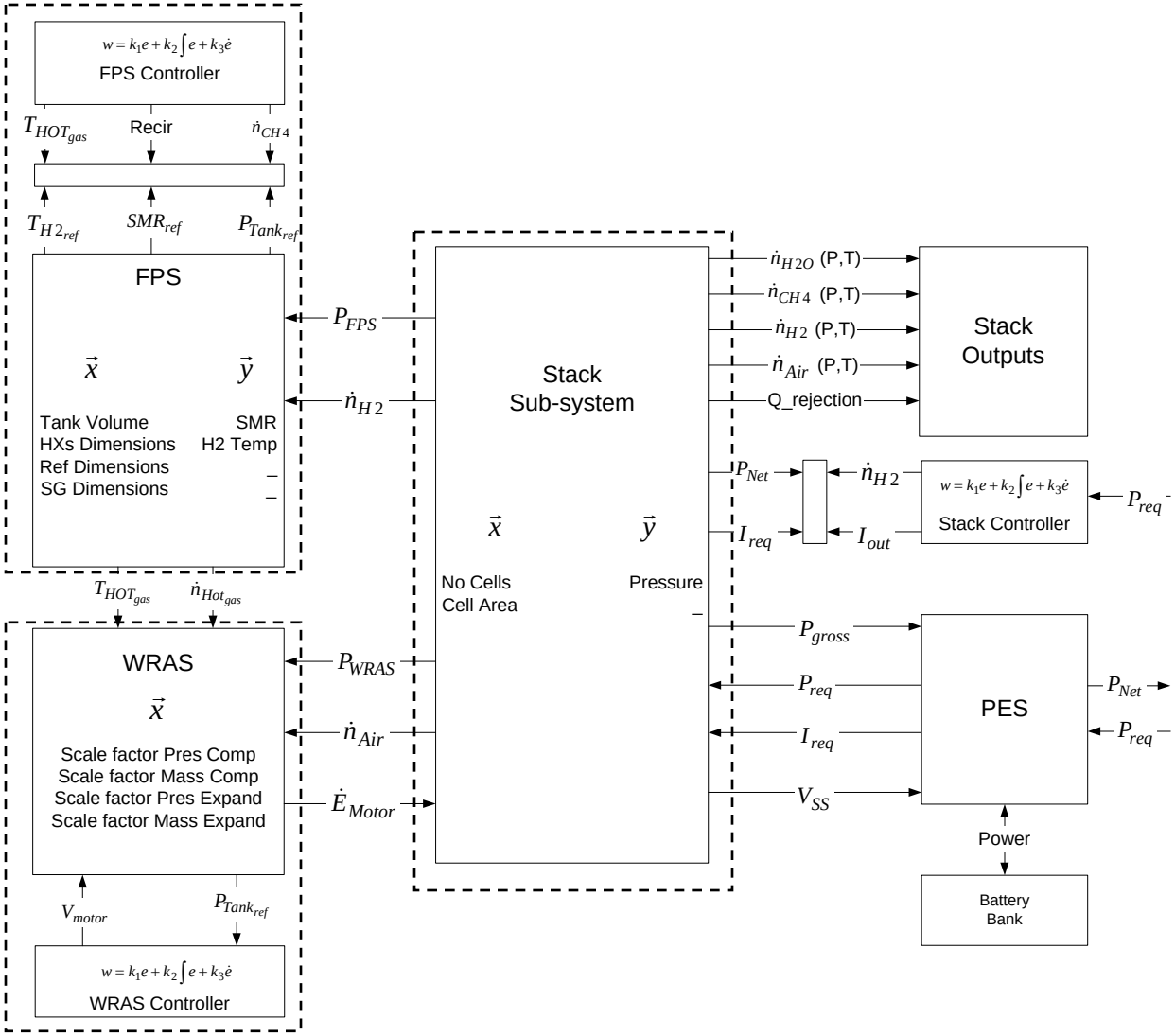

Figure 5.5. Sub-systems (including controllers) and sub-system coupling functions.

In order to apply DILGO to the system-level optimization problem for total life cycle cost, system-level, unit-based optimization problems are defined for the units to be optimized. The boundaries of each unit (sub-system), their associated local decision variables as well as the coupling functions connecting each unit to the rest are clearly seen in Figure 5.5. This figure illustrates the decomposition of the system-level problem for FCS synthesis/design into four separate but integral sub-problems (the fourth sub-problem, i.e. that for the PES is not considered here).

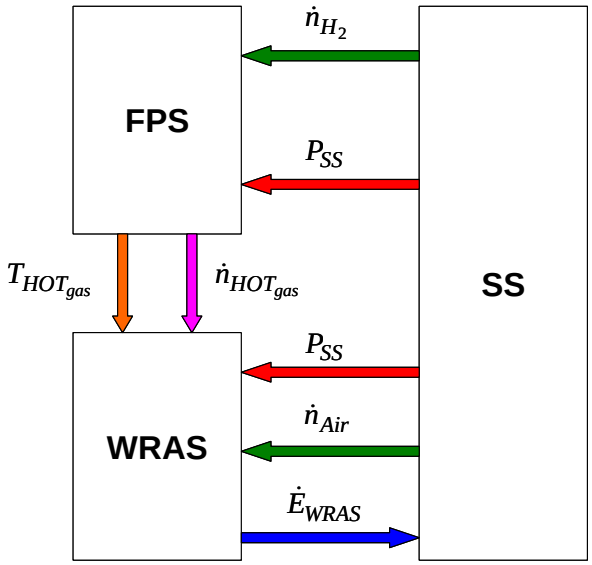

Figure 5.6. Systems coupling functions.

Table 5.1. Coupling function definition.

Sub-system	Coupling Function	Symbol
SS	Hydrogen molar flow	$\dot{n}_{H_2}$
	System tank pressure	P_{FPS} and P_{WRAS}
	Air molar flow	$\dot{n}_{Air}$
WRAS	Motor parasitic power	$\dot{E}_{WRAS}$
FPS	Hot gases exit temperature	T_{HOTgas}
	Hot gases molar flow	$\dot{n}_{HOTgas}$

The material and energy streams linking the above three units are identified as the coupling functions of the FCS. The coupling functions are considered as intermediate products and/or feedbacks going to or coming from the units. The application of the DILGO decomposition technique makes it necessary to define the coupling functions shown in Figure 5.5. A more detailed description of these coupling functions is given below in Figure 5.6. A list per sub-system appears in Table 5.1.

The SS must satisfy (apart from its internal parasitic power demand and the residential total electrical load) the power demand, $\dot{E}_{WRAS}$, required to run the WRAS. In order for the SS to produce the required gross power, the necessary molar flow rate of hydrogen in the hydrogen-rich gas stream, $\dot{n}_{H_2}$, must be supplied by the FPS. In the same way, the necessary molar flow rate of air, $\dot{n}_{Air}$, must be supplied by the WRAS. In addition, the FPS provides hot gases to the WRAS at a given rate and temperature, $\dot{n}_{HOTgas}$ and T_{HOTgas}, used to recover work at the expander. Moreover, the pressure of the hydrogen-rich gas and air streams, P_{FPS} and P_{WRAS}, exiting the FPS and WRAS, respectively, must match the inlet stack pressure of the SS. In addition to the coupling functions mentioned above, the hydrogen and oxygen utilization factors can be defined as functions linking the SS, FPS, and WRAS units. In this doctoral work, however, these two factors are treated as fixed parameters in the SS model for reasons of simplicity.

Given the high fidelity of the simulations and the number and type of decision variables and constraints (see Tables 5.2 to 5.5), one can clearly see that one is confronted with a very complex, large-scale, mixed integer, non-linear, dynamic optimization problem. The difficulties associated with solving this problem are exacerbated by the following:

- The dynamic simulations tools are not specifically designed to handle large scale optimizations. Each time a simulation is run, it is necessary to launch the program and read the necessary software licenses. This is very expensive computationally.
- The presence of both continuous and discrete decision variables makes it necessary to use a heuristic approach: either a genetic algorithm or simulated annealing. There are no general gradient-based methods able to solve this dynamic mixed integer,

non-linear programming (DMINLP) problem. However, heuristic algorithms impose a significant computational penalty in terms of solution time.

What follows in section 5.3.1 is the formulation of the system-level, unit-based optimization problems for the three units considered, namely the SS, WRAS, and FPS, along with a detailed description of their independent (decision) variables and a definition of their dynamic shadow prices.

5.4.1 SS System-Level, Unit-Based Optimization Problem Definition

The SS unit-based, system-level optimization problem is formulated as follows

Minimize

$$\begin{aligned} C'_{SS} &= C_{SS} + C^*_{FPS} + C^*_{WRAS} + C^*_{fuel} \\ &+ \int_{t=0}^{T} \dot{\lambda}_{H_2}(t)\Delta\dot{n}_{H_2}(t)dt + \int_{t=0}^{T} \dot{\lambda}_{Air}(t)\Delta\dot{n}_{Air}(t)dt \\ &+ \int_{T=0}^{T} \dot{\lambda}_{pres_{FPS}}(t)\Delta P_{FPS}(t)dt \int_{T=0}^{T} \dot{\lambda}_{pres_{WRAS}}(t)\Delta P_{WRAS}(t)dt \end{aligned} \tag{5.3}$$

w.r.t. $n_{cells}, A_{act}, \vec{K}_{SS}$

subject to

$$\vec{h}_{SS} = \vec{0} \tag{5.3.1}$$

$$\vec{g}_{SS} \le \vec{0} \tag{5.3.2}$$

$$\left[\dot{E}_{WRAS} - \dot{E}^*_{WRAS}\right] = \vec{0} \tag{5.3.3}$$

where the vector of equality constraints, $\vec{h}_{SS}$, represents the thermodynamic model of the SS while the vector of inequality constraints, $\vec{g}_{SS}$, represents physical limitations imposed upon the sub-system. Equations (5.3.3) indicate that the coupling function $\dot{E}_{WRAS}$ must take the proper values dictated by the solution of the WRAS unit-based, system-level optimization problem described in the following section. The synthesis/design and

operational decision variables for the SS along with their ranges, as well as the physical constraints imposed upon the sub-system, are shown in Table 5.2. It has been assumed in equation (5.3) that the dynamic shadow prices are constant for a particular operational point over the range of hydrogen and air mass flow and FPS pressure. This assumption is later probed in *Chapter 6* to confirm its validity which has been assumed based on the fact that the SS model is a steady state and not transient one. The same assumption was made for the WRAS sub-system which must also be verified since in this case the WRAS model is transient. Note that the coupling functions have been represented in the above equations by mole flow rates and pressure differences. The work of Muñoz and von Spakovsky (2000b) suggest that there is a mathematical advantage with the use of quantities as coupling functions that make the shadow prices monotonic and, ideally, linear. This is an aspect of the coupling functions chosen which is also proved in Chapter 6.

Table 5.2: SS decision and principal dependent optimization variables and constraints.

Synthesis/Design Decision Variable Description		**Constraints**
n_{cells}	Number of cells	$50 \le n_{cells} \le 400$
A_{act}	Cell active area (cm^2)	$100 \le A_{act} \le 400$
Operational Decision Variable Description		**Constraints**
P_{oper}^{FC}	Stack operating pressure (bar)	$3 \le P_{oper}^{FC} \le 14$
Dependent Variable Description		**Constraints**
V_{cell}^{actual}	Actual cell voltage (V)	$V_{cell}^{actual} \ge 0.4$
Operational Parameter		**Constraints**
T_{oper}	Stack temperature	$T_{oper} = 1000^o K$

Problem (5.3) represents the minimization of the system-level objective function, i.e. the total cost of the FCS, C_{FCS}, by varying the local (SS unit) decision variables only. Apart from the local objective function C_{SS} and the optimum values for the FPS and WRAS annualized capital costs as well as the optimum operating cost, the expression for the unit-based, system-level objective function, $C_{SS}^{'}$, includes the dynamic shadow price

rates of the three coupling functions $\dot{n}_{H_2}$, $\dot{n}_{Air}$ and P_{FPS}. These shadow price rates are defined as

$$\dot{\lambda}_{H_2}(t) = \frac{\partial \dot{C}^*_{FPS}}{\partial \dot{n}_{H_2}(t)} \tag{5.4}$$

$$\dot{\lambda}_{Air}(t) = \frac{\partial \dot{C}^*_{WRAS}}{\partial \dot{n}_{Air}(t)} \tag{5.5}$$

$$\dot{\lambda}_{pres_{FPS}}(t) = \frac{\partial \dot{C}^*_{FPS}}{\partial P_{FPS}(t)} \tag{5.6}$$

$$\dot{\lambda}_{pres_{WRAS}}(t) = \frac{\partial \dot{C}^*_{WRAS}}{\partial P_{WRAS}(t)} \tag{5.7}$$

where $\dot{C}^*_{FPS} = \dot{C}^*_{fuel}$ (5.8)

The $\dot{\lambda}$ represent the arte of the marginal changes in the optimum value of the FPS total cost due to marginal changes in the value of the coupling functions $\dot{n}_{H_2}$, $\dot{n}_{Air}$, P_{FLS} and P_{WRAS}, respectively.

Finally, the terms $\Delta\dot{n}_{H_2}$, $\Delta\dot{n}_{Air}$, ΔP_{FPS} and ΔP_{WRAS}, which appear in equation (5.3), characterize the effect that the variation in the SS decision variables has on the above mentioned coupling functions and are given by

$$\Delta\dot{n}_{H_2} = \dot{n}_{H_2} - \left(\dot{n}^*_{H_2}\right)^o \tag{5.9}$$

$$\Delta\dot{n}_{Air} = \dot{n}_{Air} - \left(\dot{n}^*_{Air}\right)^o \tag{5.10}$$

$$\Delta P_{FPS} = P_{FPS} - \left(P^*_{FPS}\right)^o \tag{5.11}$$

$$\Delta P_{WRAS} = P_{WRAS} - \left(P^*_{WRAS}\right)^o \tag{5.12}$$

where the superscript "o" refers to the optimum coupling function value obtained in the previous DILGO iteration.

5.4.2 FPS System-Level, Unit-Based Optimization Problem Definition

The unit-based, system-level optimization problem for the FPS is defined as

Minimize

$$C_{FPS}^{'} = C_{FPS} + C_{fuel} + C_{SS}^{*} + C_{WRAS}^{*} + \int_{t=0}^{T} \dot{\lambda}_{T_{HOT_{gas}}}(t)\Delta T_{HOTgas}(t)dt + \int_{t=0}^{T} \dot{\lambda}_{\dot{n}_{HOTgas}}(t)\Delta \dot{n}_{HOTgas}(t)dt \quad (5.13)$$

w.r.t.

$$\left\{\vec{x}_{FPS}, \vec{y}_{FPS}, \vec{K}_{FPS}\right\}$$

subject to

$$\vec{h}_{FPS} = \vec{0} \quad (5.13.1)$$

$$\vec{g}_{FPS} \leq \vec{0} \quad (5.13.2)$$

$$\begin{bmatrix} \dot{n}_{H_2} - \dot{n}_{H_2}^{*} \\ \dot{n}_{Air} - \dot{n}_{Air}^{*} \end{bmatrix} = \vec{0} \quad (5.13.3)$$

where the vector of equality constraints, $\vec{h}_{FPS}$, represents the thermodynamic, kinetic, and geometric models of the FPS unit while the vector of inequality constraints, $\vec{g}_{FPS}$, represents physical limitations imposed upon the sub-system. Equations (5.13.3) indicate that the coupling functions $\dot{n}_{H_2}$ and $\dot{n}_{Air}$ must take the appropriate values provided by solving the SS and WRAS unit-based, system-level optimization problems.

Problem 5.13 represents the minimization of the system-level objective function exclusively due to variations in the local (FPS) decision variables. The unit-based, system-level objective function, $C_{FPS}^{'}$, is comprised of the local contributions (i.e. the FPS annualized total capital cost as well as the cost of the fuel consumed), the optimum value for the capital cost of the SS and WRAS obtained from solving problems (5.3) and (5.18), and additional terms that indicate the impact that variations in the FPS decision variables have on the local objective of the WRAS. These variations in the local decision

variables propagates into the SS and WRAS units by means of the following dynamic shadow prices:

$$\dot{\lambda}_{T_{HOT_{gas}}}(t) = \frac{\partial \dot{C}^{*}_{WRAS}}{\partial T_{HOT_{gas}}(t)} \tag{5.14}$$

$$\dot{\lambda}_{\dot{n}_{HOT_{gas}}}(t) = \frac{\partial \dot{C}^{*}_{WRAS}}{\partial \dot{n}_{HOT_{gas}}(t)} \tag{5.15}$$

whose sign and absolute value dictate the appropriate incremental change in the coupling functions $T_{HOT_{gas}}$ and $\dot{n}_{HOT_{gas}}$ given by

$$\Delta T_{FPS_{HOTgas}} = T_{FPS_{HOTgas}} - \left(T^{*}_{FPS_{HOTgas}}\right)^{o} \tag{5.16}$$

$$\Delta \dot{n}_{HOT_{gas}} = \dot{n}_{HOT_{gas}} - \left(\dot{n}^{*}_{HOT_{gas}}\right)^{o} \tag{5.17}$$

so that an improved optimum value of the system-level objective function is guaranteed. The synthesis/design and operational decision variables for the FPS along with their ranges are presented in Tables 5.3 and 5.4.

Table 5.3: FPS synthesis/design decision variables and constraints.

Component	Synthesis/Design Decision Variable Description		Constraints
SMR reactor	d_i^{SMR}	SMR reactor tube diameter (m)	$0.01 \le d_i^{SMR} \le 0.02$
	n_{tubes}^{SMR}	Number of SMR reactor tubes	$100 \le n_{tubes}^{SMR} \le 500$
	L_{SMR}	SMR reactor length (m)	$0.05 \le L_{SMR} \le 1$
Steam generator	d_i^{EG}	tube diameter (m)	$0.01 \le d_i^{SG} \le 0.02$
	n_{tubes}^{EG}	Number of tubes	$100 \le n_{tubes}^{EG} \le 500$
	L_{EG}	length (m)	$0.05 \le L_{EG} \le 1$
Compact heat exchangers	N_{plates}	Number of plated	$4 \le N_{plates} \le 60$
	L_h	Hot-side length (m)	$0.03 \le L_h \le 1.5$
	L_c	Cold-side length (m)	$0.03 \le L_c \le 1.5$

Component	Synthesis/Design Decision Variable Description		Constraints
Reformate pressure control	K_P	Proportional gain	$10^{-8} \le K_p \le 10^{-2}$
	K_I	Integral gain	$10^{-13} \le K_I \le 10^{-8}$
SMR control	K_P	Proportional gain	$0.1 \le K_p \le 500$
	K_I	Integral gain	$10^{-2} \le K_I \le 10$
Reformate temperature control	K_P	Proportional gain	$0.1 \le K_p \le 500$
	K_I	Integral gain	$10^{-2} \le K_I \le 10$
Reformate tank output control	K_P	Proportional gain	$0.1 \le K_p \le 500$
	K_I	Integral gain	$10^{-2} \le K_I \le 10$

Table 5.4: FPS operational decision variables and constraints.

Component	Operational Decision Variable Description		Constraints
SMR reactor	T_o^{SMR}	SMR reactor outlet temperature, ºC	$550 \le T_o^{SMR} \le 1300$
Reformate mixer	ζ_{H_2O/CH_4}	Steam-to-methane ratio	$1.5 \le \zeta_{H_2O/CH_4} \le 6$

5.4.3 WRAS System-Level, Unit-Based Optimization Problem Definition

The unit-based, system-level optimization problem for the WRAS is defined as

Minimize

$$C'_{WRAS} = C_{WRAS} + C^*_{FPS} + C^*_{fuel} + C^*_{SS} + \int_{t=0}^{T} \dot{\lambda}_{E_{WRAS}} \Delta \dot{E}_{WRAS} dt \tag{5.18}$$

w.r.t.

$$\left\{ \vec{x}_{WRAS}, \vec{y}_{WRAS}, \vec{K}_{WRAS} \right\}$$

subject to

$$\vec{h}_{WRAS} = \vec{0} \tag{5.18.1}$$

$$\vec{g}_{WRAS} \le \vec{0} \tag{5.18.2}$$

$$\begin{bmatrix} \dot{n}_{Air} - \dot{n}^{*}_{Air} \\ \dot{n}_{HOTgas} - \dot{n}^{*}_{HOTgas} \\ T_{HOT_{gas}} - T^{*}{}_{HOT_{gas}} \end{bmatrix} = \vec{0} \tag{5.18.3}$$

where the vector of equality constraints, $\vec{h}_{WRAS}$, represents the thermodynamic, kinetic, and geometric models of the WRAS while the vector of inequality constraints, $\vec{g}_{WRAS}$, represents the physical limitations imposed upon the sub-systems. Equations (5.18.3) indicate that the coupling functions $\dot{n}_{Air}$, $\dot{n}_{Hotgas}$, and $T_{FPS_{HOTgas}}$ must take the appropriate values provided by solving the SS and FPS unit-based, system-level optimization problems. Problem (5.17) represents the minimization of the system-level objective function exclusively due to variations in the local (WRAS) decision variables. The unit-based, system-level objective function, $C^{'}_{WRAS}$, is now comprised of the local contributions (i.e. the WRAS annualized capital cost as well as the cost of the fuel consumed), the optimum value for the total cost of the SS and FPS obtained from solving problems (5.3) and (5.13), and two additional terms that indicate the impact that the variation in the WRAS decision variables has on the local objective of the SS unit. This variation in the local decision variables propagates into the SS unit by means of the following dynamic shadow price:

$$\dot{\lambda}_{\dot{E}_{WRAS}} = \frac{\partial \dot{C}^{*}_{SS}}{\partial \dot{E}_{WRAS}} \tag{5.19}$$

whose sign and absolute value dictate the appropriate incremental change in the coupling function $\dot{E}_{WRAS}$ given by

$$\Delta \dot{E}_{WRAS} = \dot{E}_{WRAS} - \left(\dot{E}^{*}_{WRAS} \right)^{o} \tag{5.20}$$

so that an improved optimum value of the system-level objective function is guaranteed. The synthesis/design and operational decision variables for the WRAS along with their ranges are presented in Table 5.54.

Table 5.5: WRAS decision and principal dependent optimization variables and constraints.

Component	Synthesis/Design Decision Variable Description		Constraints
Compressor	$P_{designCOMP}$	Compressor design pressure (bar)	$3 \le P_{designCOMP} \le 10$
	$F_{designCOMP}$	Compressor design flow (kmol/sec)	$3e-6 \le F_{designCOMP} \le 10e-5$
Expander	$P_{designEXP}$	Expander design pressure (bar)	$3 \le P_{designEXP} \le 10$
	$F_{designEXP}$	Expander design flow (kmol/sec)	$3e-6 \le F_{designEXP} \le 10e-5$
Air tank control	K_P	Proportional gain	$0.1 \le K_p \le 500$
	K_I	Integral gain	$10^{-2} \le K_I \le 10$
Electric motor control	K_P	Proportional gain	$10^{-4} \le K_p \le 10^{-1}$
	K_I	Integral gain	$10^{-5} \le K_I \le 10^{-2}$

5.5 Solution Approach

The necessary steps for applying DILGO to the FCS in order to identify of the final synthesis/design and operational/control that minimizes the total life cycle cost of the FCS over the entire load profile are summarized below.

1. Solve the unit-based, system-level optimization problem for the SS, i.e. Problem (5.3). Since no information about the FPS and the WRAS exists in the first iteration of DILGO, set the shadow prices $\dot{\lambda}_{H_2}$, $\dot{\lambda}_{air}$, and $\dot{\lambda}_{pres}$ equal to zero and use initial estimates for the parasitic power demand, $\dot{E}_{WRAS}$, and the inlet stack pressures, P_{FPS} and P_{WRAS}.
2. Calculate the shadow prices based on the optimum SS capital cost, C^*_{SS}, by using equation (5.19). Make sure that the ranges within which the coupling function $\dot{E}_{WRAS}$ is allowed to vary, preserve the validity of the dynamic shadow price rates constant behavior assumption.
3. Solve the unit-based, system-level optimization problem for the combined FPS unit, i.e. Problem (5.13), by using as values for the coupling functions calculated in steps

1 and 2, respectively. Since no information about the WRAS exists in the first iteration of DILGO, set the shadow price $\dot{\lambda}_{T_{FPS_{HOTgas}}}$ and $\dot{\lambda}_{\dot{n}_{HOTgas}}$ equal to zero and use initial estimates for the parasitic power and air tank temperature.

4. Calculate the shadow prices based on the optimum FPS total cost, C^*_{FPS}, by using equations (5.4) and (5.6). Make sure that the ranges within which the coupling functions $\dot{n}_{H_2}$ and P_{FPS} are allowed to vary, preserve the validity of the dynamic shadow price rates constant behavior assumption.
5. Solve the unit-based, system-level optimization problem for the combined WRAS unit, i.e. Problem (5.18), by using the values for the coupling functions calculated in steps 2 and 4, respectively. At this point enough information is available from the SS and FPS. i.e. their shadow prices are known. However if parallel computation is being used, for the first iteration of DILGO the shadow prices $\dot{\lambda}_{\dot{E}_{WRAS}}$, $\dot{\lambda}_{T_{FPS_{HOTgas}}}$ and $\dot{\lambda}_{\dot{n}_{HOTgas}}$ can be set equal to zero and initial estimates for the hot gas inlet temperature, mass flow, and required system pressure
6. Calculate the shadow prices based on the optimum WRAS total cost, C^*_{WRAS}, by using equations (5.5) , (5.7), (5.14), and (5.15),. Make sure that the ranges within which the coupling functions P_{SS}, $T_{FPS_{HOTgas}}$, $\dot{n}_{HOTgas}$, and $\dot{n}_{Air}$ are allowed to vary, preserve the validity of the dynamic shadow price rates constant behavior assumption.
7. Repeat steps 1 through 6 until no further improvement in the system-level objective function, i.e. C_{FCS}, is achieved or until the coupling functions have reached the minimum or maximum allowable values.
8. Identify the synthesis/design and dynamic/operational values of the decision variables that minimizes the total cost of the FC over the entire load profile.
9. Proceed with a control stability analysis. If stability problems are found, redefine the range for the control gains or apply conceptual decomposition by adding a new segment to the load profile which challenges the system. This was not necessary in this doctoral work.

The optimization tool of the commercial dynamic development environment package gPROMS® (2003) was used to solve optimization problems (5.3), (5.13), and (5.18). This software provides a MINLP optimization algorithm suitable to solve dynamic problems. The procedure described above is the same regardless of whether or not the objective function is the total life cycle cost or system time response. Figure 5.6 shows the coupling function flows between sub-systems and the system optimization scheme.

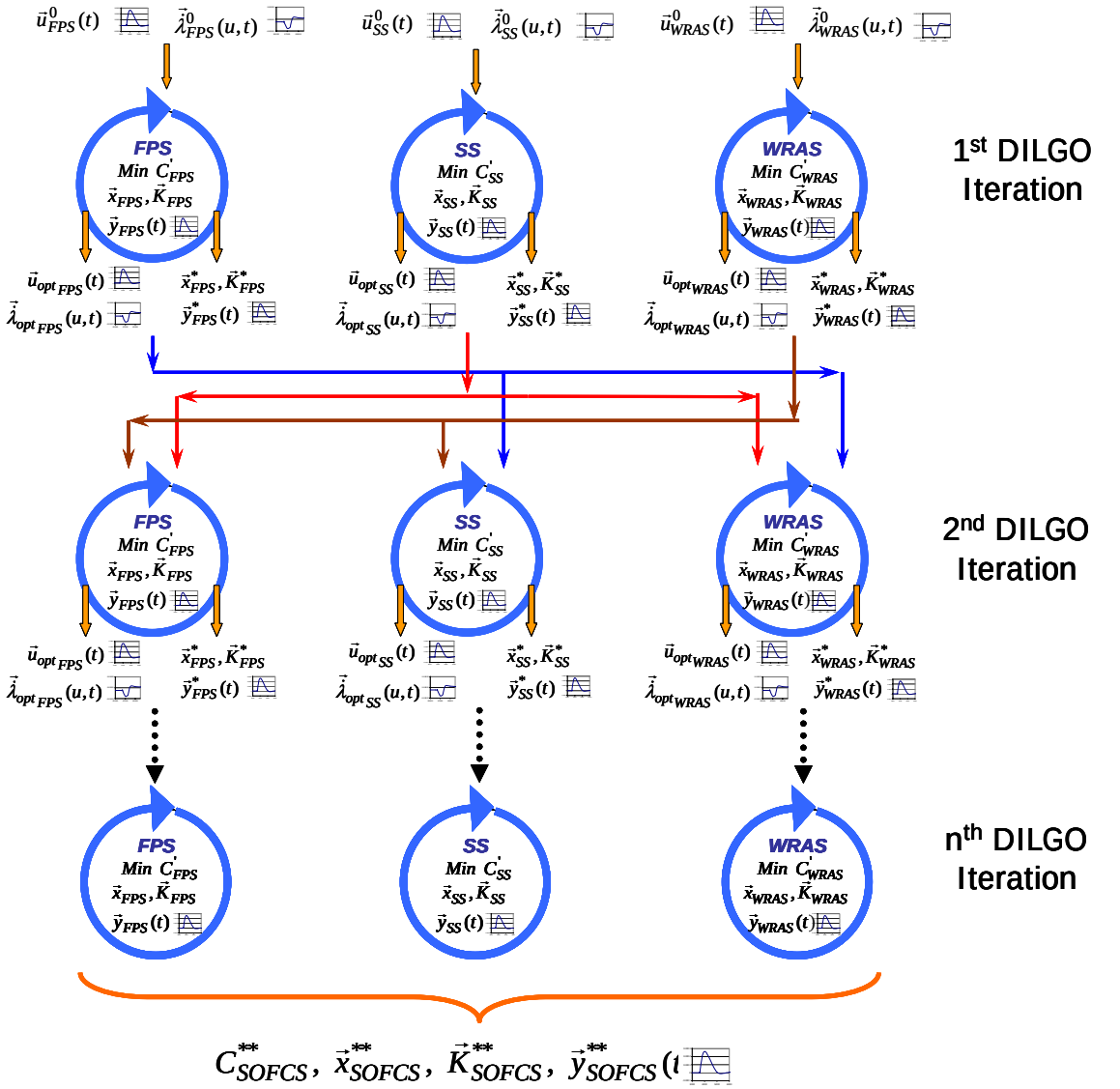

Figure 5.7. Parallelization scheme of the DILGO optimization approach for the SOFC based APU.

Once the shadow prices are computed for the first DILGO iteration and new feasible values of the coupling functions are defined, this information can be used to proceed with the second DILGO iteration. Thus all the subsystem optimizations can be performed in parallel (see Figure 5.7) from the second DILGO iteration onward. At the end of each DILGO iteration, new values of the coupling functions are generated and new values of the shadow prices are computed. This information is updated into each subsystem optimization problem. The procedure from steps 1 to 6 is repeated until convergence is reached. Convergence implies that the variation in the system-level, unit-base objective function for each subsystem is below a predefined limit (e.g., less than 0.2 %).

Chapter 6

Results and Discussion

The results for the dynamic synthesis/design and operational/control optimization of the proposed SOFC based APU are discussed in this chapter. A presentation of the optimum solution obtained for this highly complex problem with 71 degrees of freedom using the DILGO decomposition technique is followed by a presentation of the system dynamic response as seen via the behavior of the dynamic operational decision variables and the most important dynamic dependent variables. The control and controlled variables pairing is presented next followed by the optimum system synthesis. The system optimum start-up strategy is defined and the most relevant start-up results are discussed. A detailed system life cycle cost analysis, which is product of the optimization, is presented. Coupling function dynamic shadow price rates for the corresponding sub-systems are shown. Finally, the system's efficiency and component geometry effect on dynamic behavior are analyzed and discussed in the last section of this chapter.

6.1 Dynamic Synthesis/Design and Operational/Control Optimization Problem Results Using the DILGO Approach

As indicated in Chapter 5, the DILGO physical decomposition technique for dynamic system is used in order to optimize the SOFC based APU synthesis/design and operational/control for an entire residential load profile. The solutions to the FPS,

WRAS, and SS unit-level and system-level, unit-based optimization problems in terms of life cycle cost for each iteration of the DILGO approach as well as the corresponding total life cycle cost for the SOFC system (SOFCS) are presented in Table 6.1. A graphical representation of this tabulated data is given in Figures 6.1 and 6.2.

Table 6.1. Optimum cost of the total SOFC system and subsystem for each iteration of the DLGO approach.

DILGO Iteration No.	SOFCS ($)	FPS ($)	WRAS ($)	SS ($)	FUEL ($)	Percentage Improvement
1	38230	10947	2203	5541	19539	---
2	30673	8400	2150	4120	16003	19.7672
3	28130	7720	1890	3420	15100	8.29068
4	26816	6732	1716	3900	14468	4.67117
5	24919	6266	1635	3768	13250	7.07413
6	24843	6239	1625	3752	13227	0.30499

What is believed to be the global optimum[51] value for the total life cycle cost of the SOFCS is obtained in six iterations of DILGO. A significant improvement in the value of the system-level objective function is observed upon completion of the second DILGO iteration. In particular, the final total life cycle cost is lower by $13,387 (US) than that of the first iteration, which translates into a 35.017% decrease.

Figures 6.1 and 6.2 show the evolution of the capital cost of all sub-systems, the life cycle fuel cost, and total life cycle cost for the different iterations of the DILGO process. It is clearly evident that for every iteration some improvement was achieved in the system-level objective function (total life cycle cost). The flat behavior of total life cycle cost for the last two iterations indicates that the overall iterative optimization scheme converged, i.e. no significant improvement is achieved after iteration 6. This observation was verified by running the problem a seventh time with no observable change in the independent variables or the system-level objective function.

[51] See footnotes 2, and 13 for a discussion of what is meant here in regards to the use of the term “global optimum”.

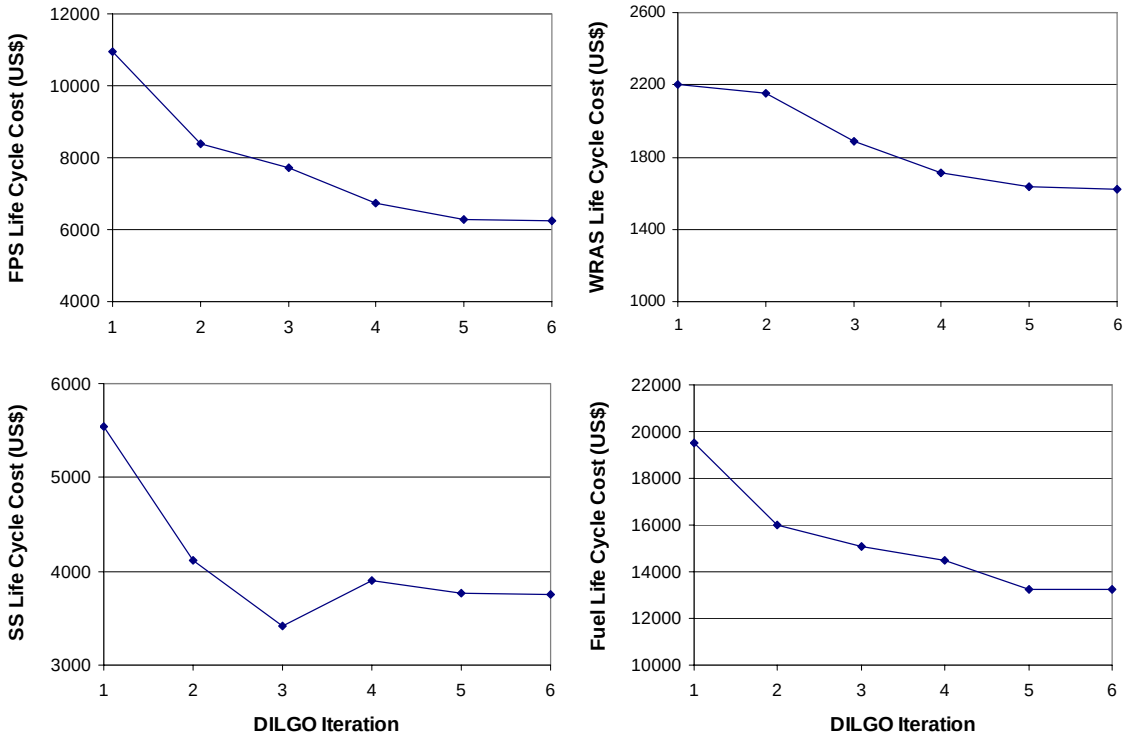

Figure 6.1. Evolution of the capital cost for all sub-systems and the fuel cost at different points of the dynamic iterative local-global optimization (DILGO) approach.

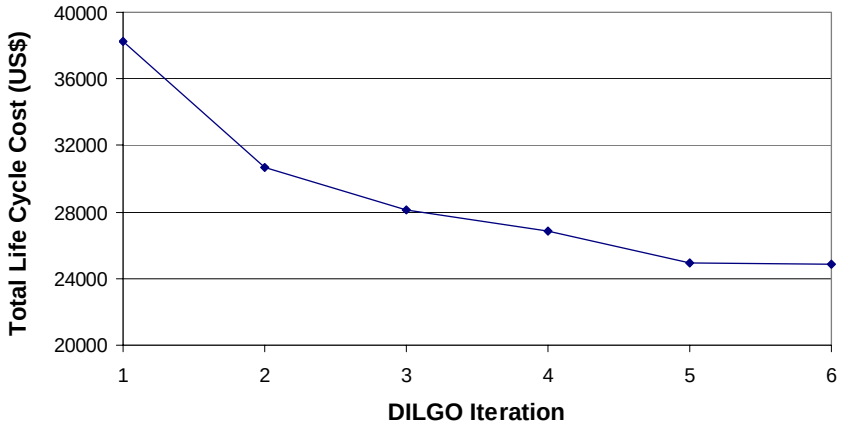

Figure 6.2. Evolution of the Total Life Cycle Cost at different points of the dynamic iterative local-global optimization (DILGO) approach.

Optimum results for the SS, FPS, and WRAS independent synthesis/design decision variables appear in Tables 6.2 and Table 6.3. The reader is reminded that in this doctoral work the controller gains are treated as synthesis/design decision variables (see table 6.3). In fact, it is recommended that for future work these variables to be treated as well as dynamic operational decision variables. This is

possible if gain scheduling or non-linear control architecture is applied. Detailed optimum cost function values appear in Table 6.4. Three dynamic operational decision variables per time interval for a total of 30 based on Figures 5.3 and 5.4) were selected to be part of the optimization problem (i.e., stack operating pressure, steam-methane reformer reformate exit temperature, and steam-to-methane ratio). In the next section, the optimum dynamic trajectory of these decision variables are presented along with the optimum trajectory of the most important dynamic dependent variables.

Table 6.2. FPS, WRAS, and SS optimum values for the synthesis/design variables.

Sub-System	**Component Variable**	**Value**	**Sub-System**	**Component Variable**	**Value**
FPS			**FPS**		
HX I	L_h *(m)*	0.061	HX IV	L_h *(m)*	0.1818
	L_c *(m)*	0.061		L_c *(m)*	0.2129
	N_{Plates}	8		N_{Plates}	5
HX II	L_h *(m)*	0.1643	HX V	L_h *(m)*	0
	L_c *(m)*	0.1734		L_c *(m)*	0
	N_{Plates}	5		N_{Plates}	0
HX III	L_h *(m)*	0.03262	SMR	L *(m)*	0.1762
	L_c *(m)*	0.03262		d_i *(m)*	0.01
	N_{Plates}	5		N_{tubess}	145
				t_h *(m)*	0.00006
SS			**WRAS**		
	A_{cell} *(cm^2)*	1221.43	Comp.	PR_{design}	3.1
	N_{cells}	26		m_{design} *(kg/s)*	0.00453
			Exp.	PR_{design}	2.94
				m_{design} *(kg/s)*	0.01605

Table 6.3. Optimum values for the control gains[52]

Component	Control Variable	State Variable	Proportional Gain (K_P)	Integral Gain (K_I)
Steam-methane reformer	Hot gases inlet temperature	Reformate exit temperature	22.1505	0.81187
	Anode recirculation fraction	Steam-to-methane ratio	19.74604	0.30227
Reformate tank	Methane mass flow	Tank pressure[53]	1.9375e-6	1.0084e-10
Air Tank	Electric motor volts	Tank pressure	0.00652	0.000118
Fuel Cell Anode	Valve voltage	Reformate mass flow	34.05	1.447
Fuel Cell Cathode	Valve voltage	Air mass flow	92.05	3.18

Table 6.4: FPS, WRAS, and SS optimum capital and operational cost[54].

SOFCS (US$)	**24,843**
FPS (US$)	**6,239**
WRAS (US$)	**1,625**
SS (US$)	**3,752**
Fuel (US$)	**13,227**
WRAS (US$)	**1,625**
Compressor	487
Expander	745
Motor	243
Auxiliary	147

FPS (US$)	**6,239**
HX I	611
HX II	358
HX III	15.28
HX IV	487
HX V	0
Bare Reactor	1,212
Catalyst	1,928
Steam Generator	1,618
SS (US$)	**3,752**

6.1.1 System Dynamic Response

In this doctoral work, the dynamic independent (decision) and dependent decision variables listed on the previous page and in Table 6.3 are defined as system outputs or state variables. As state variables, they are regulated by the set of controllers defined in Chapter 4 (see, e.g., Figure 4.24). These variables are also called controlled variables and serve as reference values for the controllers. The variables that are manipulated in order to keep controlled variables at their optimum

[52] The controller gains are treated as synthesis/design decision variables in the optimization problem. No derivative gain was used in the controller architecture due to instability and model robustness problems.
[53] Note that the reformate and air tank pressures are constrained through the pressure coupling function to essentially coincide (except for a fixed pressure drop) with the dynamic operational decision variable, the stack operating pressure
[54] Cost includes purchase cost, amortization cost, and maintenance cost.

values are defined as control variables. Figures 6.3 to 6.8 show the dynamic optimum trajectories of the dynamic independent (decision) and dependent variables along with the dynamic trajectories of their respective control variables. Figure 6.3 shows how the actual reformate tank pressure very closely follows the optimum pressure trajectory. It should be noticed how the optimum tank pressure (i.e., in effect the system pressure) is a function of system demand (Figures 5.3 and 5.4). At high loads the optimum pressure is higher. This is explained by the fact that a low loads both the SS and the FPS efficiency is higher and the pressure increase has only a minor effect on the stack efficiency increment. On the other hand, the WRAS is less efficient at low loads; and therefore, the parasitic power due to the electrical motor at low load increases as the system pressure increase.

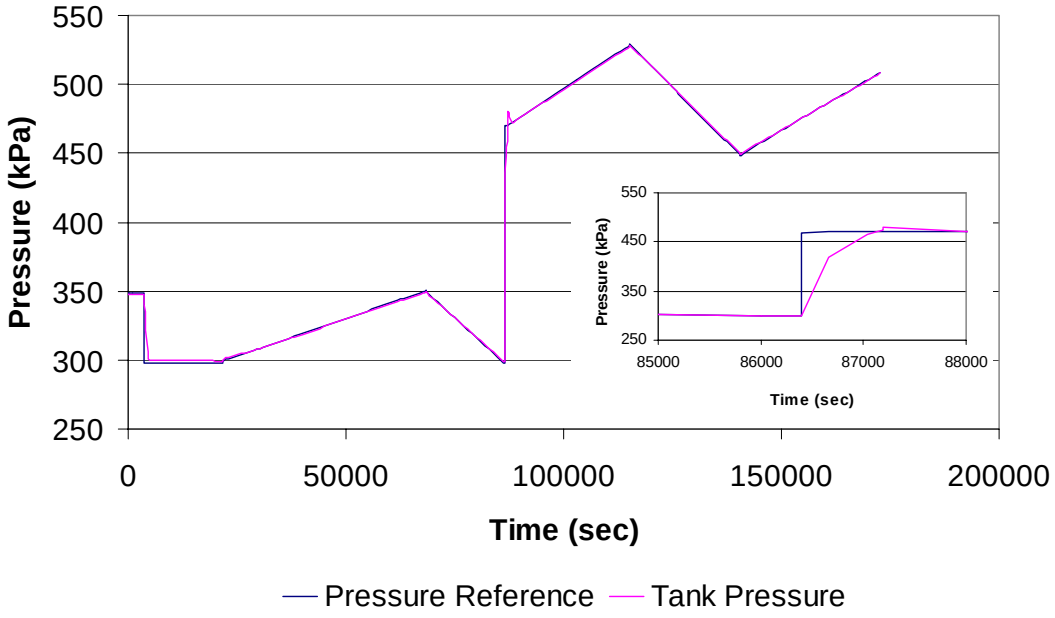

Figure 6.3. Reformate tank pressure (state variable) optimum dynamic response.

The insert in Figure 6.3 shows the behavior of the system pressure during a very strong operational change at 86,400 sec (24 hr). At this point the load changes from 1.5 kWe to 5.55 kWe and the optimum operational pressure changes from 297 kPa to 472 kPa. The system pressure matches the optimum system pressure after approximately 1300 sec (21.7 min). The apparent slow response is not due to the lack of system capacity but rather to the need to take into account efficient operation during the transient, since as the mass flow of steam-methane mixture into the reformer increases, the reformer conversion efficiency decreases due to the reduction in gas residence time and the slow dynamics of the heat transfer process through the

reformer walls. Thus, an indiscriminate increase in methane mass flow would rapidly increase the reformate tank pressure, but the hydrogen mole fraction would drop. Figure 6.4 shows the dynamic trajectory of the methane flow rate into the reformer, which in turn is the control variable to the reformate tank pressure. This mass flow is in fact regulated by a flow control valve as modeled in Chapter 4. The rapid increase in the mass flow at 86,400 sec is due to the sudden change in the reference pressure which produces an instantaneous error signal, which the controller tries to correct.

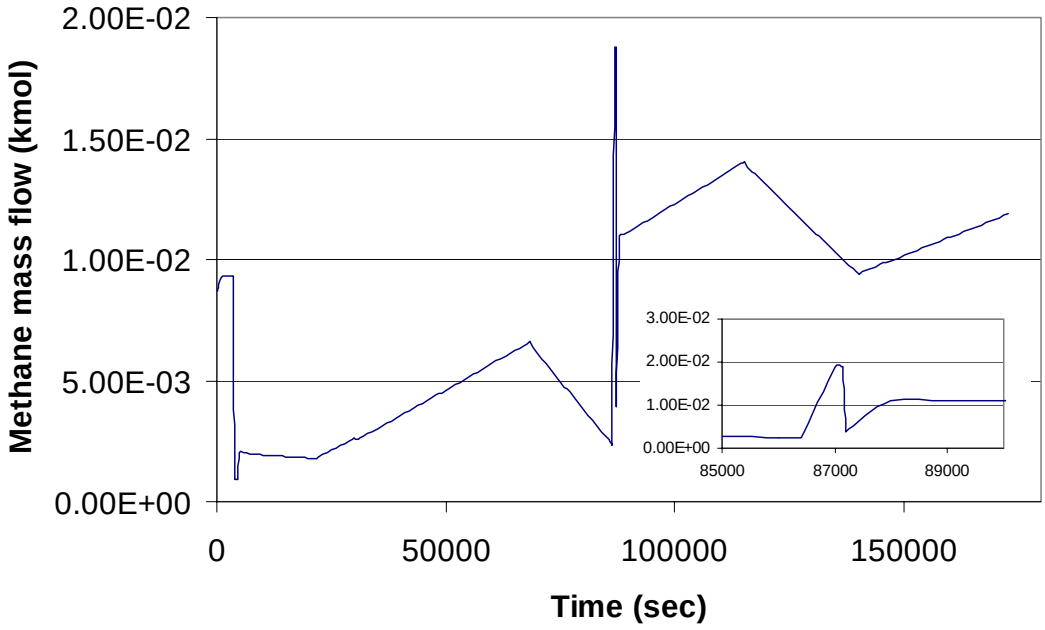

Figure 6.4: Steam-methane reformer optimum inlet methane mass flow (control variable).

Figure 6.5 shows how the actual air tank pressure very closely follows the optimum system pressure trajectory. Again the optimum system pressure is a function of system demand. In general, the faster the response with respect to the reformate tank is due to the fact that a higher loads the expander is able to provide all the energy required by the compressor. Figure 6.6 shows how the air tank pressure control variable, the electric motor voltage feed is zero for most of the load profile. Only between 3,600 sec (1 hr) and 31,000 sec (8.61 hr) parasitic power for the motor is required. This coincides with the lowest load requirement regime.

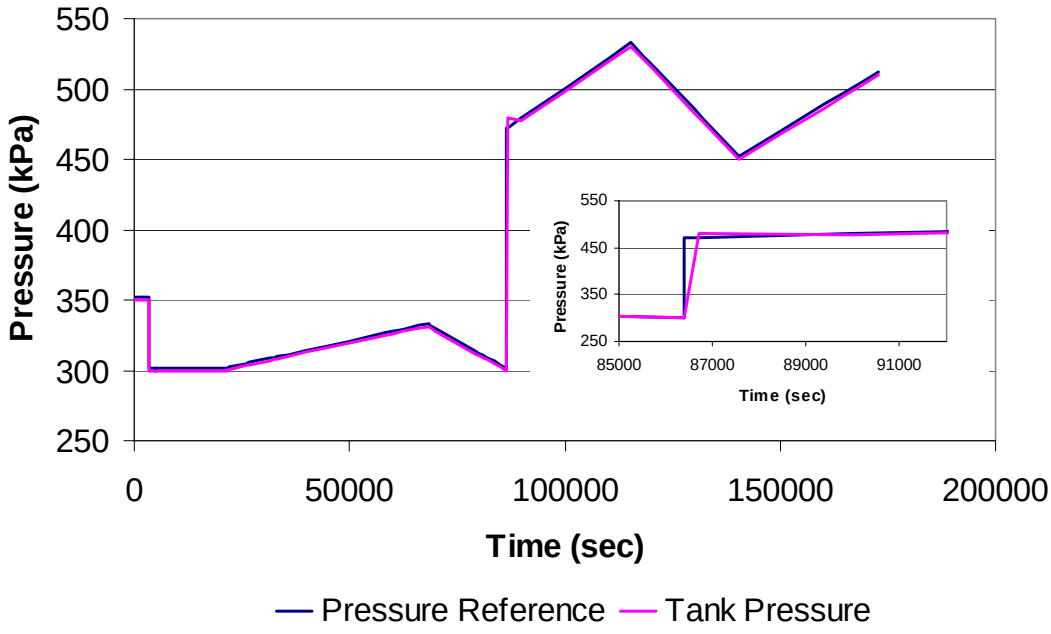

Figure 6.5. Air tank pressure (state variable) optimum dynamic response.

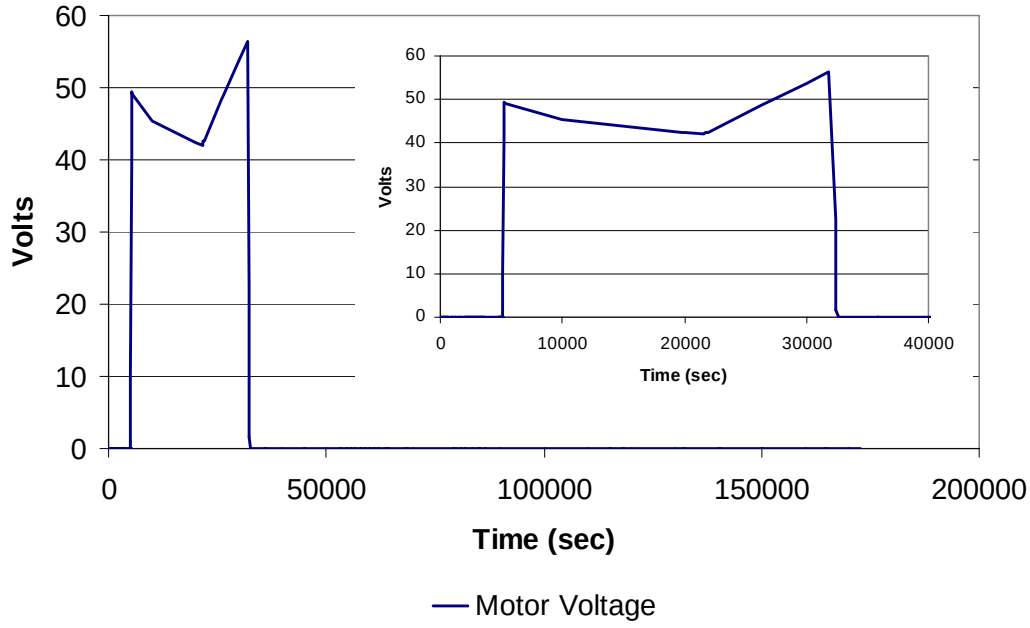

Figure 6.6. Electrical motor (control variable) optimum voltage input.

Figure 6.7 shows the optimum and the actual dynamic trajectory for the steam-methane reformer reformate exit temperature. This figure shows how the actual reformate exit temperature very closely follows the optimum temperature trajectory. This, optimum reformate exit temperature is a function of system demand. At high loads, the optimum temperature is higher. This is explained by the fact that at high

loads the reformate residence time is lower; thus, the conversion efficiency is lower. In order to increase the conversion capacity an increase in the reformate's exit temperature is required. However, a temperature increase is restricted by the additional fuel consumption. Again, let us analyze the system behavior as a very strong operational change occurs at 86,400 sec (24 hr). At this point the load changes from 1.5 kWe to 5.55 kWe and the optimum reformate exit temperature changes from 1051.8 K to 1061.4 K. The system pressure matches the optimum system pressure after approximately 1450 sec (24.2 min). The apparent slow response is due to the slow transient of the heat transfer process through the reformer walls. Figure 6.8a shows the dynamic trajectory of the hot gases reformer inlet temperature, which in turn is the control variable for the reformate exit temperature. As can be seen, the hot gases temperature can rapidly be increased, by regulating the methane mass flow into the burner through a flow control valve.

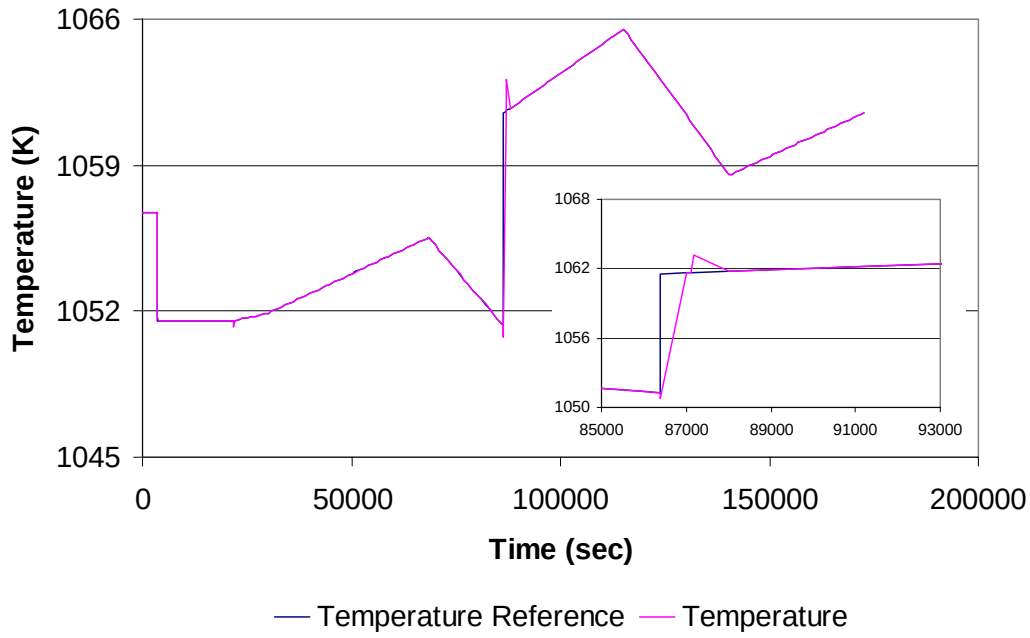

Figure 6.7: Steam-methane reformer reformate gas exit temperature (state variable) optimum dynamic response.

Figure 6.8b shows the dynamic response of the hot gases temperature along the reformer for this. The rapid increase in the hot gases temperature is due to two reasons. The first is the sudden change in the reference temperature (optimum temperature) which produces an instantaneous error signal, and the second is the change in reformate exit temperature due to the change in mass flows. Both conditions introduce an error which the controller tries to correct.

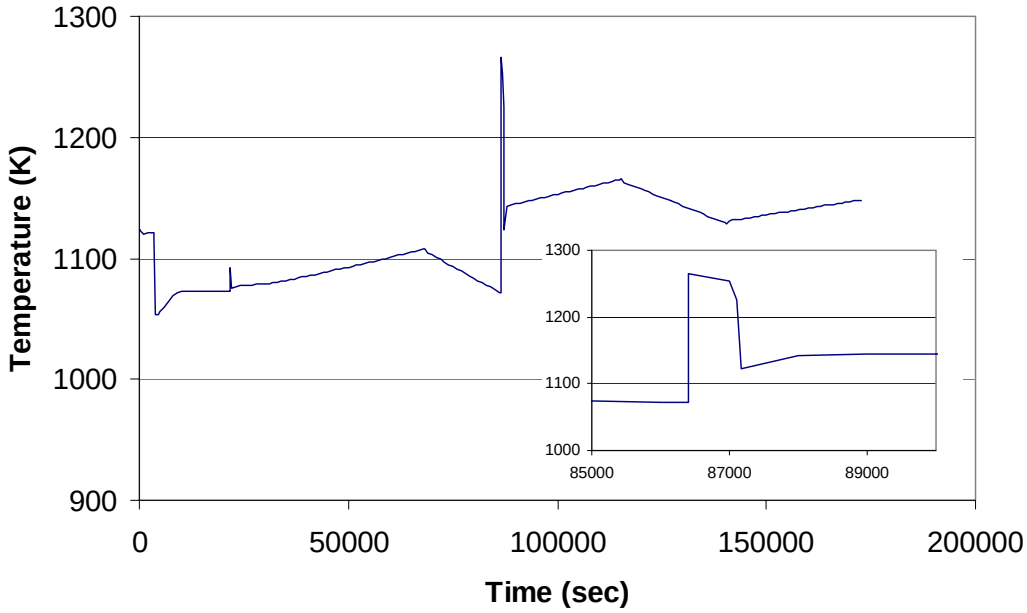

Figure 6.8a. Steam-methane reformer optimum hot gases inlet temperature (control variable) dynamic response.

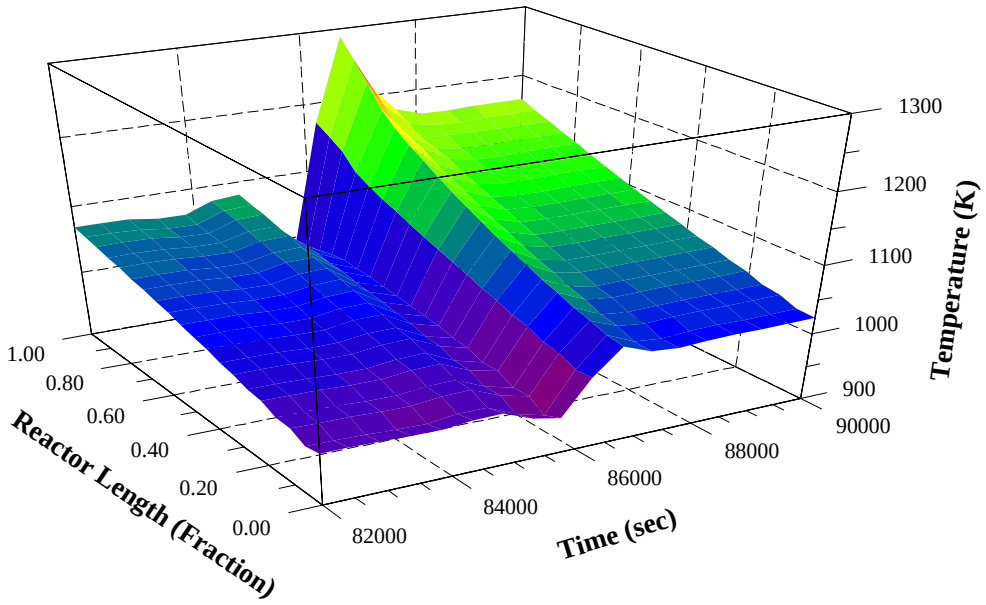

Figure 6.8b. 3D depiction of the steam-methane reformer optimum hot gases inlet temperature (control variable) dynamic response.

Figure 6.9 shows the dynamic trajectory of the optimum and actual steam-to-methane ratio (SMR). As it can be seen, the reference (optimum) and the actual SMR trajectory are strongly integrated. This behavior is due to the rapid regulation of the recirculation fraction shown in Figure 6.10 which in turn is controlled by a three-way flow control valve. A high SMR ratio is desired in order to have a more efficient methane conversion in the reactor. However, the recirculation fraction is limited

because an increment in reformate mass flow requires additional fuel in order to maintain appropriate reforming temperatures. Analyzing the system behavior during the operational change occurring at 86,400 sec (24 hr) shows that the actual SMR matches the reference (optimum) value rapidly for the reason presented above. Despite this behavior, the anode exit recirculation fraction only stabilizes after 400 sec (6.6 min) due to the time delay through the stack and reformer and transient effects, i.e. as the flow through the reformer to the stack increases, the output flow from the stack does not increase at the same speed. Additionally, the methane flow is changing as shown in Figure 6.4.

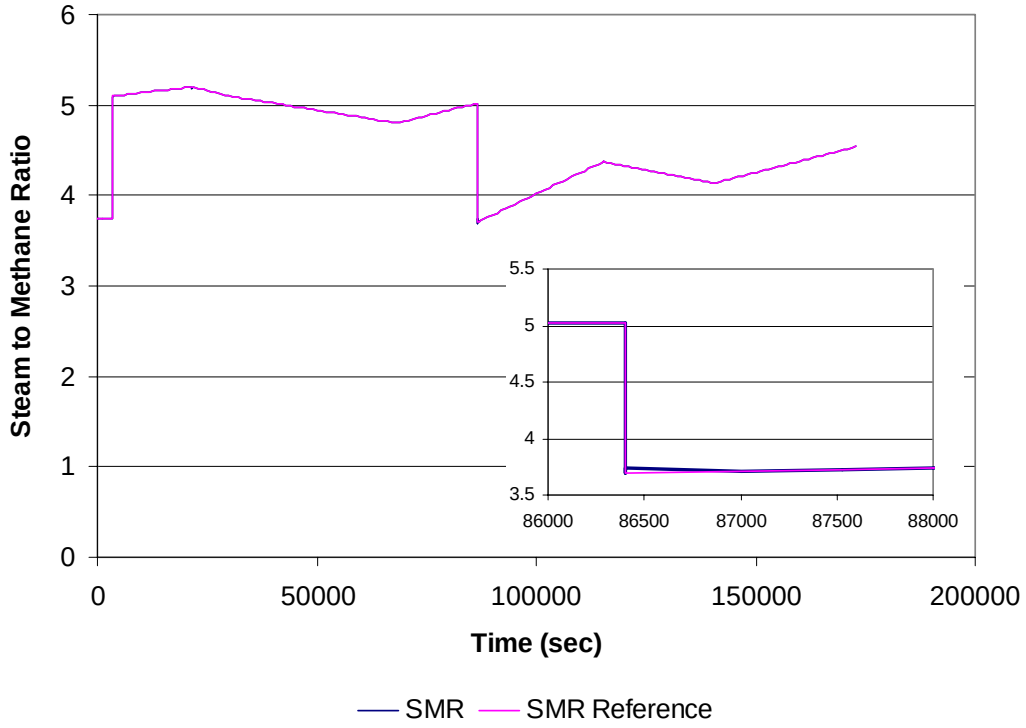

Figure 6.9. Steam-to-methane ratio (state variable) optimum dynamic response.

Figure 6.11 shows the most important system operational constraint's dynamic response. As mentioned above, regulating the temperature difference between the anode and the cathode inlet is extremely important in order to avoid thermal stresses. The maximum acceptable absolute temperature difference used in this doctoral work was 5 ^{o}K. As can be seen, this constraint is met through the entire load profile, including during the strong transients present at 3,600 sec (1 hr) and 84600 sec (24 hr). The higher temperature difference is present at very low loads. In general, the temperature difference is a function of the operational conditions (e.g., mass flow and temperatures). Due to configurational reasons explained below, the anode inlet

temperature is easy to regulate (the chosen stack operational temperature is 1000 ^{o}K). However, the cathode inlet temperature depends more strongly on system synthesis/design, which is used instead of an additional controller. This solution is more fuel efficient and more reliable.

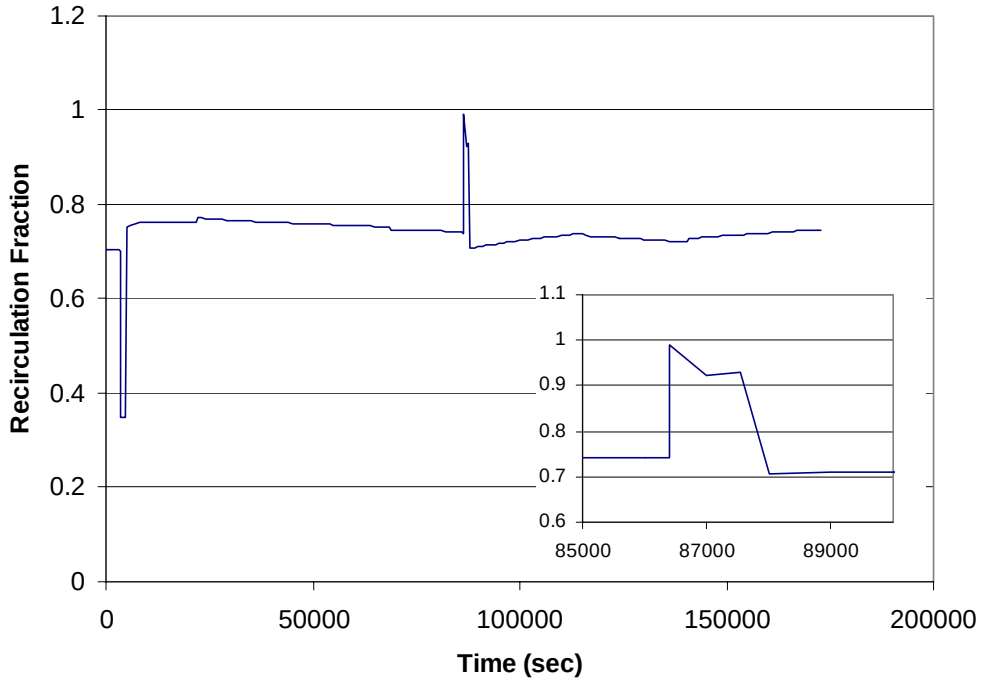

Figure 6.10. Anode exit optimum recirculation fraction (control variable) dynamic response.

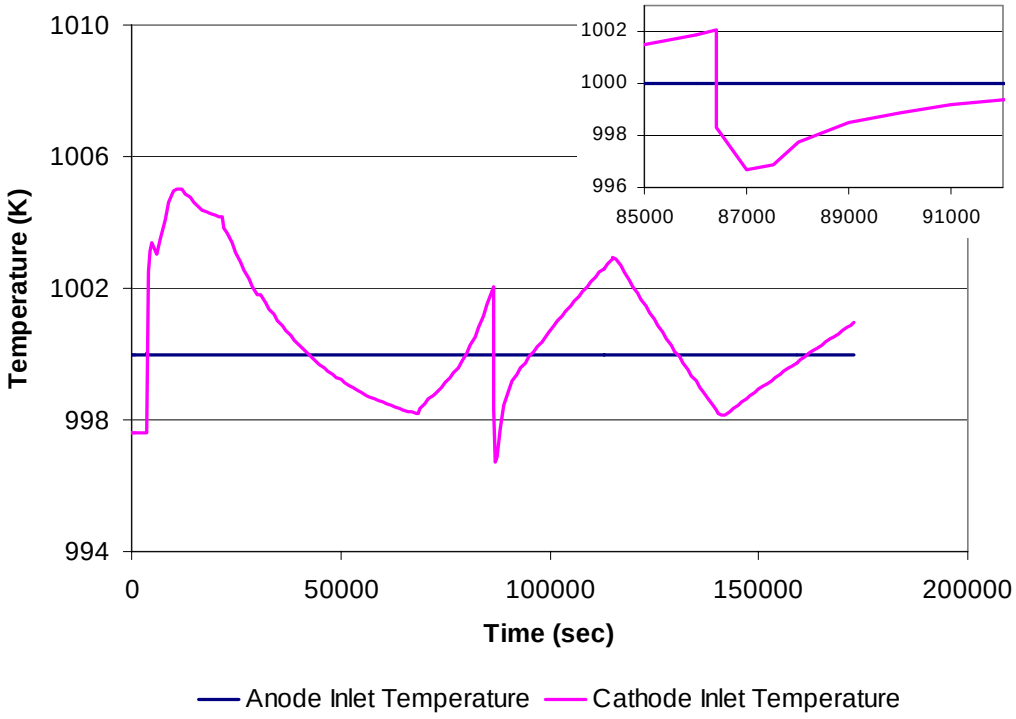

Figure 6.11. Anode and cathode inlet temperature optimum dynamic behavior.

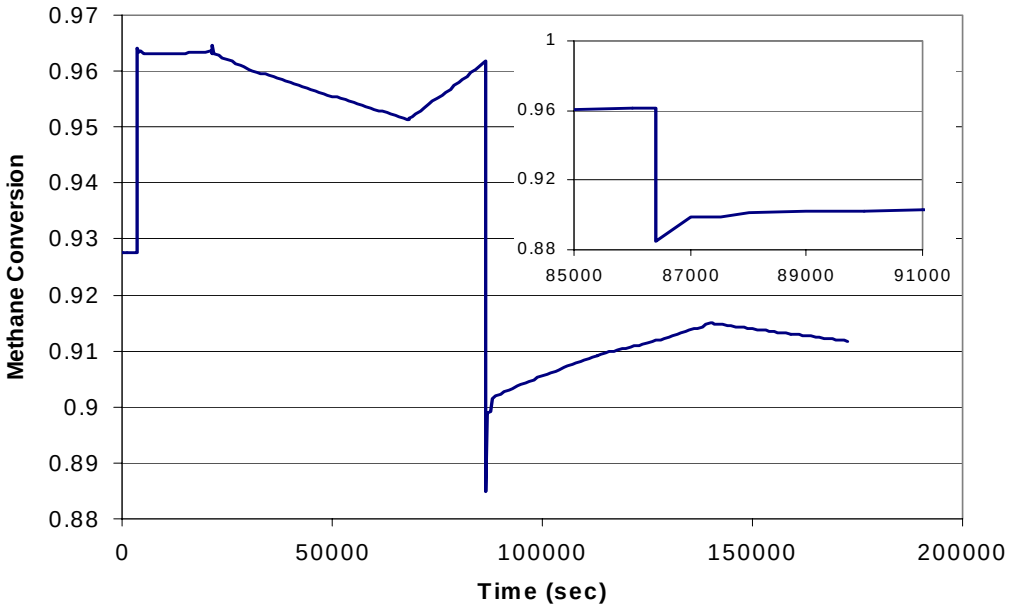

Figure 6.12a. Methane conversion optimum dynamic response.

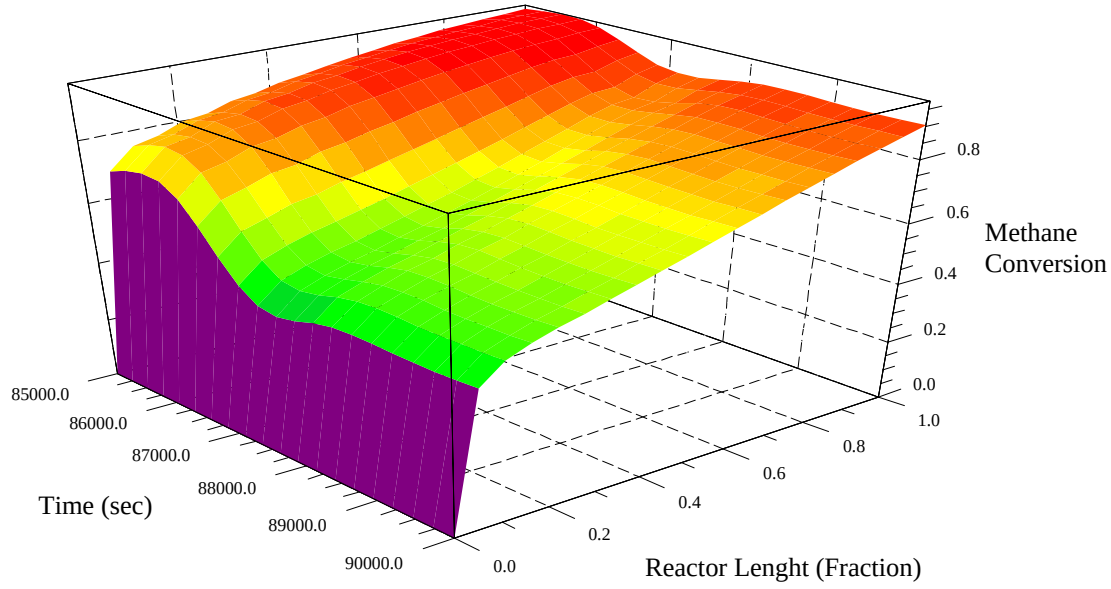

Figure 6.12b: 3D depiction of the methane conversion optimum dynamic response.

Figure 6.12a shows the methane conversion optimum dynamic trajectory. As expected, the conversion at low load (low mass flows) is higher even though the reformate exit temperature is lower. This is explained by the higher recidence time through the reformer. In addition, after the step load change at 86,400 sec (24 hr) the methane conversion decreases suddenly due to the rapid increase in reformate mass flow. The methane conversion stabilizes at about 89,000 sec (24.7 hr). Figure 6.12b shows the optimum dynamic response of the methane conversion along the reformer for the step-up load change. In general, it should be pointed out as a major conclusion

that the capacity of the system to reach steady state is faster for a step-down in load (at 3600 sec (1 hr)) than for a step-up in load (at 84600 sec (24 hr)). This can be seen in Figures 6.3 to 6.13.

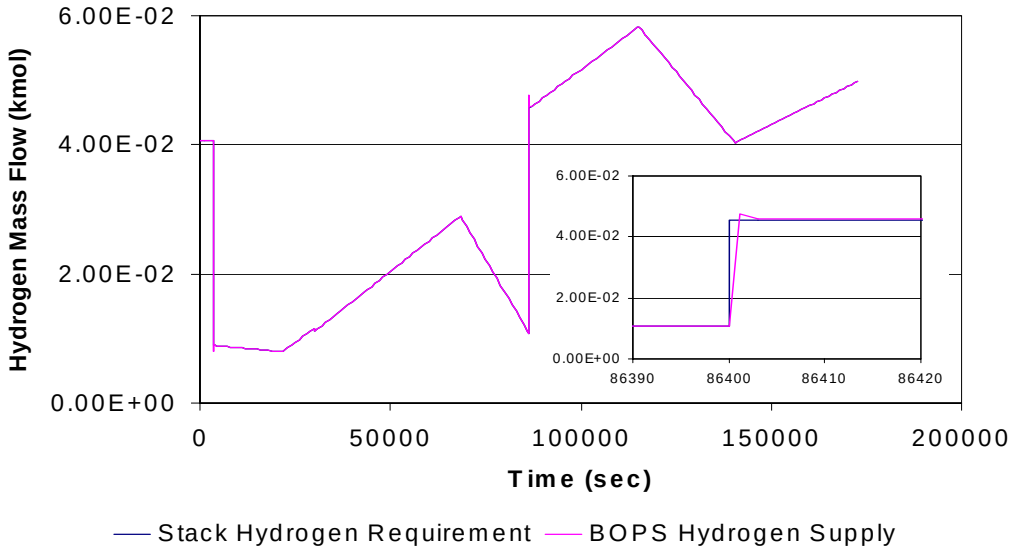

Figure 6.13. Stack hydrogen requirements and BOPS optimum hydrogen supply (part of the reformate mass flow which is a state variable) from the reformate tank.

Figure 6.13 shows the stack hydrogen requirements compared to the BOPS hydrogen supply from the reformate tank. The rapid response is evident. This unique and very desirable feature is due to the existence of reformate and air buffers. It should be pointed out that the time response is a limiting characteristic of SOFC systems when applied to APUs. Without the buffers, the time response for an increment in load beyond admissible ranges for several reasons. First, the methane and the anode products are subject to transport delays. Second, an increase in mass flow through the reformer implies a reduction in conversion, which from Figure 6.12 takes about 400 sec (6.7 min) to stabilize. Finally, a faster response requires a stronger intervention on the part of the hot gases (i.e. an increase in the hot gases temperature above efficient values) which additionally may introduce excessive temperature gradients in the reformer. Furthermore, without buffering, a reduction in load would generate waste, since the extra hydrogen generated during the transient cannot be used in the stack and instead must be used in the burner. Figure 6.14 shows the optimum dynamic response of the hot gases inlet temperature to the expander. In general, the lower the load, the higher the inlet temperature. Figure 6.15 shows the optimum dynamic response of the inlet mass flow inlet to the expander.

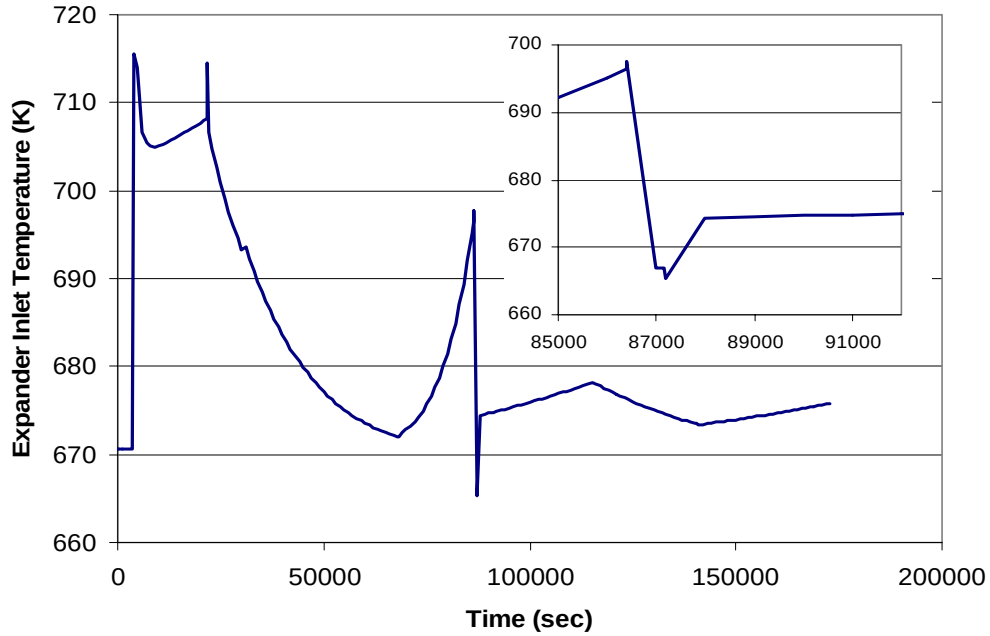

Figure 6.14. Optimum dynamic response of the hot gases expander inlet temperature.

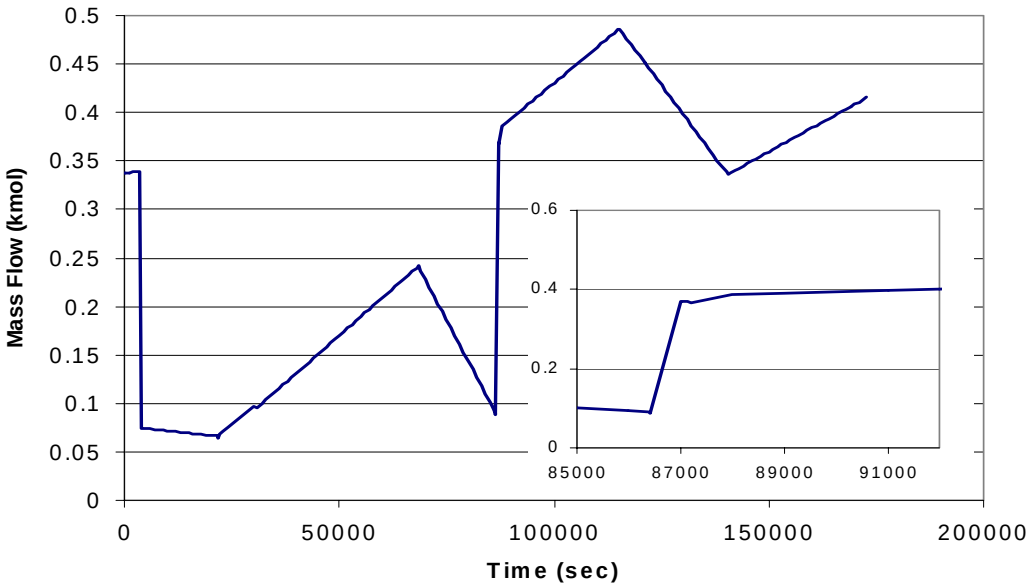

Figure 6.15. Optimum dynamic response of the expander inlet hot gases mass flow.

Figure 6.16 shows the optimum dynamic response of the electrical motor parasitic power. As shown in this figure, after the step change at 3600 sec, the required air mass flow decreases, but the mass flow into the expander decreases as well. Therefore, both the compressor and expander operate under conditions of low efficiency. As a result, the work generated by the expander is not enough to drive the compressor. In contrast, after about 32,000 sec (8.8 hr), the optimum compressor and expander design decision variable values yield zero parasitic power for the remainder of the load profile.

Figure 6.17 shows the heat rejection from the stack, which in fact is not negligible. Theoretically, this heat can be recover and used for the reforming process. However, the implementation of the heat recovery cycle introduces additional capital costs as well as technical problems. Therefore, in this doctoral work, the heat is rejected to the ambient using a fan, which in fact represents a parasitic load. Finally, Figure 6.18 shows the optimum dynamic response of the air tank temperature and the compressor exit air temperature, the most important feature is the increase in the air temperature as the optimum pressure ratio increases.

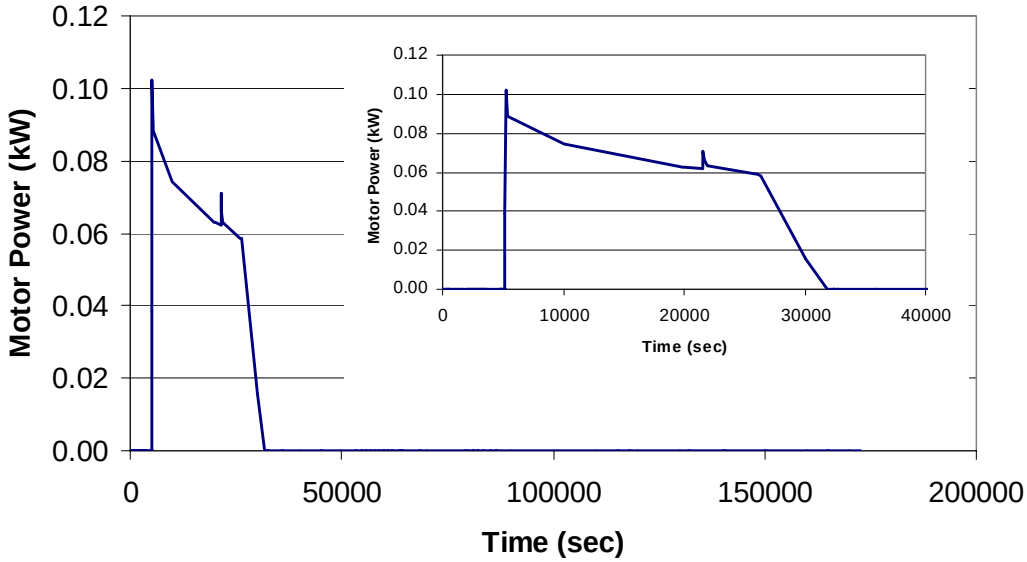

Figure 6.16. Optimum dynamic response of the electrical motor power output.

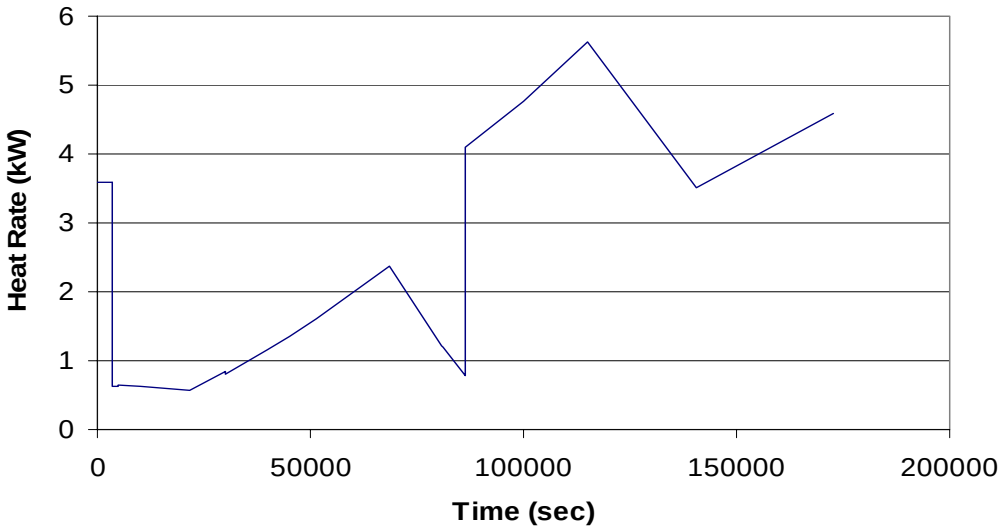

Figure 6.17. Stack heat rejection Optimum dynamic response.

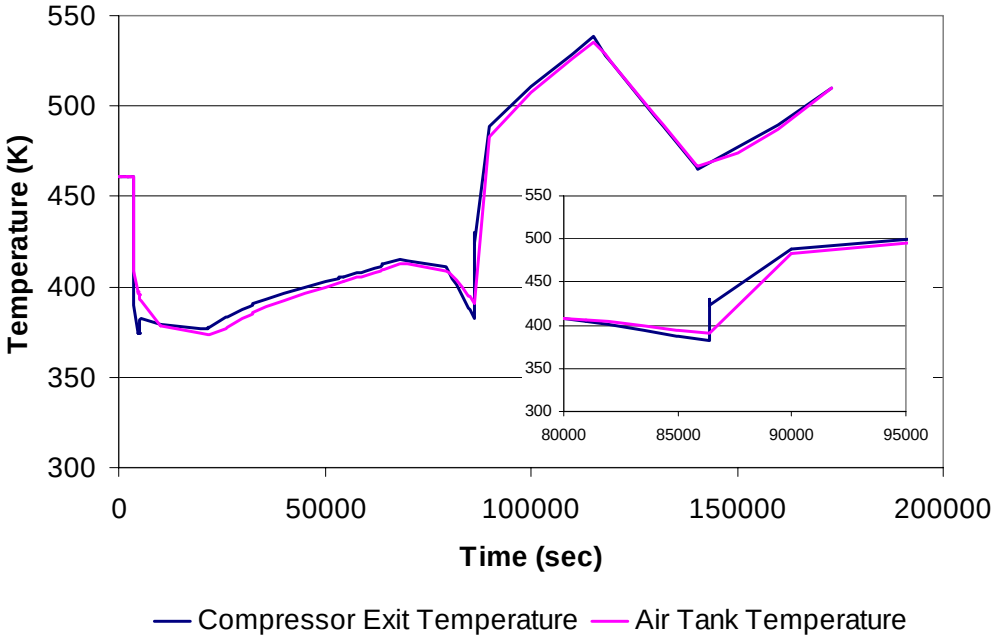

Figure 6.18. WRAS inlet air temperature optimum dynamic response.

6.1.2 Control and Controlled Variable Pairing Determination

Table 6.5 shows the control and controlled variables pairing. The determination of control variables requires preliminary analysis in order to find the control variable that can best change a given state variable in the desired manner. This task is relatively straightforward when dealing with a plant element with a single state variable to be controlled (e.g., the reformate tank pressure should be controlled by regulating the amount of mass flow coming in). However, when dealing with multiple control-state variables in a single component such as in the case of the reformer, the variable coupling must be establish by determining the effects of each possible control variables on each state variable. In the case of the steam-methane reformer, it is necessary to control the reformate exit temperature, composition (methane conversion), and mass flow. There are three proposed control variables which are the hot gases inlet mass flow and temperature and the steam-to-methane ratio. What follows describes the results of the pairing process.

Table 6.5. Control and controlled variables pairing.

Element	Control Variable	Controlled (state) variable
Steam-methane reformer	Hot gases inlet temperature[55]	Reformate exit temperature
Steam-methane reformer	Hot gases mass flow[55]	Methane conversion
Steam-methane reformer	Anode recirculation fraction[55]	Steam-to-methane ratio
Reformate tank	Methane mass flow into the SMR[55]	Reformate tank pressure
Reformate tank	Anode reformate inlet mass flow[55]	Stack gross output power
Air tank motor	Electrical motor input voltage	Air tank pressure
Air tank motor	Cathode air inlet mass flow[55]	Air-fuel ratio at the stack

The Relative Gain Matrix (RGM) technique was used to find the relative effects of the control variables ($\vec{w}$) on the state variables ($\vec{y}$). The RGM measures this effect by determining the derivative of each stated variable with respect to the each control variable. With this information, a matrix ($M_{n \cdot m}$) is created where *n* is the number of control variables and *m* is the number of state variables. In this case, a 3x2 matrix is generated. By comparing the elements of the resulting matrix, the coupling is found. In this doctoral work, the resulting RGM is shown below in Table 6.6, where K_{ij} is the gain of the i^{th} control variable with respect to the j^{th} state variable. Figure 6.19 shows the relationship between the state variables and the proposed control variables.

Table 6.6. Relative Gain Matrix (RGM) for the steam-methane reformer.

	Hot gas inlet temperature (w_1)	**Hot gas mass flow (w_2)**	**Steam-to-methane ratio (w_3)**
Reformate exit temperature (y_1)	$K_{11} = \frac{\partial y_1}{\partial u_1} = 9.51$	$K_{12} = \frac{\partial y_1}{\partial u_2} = 1.31$	$K_{13} = \frac{\partial y_1}{\partial u_3} = 1.74$
Methane conversion (y_2)	$K_{21} = \frac{\partial y_2}{\partial u_1} = 0.25$	$K_{22} = \frac{\partial y_2}{\partial u_2} 0.0028$	$K_{23} = \frac{\partial y_2}{\partial u_3} = 0.0026$

[55] This variable is in fact affected by the control of a flow valve as presented in section 4.6. By varying the input voltage to the valve, the opening of the valve is changed, which in turn affects the mass flow through it. In this doctoral work, no reference to the voltage input is made, since it says little about the flow condition. Instead, the actual value of the mass flow is given. The correlation of the voltage-mass flow is rather easy to determine and is given by the valve characteristics.

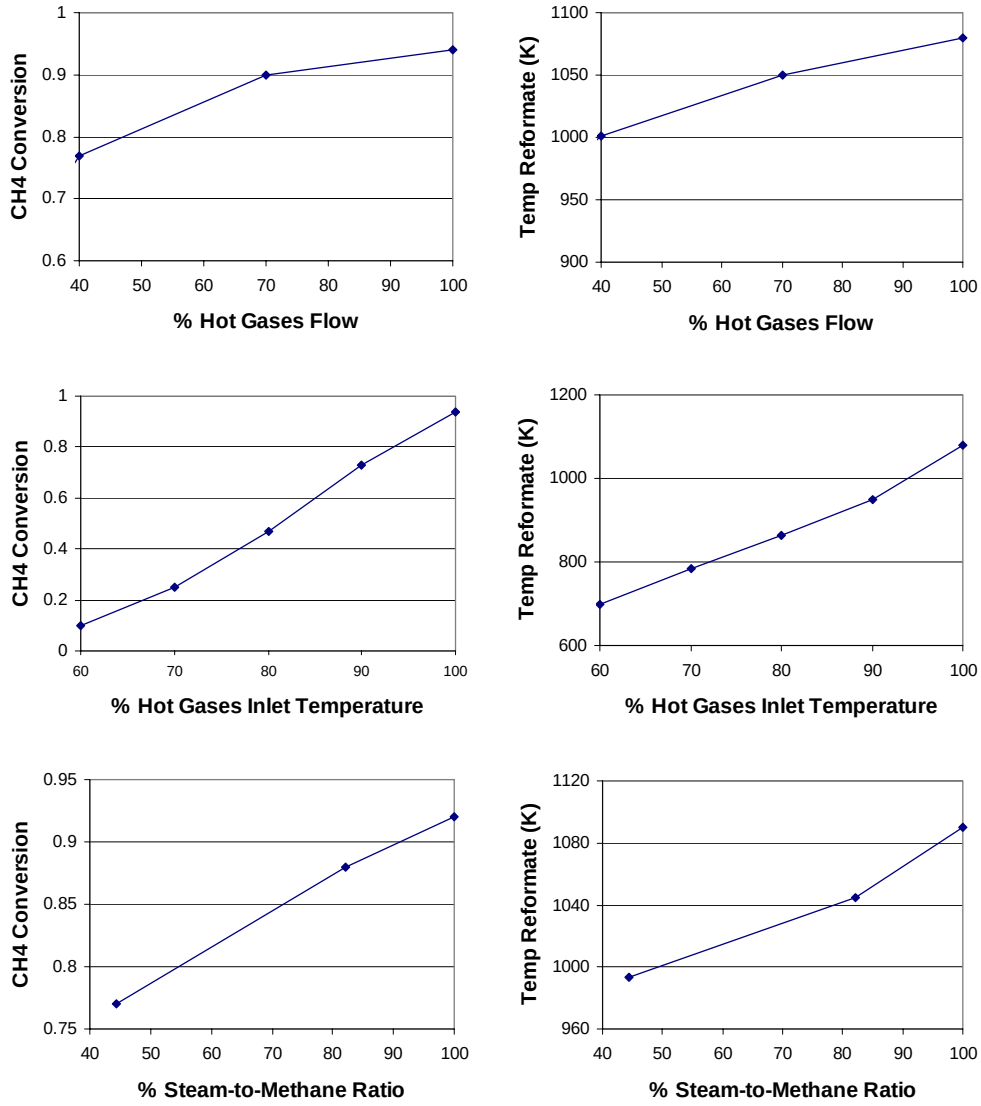

Figure 6.19: Controlled and control variables relationship.

As it can be seen from Table 6.6, the hot gases inlet temperature has the highest relative capacity to affect both state variables. However, the hot gases inlet temperature is maximum gain is that related to the reformate exit temperature. Therefore, these two variables are paired. Note that the gain of the hot gases inlet temperature with respect to the methane conversion is two orders of magnitude higher that those of the hot gas mass flow and steam-to-methane ratio. Therefore, it may be also appealing to pair the hot gases inlet temperature to the methane conversion and to either use the hot gas mass flow or the steam-to-methane ratio to control the reformate exit temperature. Even though this approach seems correct, it has a flaw. The hot gas

mass flow and the steam-to-methane ratio effect on the reformate exit temperature is limited. The reformate exit temperature will never exceed the hot gases inlet temperature whatever the hot gas mass flow and anode recirculation mass flow are. This means that as the hot gas mass flow and the anode recirculation mass flow increased, their respective gains would go to zero.

Regarding the methane conversion, it can be seen from Table 6.6 that the hot gas mass flow and the steam-to-methane ratio have a similar effect on the methane conversion. The selection of which control variable to pair to the methane conversion is based on parametric analysis and preliminary optimization results. It was observed that a high methane conversion is desired in order to achieve high conversion efficiency. In order to achieve this, a high hot gas mass flow and high steam-to-methane ratio are required. However, for most operational segments, in order to reach a high methane conversion with a given steam-to-methane ratio, it is necessary to generate more hot gases than those available from the anode and cathode exits. In order to do this, additional air from the air tank is required, which means additional work from the compressor and additional fuel to reach the required temperature. Thus, the efficiency gain achieved by increasing the methane conversion does not compensate the additional cost due to the increase in power requirement and additional fuel. Consequently, the optimum operating regime is found when all the anode and cathode exhaust are used with no extra air and the steam-to-methane ratio is used as the control variable for the methane conversion. This in fact produces a change in the system configuration since no connection between the air tank and the fuel-anode and cathode exhaust mixer is now required.

6.1.3 Solid Oxide Fuel Cell System Optimum Synthesis

This research work is part of a project sponsored by the DOE SECA Program which intends to advance the state-of-the art of SOFC systems. This project is divided into two phases. During Phase I an important objective was to establish feasible system super-configuration which provides high efficiency and reliability. Based on this super-configuration, detailed dynamic models for each component where developed and then coupled in order to generate a system level dynamic model. Using the system level dynamic model, parametric studies were done in order to determine system behavior for various combinations of system-level parameters and components

locations and dimensions. The interested reader is referred to Mazumder et. al. (2004) and Rancruel and von Spakovsky (2004).

The results of the parametric studies were used to determine the most promising subset of this super-configuration i.e. reduced super configuration based on system response, fuel consumption, capital cost, operational constraints, etc. During Phase II, the resulting reduced super-configuration was subjected to a large scale synthesis/design optimization while taking into account its effects on system operation, i.e. on the dynamic response of the system.

Figure 4.10 and 6.20 shows the most promising super-configuration established at the beginning of Phase I. The purpose of each component is explained in detail in Chapter 4. The parametric studies showed this configuration to provide adequate fuel efficiency. However, the system cannot offer proper control of the temperature difference between the anode and the cathode inlets. Current solid oxide fuel cell stack materials require that the temperature gradients along and across the stack to be controlled within a very small range. This information is mostly proprietary and not available in the literature. However, at a 2004 fuel cell conference in Rochester, New York; a 5 ^{o}K difference between anode and cathode inlets was suggested by several manufacturers. Therefore, this value was used for this doctoral work.

The main reason for a high temperature difference at the stack inlet is the fact that the mass flow at the cathode exit is reduced due to oxygen conversion during the electrochemical reactions. This reduction is in fact significant due to the relatively low oxygen to hydrogen ratio used to run the stack. For this doctoral work, the oxygen to hydrogen ratio was set to 2.2 based on available information. Furthermore, the available stack model at this stage of the project does no consider the effects of the oxygen to hydrogen ratio.

Additionally, the mass flow at the cathode exit has a time delay with respect to the mass flow at the inlet. This behavior is most critical while driving the system from low to high load. During this operational condition, the mass flow of cold gases through heat exchanger II increases rapidly while the hot gases coming out of the stack increase at a slower rate due to the stack time delay. The same phenomenon is present in the anode and heat exchanger I. This behavior makes the stack inlet temperature difficult to control unless additional control forces are integrated (e.g.,

hot gases and cathode products mixing). This solution is not desirable because it implies additional capital and operational costs.

In order to provide a system-level solution for the problem mentioned above, heat exchanger I is relocated. Instead of transferring energy from the anode exit to the anode inlet stream, heat exchanger I is used to transfer energy from the reformate tank exit stream to the cathode exit stream. The products of the cathode at a higher temperature are then passed through heat exchanger II. This modification has proved to be effective in controlling both the anode and the cathode inlet temperatures. The stack exit temperature is held constant at 1000^{o}K by separately controlling it with a fan based cooling system. Furthermore, in general the anode inlet mass flow is much smaller that the cathode's. This means that the heat exchanger I hot gas exit temperature (i.e. anode inlet temperature) is always very close to 1000^{o}K. Furthermore, the additional energy put into the cathode exhaust helps to level the heat exchanger II cold stream exit temperature (i.e. cathode inlet temperature) rapidly and closer to 1000^{o}K.

Regarding the anode exhaust, if was found that recirculating a fraction of it back into the steam-methane mixer provides sufficient water content for the steam-methane reformer, thus, eliminating the need for a steam generator during regular operation and even during transients. This in fact elevates the system efficiency due to the elimination of all parasitics related to the steam generator operation (i.e. pump motor and hot gases). The steam generator is still required for start-up. It was also concluded that due to the high temperature of the recirculated anode products, heat exchanger III was not required at this location. This component was, thus, relocated in order to transfer energy to the hot gases going into the expander so as to reduce the dependence of the WRAS on the electrical motor. Figure 6.21 shows the resulting reduced super-configuration established at the end of Phase I. This Phase I/Phase II reduced super-configuration is used in order to perform the dynamic synthesis/design and operational/control optimization of the SOFC system, resulting in the final optimal system configuration.

Figure 6.22 shows this optimum configuration for the during-operation regime (i.e. no start-up included). The synthesis/design optimum no longer requires heat exchanger V since recovering additional energy from the expander exhaust increases the compressor inlet temperature, which in turn increases the power requirement. This

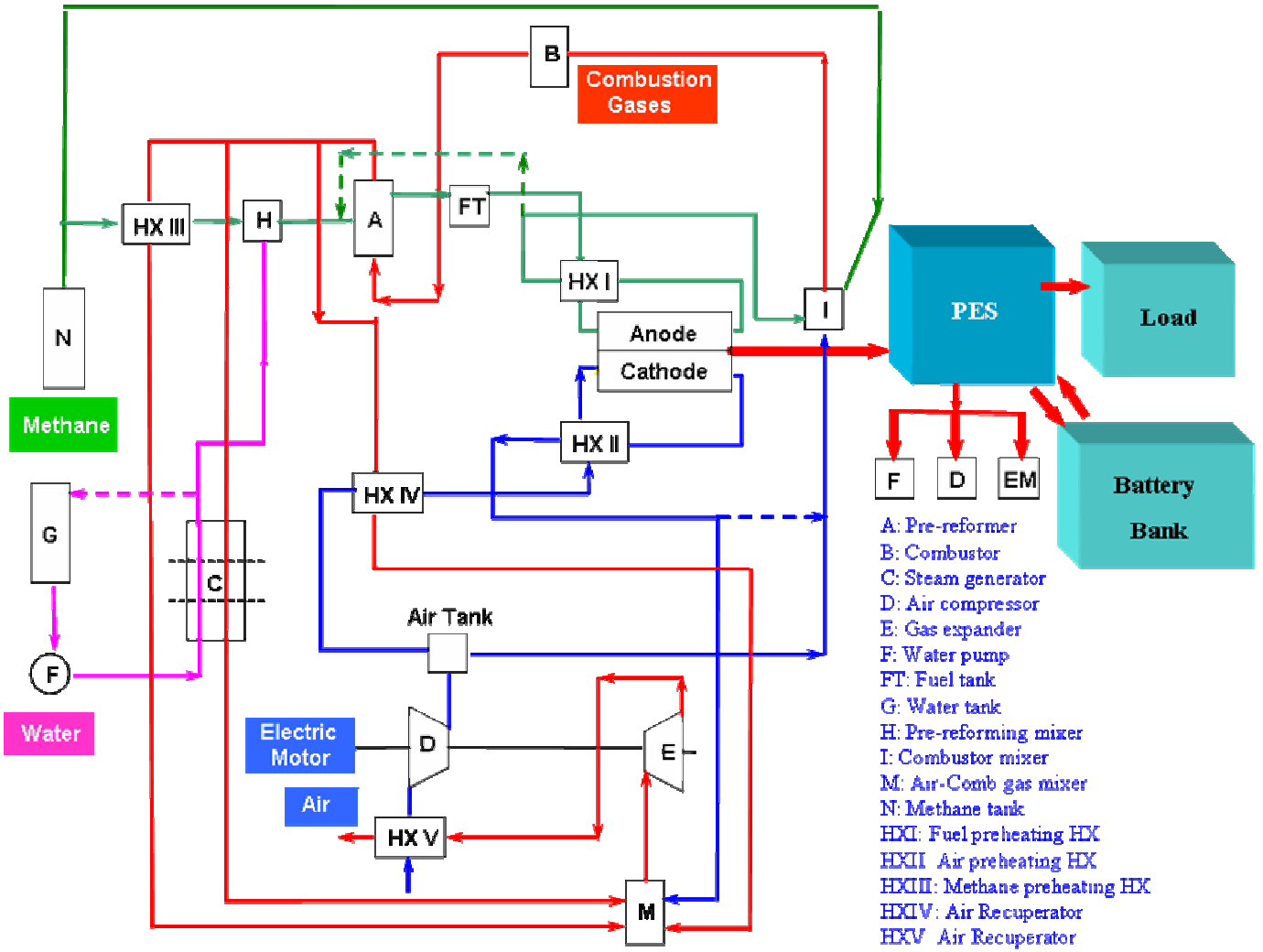

Figure 6.20. SOFC Phase I reduced super-configuration (also given in Figure 4.10) established at the beginning of Phase I.

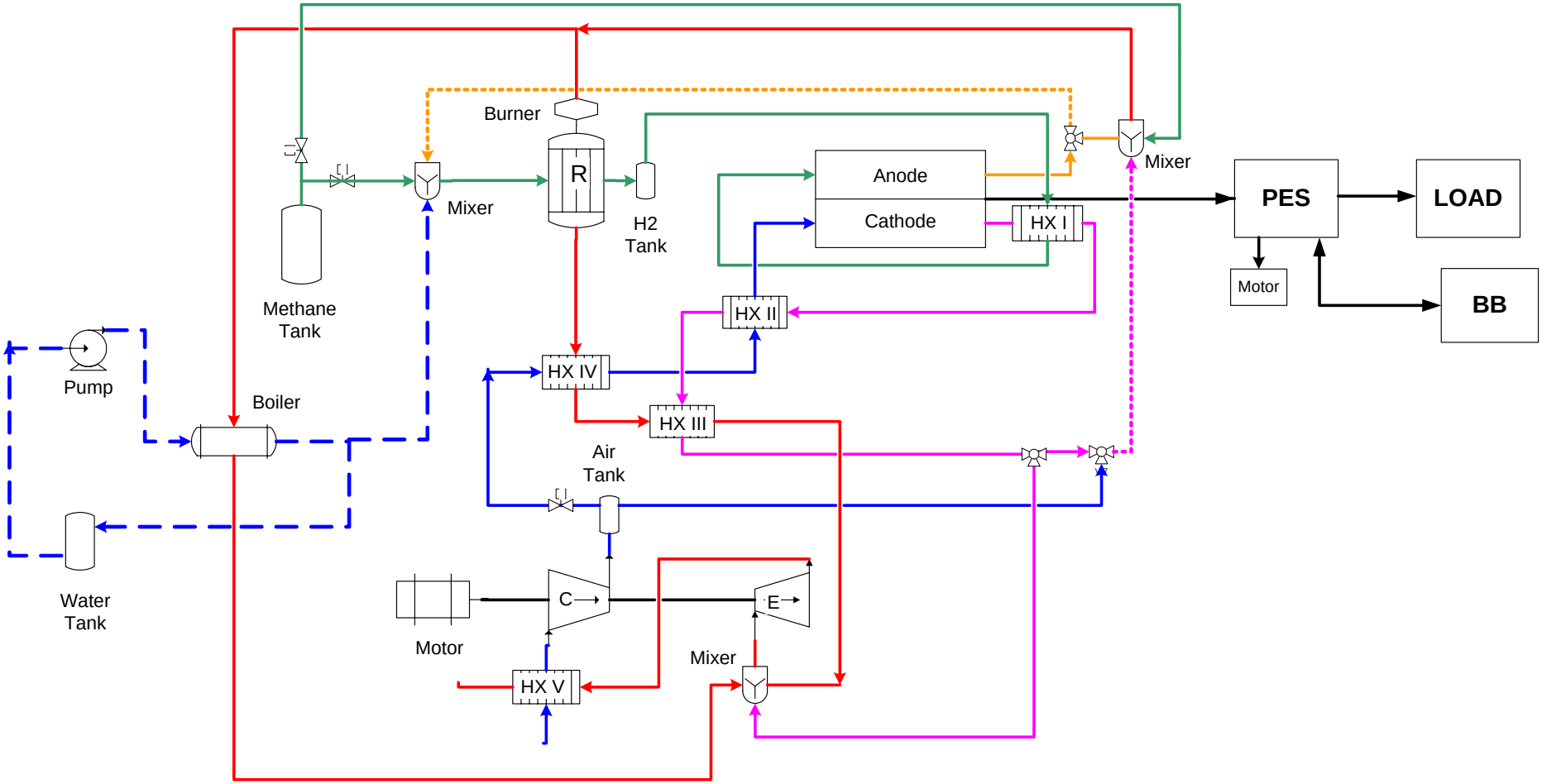

Figure 6.21. SOFC system phase I/Phase II reduced super-configuration established at the end of Phase I for purposes of dynamic synthesis/design optimization in Phase II.

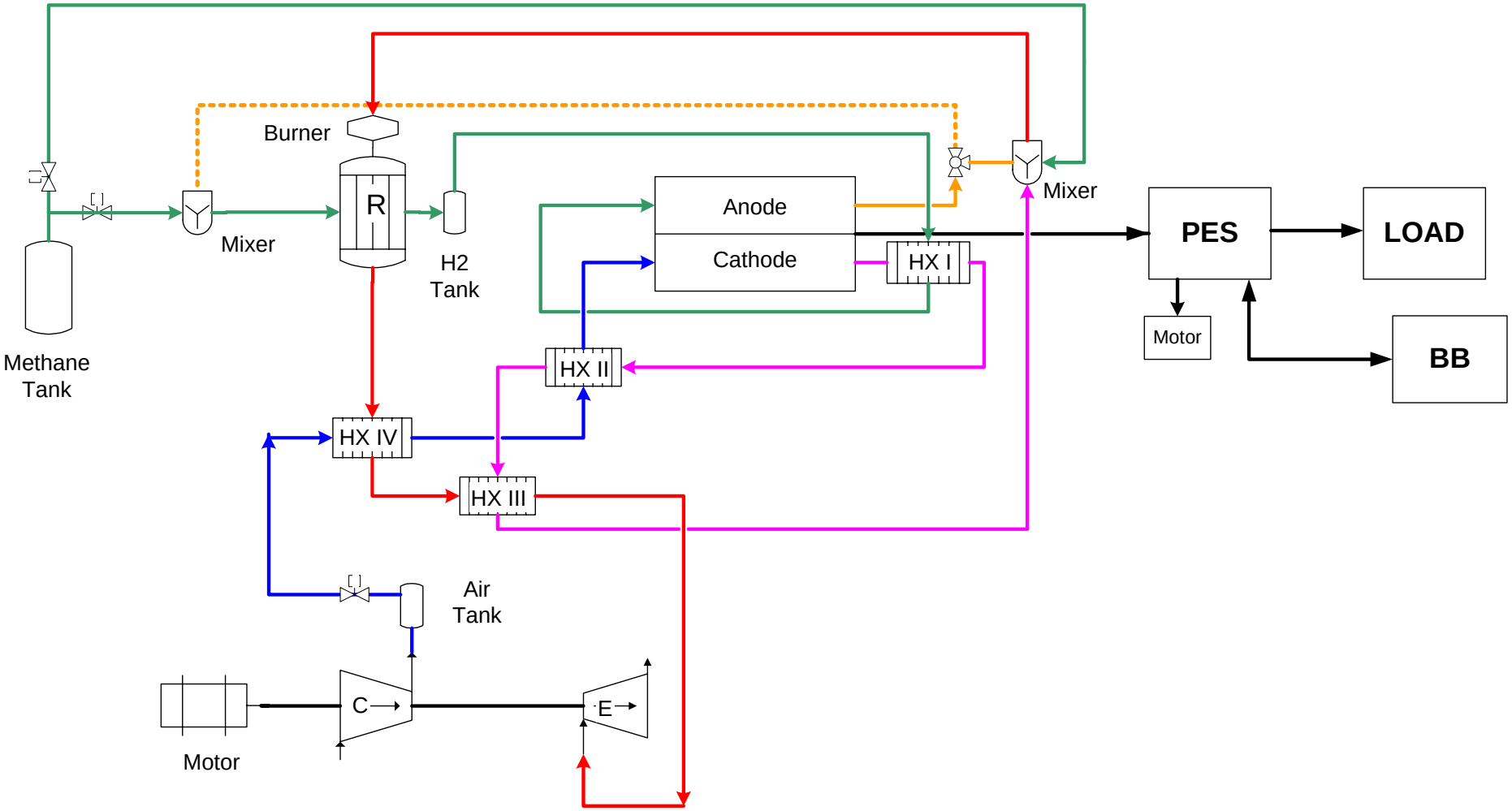

Figure 6.22. Optimum configuration resulting from the Phase I/Phase II reduced super-configuration during synthesis/design and operational/control optimization.

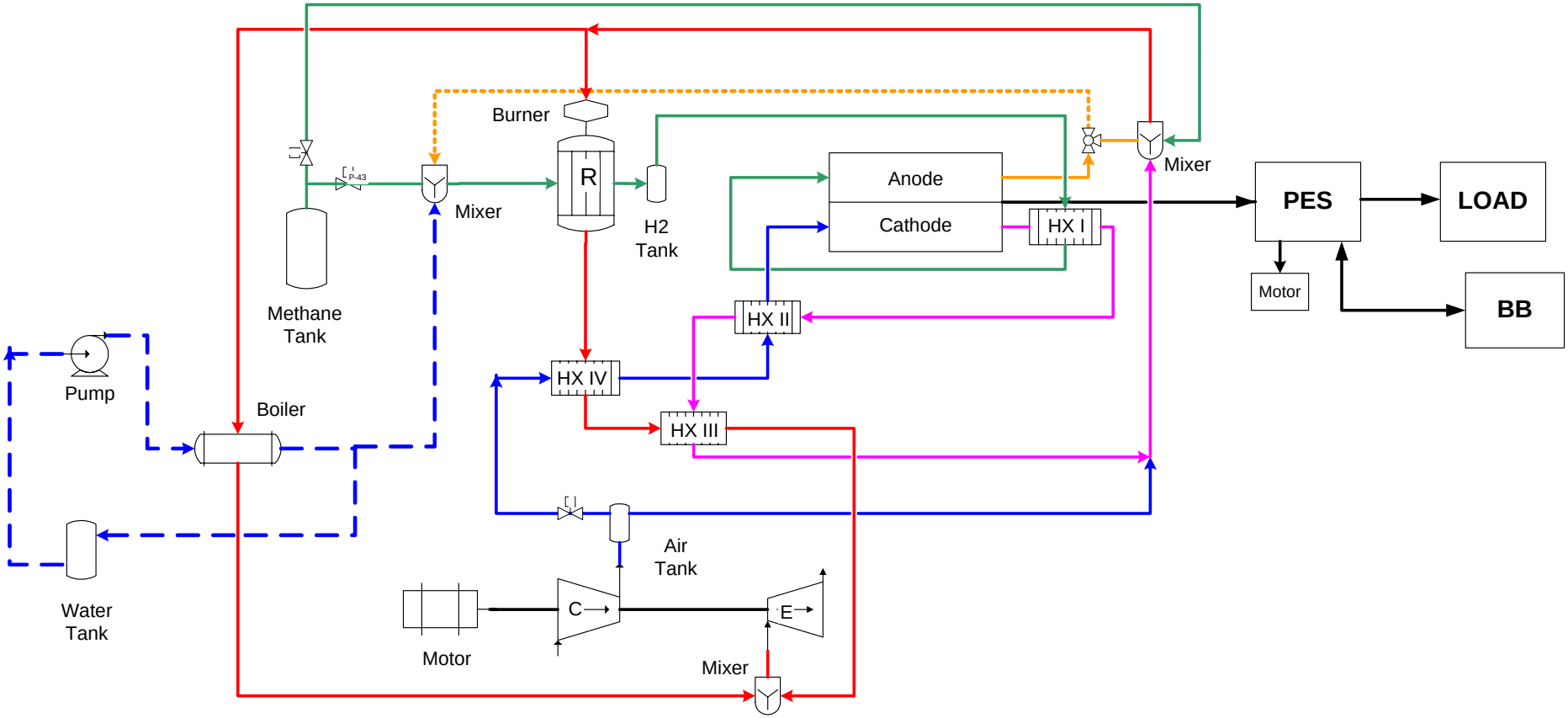

Figure 6.23. Optimum start-up configuration resulting from the dynamic synthesis/design and operation/control optimization process.

in fact was expected. However, the increment in the air temperature into the BOPS does not compensate the additional power requirement at any operational condition.

As mentioned in Section 6.1.2, the dynamic operational optimum does not take the products of the cathode directly to the expander mixer, thereby, eliminating the piping connecting the expander mixer and the cathode products line. Moreover, the dynamic operational optimum yields no air taken directly from the air tank for combustion for the during-operation regime, consequently, eliminating the respective piping.

Figure 6.23 shows the optimum configuration for start-up. The fundamental differences in reference to the during-operation regime lie in the need for a steam generator and a line that provides air directly from the air tank for combustion. Before steam is generated at the proper temperature, the output of the steam regenerator is recirculated into the water tank in order to increase the water temperature and speed up the process. The start-up process is explained in detail in the next section.

6.1.4 Start-up Strategy with Battery Bank

An analysis of the proposed configuration and control strategies and a consideration of the need for a fast response to load changes leads to the following system start-up control strategy:

1. First the turbo-machinery is started. At this point energy is taken from the battery bank.
2. Once the turbo-machinery is operating, the BOPS starts. Fuel and air is delivered to the combustor and hot combustion gases are produced in order to generate steam and heat up the system components.
3. Once the heat source is available, the steam generation process starts. The hot gas mass flow through the steam generator during start-up is such that design thermal stresses are not exceeded but operating conditions are reached promptly. Until operating conditions are reached, the water coming out of the steam generator is recirculated. Thus, no water is wasted and the inlet temperature is increased.

4.1 While adequate vapor temperatures are being reached, hot combustion gases are used for thermal conditioning of the heat transfer devices. Thus, hot gases are passed through the hot-side of the system's heat exchangers and reformer. Hot gas flow through components is constrained by temperature gradient limits.

4.2 At the same time, the SOFC stack is conditioned for high temperature operation.

5.1 The streams of hot gases coming out of the BOPS are mixed together. If the output temperature is high enough, the WRAS starts: the expander is coupled to the air compressor.

5.2 The SOFC stack starts using reformate fuel and air from the high pressure tanks: SOFC electrical energy generation commences.

5.3 The SOFC and the PES are coupled in order to start the generation of alternating current.

6. The turbo-machinery stops taking energy from the battery bank, which begins to be recharged.

7.1 With the FPS components and steam at operational temperatures, the steam generator stops and the fuel processing begins working with steam from the products of the anode.

7.2 The FPS and the SOFC stack are coupled through the high pressure reformate tank. A minimum level of mass in the tank is required at all times.

8. The FPS and air compressor are never shut-down until proper levels in the air and reformate tanks are reached.

Start-up Results

For start-up, the BOPS was first analyzed at the component level. Before the production of hydrogen starts at the reformer, it is necessary to generate steam at temperatures above 800 ^{o}K. To reach these conditions as soon as possible while assuring material integrity, the temperature and mass flow of the hot gases are controlled. The higher the gas inlet conditions are, the faster the steam reaches operational conditions.

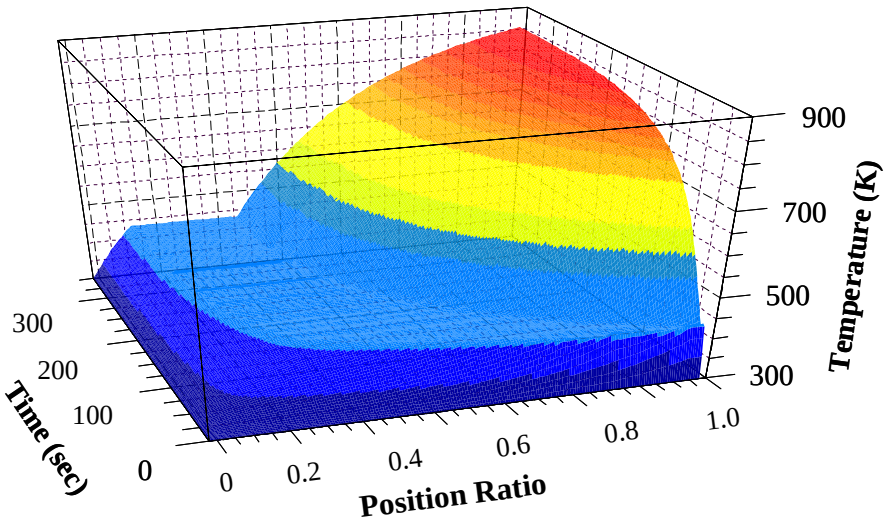

Figure 6.24: Steam generator start-up temporal and spatial thermal responses on the water side.

To reach these conditions as soon as possible, both cold water and hot gases are passed through the steam generator; and until operational conditions are reached, the water coming out of the steam generator is recirculated to the water tank. Two advantages result from this approach. No water is wasted, and the water inlet temperature increases with time, which increases the rate at which the metal heats up. Figure 6.24 shows the spatial and temporal thermal responses of steam generator start-up on the water side. The figure shows that water exit temperatures higher than 800 ^{o}K are reached in about 150 sec while steady state is reached in 300 sec.

During transient operation, especially at start-up and shut-down, material resistance to thermal stresses were taken into account in order to assure the integrity of all components. This was controlled by introducing temperature gradient and heat flux constraints into the synthesis/design and operational/control problem. For the present study, it was found that the heat flux occurring throughout the steam generator during start-up is never more than 150 kW/m^2, which is significantly less than the maximum allowable value (burnout flux) of 340 kW/m^2.

Figure 6.25 shows the spatial and temporal performance of the steam-methane reactor during start-up. Notice that the plot starts at about 100 seconds, which is the time that it takes for the steam generator to produced steam at operational temperatures and at which point the recirculation is stopped. During recirculation, all thermal components are pre-heated. This means that hot gases are passed through these components without any cold-side flow. The final conditions (metal

temperature) after the pre-heating period depend on the mass flow and temperature of the hot gases and on the mass of the component. Again, temperature gradients must be taken into account. To generate the results shown in Figure 6.25 a mass flow of hot gases of 0.000503 kmol/sec was used during pre-heating. It took the reformer about 210 seconds to reach steady state at a maximum methane conversion rate of 90%. Without pre-heating, steady state is reached in 625 seconds. The duration of the transient depends on the degree of pre-heating and the mass flow conditions on both sides of the reactor. Notice that the initial conversion rate at the reformer exit may not be zero if the pre-heating is high enough.

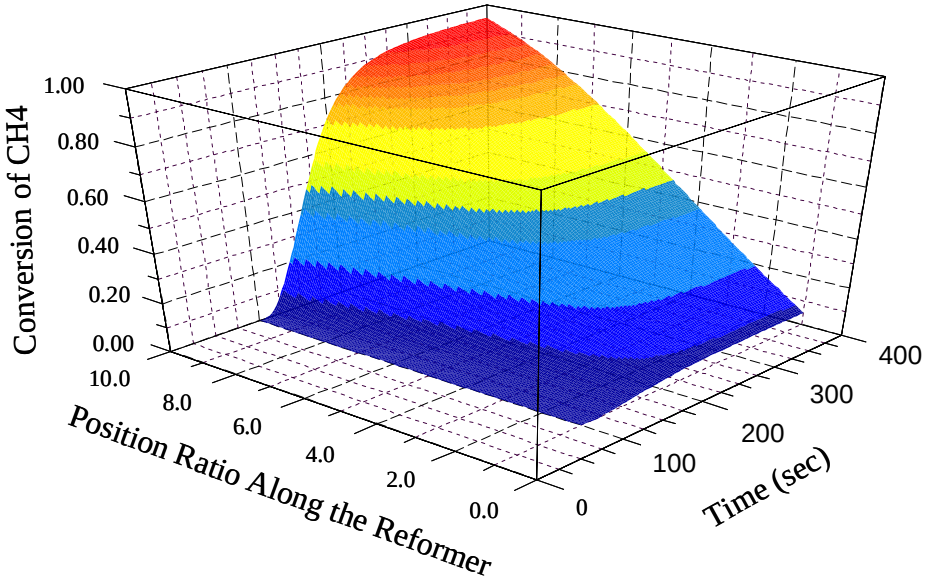

Figure 6.25: Steam-methane reformer start-up dynamic response for low pre-heating.

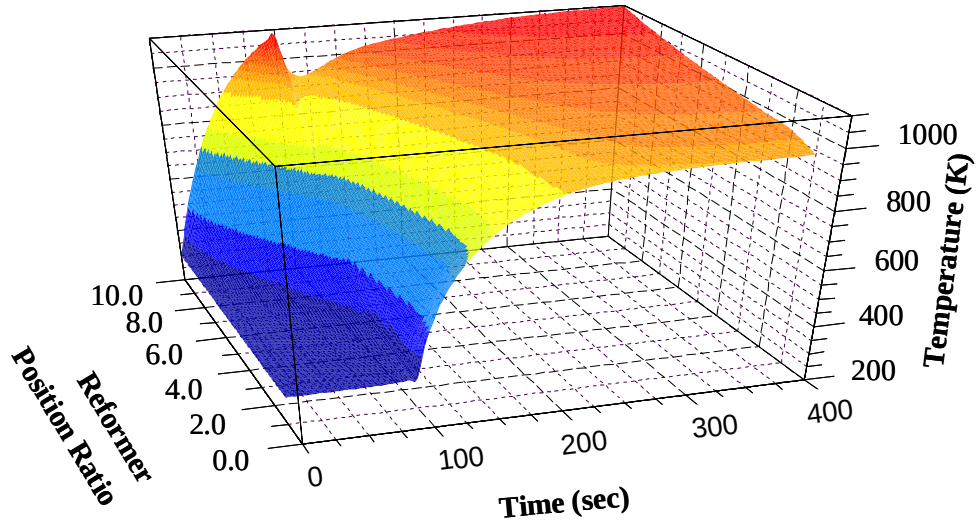

Figure 6.26: Steam methane reformer wall temperature start-up response for high pre-heating.

Figure 6.26 shows the reformer wall temperature response during start-up. The first 105 sec corresponds to the preheating period. Initially, the temperature of the metal starts increasing at a higher rate on the hot-gas inlet side. At the end of the pre-heating period, the temperature of the metal close to the hot-gas inlet side (position ratio 10.0 at 105 sec) is slightly higher than the steady state temperature; and the temperature of the metal close to the reformate-gas inlet side (position ratio 0.0 at 200 sec) is lower than the steady state temperature. This behavior produces higher thermal stress in the axial direction than those present during steady state operation. Thus, for start-up, both control variables and physical limits or constraints are taken into account during the synthesis/design process.

A comparison between the thermal responses of heat exchanger III for the cases with and without pre-heating is shown in Figure 6.27. Again, the pre-heating time is 100 sec. When pre-heating finishes and cold-side flow starts, conditions are such that the cold stream exit temperature is at operational conditions. If no pre-heating is used, 98 additional seconds are required to reach operational conditions.

Finally, the heat exchanger model uses a two-dimensional grid of 400 discrete elements, which allows a detailed and fairly accurate prediction of the temperature distribution in each compact heat exchanger. Figure 6.28 shows this two-dimensional temperature distribution on the cold side for heat exchanger III. The y and x axes are scaled on the basis of the number of discrete segments in each direction.

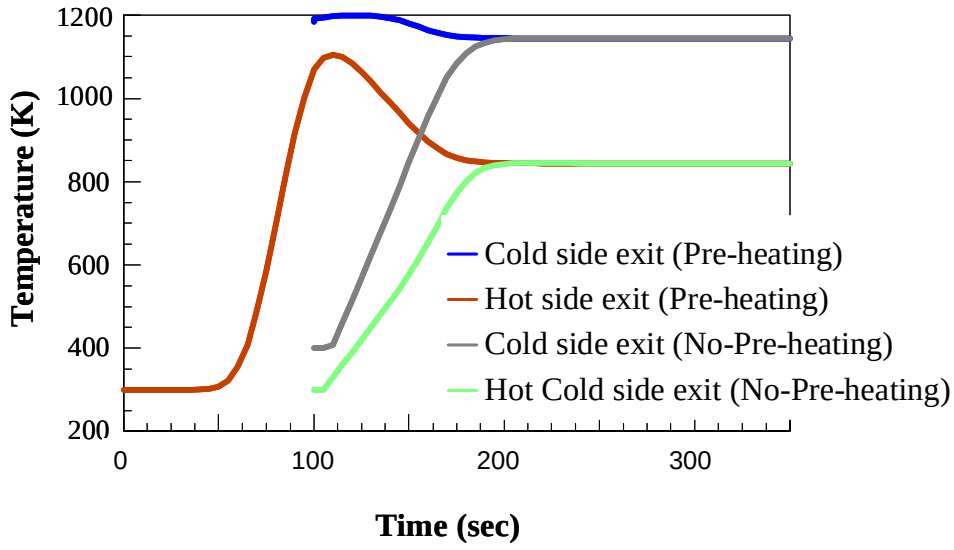

Figure 6.27: Compact heat exchanger III start-up thermal time response comparison between pre-heating and no pre-heating.

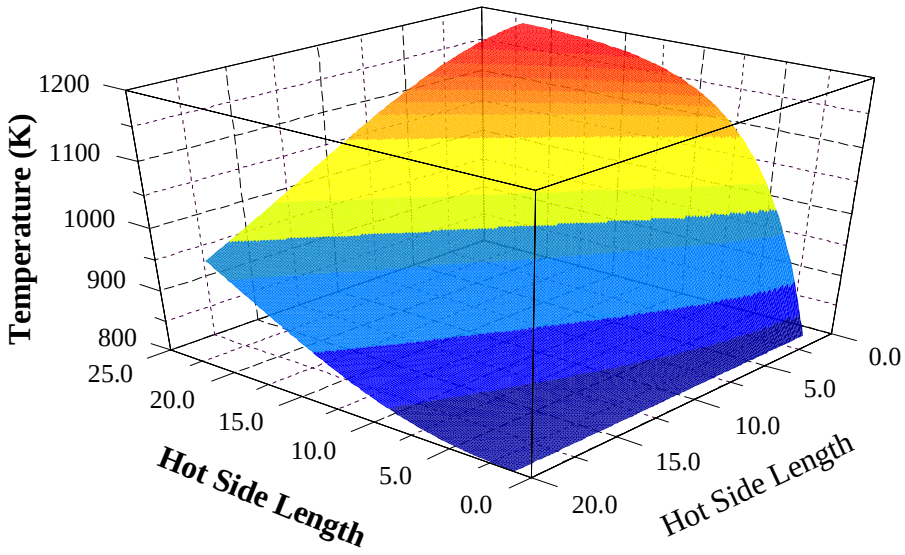

Figure 6.28. Compact heat exchanger III 2D spatial temperature distribution at steady state for the cold-side stream.

6.1.5 Optimal Costs

The optimal costs for the proposed SOFC based APU configuration are presented in this section. The details of the cost models used and the economic assumptions associated with them are described in Chapter 4. However, it should be emphasized that the costs given below are based on a production volume of 200,000 units per year and a maximum net power output of 6.6 kW. Obviously, a significant change in the number of units produced per year could significantly modify these costs.

The optimum values for the purchase costs of the FPS components are presented in Table 6.7. A graphical representation of the sub-system purchase cost breakdown is given in Figure 6.29. It is obvious that the FPS cost is well distributed among the three major components (i.e. reactor, steam generator, and heat exchangers). The purchase cost of the SMR and the catalyst bed for one year is approximately equal to 103.3 $/kWe. Notice that the steam generator accounts for a little more than a third of the FPS purchase cost. Therefore, it is appropriate to investigate the integration of auto-thermal reforming (ATR) which does not need steam for start-up. However, ATR is significantly less efficient than SMR. New SOFC technology introduces the concept of a single reformer capable of starting-up as an ATR and then switching to SMR (Delphi Corporation, 2004).

Table 6.7. Optimum purchase costs of the FPS components (based on a production volume of 200,000 units per year).

Cost Description		Value ($)
$C_{bare\ reactors}$	Bare reactors purchase cost	579.57
$C_{catalyst}$	Catalyst beds purchase cost (first year)	91.83
C_{SG}	Steam generator purchase cost	770.82
C_{HX}	Compact heat exchangers purchase cost	701
$C_{FPS}^{purchase}$	FPS purchase cost	**2,143.22**

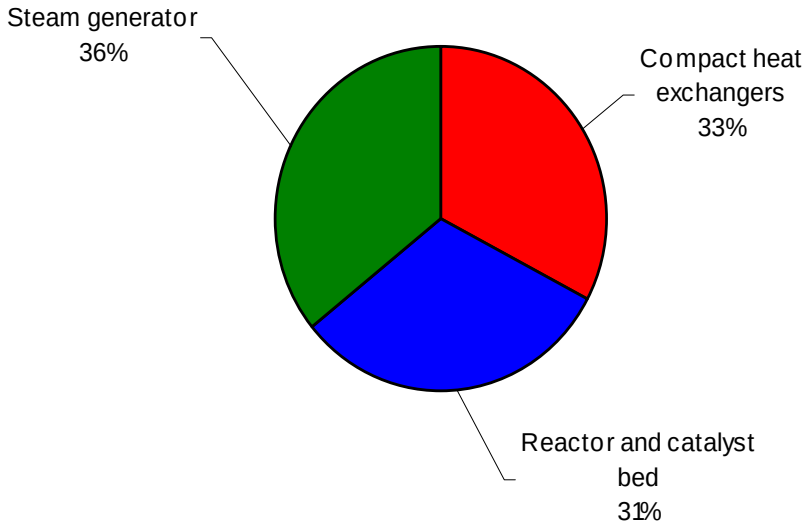

Figure 6.29. FPS purchase cost breakdown (based on a production volume of 200,000 units per year).

The optimum purchase cost of the fuel cell stack and its breakdown in addition to the auxiliary equipment (i.e. cooling system, sensors, and control valves, etc.) optimum purchase costs are presented in Table 6.8. The fact that the cost of the anode-cathode assembly represents 55% of the fuel cell stack purchase cost comes as no surprise taking into account its costly materials. Furthermore, the SS purchase cost breakdown displayed in Figure 6.30 clearly shows that anode-cathode assembly dominates the SS purchase cost, which adds up to 274.7 $/kWe.

Table 6.8. Optimum purchase costs of the SS components (based on a production volume of 200000 units per year).

Cost Description		Value ($)
C_{ass}	Stack purchase cost	1221.76
$C_{extra\ material}$	Endplates, collectors, insulators, and tie bolts	346.88
$C_{assembly}$	Stack assembly cost	55.7
C_{stack}	Fuel cell stack purchase cost	**1,624.35**
C_{aux}	Auxiliary equipment purchase cost	162.43
$C_{SS}^{purchase}$	SS purchase cost	**1,786.78**

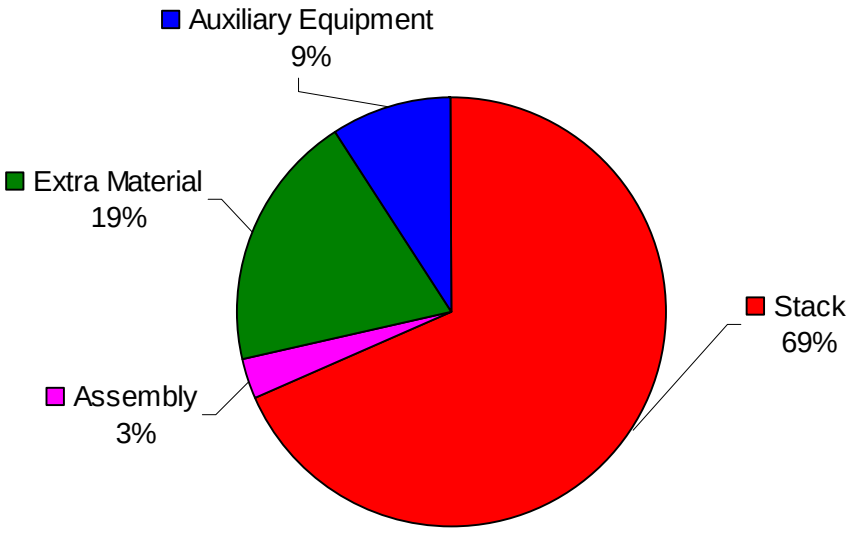

Figure 6.30. SS purchase cost breakdown (based on a production volume of 200,000 units per year).

The optimum purchase cost of the WRAS and its breakdown in addition to the auxiliary equipment (i.e. tank, sensors, and control valves, etc.) optimum purchase costs are presented in Table 6.9. The fact that the cost of the expander represents 46% of the WRAS purchase cost also comes as no surprise, taking into account that this component introduces new technology in order to maintain high pressures for all operational conditions, especially in a system with relatively small flow rates. Furthermore, the WRAS purchase cost breakdown displayed in Figure 6.31 clearly shows that the expander dominates the WRAS purchase cost. The sub-system purchase cost adds up to 118.92 $/kWe.

Table 6.9: Optimum purchase costs of the WRAS components (based on a production volume of 200,000 units per year).

Cost Description		Value ($)
C_{Comp}	Compressor purchase cost	232.10
C_{Mot}	Electrical motor purchase cost	116.05
C_{Exp}	Expander purchase cost	355.33
C_{Aux}	Auxiliary equipment purchase cost	70.34
$C_{WRAS}^{purchase}$	WRAS purchase cost	**773.84**

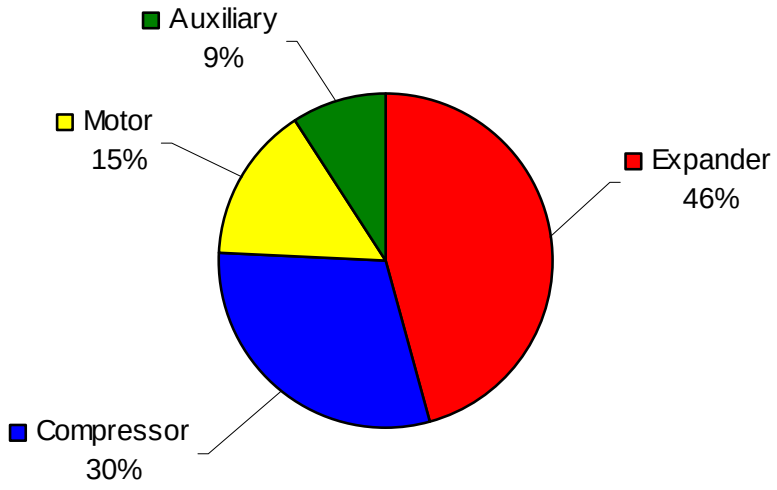

Figure 6.31. WRAS purchase cost breakdown (based on a production volume of 200,000 units per year).

Table 6.10 lists the optimum capital costs of the three sub-systems considered in this doctoral work, namely the FPS, the SS, and the WRAS. The capital cost of each of these sub-systems is comprised of the corresponding purchase cost together with its amortization cost and the maintenance cost of the sub-system. Apart from the optimum capital costs of the three aforementioned sub-systems, the value for the SOFCS optimum total cost given in Table 6.10 includes the operating cost of the SOFCS over the entire load profile, which in fact the includes the transient segments.

Table 6.10. Optimum costs for the proposed SOFCS and for its sub-systems (based on a production volume of 200,000 units per year).

Cost Description		Value ($)
$C_{FPS}^{purchase}$	FPS purchase cost [56]	2,969.69
C_{FPS}^{amort}	FPS amortization cost	2,969.69
C_{FPS}^{maint}	FPS maintenance cost	296.96
C_{FPS}	FPS capital cost	**6239.34**
$C_{SS}^{purchase}$	SS purchase cost	1786.78
C_{SS}^{amort}	SS amortization cost	1786.78
C_{SS}^{maint}	SS maintenance cost	178.67
C_{SS}	SS capital cost	**3752.24**
$C_{WRAS}^{Purchase}$	WRAS purchase cost	773.84
C_{WRAS}^{Amor}	WRAS amortization cost	773.84
C_{WRAS}^{Main}	WRAS maintenance cost	77.38
C_{WRAS}	WRAS capital cost	**1,625.06**
C_{fuel}	SOFCS operating cost	13,227.02
C_{TES}	SOFCS total cost	**24,843.70**

Figure 6.32 indicates that the cost associated with the consumption of natural gas (methane) throughout the lifetime of the SOFCS is the major contributor to the total cost of the SOFCS and that the FPS is the second most costly sub-system. This, in fact, is due to the additional cost imposed by the steam generator. Therefore, it may be important to investigate FPS configurations based on auto-thermal reforming.

[56] Includes the 10-year cost of the catalyst bed.

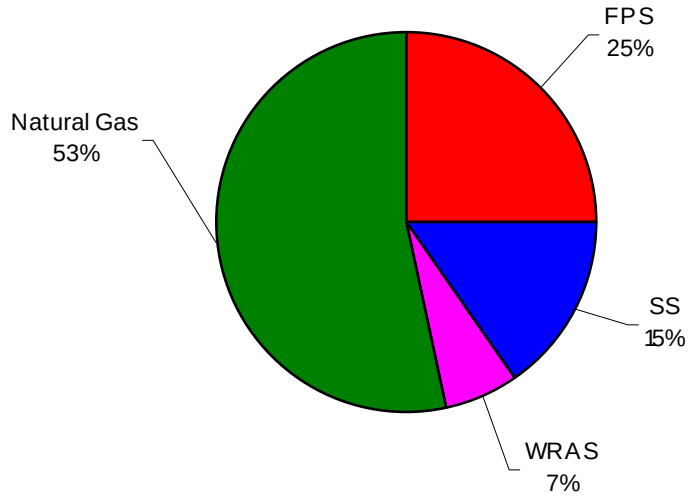

Figure 6.32 SOFC system total cost breakdown (based on a production volume of 200,000 units per year).

6.1.6 Dynamic Shadow Price Rates

Figure 6.33 shows the hydrogen dynamic shadow price rate through the operational profile. It can be seen that the hydrogen consumption rate effect on the BOPS cost rate is a function of the operational point of the system, i.e. the higher the hydrogen consumption is the higher the effect on cost rate due to variations in the hydrogen rate. However, during step changes in load at 3,600 sec (1 hr) and 86,400 sec (24 hr) the hydrogen dynamic shadow price rate changes dramatically and rapidly. Under those conditions the dynamic shadow price rate is a measure not only of the effect of a change in the operational point but also of the effects of the systems dynamics and the controls. At 3,600 sec (1 hr) the hydrogen dynamic shadow price rate increases rapidly because the hydrogen rate into the stack changes first and faster than the fuel going into the BOPS from the methane tank. As the controllers reach zero error and the system reaches stable conditions, the dynamic shadow price rate stabilizes at about 500 sec (8.33 min) and at 86,400 sec (24 hr) a similar phenomenon occurs, the hydrogen dynamic shadow price rate reduces dramatically because the change in hydrogen into the stack changes faster than the rate of methane into the BOPS.

Figure 6.34 shows the hydrogen molar flow rate dynamic shadow price rate profile for all 6 DILGO iterations. This figure in fact is an indication of the linearity of the dynamic shadow price rates for a given instant of time in that their behavior

tend to be constant for a given instant of time. This means that a representation of cost rate, hydrogen molar flow rate, and time will show a linear behavior with respect to time. In fact, this behavior was observed for all dynamic shadow prices rates, which confirms the hypothesis of near hyper plane behavior for the system-level ORS which aids in solving the three system-level, unit-based optimization problems and in quickly converging the system-level optimization problem.

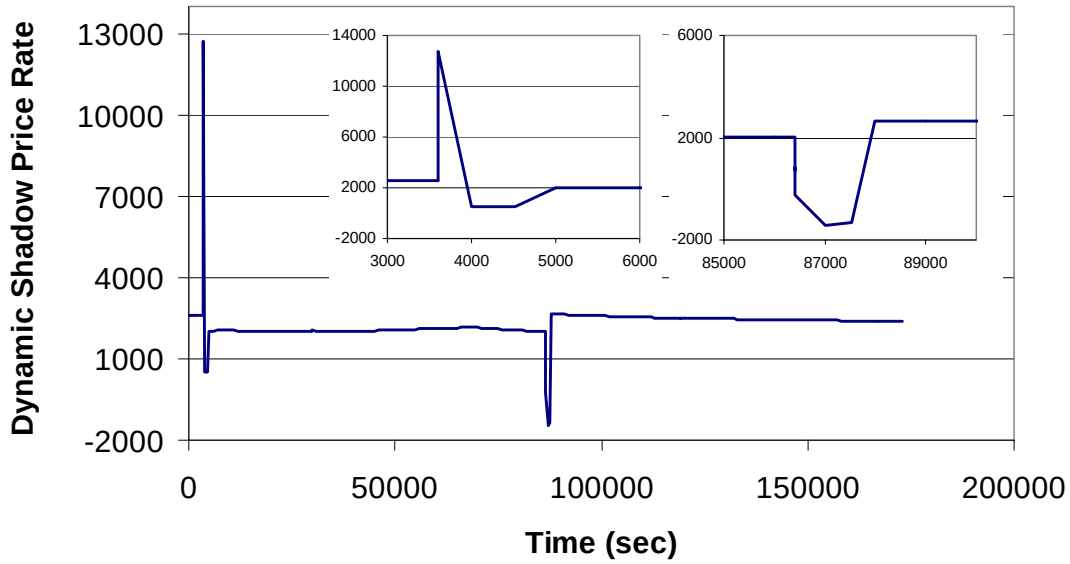

Figure 6.33. Hydrogen molar flow dynamic shadow price rate profile for the last iteration of the DILGO approach.

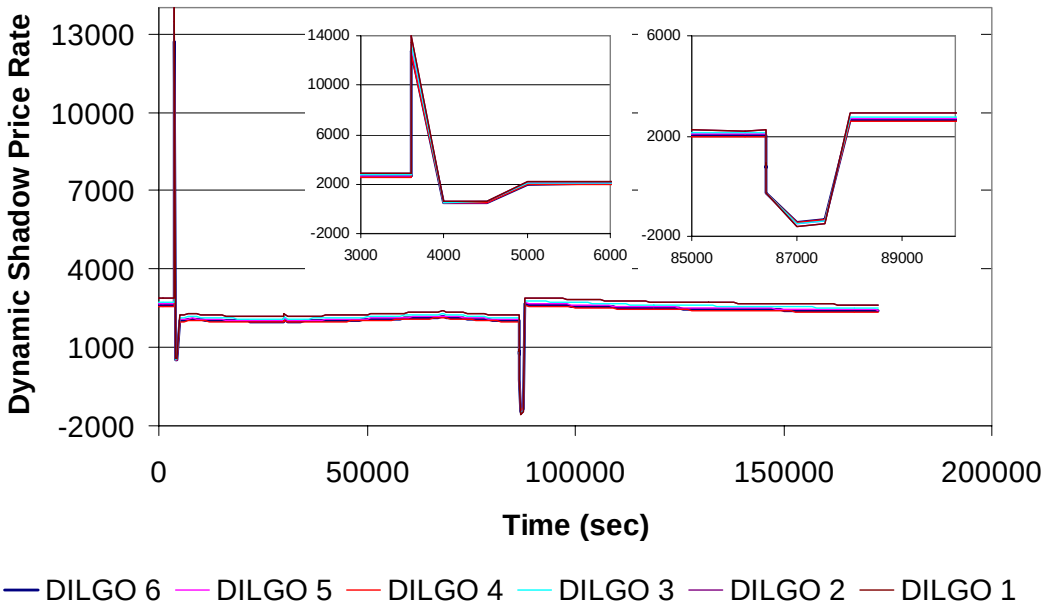

Figure 6.34. FPS hydrogen molar flow rate dynamic shadow price rate profile for all DILGO iterations.

Figure 6.35 shows the unit-level optimum response surfaces for the FPS at four given instances of time. It shows that the optimum values of the FPS (at a given instant of time) versus the hydrogen molar rate and the FPS pressure (i.e. two coupling functions). Four different operational points (i.e., 21,600 sec (6 hr), 68,400 sec (19 hr), 87,000 sec (24.2 hr), and 115,000 sec (31.9 hr)) on the load profile were chosen to show the ORSs near linearities with respect to time, one of them (Figure 6.35c) located close after the step-up change in load where the transients are more significant. It is obvious that the minimum total cost for the FPS at all time corresponds to the minimum possible hydrogen molar flow rate requirement and system pressure. However, Figure 6.35a shows that the variations in system pressure are more significant during low loads. Figure 6.35c and 6.35d show that variations in hydrogen molar flow rate requirements have a bigger impact on the sub-system cost as the load becomes larger.

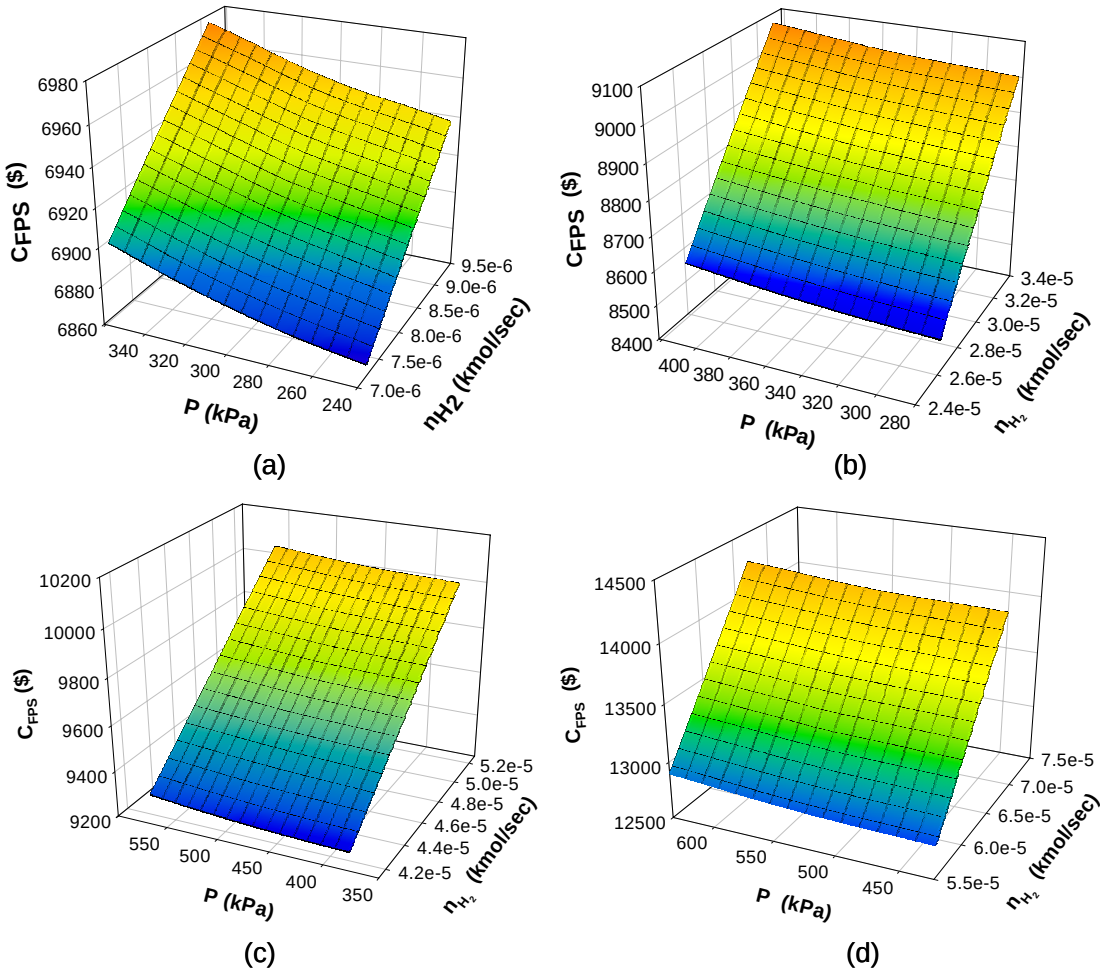

Figure 6.35. The FPS unit-level ORSs in the $\dot{n}_{H_2}$ and P_{FPS} dimensions for four different instants of time.

Figure 6.36 shows the FPS pressure (reformate tank pressure) dynamic shadow price rate through the operational profile. Again, it can be seen that the pressure effect on the BOPS cost rate is a function of the operational point of the system, i.e. the higher the pressure the higher the effect on cost rate due to variations in FPS pressure. As with the hydrogen dynamic shadow price rate during the step change in load profile, the pressure shadow price rate changes rapidly. For instance at 86,400 sec (24 hr), initially the effect of a change in the system pressure increases the dynamic shadow price rate due to the change in reference pressure. However, at some point, this behavior is inverted, and the pressure dynamic shadow price rate effect reduces until the controller reaches zero error and stable conditions are reached. The dynamic pressure shadow price rate stabilizes after about 2,500 sec (41.7 min). Figures 6.33 and 6.36 should be analyzed considering the load profile, the FPS pressure dynamic response, and the FPS methane consumption through the entire load profile.

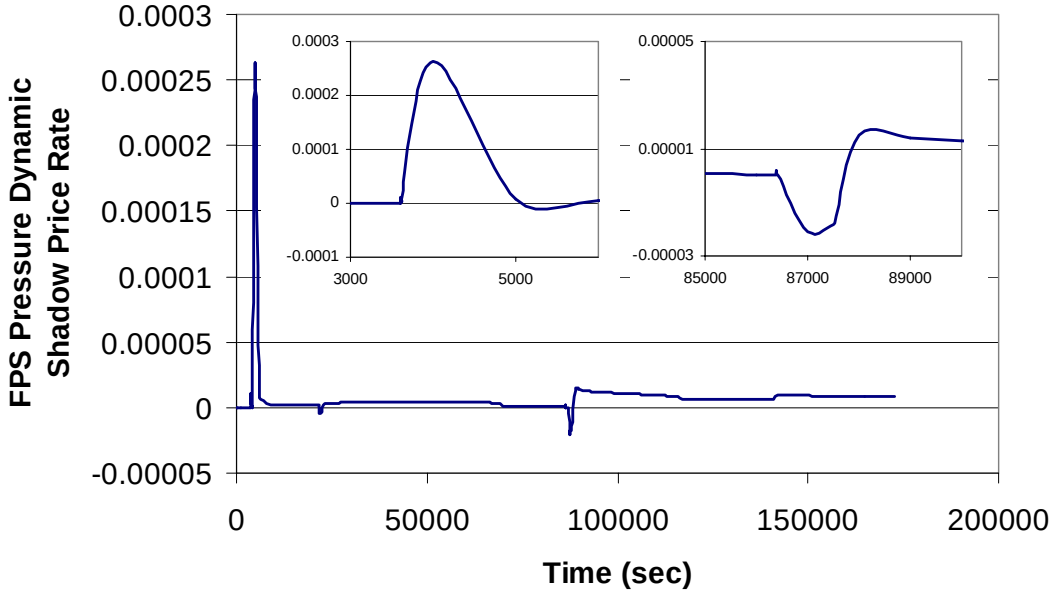

Figure 6.36. FPS pressure dynamic shadow price rate profile for the last DILGO iteration.

6.1.7 System Efficiency

Figure 6.37 shows the FPS and SOFC system optimum efficiencies through the entire load profile. The BOPS efficiencies are not shown because they coincide with the FPS efficiency except for and small interval of time at the start of the profile

(see Figure 6.16) and even in this interval the deviations are very small. In this doctoral work four efficiencies are defined as follow:

$$\eta_{FPS} = \frac{\dot{m}_{H_2} LHV_{H_2}}{(\dot{m}_{CH_4} LHV_{CH_4})_{\text{to reformer}} + (\dot{m}_{CH_4} LHV_{CH_4})_{\text{to combustor}}} \tag{6.1}$$

$$\eta_{BOPS} = \frac{\dot{m}_{H_2} LHV_{H_2}}{(\dot{m}_{CH_4} LHV_{CH_4})_{\text{to reformer}} + (\dot{m}_{CH_4} LHV_{CH_4})_{\text{to combustor}} + \dot{E}_{WRAS}} \tag{6.2}$$

$$\eta_{SS} = \frac{\dot{E}_{SS}}{\dot{m}_{H_2} LHV_{H_2}} \tag{6.3}$$

$$\eta_{SOFCS} = \frac{\dot{E}_{net}}{(\dot{m}_{CH_4} LHV_{CH_4})_{\text{to reformer}} + (\dot{m}_{CH_4} LHV_{CH_4})_{\text{to combustor}}} \tag{6.4}$$

where η_{FPS}, η_{BOPS}, η_{SS}, and η_{SOFCS} are the FPS, BOPS, SS, and the SOFC system efficiencies respectively. LHV_{H_2} and LHV_{CH_4} are the hydrogen and methane low heating value, $\dot{m}_{H_2}$ and $\dot{m}_{CH_4}$ are the hydrogen and methane mass flow rates. $\dot{E}_{WRAS}$ is the parasitic power from the WRAS and $\dot{E}_{net}$ is the system net power. The efficiency definition in equation (6.1) to (6.4) are steady state efficiencies which represent the system performance at a given instant. Using these definition helps to determine the dynamic effects on system performance.

There are several interesting features and behaviors that should be noted from Figure 6.37. First, FPS efficiencies higher than one are due to the fact that no additional energy is required to generate steam. Therefore, the required extra heat is used only for the methane reforming. Moreover, the extensive heat and work recovery achieved by the optimum system configuration enhances the FPS efficiency. Note that the WRAS is able to provide the required power for air compression for most of the load profile, and even during the low load segment, additional parasitic power is small. The synergy effect of recirculating the anode exhaust is increased by the fact that the steam is at high temperature, eliminating the need for methane pre-heating.

As expected the FPS efficiency is higher at low load regimes. This is due to reasons previously mentioned (i.e. the residence time in the reformer increases,

improving the conversion). In the same manner, the SS efficiency at low loads increases. The same behavior is true for the system total efficiency. The high value and relatively flat behavior of system efficiency with respect to the load requirement is one of the characteristics that make fuel cell systems appealing over conventional technologies. A total system efficiency ranging from 0.3 at low load (86,400 sec or 24 hr) to 0.94 at high load (3,600 sec or 1 hr) shows a remarkable system performance. As shown in figure 6.38 during the two drastic step changes in load at 3,600 sec and 86,000 sec dramatic changes in system efficiency are generated due to the system dynamic effects such as transport delays, the slow transients of the reformer, and control effects. This shows the importance of considering the dynamic effects when optimizing the system configuration, component designs, and controls in order to minimize the negative effects and take advantages of the positive ones.

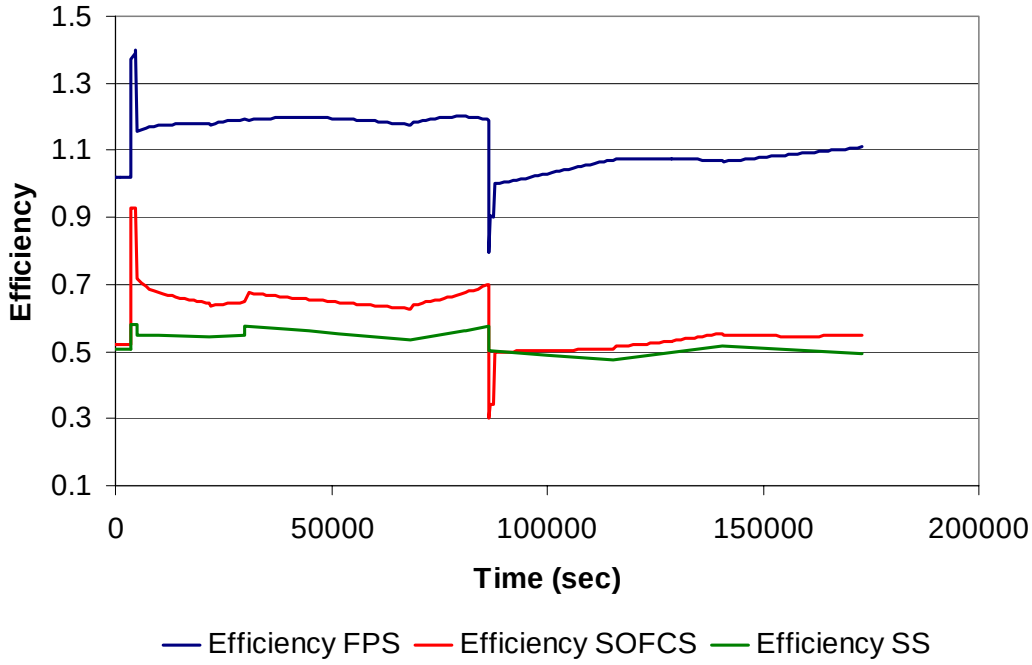

Figure 6.37. FPS, SS, and SOFC system optimum dynamic efficiency profile.

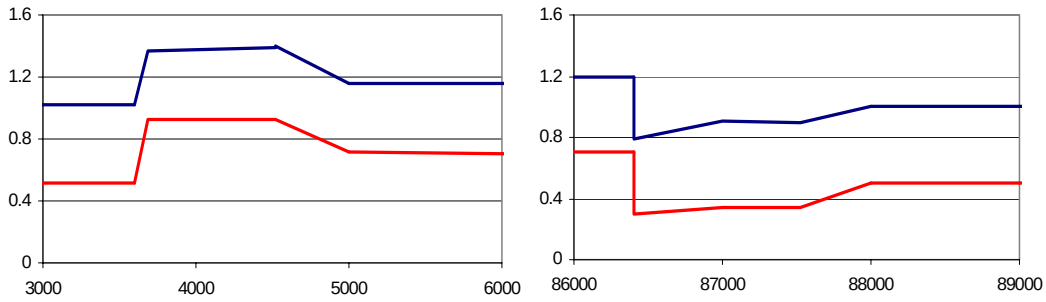

Figure 6.38. FPS and SOFC system optimum dynamic efficiency profiles at each of the two drastic load changes (at 1 hr and at 24 hr).

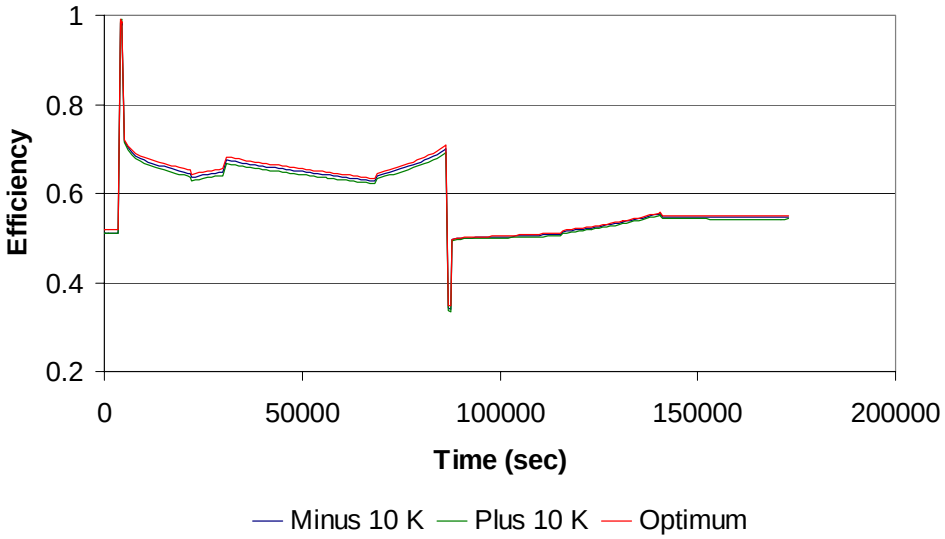

Figure 6.39. Reformer reference temperature effect on system efficiency.

Figure 6.39 shows the effect of one of the dynamic operational decision variables on SOFC system efficiency. An incremental increase in the reformer reference temperature (optimum reformate exit temperature) with respect to the optimum reduces the system efficiency due to the extra fuel required to maintain a hotter temperature. A reduction in this temperature with respect to the optimum reduces the system efficiency due to the reduction in the reforming efficiency (i.e. the higher the temperature the better the demethanation reaction) and the reduction in the hot gases inlet temperature into the expander. This shows, once again, the delicate balance to be achieved in order to find the optimum synthesis/design and dynamic operational decision variable values.

6.1.8 Design Variable Effects on System Dynamics and Operational Costs

Figure 6.40 shows the effect of the steam-methane reformer size on the temperature difference between the anode and cathode inlet streams, which in turn is the most important operational constraint applied in this doctoral work. Table 6.11 show the effect of the steam-methane reformer size on the fuel and component capital costs. The figure shows how a reformer 10% larger than the optimum generates a temperature difference larger than that allowed (i.e. 5 ^{o}K). Additionally, the reduction in fuel consumption due to a larger reformer does not compensate the increase in capital cost. Hence, this option is not feasible from an operational and an economical

standpoint. A reformer 10% smaller still meets the temperature difference constraint. However, the reduction in capital cost does not compensate the increment in fuel consumption, yielding a more expensive system than the optimum. Therefore, this option is not economically optimal.

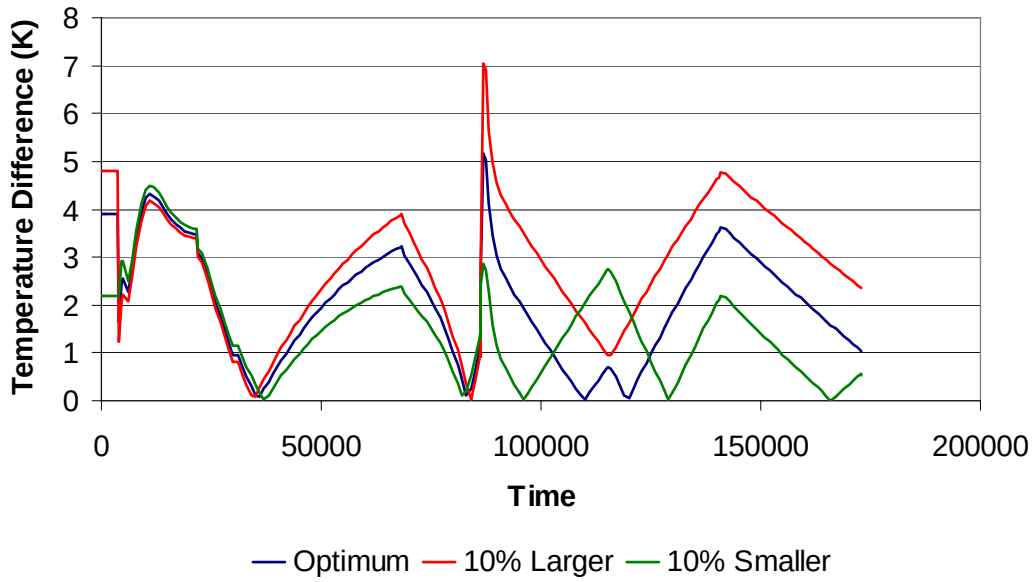

Figure 6.40 Effects of variations in steam-methane reformer size on system dynamics.

Table 6.11 Effects of variation in steam-methane reformer size on life cycle costs.

	Optimum	10% Larger	10% Smaller
Fuel Cost	US$ 13,227	US$ 13,090	US$ 13,511
Reformer Capital Cost	US$ 2,252	US$ 2,526	US$ 2,080
Total	US$ 15,529	US$ 15,616	US$ 15,591

Figures 6.41a and 6.41b show the effect of variation in the steam-methane reformer size on the cost rate. As previously concluded, the larger the reformer the lower the cost rate. However, Figure 6.41 shows clearly that the variation in cost rate depends on the operational condition, i.e. load requirement. At low loads, the reformer size effect is small compared to its effect at high loads. Additionally, Figure 6.42 shows a zoom-in of figure 6.41a exactly at the moment of the step load increment at 86,400 sec (24 hr). As can be seen, the same trend as before applies. The cost rate during the transient is lower as the reformer size goes up. Hence, one can conclude that the operational/control cost goes down as the reformer size goes up. Obviously, the optimum balance between reformer size and cost rate is a trade-off

problem, which has been successfully solved in this doctoral work by implementing dynamic shadow price rates.

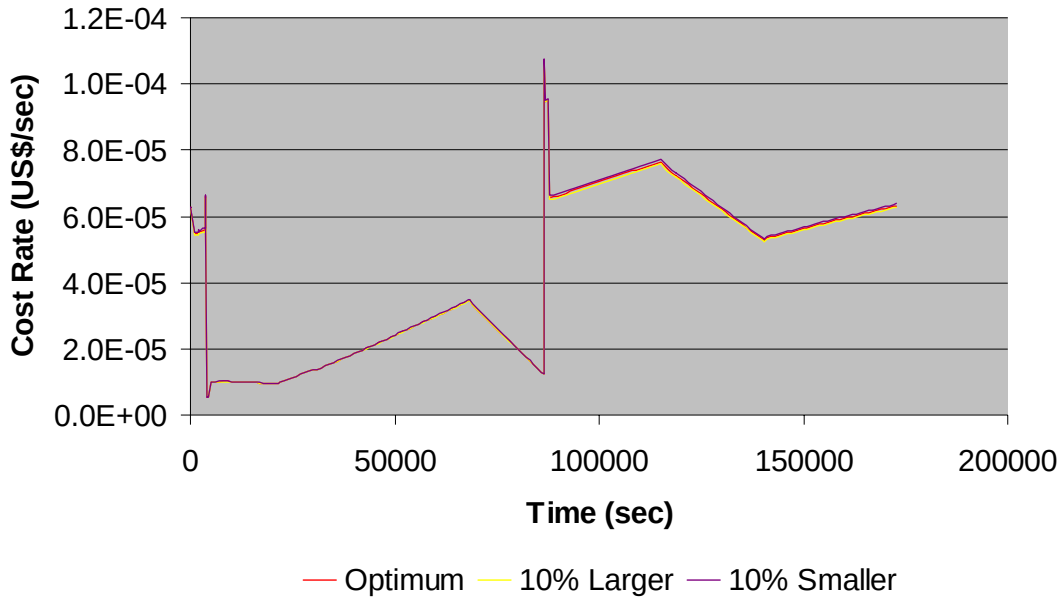

Figure 6.41a. Effect of variation in steam-methane reformer size on cost rate.

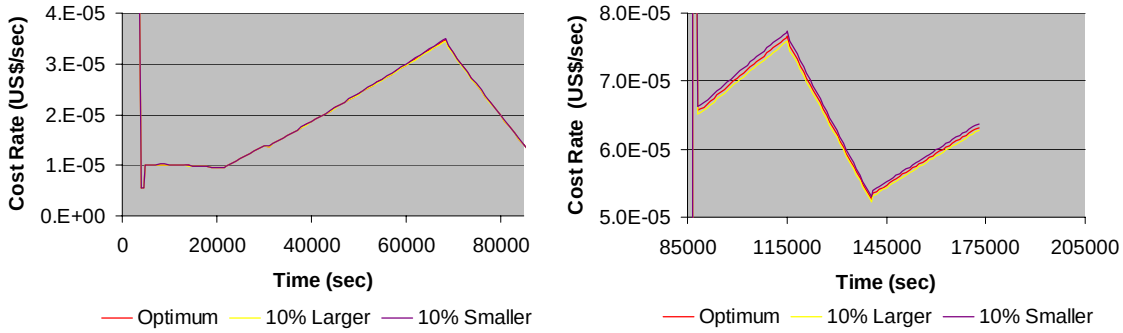

Figure 6.41b. Effect of variation in steam-methane reformer size on cost rate at 1 hr and 24 hr.

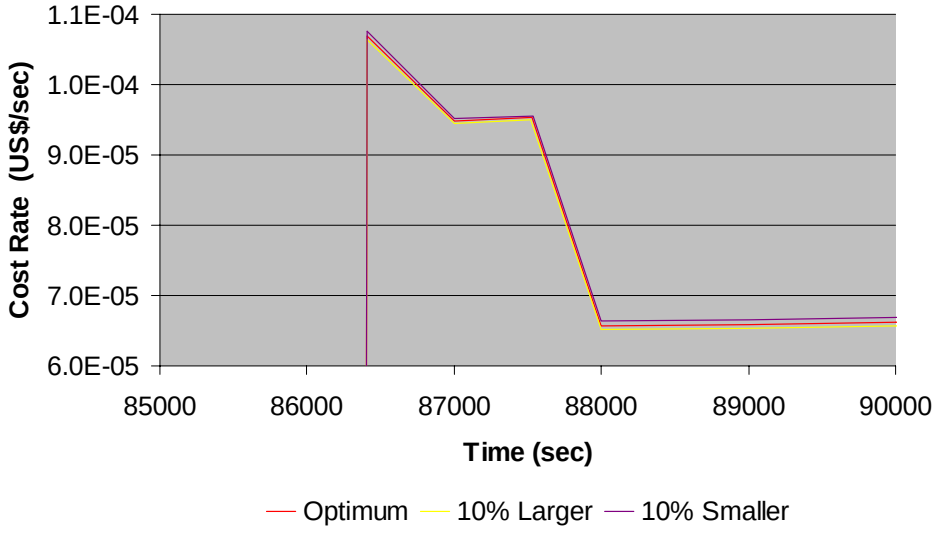

Figure 6.42. Zoom-in at 24 hr of the effects of variation in steam-methane reformer size on cost rate.

Figure 6.43 shows the effects of variations in the heat exchanger II size on the temperature difference between the anode and cathode inlet streams. Table 6.12 shows this effect on the fuel and component capital costs. This figure shows how a reformer 10% larger than the optimum generates a temperature difference larger than that allowed (i.e. 5 ^{o}K) during the step-up change in load at 86,400 sec (24 hr). A heat exchanger 10% smaller violates the temperature difference constraint at low loads (about 21,600 sec (6 hr)). Therefore, both modifications are operationally unacceptable. Table 6.12 shows that a smaller heat exchanger is economically feasible if higher temperature difference are allowed. This effect shows how progress in one technology (i.e. stack materials) can produce FPS cost reductions.

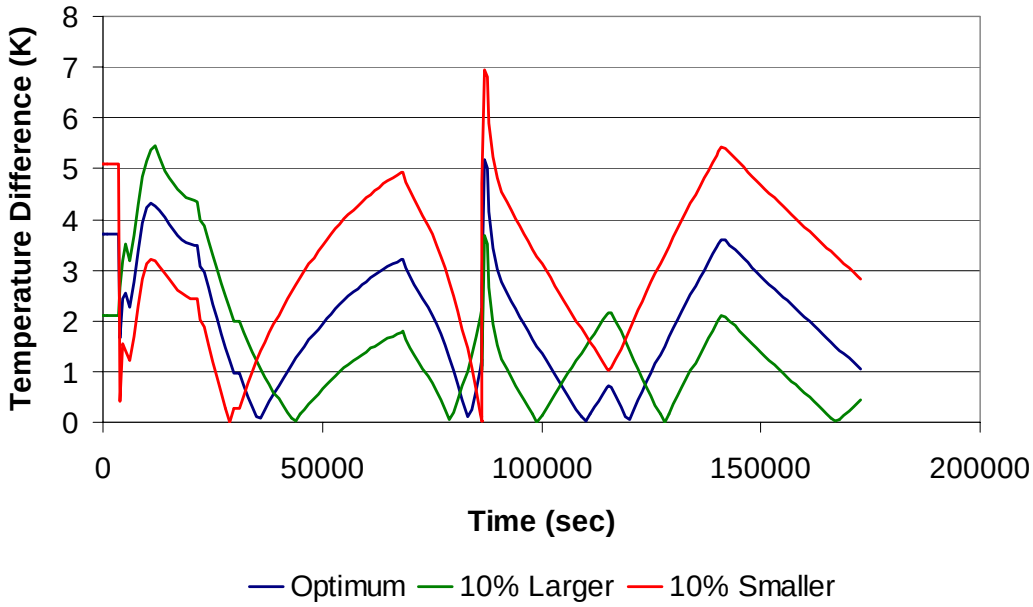

Figure 6.43. Effects of variation in heat exchanger II size on system dynamics.

Table 6.12. Effects of variation in heat exchanger II size on life cycle costs.

	Optimum	10% Larger	10% Smaller
Fuel Cost	US$ 13,227	US$ 13,291	US$ 13,260
Reformer Capital Cost	US$ 308.7	US$ 378	US$ 252
Total	US$ 13,535.7	US$ 13,669	US$ 13,512

6.1.9 Total System Response to Load Changes

Figure 6.44 shows the system's relatively fast response for a change in load requirements from 1 kWe to 4 kWe. Thanks to the air and reformate tanks (buffers),

the system response is fairly fast (i.e. a fraction of a second). This response would not be possible without buffering because of the transport delays and the time response of the reformer. Figures 6.44 also shows an overshoot, which translates into an energy surplus stored in the battery bank. Figure 6.45 shows the system's relatively fast response for a change in load requirements from 5 kWe to 1 kWe. Again, the time response is rather fast. Figure 6.45 shows undershoot, the energy for which is supplied by the battery bank.

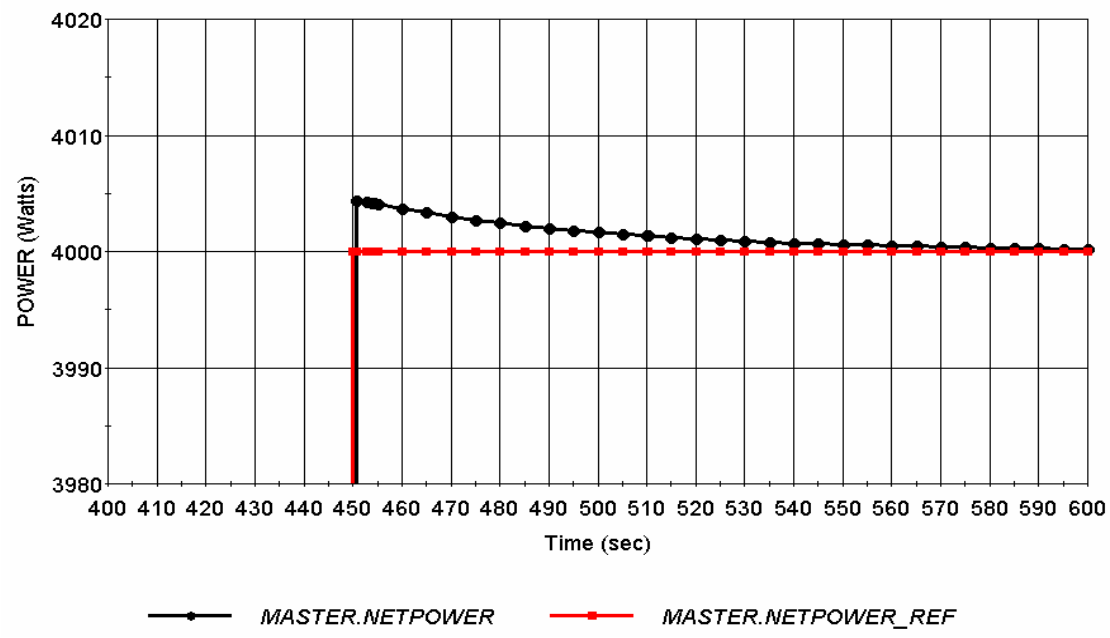

Figure 6.44. Low load (1 kWe) to high load (4 kWe) system transient response.

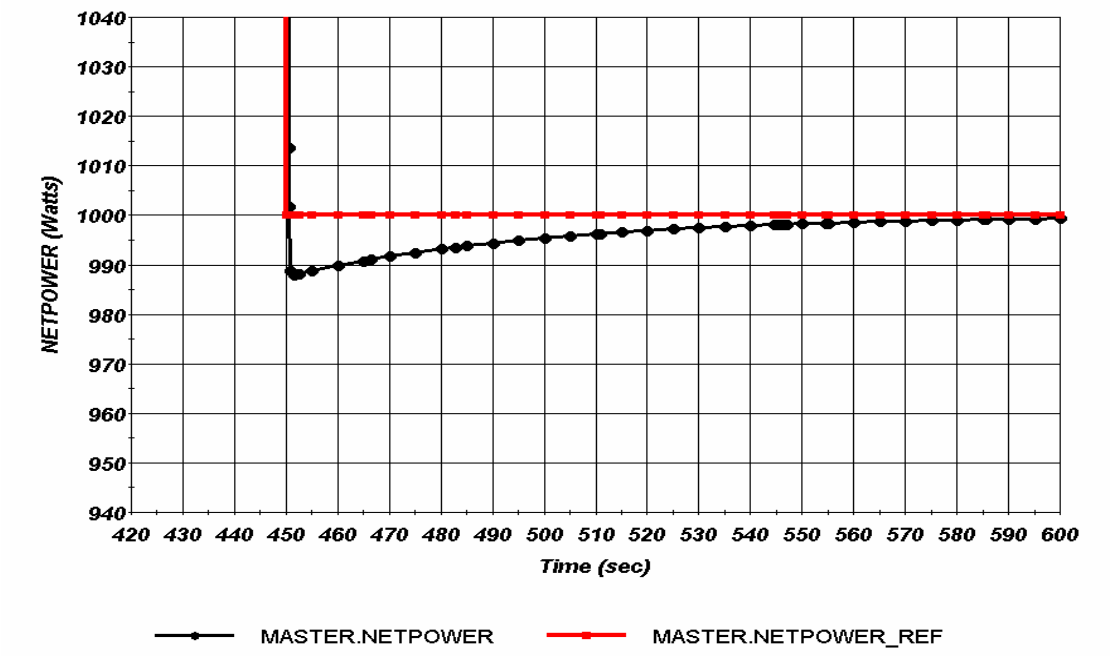

Figure 6.45. High load (5 kWe) to low load (1 kWe) system transient response.

Chapter 7

Conclusion

A number of conclusions on the effectiveness of the physical decomposition approach for dynamic optimization developed and implemented in this doctoral work for the synthesis/design and operation/control optimization of a SOFC based APU as well as the main conclusions derived from the results of this research are summarized as follow:

1. DILGO has shown its ability to handle large-scale DMINLP problems for energy system and energy sub-systems under transient operation and subject to abrupt and large disturbances. This opens the possibility of successfully applying DILGO and physical decomposition to a broad number of applications, involving diverse disciplines and objective functions. DILGO effectively handles the information transfer problem between sub-systems when subject to external forces (e.g., change in load) and internal regulation (e.g. system control system) in such a way as to be able to ensure that the decomposed unit optimizations result in an overall system-level optimum. Furthermore, the number of sub-systems which DILGO can handle shows no limits other than those due to practical considerations.

2. DILGO constitutes a powerful way of not only obtaining a global optimum solution for dynamic problems but of gaining a vast amount of insight into the relative effect that each unit and its respective decision variables have in terms of the overall objective function (i.e. total life cycle cost).

3. This original DILGO decomposition strategy is the first to successfully closely approach the theoretical condition of “thermoeconomic isolation” when applied to the transients and control of highly complex, highly dynamic, non-linear systems. In fact, as can be determined from the literature, there is not even a reported attempt to consider dynamic, control, and operational requirements all together at the early stages of the conceptual and preliminary synthesis/design stage. This was achieved in this doctoral work in such a way that it was possible to pose a synthesis/design and operation/control system optimization problem.

4. By dividing the total energy system into sub-systems, the technique of physical decomposition (DILGO in particular) has the advantage of breaking the overall optimization problem into a set of much smaller, unit sub-problems, which simplifies a highly complex, highly dynamic, non-linear problem of synthesis/design and operation/control optimization and allows one to take into account a larger number of decision variables (degrees of freedom) than would otherwise be possible. Therefore, this physical decomposition strategy makes it possible to simultaneously optimize not only at a system level, i.e. with respect to the system’s performance and configuration al synthesis, but also at a detailed component/sub-system level, i.e. with respect to the detailed geometry, capacities, and performance of the components themselves.

5. DILGO uses dynamic shadow price rates and coupling function changes to reduce the number of unit optimizations required. The effect of the different units’ independent (decision) variables and dynamics are assessed in terms of the unit’s (local) cost and their effect on the rest of the system. Thus, in DILGO, unit-based, system-level optimization sub-problems (as opposed to purely local objective functions) are defined. Each of these sub-problems while using strictly local (unit) independent (decision) variables approximates the system-level optimum cost. The dynamic shadow price rates are in fact the dynamic marginal cost rates based on the optimum cost rates of the units. The dynamic shadow price rates are an approximation of the dynamic optimum response surface (ORS).

6. Physical decomposition (in particular DILGO) allows different sub-systems to be modeled using the most appropriated software. As a matter of fact, different sub-systems are often times synthesized/designed by different groups and even different companies, which in turn are most probably in different geographical locations. Therefore, diverse modeling platforms are almost assuredly unavoidable.

7. Neither time or conceptual decomposition was used to solve the synthesis/design operation/control optimization problem. Their application was not necessary due to practical considerations such as the number of segments, the number of sub-systems, and the continuous load profile. However, the mathematical concepts behind DILGO completely support conceptual and time decomposition, i.e. the decomposition of the optimization problem into independent steady or dynamic operational segments or even into quasi-stationary time segments if the assumption proves adequate (i.e. only slow transients are presented).

8. The dynamic, mixed integer, non-linear programming (DMINLP) problem for the SOFC based APU was solved and the global convergence of the DILGO method was verified. From the calculation of the dynamic shadow price rates, a very important conclusion is drawn. The relatively constant behavior of the dynamic shadow price rates is a significant contributing factor to the rather fast convergence of the DILGO approach. This constant behavior of the dynamic shadow price rates allows one to infer that they are linear or at least monotonic (e.g., convex) with respect to the coupling functions but not necessarily with respect to time. Furthermore, this behavior shows that the appropriate selection of the coupling functions for the units has been made.

9. It should be pointed out that the linearity of the dynamic shadow price rates mentioned above was obtained by representing the coupling functions with quantities that were non-exergy or even non-energy-based. The quantities also opens up the opportunity to apply DILGO to the dynamic optimization of non-energy based sub-systems or systems (e.g., aircraft airframe, etc.).

10. The methods presented in this work constitute a powerful approach for performing the decomposed synthesis/design and operation/control optimization of highly coupled, highly complex energy systems. The fundamental purpose of DILGO is to complement and integrate current engineering practices and processes, and is not intended to substitute or neglect them. Furthermore, these methods were developed to support the use of existing codes that use common engineering concepts. In addition, all of the methods presented here do not create any of the cultural and logistical barriers that may result when integrating different technologies, models, or disciplines.

11. As ILGO (Muñoz and von Spakovsky, 2000) meets a number of practical considerations for system optimization under steady state conditions, DILGO does likewise but for dynamic systems such that the analysis and optimization of each unit (sub-system) is modular and divided into clearly separated tasks. The unit optimizations may be performed in parallel and human intervention is supported. Sophisticated, high-fidelity tools for the sub-systems and load simulations can be used. In each iteration of DILGO, improvements in the objective functions are achieved. In the event of a stop in the optimization process, an improved objective function value over that of the starting or reference system will already have been achieved.

12. The optimum system configuration is able to meet all of the load requirements and system constraints. In particular, using reformate and air tanks as buffers between the BOPS and the SS was shown to be an operational and cost effective method to minimized the transient effects on the SOFC stack due to changes in load. Additionally, buffering reduced the temperature fluctuations of the streams throughout the system. Furthermore, buffering allows one to better regulate the change in operational conditions both at the reformer and in the WRAS, which in turn yields more efficient transitions due to load changes.

13. The thermal energy recovery and thermal management cycle made up of a heat exchanger network and expander show internal energy can both dramatically enhance system efficiency and effectively regulate the anode and cathode inlet

temperatures. In particular, the location of heat exchanger I (HX I) permits the regulation of the anode inlet temperature and preconditions the cathode exit to interact with the cathode inlet at the heat exchanger II (HX II) where the cathode inlet temperature is regulated. Dynamic simulation through the whole operational regime, which includes drastic transients, showed that temperature differences between the anode and cathode inlet never exceeded 5 ^{o}K. Heat exchanger IV (HX IV) effectively recovers the required heat to precondition the air passing through HX II before entering the cathode while heat exchanger III (HX III) transfers energy from the cathode exhaust to the combustion gases in order to reach high temperatures at the expander inlet. The expander in the WRAS then effectively recovers energy to significantly offset the parasitic load due to compressor operation. The end result of all of this is that, taking capital cost into account, an incredibly efficient and cost effective system has been developed which achieves an average efficiency (see conclusion 15) that is superior to the best combustion technology available today.

14. Recirculating the anode products back to the steam-methane reformer was shown to be an extremely synergistic strategy. On the one hand, the anode products are so rich in water content that steam-to-methane ratios as high as 7 can be reached, thus eliminated the need of requiring steam generation during the in-operation regime. In fact, using the steam generator to produce enough steam to reach steam-to-methane ratios of 7 would drop the system efficiency severely. Additionally, the reforming efficiency increases as the steam-to-methane ratio increases.

15. In general the optimum configuration, which is a product of this research, is shown to enhance the total system efficiency significantly in such way that the average system efficiency through the entire load profile is 56%. The system is able to operate at low loads (approximately 20 % of the maximum system power) without sacrificing system performance. In fact, at low load system performance increases because the increase in the FPS and SS efficiencies surpass of the reduction in efficiency due to the parasitic load for air compression.

16. The fact that the consumption of natural gas throughout the system's lifetime represents more than half (54%) of the total cost indicates that the proposed system is theoretically more attractive at locations where natural gas is cheaper. Additionally, a total life cycle cost breakdown shows that operational costs are dramatically important in considering system feasibility, so that, issues such as system efficiency and performance during steady and transient states are of great importance during the optimization process.

17. The observation that the FPS cost represents 25% of the system total life cycle cost indicates that special attention should be paid to minimizing the FPS capital cost. A major contributor in this cost is the need for a steam generator to be used for start-up; therefore, it is recommended to investigate the application of auto-thermal reforming, which is less efficient than steam reforming but does not required steam generation.

18. The proposed control sub-system architecture composed of a set of PID controllers was shown to be able to effectively and efficiently handle the total system transient. In particular, DILGO was able to execute the synthesis/design and operation/control optimization at once for separate units. However, the theoretical basis of DILGO does not constrain the control sub-system to have PID architecture. Consequently, it is recommended to explore the applicability of new architectures such as internal model control, adaptive control, etc. in the total system optimization problem.

Chapter 8

Recommendations for Future Work

There are a number of additional issues that may be considered the natural "next steps" to this work. Some of these issues are listed below.

- The ever increasing complexity of systems and simulators and the need to account for transient behavior create a severe computational burden for simulation and accordingly for optimization. To alleviate this problem, two possible approaches are recommended. The first is the use of models of different complexity for the modeling of the different units. The second is the use of approximations that could replace the actual modeling at certain stages of the optimization. Consider, for example, the case of the FPS simulator developed in this doctoral work. The extreme expense resulting from the use of this tool combined with a global search type of optimization algorithm, e.g., a GA, could be alleviated in great measure by any or both of the schemes proposed. In the first approach, a simple model that contains most of the thermodynamic features of the problem along with simplified sizing functions could potentially aid in the search of the synthesis/design space. Once a few "promising areas" are found one could switch to a less expensive (in term of computational burden) gradient-based algorithm that uses the actual FPS model. The second suggestion is to use actual simulation results to generate a model of the system. This technique replaces the objective and/or the constraints with relatively simple functions, which are typically polynomials.

- The steam generator represents 33% of the FPS total life cycle cost, which in turn accounts for about 25% of the SOFC system total life cycle cost. Therefore, it is absolutely important to explore the application of fuel processing technologies that do not require steam during start-up or even during operation. Since steam reforming is

the most efficient fuel processing method available today, the application of reforming technologies different from steam reforming will allow one to measure the inherent trade-off between system efficiency and capital cost, noting, of course, that these other reforming technologies are significantly less efficient than the steam reforming approach used here.

- Currently, research efforts are being directed to implement advanced control architectures (i.e. adaptive control, model control, multivariable control, etc.) in order to solve the fuel cell control problem. Even though progress is being made, these efforts use the traditional control sub-system design approach (i.e. do not consider the operational/control problem early on in the conceptual and preliminary total system synthesis/design stage). In this doctoral work, a PID control sub-system architecture was implemented using the DILGO approach. However, the mathematical basis of DILGO does not constrain its application to PID architectures. Therefore, it is recommended to exploit the current advancement in the control arena in order to solve the dynamic synthesis/design operational/control optimization problem using DILGO, while considering the control architecture as a set of synthesis/design decision variables.

- The load profile used in this doctoral work is based on the work by Ellis and Gunes, 2001. In fact, this profile is a statistical simplification of the real loads which present more frequent variations than this simplify profile. It should be clear that the load profile defines in part the system interaction with the environment and that changes in the load profiles may induce changes in the "global optimum". Therefore, the inclusion of abrupt load changes closer to each other as part of the load profile may provide better insight on sub-systems dynamic interaction effects and total system dynamic performance. How frequent and how close to each other these changes are should be defined, taking into account simulation times and computational tools.

- Finally, the DILGO capabilities were proven by solving a large-scale dynamic optimization problem such as the one for the dynamic synthesis/design of the and operational/control SOFC based APU. However, the solution of a larger-scale dynamic problem that incorporates various research groups using different methods

and software will significantly prove the generality of the method developed in this doctoral work. This opportunity may become available as the DOE SECA initiative advances and dynamic models for the power electronics and stack sub-systems are made available.

References

Acharya, K., Mazumder, S.K., Burra, R., Williams, R., Haynes, C., 2003, System-interaction analyses of solid-oxide fuel cell (SOFC) power-conditioning system, in press, Proceedings of IEEE IAS Conference.

Achenbach, E., 1995, Response of a solid oxide fuel cell to load change, Journal of Power Sources, vol. 57, pp. 105-109.

Adelman, S. T., Hoffman, M. A., and Baughn, J. W., 1995, A methane-steam reformer for a basic chemically recuperated gas turbine, Journal of Engineering for Gas Turbines and Power, vol. 117, pp. 16-23, January.

Alatiqi, I. M., Meziou, A. M., and Gasmelseed, G. A., 1989, Modeling, simulation, and sensitivity analysis of steam-methane reformers, International Journal of Hydrogen Energy, vol. 14, No. 4, pp. 241-256.

Arthur D. Little, 1994, Multi-Fuel Reformers for Fuel Cells Used in Transportation, Final Report for the U.S. Department of Energy, Report No. DOE/CE/50343-2, Cambridge, Massachusetts.

Arthur D. Little, 1999, Assessment of Planar Solid Oxide Fuel Cell Technology, Final Report for the U.S. Department of Energy, Report No. DOE/CE/39436-02, Cambridge, Massachusetts.

ASHRAE, 1993, Hand Book Fundamentals. ASHRAE, Inc.

Azevedo, J. L. T. and Cunha, J., 2000, Modeling the integration of a compact plate steam reformer in a fuel cell system, Journal of Power Sources, vol. 86, pp. 515-522.

Balling R.J.and Sobieszczanski-Sobieski, J, 1996, Optimization of Coupled Systems: A Critical Overview of Approaches, AIAA Journal, Vol. 34, No. 1, January

Bausa J., Tsatsaronis G., 1998. Dynamic Optimization of Start-up and Load-Increasing Processes in Power Plants Methodology and Application. ASME advanced Energy Systems Division, vol 38. 1998.

Bejan, A., Tsatsaronis, G., et al., 1996, Thermal Design and Optimization, John Wiley and Sons, New York.

Balchen J. and Mumme K., “Process Control: Structures and Applications”, Aspen Publishers, Inc. January, 1988.

Bequette B. W., 2003. Process Control Modeling, Design, and Simulation. Prentice Hall International Series in the Physical and Chemical Engineering Series.

Bessette, N., 1994, Modeling and Simulation for Solid Oxide Fuel Cell Power Systems, Ph.D. Thesis, Georgia Institute of Technology, Atlanta, Georgia.

Bianchi M., Peretto A., and Spina P, 1998. Modular Dynamic Model of a Multi-Shaft gas Turbine and Validation Test. ASME advanced Energy System Division, Vol. 38, 1998.

Boehm, R. F., 1987, Design Analysis of Thermal Systems, John Wiley and Sons, Inc., New York.

Boland, D. and Linnhoff, B., 1979, The Preliminary Design of Networks for Heat Exchange by Systematic Methods, Chemical Engineer, pp 222-228.

Bodrov, N. M., Apel’baum, L. O., and Temkin, M. I., 1964, in Murray, A. P. and Snyder, T. S. (Editors), Steam-Methane Reformer Kinetic Computer Model with Heat Transfer and Geometry Options, Industrial Engineering Chemical Process Design and Development, Vol. 24, No. 2, p. 289.

Chemical Engineering Plant Cost Index, 2001, Chemical Engineering, McGraw-Hill, New York.

Chong, E.K.P., and Zak, S.H., 1996, An Introduction to Optimization, Wiley-Interscience, New York, New York.

CRC, 1976, Handbook of Tables for Applied Engineering Science. CRC Press.

Curti, V., von Spakovsky, M.R., Favrat, D., 2000, An Environomic Approach for the Modeling and Optimization of a District Heating Network Based on Centralized and Decentralized Heat Pumps, Cogeneration and/or Gas Furnace (Part I: Methodology), International Journal of Thermal Sciences, vol. 39, no. 6, June, Elsevier, France.

Curti, V., von Spakovsky, M.R., Favrat, D., 2000, An Environomic Approach for the Modeling and Optimization of a District Heating Network Based on Centralized and Decentralized Heat Pumps, Cogeneration and/or Gas Furnace (Part II: Application), International Journal of Thermal Sciences, vol. 39, no. 6, June, Elsevier, France.

Dieckmann, R. R., Watson, A. C., and Glover, S. F., 1972, "Development of Integrated Environmental Control Systems for Aircraft", Air Force Flight Dynamics Laboratory, Wright-Patterson Air Force Base, Ohio, May.

Directed Technologies, Inc., 2001, http://directedtechnologies.com.

El-Sayed Y., 1989, A Decomposition Strategy for Thermoeconomic Optimization, ASME Journal of Energy Resources Technology, vol. 111, pp 1-15

El-Sayed Y., 1996, A Second-Law-Based Optimization: Part I Methodology & Part 2, ASME Application, Journal of Energy Resources Technology, Vol. 118, pp. 693-703.

El-Sayed, Y.M. and Evans, R.B., 1970, Thermoeconomics and the Design of Heat Systems, Journal of Engineering for Power, ASME Transactions, Vol. 92, 27, Jan.

El-Sayed, Y.M., 1996, A Second-Law-Based Optimization: Parts 1 and 2, Journal of Engineering for Gas Turbines and Power, ASME Transactions, vol. 118, October, N.Y.

Ellis, M.W., von Spakovsky, M.R., and Nelson, D.J., 2001, Fuel cell systems: efficient, flexible energy conversion for the 21st century, Proceedings of the IEEE, vol. 89, no. 12, pp. 1808-1818.

Energy Information Administration, 2000, "U.S. Natural Gas Prices", http://www.eia.doe.gov.

Escombe, F. M., 1995, Fuel Cells: Applications and Opportunities - Executive Summary, ESCOVALE Consultancy Services, Report No. 5020, Surrey, United Kingdom, January.

Evans, R.B. and Tribus, M., 1962, A Contribution to the Theory of Thermoeconomics, UCLA Dept. of Engineering: Report No. 62-63, Los Angeles, CA, August.

Evans, R.B. and von Spakovsky, M.R., 1993, Engineering Functional Analysis (Parts II), Journal of Energy Resources Technology, ASME transactions, Vol. 115, No. 2, N.Y., N.Y., June.

Evans, R.B. and von Spakovsky, M.R., 1993, Engineering Functional Analysis (Parts II), Journal of Energy Resources Technology, ASME transactions, Vol. 115, No. 2, N.Y., N.Y., June.

Evans, R.B., 1980, Thermoeconomic Isolation and Exergy Analysis, Energy: The International Journal, Vol. 5, Nos. 8-9, 805-821.

Floudas, A., 1995, Nonlinear and Mixed-Integer Optimization, Oxford University Press, New York.

Fogler Scott H., 1999, Elements of Chemical Reaction Engineering. Prentice Hall International Series in the Physical and Chemical Engineering Series.

Frangopoulos, C. A., 1994, Application of the Thermoeconomic Functional Approach to the CGAM Problem, Energy-The International Journal, Vol. 19, No. 3, pp. 323-342.

Frangopoulos, C.A., 1983, Thermoeconomic Functional Analysis: A Method for Optimal Design or Improvement of Complex Thermal Systems, School of Mechanical Engineering, Georgia Institute of Technology, Ph.D. Dissertation.

Frangopoulos, C.A., 1984, Thermoeconomic Functional Analysis: An Innovative Approach to Optimal Design of Thermal Systems, Second Law Aspects of Thermal Design. HTD Vol. 33, ASME, N.Y., N.Y., August.

Frangopoulos, C.A., 1989, Optimal Synthesis and Operation of Thermal Systems by the Thermoeconomic Functional Approach, ASME Winter Annual Meeting, AES 10-3, 49.

Frangopoulos, C.A., 1994, Application of Thermoeconomic Optimization Methods to the CGAM Problem, Energy: The International Journal, special edition, Vol. 19, No. 3, pp. 323-342, Pergamon Press, Great Britain.

Frangopoulos, C.A., and von Spakovsky, M.R., 1993, The Environomic Analysis and Optimization of Energy Systems (Part I), Proceedings of the International Conference on Energy Systems and Ecology: ENSEC'93, Vol. I, pp. 123-132, ASME, Cracow, Poland, July.

Frangopoulos, C.A., Evans R.B., 1984, Thermoeconomic Isolation and Optimization of Thermal System Components, Second Law Aspects of Thermal Design. HTD Vol. 33, ASME, N.Y., N.Y., August.

Frangopoulos C., von Spakovsky M., and Sciubba E., 2002. A Brief Review of Methods for the Design and Synthesis Optimization of Energy Systems. Internatonal Centre for Applied Thermodynamics / Journal. Vol. 5 No. 4 pag 151-160, 2002

Froisy G., 1995. Design of robust constrained model-predictive controllers with volterra series, AIChE J. 41(9): 2098-2107.

Fuel Cell Handbook, 2000, 5th edition, Office of Fossil Energy, National Energy Technology Laboratory, Morgantown, West Virginia, October.

Gaggioli R. and El-Sayed Y., 1989, A Critical Review of Second Law Costing Methods, Journal of Energy Resources Technology, ASME Transactions, vol. 111, pp 1-15.

Gaggioli, R., Sama, D.A., Qian, S., and El-Sayed, Y. M., 1991, Integration of a New Process into an Existing Site: A Case Study in the Application of Exergy Analysis, Journal for Engineering for Gas Turbines and Power, ASME Transactions, vol. 113, no. 2.

George, R.A. and Bessette, N.F., 1998, Reducing the Manufacturing Cost of Tubular SOFC Technology, Journal of Power Sources, vol. 71, pp. 131-137.

Georgopoulos, N., 2002, *Application of a Decomposition Strategy to the Optimal Synthesis/Design and Operation of a Fuel Cell Based Total Energy System*, M.S. thesis, Department of Mechanical Engineering, Virginia Polytechnic Institute and State University, Blacksburg, VA.

Georgopoulos, N., von Spakovsky, M. R., and Muñoz, J. R., 2002, Application of a decomposition strategy to the optimal synthesis/design and operation of a fuel cell based total energy system for residential applications, International Mechanical Engineering Congress and Exposition – IMECE'2002, ASME, N.Y., N.Y., November.

Goldberg, D. E., 1989, Genetic Algorithms in Search, Optimization and Machine Learning, Addison Wesley, Reading, MA.

Golbert J. and. Lewin D., Fuel Efficient Model Predictive Control of PEM Fuel Cells. PSE Research Group, Wolfson Department of Chemical Engineering, Technion I. I. T., Haifa 32000, Israel

gPROMS, 2000, User Guide, version 2.2, Process Systems Enterprise Ltd., London, United Kingdom.

Greene R., 1992, Compressors, Selection, Usage, and Maintenance. Mc Graw Hill Inc, USA.

Gunes, M. B., 2001, Investigation of a Fuel Cell Based Total Energy System for Residential Applications, M.S. Thesis, Department of Mechanical Engineering, Virginia Polytechnic Institute and State University, Blacksburg, Virginia.

Gyftopoulos, E. P. and Beretta, G. P., 1991, *Thermodynamics: Foundations and Applications*, Macmillan Publishing Company, New York.

Hajela P., 1999, Nongradient Methods in Multidisciplinary Design Optimization-Status and Potential, Journal of Aircraft, Vol. 36, No.1, Jan-Feb.

Hill P. and Peterson C., 1992, Mechanics and Thermodynamics of Propulsion. Addison-Wesley Publishing Company, Inc.

Huang, X. and Reifsnider, K., 2001, Modeling long-term performance of solid oxide fuel cells: A phenomenological approach.

Incropera F. and DeWitt D., 1990, Fundamental of Heat and Mass Transfer. John Wiley and Sons, Inc.

JANAF Thermochemical Tables, 1971, 2nd edition, Stull, D. R. and Prophet, H. (Project Directors), NSRDS-NBS37.

James, B. D., Lomax, F. D., Thomas C. E., and Colella, W. G., 1997, "PEM Fuel Cell Power System Cost Estimates: Sulfur-Free Gasoline Partial Oxidation and Compressed Direct Hydrogen", Final Report for the Ford Motor Company, Arlington, Virginia, October.

Kakac S. and Liu H., 2002, Heat Exchangers Selection, Rating, and Thermal Design. CRS press.

Kays, W.M. and London, A.L., 1998, Compact Heat Exchangers, Krieger Publishing Company, Malabar, FL.

Kern, D. Q., 1950, *Process Heat Transfer*, McGraw-Hill, New York.

Keiski, R. L., Desponds, O., Chang, Y. –F., and Somorjai, G. A., 1993, Kinetics of the Water-Gas Shift Reaction over Several Alkane Activation and Water-Gas Shift Catalysts, Applied Catalysis A, Vol. 101, No. 2, pp. 317-338, August.

Khandkar, A., Hartvigsen, J., and Elangovan, S., 1998, Selection of SOFC stack operating point for optimal balance of efficiency and power. Proceedings of the Third European Solid-oxide Fuel Cell Forum.

Kim, J.W., Virkar, A.V., Fung, K.Z., Mehta, K., and Singhal, S.C., 1999, Polarization Effects in Intermediate Temperature, Anode-Supported Solid Oxide Fuel Cells. Journal of the Electrochemical Society, vol. 146, no. 1, pp. 69-78.

Kotas T.J., 1985, The Exergy Method of Thermal Plant Analysis, Krieger Publishing Company, Malabar, Florida.

Le Claire, R., 1975, Evaluation of the Overall Fuel Mass Penalty of an Aircraft System, Aeronautical Journal, May, pp 225-228.

Linhoff, B., 1989, Pinch Technology for the Synthesis of Optimal Heat and Power Systems, Journal of Energy Resources Technology, ASME Transactions. Vol. 111, pp. 137-147.

Linhoff, B. and Alanis, F.J., 1991, Integration of a New Process Into an Existing Site: A Case Study in the Application of Pinch Technology, Journal of Engineering for Gas Turbines and Power, ASME Transactions, Vol. 113, pp. 159-169.

Linnhoff, B., 1993, Pinch Technology for the Synthesis of Optimal Heat and Power Systems, Journal of Energy Resources Technology, ASME Transactions, vol. 111.

Manglik, R.M. and Bergles, A.E., 1990, The Thermal-Hydraulic Design of the Rectangular Offset-Strip-Fin Compact Heat Exchanger in Compact Heat Exchangers, R.K. Shah, A.D. Kraus, and D. Metzger editors, Hemipshere Publishing Corporation, pp 123-149.

Marshall and Swift Equipment Cost Index, 2001, *Chemical Engineering*, McGraw-Hill, New York.

Mazumder, S. K., Acharya K., Burra R., Haynes C., Willian R., von Spakovsky M. R., Rancruel D. F., Nelson D., Hertvigsen J., Elangovan S., Mckintyre, C., Herbison D., 2003, An Investigation to Resolve the Interaction Between Fuel Cell,

Power Conditioning System And Application Loads. Topical report, U.S. Department of Energy, Cooperative Agreement Number: DE-FC26-02NT41574, October.

Mazumder, S. K., Acharya K., Haynes C., Willian R., von Spakovsky M. R., Rancruel D. F., Nelson D., Hertvigsen J., Gemmen R. S., 2004. Solid-Oxide Fuel Cell Performance and Durability: Resolution of the Effects of Power-Conditioning System and Application Loads, Journal of Power Electronics, special issue on Distributed Power Generation (DG), IEEE.

Mazumder, S.K., Burra, R., Acharya, K., Von Spakovsky, M.R., Nelson, D.J., Rancruel, D., Haynes, C., Williams, R., 2003, "Development of a comprehensive simulation platform to investigate system interactions among solid-oxide fuel cell, power-conditioning systems, and application loads", *Proceedings of ASME First International Conference on Fuel Cell Science, Engineering and Technology.*

Metropolis N., Rosenbluth A. W., Rosenbluth M. N., Teller A. H., and Teller E., 1953. Equation-of-state calculations by fast computing machines. J. Chem. Phys. 21 1087

Muñoz J. R., von Spakovsky M.R., 1999, A Second Law Based Integrated Thermoeconomic Modeling and Optimization Strategy for Aircraft / Aerospace Energy System Synthesis and Design (Phase I - Final Report), final report, Air Force Office of Scientific Research, New Vista Program, December.

Muñoz, J.R. and von Spakovsky, M.R., 2000a, An Integrated Thermoeconomic Modeling and Optimization Strategy for Aircraft / Aerospace Energy System Design, Efficiency, Costs, Optimization, Simulation and Environmental Aspects of Energy Systems (ECOS'00), Twente University, ASME, Netherlands, July 5-7.

Muñoz, J.R. and von Spakovsky, M.R., 2000b, The Use of Decomposition for the Large Scale Synthesis/ Design Optimization of Highly Coupled, Highly Dynamic Energy Systems: Part I - Theory, 2000 ASME International Mechanical Engineering Congress and Exposition, Orlando, FL, Nov 5-10.

Muñoz, J.R. and von Spakovsky, M.R., 2000c, The Use of Decomposition for the Large Scale Synthesis/ Design Optimization of Highly Coupled, Highly Dynamic Energy Systems: Part II - Applications, 2000 ASME International Mechanical Engineering Congress and Exposition, Orlando, FL, Nov 5-10.

Mutambara, A., Design and Analysis of Control Systems. CRC Press LLC, Boca Raton, USA, 1999

Oei, D., Adams, J. A., Kinnelly, A. A., Purnell, G. H., Sims, R. I., Sulek, M. S., and Wernette, D. A., 1997, "Direct-Hydrogen-Fueled Proton-Exchange-Membrane Fuel Cell System for Transportation Applications", Final Report for the U.S. Department of Energy, Report No. DOE/CE/50389-503, Dearborn, Michigan, July.

Olsommer, B., von Spakovsky, M.R., Favrat, D., 1999a, An Approach for the Time-dependent Thermoeconomic Modeling and Optimization of Energy System Synthesis, Design and Operation (Part I: Methodology and Results), *International Journal of Applied Thermodynamics*, Vol. 2, No. 3.

Olsommer, B., von Spakovsky, M.R., Favrat, D., 1999b, An Approach for the Time-dependent Thermoeconomic Modeling and Optimization of Energy System Synthesis, Design and Operation (Part II: Reliability and Availability), *International Journal of Applied Thermodynamics*, Vol. 2, No. 4.

Paulus, D. and Gaggioli, R., Rational Objective Functions for Vehicles, AIAA Paper No. 2000-4852, 8th AIAA/USAF/NASA/ISSMO Symposium on Multidisciplinary Analysis and Optimization, Long Beach, California, September 6-8, 2000.

Rao, S. S., 1996, Engineering Optimization-Theory and Practice, John Wiley and Sons, N.Y.

Rancruel D. and von Spakovsky M.R., 2003, Decomposition with Thermoeconomic Isolation Applied to the Optimal Synthesis/Design of an Advanced Fighter Aircraft System, International Journal of Thermodynamics, Vol. 6, No.3, pp. 93-105, September.

Rancruel, D. F. 2003 "A Decomposition Strategy Based on Thermoeconomic Isolation Applied to the Optimal Synthesis/Design and Operation of an Advanced Fighter Aircraft System", Master thesis, Virginia Polytechnic Institute and State University, Blacksburg,VA.

SAE Aerospace Applied Thermodynamics Manual, 1969, Society of Automotive Engineers, New York.

Sama D. A., 1995, Differences Between Second Law Analysis and Pinch Technology, Journal of Energy Resources Technology, ASME Transactions. Vol. 117, pp. 186-190

Sama, D.A., Qian, S., Gaggioli, R., 1989, A common Sense Second Law Approach for Improving Process Efficiencies, International Symposium on the Thermodynamic Analysis and Improvement of Energy Systems, ASME, Pergamon Press, Beijing.

Sastry S. and Bodson M., 1989. “Adaptive Control: Stability, Convergence, and Robustness”. Prentice-Hall Advanced Reference Series (Engineering) Prentice-Hall, 1989-1994.

Schmuller J., 1991, 1992."Expert System Shells at Work" series by Schmuller PC AI, (1991, 1992).

Sciubba, E., 1995, Artificial Intelligence Applications to the Synthesis of Thermal Processes, Second Law Analysis of Energy Systems: Towards the 21st Century, ASME, Univ. di Roma.

Sciubba, E., 1998, Artificial Intelligence in Thermal Systems Design: Concepts and Applications, Nova Science Publishers, Commack, N.Y.

Scott H., 1999, Elements of Chemical Reaction Engineering. Prentice Hall International Series in the Physical and Chemical Engineering Series.

Shah, R.K. and Webb, R.L., 1982, Compact and Enhanced Heat Exchangers, in Heat Exchangers: Theory and Practice, J. Taborek, G.F. Hewitt, and N. Agfan editors, Hemisphere Publishing Corporation, pp 435-468

Shah, R.S., 1981, Compact Heat Exchanger Design Procedure, in Heat Exchangers, Thermal-Hydraulic Fundamentals and Design, S. Kakac, A.E. Bergles and F. Matinger editors, Hemisphere Publishing Corporation, pp 495-536.

Sinott, R. K., 1994, in Coulson, J. M. and Richardson, J. F. (Editors), *Coulson and Richardson’s Chemical Engineering*, 5th edition, Butterworth-Heinemann Publishers, Woburn, Massachusetts.

Sobieszczanski-Sobieski, J, 1989, Optimization by Decomposition: A step from Hierarchic to Non-hierarchic Systems, NASA CP-3031, Part 1.

Sobieszczanski-Sobieski, J, 1990, Sensitivity of Complex, Internally Coupled Systems, AIAA Journal, Vol. 28, pp.153-161, January.

Sobieszczanski-Sobieski, J. and Haftka, 1997, Multidisciplinary Aerospace Design Optimization: Survey of Recent Developments, Structural Optimization, Vol. 14, No. 1, pp 1-23.

Tsatsaronis, G. and Pisa, J., 1994, Exergoeconomic Evaluation and Optimization of Energy Systems-Application to the CGAM Problem, Energy-The International Journal, Vol. 19, No. 3, pp. 287-321.

Tsatsaronis, G. and Winhold, M., 1984, Thermoeconomic Analysis of Power Plants, EPRI AP-3651 Project 2029-8, Palo Alto, California, Electric Power Research Institute.

Tsatsaronis, G., 1985, Thermoökonomische Analzse von Energieumwandlungs-prozessen, Dr. Habilitatus Thesis, Dept. of Mechanical Engineering, Technical University of Aachen, West Germany.

Tsatsaronis, G., and Pisa, J., 1994, Exergoeconomic Evaluation and Optimization of Energy Sytsems: Application to the CGAM Problem, Energy: The International Journal, Vol. 19, No. 3, pp. 287-321, Pergamon, Great Britain.

Tsatsaronis, G., Pisa, J., et al., 1989, Thermodynamic Analysis and Improvement of Energy Systems, Proceeedings of the International Symposium, Beijing, China, Pergamon Press, pp. 195-200.

Union Gas, 2001, “Natural Gas Composition”, http://www.uniongas.com.

Valero, A., Lozano, M., et al., 1994, Application of the Exergetic Cost Theory to the CGAM Problem, Energy-The International Journal, Vol. 19, No. 3, pp. 365-381.

Valero, A., Lozano, M., et al., 1994, CGAM Problem: Definition and Conventional Solution, Energy-The International Journal, Vol. 19, No. 3, pp. 279-286.

Valero, A., Lozano, M.A., and Muñoz, M., 1986, A General Theory of Exergy Savings (Parts I, II, and III), Computer-Aided Engineering of Energy Systems, ASME, AES-Vol. 2-3, pp. 1-21.

Valero, A., Serra, L., Lozano, M.A., 1993, Structural Theory of Thermoeconomics, Thermodynamics and the Design, Analysis and Improvement of Energy Systems, ASME, AES-Vol. 30, N.Y., N.Y..

Valero, A., Serra, L., Lozano, M.A., and Torres, C., 1994, Application of the Exergetic Cost Theory to the CGAM Problem, Energy: The International Journal, Vol. 19, No. 3, pp. 365-381, Pergamon, Great Britain.

Varigonda S., Pukrushpan J., Stefanopoulou A., 2003. "Challenges in Fuel Cell Power Plant Control: The Role of System Level Models" AIChE Spring Meeting

Virkar, A.V., Kim, J.W., Mehta, K., and Fung, K.Z. Low temperature, high performance, planar solid oxide fuel cells and stacks. *www.netl.doe.gov/publications/proceedings/97/97fc/FC6-5.PDF*.

von Spakovsky M.R., 1986, A Practical Generalized Analysis Approach for the Optimal Thermoeconomic Design and Improvement of Real-World Thermal Systems, School of Mechanical Engineering, Georgia Institute of Technology, Ph.D. Dissertation.

von Spakovsky M.R., Evans R.B., 1984, Detailed Second Law Design of Components in Complex Thermal Systems, Second Law Aspects of Thermal Design. HTD Vol. 33, ASME, N.Y., N.Y., August.

von Spakovsky M.R., Evans R.B., 1990, The design and performance Optimization of thermal systems. Journal of Engineering for Gas Turbines and Power. ASME Vol. 112. January 1990.

von Spakovsky, M., 1994, Application of the Functional Analysis to the Analysis and Optimization of the CGAM Problem, Energy-The International Journal, Vol. 19, No. 3, pp. 343-364.

von Spakovsky, M.R., 1994, Application of Engineering Functional Analysis to the Analysis and Optimization of the CGAM Problem, Energy: The International Journal, Vol. 19, No. 3, pp. 343-364, Pergamon, Great Britain.

von Spakovsky, M.R., and Evans, R.B., 1993, Engineering Functional Analysis (Part I), Journal of Energy Resources Technology, ASME Transactions, Vol. 115, No. 2, N.Y., June.

von Spakovsky, M.R., and Evans, R.B., 1993, Engineering Functional Analysis (Part II), Journal of Energy Resources Technology, ASME Transactions, Vol. 115, No. 2, N.Y., June.

von Spakovsky, M.R., and Frangopoulos, C.A., 1993, The Environomic Analysis and Optimization of Energy Systems (Part II), Proceedings of the International Conference on Energy Systems and Ecology: ENSEC'93, Vol. I, pp. 123-132, ASME, Cracow, Poland, July.

von Spakovsky M.R., Frangopoulos, C.A., 1994, The Environomic Analysis and Optimization of a Gas Turbine Cycle with Cogeneration, Thermodynamics and the Design, Analysis and Improvement of Energy Systems, ASME, AES-Vol. 33, N.Y., N.Y., November.

von Spakovsky M. R., Rancruel D. F., Nelson D., Mazumder, S. K., Acharya K., Burra R., Haynes C., Willian R., Gemmen R. S., 2003. Investigation of System Demand and Component Performance and Interaction Issues for Solid-Oxide Fuel Cell Based Auxiliary Power Unit Responding to Changes in Application Load. Proceedings of the 29th Annual Conference of the IEEE Industrial Electronic Society, Roanoke, VA, 2003.

Wurster, R., 1997, "PEM Fuel Cells in Stationary and Mobile Applications: Infrastructural Requirements, Environmental Benefits, Efficiency Advantages, and Economical Implications", Ludwig-Bölkow-Systemtechnik GmbH (LBST), Ottobrunn, Germany.

Xu, J. and Froment, G. F., 1989, Methane Steam Reforming, Methanation and Water-Gas Shift: I. Intrinsic Kinetics, AIChE Journal, Vol. 35, No. 1, pp. 88-96, January.

Xu, J. and Froment, G. F., 1989, Methane Steam Reforming: II. Diffusional Limitations and Reactor Simulation, AIChE Journal, Vol. 35, No. 1, pp. 97-103, January.

Vitae

Diego Fernando Rancruel was born in Santiago de Cali, Colombia on April 3, 1972. After graduating with honors from Colegio San Juan Bosco he served as a soldier in the Colombian Army. He then attended Universidad del Valle in Cali, Colombia, and in early 1995 he received his Bachelor of Science degree with honors in Mechanical Engineering. After graduation he worked for Bayer AG. a pharmaceutical and chemical multinational company, where he worked for five years in total, one year as metrology chief engineer, two years as maintenance manager and two years as the project department manager, respectively. He attended graduate school in Universidad del Valle in Cali, Colombia; in 1997 he received an engineering degree as Specialist in Engineering Materials. He attended graduate business school in Universidad ICESI in Cali, Colombia; in 1999 he received a business degree as Specialist in Administration. He received a Master of Science in Mechanical Engineering from Virginia Tech. Upon completion of his Ph.D. he will pursue a career in the industry working for General Electric Energy.